

DATE ISSUED JUL 6 1977

ORNL-5239

761101

Radiative Heat Transfer in Arrays of Parallel Cylinders

Richard Lee Cox

APPLIED TECHNOLOGY

Any further distribution by any holder of this document or of the data therein to third parties representing foreign interests, foreign governments, foreign companies and foreign subsidiaries or foreign divisions of U.S. companies should be coordinated with the Director, Division of Reactor Research and Development, Energy Research and Development Administration.

OAK RIDGE NATIONAL LABORATORY
OPERATED BY UNION CARBIDE CORPORATION FOR THE ENERGY RESEARCH AND DEVELOPMENT ADMINISTRATION

Printed in the United States of America. Available from
the Energy Research and Development Administration,
Technical Information Center
P. O. Box 62, Oak Ridge, Tennessee 37830
Price: Printed Copy \$8.00; Microfiche \$3.00

This report was prepared as an account of work sponsored by the United States Government. Neither the United States nor the Energy Research and Development Administration/United States Nuclear Regulatory Commission, nor any of their employees, nor any of their contractors, subcontractors, or their employees, makes any warranty, express or implied, or assumes any legal liability or responsibility for the accuracy, completeness or usefulness of any information, apparatus, product or process disclosed, or represents that its use would not infringe privately owned rights.

ORNL-5239
Dist. Category UC-79c

Contract No. W-7405-eng-26

CHEMICAL TECHNOLOGY DIVISION

RADIATIVE HEAT TRANSFER IN ARRAYS OF PARALLEL CYLINDERS

Richard Lee Cox^{*} K-25

*Presently employed at ORGDP.

This report was prepared as a dissertation and submitted to the Faculty of the Graduate School of the University of Tennessee in partial fulfillment of the degree of Doctor of Philosophy with a major in Chemical Engineering.

Date Published: June 1977

OAK RIDGE NATIONAL LABORATORY
Oak Ridge, Tennessee 37830
operated by
UNION CARBIDE CORPORATION
for the
ENERGY RESEARCH AND DEVELOPMENT ADMINISTRATION

ACKNOWLEDGMENTS

This study was carried out as part of the Liquid Metal Fast Breeder Reactor Program of the Chemical Technology Division, Oak Ridge National Laboratory, which is operated by Union Carbide Corporation for the Energy Research and Development Administration. A. R. Irvine served as project leader for the study of the shipping of spent fuel elements of which this investigation was a part. B. B. Klima oversaw the preparation of the engineering drawings for the test facility. H. C. Young of the Reactor Division coordinated the installation and operation of the experimental equipment at the Y-12 Plant.

The author wishes to acknowledge the helpful suggestions of his major professor, Dr. J. S. Watson, in the preparation of this report.

Special appreciation is expressed to Janice Shannon for her speed, accuracy, and alacrity in typing this report. Sincere thanks are accorded Martha Stewart for her careful editing of the manuscript. The drawings were prepared by the Drafting Department of the Chemical Technology Division.

ABSTRACT

A theoretical and experimental study of radiative heat transfer in arrays of parallel cylinders is presented. Attention is primarily directed toward two geometries common in the nuclear industry: square arrays of cylinders on a square pitch and hexagonal arrays of cylinders on an equilateral triangular pitch.

Configuration factors for cylinders on square and equilateral triangular pitches are derived using Hottel's crossed-string method. Theoretical equations are presented for configuration factors between rods up to four rows apart for cylinders on triangular spacings and between rods up to three rows apart for cylinders on square spacings.

The usefulness of a formulation of the radiant energy exchange equations in terms of dimensionless variables is demonstrated for the case in which the heat generation rates of the cylinders are known and the temperatures are sought. Each of the major theories for treating radiation exchange within a diffuse-gray enclosure--net radiation, Gebhart's, and Hottel's methods--is examined and compared for utility in handling the steady-state and transient solutions for this case. It is shown that the net radiation method is most convenient for the steady-state problem, while either Gebhart's or Hottel's equations are superior for the transient problem.

Computer programs are presented and described for obtaining both steady-state and unsteady-state solutions for the temperatures of cylinders in hexagonal arrays of cylinders on an equilateral triangular pitch and for square arrays of cylinders on a square pitch. In the particular instance of uniform surface emissivities and uniform heat generation

rates in each of the cylinders, steady-state center-rod temperatures are given in terms of dimensionless plots which obviate the necessity of using the computer algorithms.

Experimental measurements were made of the steady-state temperatures in two 217-tube hexagonal arrays having pitch-to-diameter ratios of 1.240 and 1.367 at heat generation rates corresponding to center tube temperatures of 800 and 1000°F. The tests were carried out with the tube bundle in a vacuum to minimize the effects of gaseous conduction and natural convective heat transfer between tubes.

Theoretical calculations based on the assumption of uniform radiosity around the periphery of each tube yielded tube temperatures which were in poor agreement with the experimental observations. Replacing the assumption of uniform radiosity over the entire tube with the assumption of uniform radiosity over 30° segments yielded theoretical temperature profiles across the arrays which differed no more than 7% from the experimental profiles.

TABLE OF CONTENTS

CHAPTER	PAGE
1. INTRODUCTION.	1
2. THEORY OF RADIATION EXCHANGE AMONG DIFFUSE-GRAY SURFACES. . .	3
Basic Assumptions and Definitions	3
Net Radiation Method.	6
Gebhart's Method.	10
Hottel's Method	13
Comparison of the Methods	15
3. APPLICATION OF THEORY	16
Steady State.	16
Unsteady State.	21
4. VIEW FACTORS.	25
Defining Equations.	25
Hottel's Crossed-String Method.	31
View Factors for Cylinders on an Equilateral Triangular Pitch	36
View Factors for Cylinders on a Square Pitch.	52
Previous Work	67
5. CONSTRUCTION OF VIEW FACTOR MATRICES.	71
Hexagonal Arrays.	71
Square Arrays	77
6. THEORETICAL RESULTS	83
Steady State.	83
Unsteady State.	92
Previous Work	96

CHAPTER	PAGE
7. EXPERIMENTAL.	99
Experimental Apparatus.	99
Test Conditions and Experimental Data	105
8. COMPARISON OF EXPERIMENTAL RESULTS AND THEORETICAL CALCULA- TIONS	115
9. CONCLUSIONS AND RECOMMENDATIONS	138
Conclusions	138
Recommendations	139
LIST OF REFERENCES	141
APPENDIXES	145
A. THERMAL CONDUCTION ACROSS TUBES.	146
B. VIEW FACTORS BETWEEN WIRE-WRAPPED TUBES.	149
C. KLEPPER'S ABSORPTION FACTORS	156
D. LISTINGS OF COMPUTER PROGRAMS.	160

LIST OF TABLES

TABLE	PAGE
I. View Factors for Parallel Cylinders on an Equilateral Triangular Pitch.	53
II. View Factors for Parallel Cylinders on a Square Pitch.	66
III. Geometrical Characteristics of Experimental Arrays	100
IV. Summary of Thermal Data for Experimental Runs.	108
V. Comparison of Absorption Factors for $N = 1$ and $N = 12$ for Rods on a Triangular Pitch.	130
VI. Estimates of the Temperature Differentials Across Individual Tubes.	148
VII. Klepper's Absorption Factors for Cylinders on an Equilateral Triangular Pitch	157
VIII. Klepper's Absorption Factors for Cylinders on a Square Pitch .	158

LIST OF FIGURES

FIGURE	PAGE
1. Integration of Intensity Over Solid Angle.	26
2. Geometry for Radiant Interchange Between Two Surfaces.	28
3. Triangular Enclosure	33
4. Hottel's Crossed-String Method	35
5. Parallel Cylinders on an Equilateral Triangular Pitch.	37
6. Determination of F_{12} with Partial Shadowing.	39
7. Determination of F_{12} with No Shadowing	41
8. Determination of F_{13} with Partial Shadowing.	43
9. Determination of F_{15} with Partial Shadowing and Obstruction of One Crossed String	45
10. Determination of F_{15} with Partial Shadowing and No Obstruction of Crossed Strings	48
11. Determination of F_{18} with Partial Shadowing and Obstruction of One Crossed String	49
12. Parallel Cylinders on a Square Pitch	54
13. Derivation of F_{13} with Partial Shadowing	56
14. Derivation of F_{15} with Partial Shadowing and Obstruction of One Crossed String	59
15. Derivation of F_{15} with Partial Shadowing and No Obstruction of Crossed Strings	61
16. Derivation of F_{18} with Partial Shadowing and Obstruction of One Crossed String	63
17. Geometrical Relationship Between dA_i and A_j	69
18. Numbering of Cylinders for a Hexagonal Array with Arbitrary Temperature Distribution	73

FIGURE	PAGE
19. Matrix of F_{ij} Values for a 37-Rod Hexagonal Array with a Nonsymmetrical Temperature Distribution.	74
20. Designation of Cylinders for a Hexagonal Array with Symmetrical Temperature Distribution	76
21. Matrix of F_{ij} Values for a 91-Rod Hexagonal Array with a Symmetrical Temperature Distribution	78
22. Numbering of Cylinders for a Square Array with Arbitrary Temperature Distribution	79
23. Designation of Cylinders for a Square Array with Symmetrical Temperature Distribution and an Even Number of Rows.	81
24. Designation of Cylinders for a Square Array with Symmetrical Temperature Distribution and an Odd Number of Rows	82
25. Center-Rod Temperatures for Hexagonal Arrays of 1, 7, 19, and 37 Cylinders	86
26. Center-Rod Temperatures for Hexagonal Arrays of 61, 91, 127, 169, 217, and 271 Cylinders.	87
27. Center-Rod Temperatures for Hexagonal Arrays of 331, 397, 469, 547, and 631 Cylinders	88
28. Center-Rod Temperatures for Square Arrays of 1, 4, 9, 16, and 25 Cylinders	89
29. Center-Rod Temperatures for Square Arrays of 36, 49, 64, 81, 100, and 121 Cylinders	90
30. Center-Rod Temperatures for Square Arrays of 144, 169, 196, 225, 256, 289, 324, and 361 Cylinders.	91
31. Unsteady-State Solution for Center-Rod Temperature	95

FIGURE	PAGE
32. Tube Bundle and Sheath Prior to Assembly and Insertion into Test Vessel.	101
33. Tube Sheet	102
34. Test Vessel.	103
35. Specifications of Electrical Heaters	104
36. Cross Section of Experimental Array Showing Positions of Thermocouples.	106
37. Experimental Data for Run 1.	109
38. Experimental Data for Run 2.	110
39. Experimental Data for Run 3.	111
40. Experimental Data for Run 4.	112
41. Experimental Data for Run 5.	113
42. Comparison of Experimental Temperature Profile with Theoreti- cal Calculations--Run 1.	116
43. Comparison of Experimental Temperature Profile with Theoreti- cal Calculations--Run 2.	117
44. Comparison of Experimental Temperature Profile with Theoreti- cal Calculations--Run 3.	118
45. Comparison of Experimental Temperature Profile with Theoreti- cal Calculations--Run 4.	119
46. Comparison of Experimental Temperature Profile with Theoreti- cal Calculations--Run 5.	120
47. Emissivity of 304 Stainless Steel as a Function of Oxidation [Data of Rolling and Funai (26)]	122
48. Comparison of Experimental Data and Theoretical Calculations (Nonuniform Radiosity)--Run 1.	132

FIGURE	PAGE
49. Comparison of Experimental Data and Theoretical Calculations (Nonuniform Radiosity)--Run 2.	133
50. Comparison of Experimental Data and Theoretical Calculations (Nonuniform Radiosity)--Run 3.	134
51. Comparison of Experimental Data and Theoretical Calculations (Nonuniform Radiosity)--Run 4.	135
52. Comparison of Experimental Data and Theoretical Calculations (Nonuniform Radiosity)--Run 5.	136
53. Determination of F1'l'	150
54. Cross Section of Array at Axial Position at Which Wire Wrap Contacts Adjacent Tube	152
55. Cross Section of Array at Axial Position at Which Wire Wrap Is Farthest from Adjacent Tube	153

LIST OF SYMBOLS

A	surface area or area normal to heat flow, ft^2
B	radiosity, $\text{Btu}/(\text{hr}\text{-ft}^2)$
c	specific heat capacity, $\text{Btu}/(\text{lb}_m\text{-}^\circ\text{F})$
D	diameter of a cylinder, ft
F	black body view factor, dimensionless
G	Gebhart's absorption factor, dimensionless
H	incident radiation energy flux, $\text{Btu}/(\text{hr}\text{-ft}^2)$
k	thermal conductivity, $\text{Btu}/(\text{hr}\text{-ft}\text{-}^\circ\text{F})$
ℓ	length of path for heat flow, ft
m	number of cylinder surfaces
n	total number of surfaces, $n = m + 1$
PDR	pitch-to-diameter ratio, dimensionless
Q	rate of heat generation or rate of energy transfer, Btu/hr
R	radius of a cylinder, ft
S	cross-sectional area, ft^2
t	time, hr
T	absolute temperature, $^\circ\text{R}$
V	volume, ft^3
W	dimensionless shroud temperature parameter
X	dimensionless heat flux
Y	dimensionless temperature function
Z	dimensionless temperature function
\mathfrak{F}	Hottel's gray body view factor, dimensionless
α	absorptivity, dimensionless
γ	reflectivity, dimensionless
δ	Kronecker delta function
ε	emissivity, dimensionless
θ	dimensionless time
ρ	density, lb_m/ft^3
σ	Stefan-Boltzmann constant, $0.1712 \times 10^{-8} \text{ Btu}/(\text{hr}\text{-ft}^2\text{-}^\circ\text{R}^4)$

CHAPTER 1

INTRODUCTION

Radiative heat transfer among tubes or rods in arrays is important in many applications such as gas-fired multitube stills for heating petroleum and in the boilers of steam plants. The motivation for the work reported here arose from the need to estimate temperatures in spent nuclear fuel assemblies. These fuel assemblies are constructed either of a square array of fuel rods on a square pitch or of a hexagonal array of rods on an equilateral triangular pitch. After withdrawal from a nuclear reactor, the rods continue to generate fission product decay heat which must be dissipated to prevent the assembly from reaching excessive temperatures. The greatest concern occurs when the assembly is handled in a stagnant gas atmosphere since heat transfer by gaseous conduction and convection is relatively poor. Under such conditions, radiation is often the dominant mode of heat transfer, and an estimate of the temperatures can be obtained from an analysis of the radiative heat transfer.

Only a few analyses have appeared in the literature for radiative heat transport in rod clusters, and most of these were made using specific arrays of small size. Therefore, they are not adequate for treating larger arrays in a general manner. The work reported here was undertaken in order to treat the problem of radiative heat transfer in parallel rod arrays in a more definite manner and, in particular, to study two geometries of special interest in the nuclear industry. The following results are presented:

1. The view factors for radiative heat transfer between infinitely long parallel cylinders in both triangular pitch and square pitch arrays are derived. Tabulated results cover the range of spacings of most importance in applications such as heat exchangers and nuclear fuel rod assemblies.
2. The problems under consideration are treated using the theory of radiant exchange among diffuse-gray surfaces. The results are presented in terms of dimensionless variables so they will be in a form as general and useful as possible.
3. An algorithm is developed for solving the problem of radiant heat exchange within hexagonal arrays of cylinders on an equilateral triangular pitch -- a complex geometry of particular interest in the nuclear industry. The algorithm is capable of handling an array of any size. Computer programs are presented for both the steady-state and unsteady-state solutions.
4. A calculational scheme is evolved for treating radiative heat transfer in square arrays of cylinders on a square pitch for an array of any size. Again, computer solutions for both steady-state and transient cases are given.
5. A comparison is made of theoretically predicted and experimentally measured temperature distributions as a test of the theoretical model.

CHAPTER 2

THEORY OF RADIATION EXCHANGE AMONG DIFFUSE-GRAY SURFACES

The radiant heat exchange within an enclosure composed of diffusely emitting and diffusely reflecting gray surfaces may be determined by standard calculational methods. Possible formulations include the net radiation method, Hottel's method, and Gebhart's method. These different approaches are, however, based on an identical set of basic assumptions and yield identical numerical results. Convenience of application to a particular problem is the determinant of choice of approach. One of the goals of this study was to determine the calculational methods best suited to the classes of problems covered by this report.

I. BASIC ASSUMPTIONS AND DEFINITIONS

Five basic postulates underlie the standard calculational methods (30, 31). First, each of the surfaces considered is isothermal. This does not mean that all the surfaces are necessarily at the same temperature, but only that each one has a uniform temperature over its area. In practice, this condition may be approached by subdividing any nonisothermal surface into smaller sections, each of which is approximately isothermal.

Second, the surfaces are gray; that is, the emissivity ϵ and absorptivity α of each of the surfaces are independent of wavelength. Thus, the surfaces have no special preference with regard to their abilities to absorb or emit energy at a particular wavelength. No real materials are gray over the entire range of wavelengths. However, for practical

calculations, many materials can be considered gray because the energy that is being exchanged is concentrated in a wavelength band for which the emissivity and absorptivity are nearly independent of wavelength.

The third postulate is that radiation reflected from any surface is diffusely distributed in accordance with Lambert's cosine law (28, p. 17). No matter from what direction an incident ray strikes the surface, the reflected energy in any direction per unit of projected area normal to that direction, and per unit time and solid angle, is uniform for all angular directions. Thus, there is no need to keep account of specific rays as they interreflect between surfaces since the previous history of the radiation is completely obliterated when it strikes and is reflected. This is in contrast to specular reflection where the angle of reflection equals the angle of incidence.

Fourth, it is assumed that the energy emitted by any surface is diffusely distributed. Together, this postulate and postulate two define a diffuse-gray surface, a surface for which emissivity is independent of both wavelength and direction of emitted radiation. Application of Kirchoff's law (28) then gives

$$\epsilon = \alpha = 1 - \gamma$$

where ϵ , α , and γ (γ = reflectivity) are functions only of the temperature of the surface.

As both the emitted and reflected radiation are diffusely distributed, there is no need to make a distinction between these energy fluxes as they leave a surface. Instead, it is convenient to deal with their sum, which represents the total radiant flux leaving a surface. This sum is called

the radiosity and will be denoted by the symbol B with units of energy per unit time per unit of surface area.

The fifth assumption is that of uniform radiosity over each individual area. This requirement permits the use of view factors in the calculational methods. In the derivation of view factors between finite surfaces, the assumption is made that the energy leaving a surface — the radiosity — is constant over the surface. It will be shown later that this assumption is equivalent to assuming that the reflected energy flux is the same at every point on the surface.

A concept necessary in the following derivations is that of the view factor (alternatively designated the configuration factor, angle factor, shape factor, or geometrical factor). The view factor F_{ij} is defined as the fraction of the radiation leaving a surface i that is intercepted by surface j . The characteristics of view factors and their evaluation will be treated more comprehensively in Chapter 4. At this point, it is sufficient to state certain fundamental properties that are needed in subsequent derivations. The first property is the reciprocity rule, which relates the configuration factor for radiant energy traveling from surface i to surface j to the configuration factor for radiant energy traveling from surface j to surface i . The mathematical statement of the reciprocity rule is

$$A_i F_{ij} = A_j F_{ji} \quad (1)$$

where A_i and A_j denote the areas of surfaces i and j , respectively.

Another useful property of view factors follows from the conservation of energy. Any surface can be considered to be completely surrounded by

an envelope of other solid surfaces or open areas. This envelope, termed an enclosure, accounts for all directions surrounding the surface. The radiant energy leaving any surface, i , in an enclosure must impinge on the various surfaces making up the enclosure. It follows that

$$\sum_{j=1}^n F_{ij} = 1$$

where n is the number of surfaces in the enclosure. Note that the summation includes the term F_{ii} , which represents the fraction of the radiation leaving surface i that is intercepted by surface i itself. This term is not zero when surface i is concave.

II. NET RADIATION METHOD

The net radiation or radiosity method first devised by Poljak will now be presented (28, 3, 17). Equations will be developed for both the steady-state and unsteady-state cases.

The outgoing energy flux B_i from surface i is composed of directly emitted energy plus the reflected portion of the incident energy flux H_i . Thus

$$B_i = \epsilon_i \sigma T_i^4 + \gamma_i H_i = \epsilon_i \sigma T_i^4 + (1 - \epsilon_i) H_i \quad (2)$$

where T_i is the absolute temperature of the surface and σ is the Stefan-Boltzmann constant, 0.1712×10^{-8} Btu/(hr-ft²-°R⁴) or 5.669×10^{-12} watt/(cm²-°K⁴). The flux incident upon surface i is made up of contributions from all the surfaces within the enclosure that can see i , including surface i itself if it is concave. The energy incident on surface i for an enclosure containing n surfaces is then

$$A_i H_i = \sum_{j=1}^n A_j F_{ji} B_j = \sum_{j=1}^n A_i F_{ij} B_j = A_i \sum_{j=1}^n F_{ij} B_j, \quad (3)$$

$$H_i = \sum_{j=1}^n F_{ij} B_j, \quad (4)$$

where the reciprocity relation, Equation (1), has been employed in the simplification of Equation (3). Use of Equation (4) eliminates the term H_i in Equation (2) to yield

$$B_i = \epsilon_i \sigma T_i^4 + (1 - \epsilon_i) \sum_{j=1}^n F_{ij} B_j. \quad (5)$$

The net heat Q_i transferred per unit time from a surface is the difference between the emitted radiation and the absorbed portion of the incident radiation:

$$Q_i = A_i \epsilon_i \sigma T_i^4 - A_i \alpha_i H_i = (\epsilon_i \sigma T_i^4 - \epsilon_i H_i) A_i. \quad (6)$$

Solving for H_i gives

$$H_i = \sigma T_i^4 - \frac{Q_i/A_i}{\epsilon_i}$$

and substitution of this result into Equation (2) yields

$$B_i = \sigma T_i^4 - \left(\frac{1 - \epsilon_i}{\epsilon_i} \right) \frac{Q_i}{A_i}. \quad (7)$$

Elimination of B_i from Equation (5) by using Equation (7) gives

$$\sigma T_i^4 - \frac{Q_i/A_i}{\epsilon_i} = \sum_{j=1}^n F_{ij} \sigma T_j^4 - \sum_{j=1}^n F_{ij} \left(\frac{1 - \epsilon_j}{\epsilon_j} \right) \frac{Q_j}{A_j}. \quad (8)$$

After combining terms and allowing the index i to take on values from 1 to n , the following set of equations is obtained:

$$\sum_{j=1}^n (F_{ij} - \delta_{ij}) \sigma T_j^4 = \sum_{j=1}^n \left(F_{ij} \frac{1 - \epsilon_j}{\epsilon_j} - \frac{\delta_{ij}}{\epsilon_j} \right) \frac{Q_j}{A_j}, \quad i = 1, \dots, n \quad (9)$$

where δ_{ij} is the Kronecker delta function defined as

$$\delta_{ij} = \begin{cases} 1 & \text{if } i = j \\ 0 & \text{if } i \neq j \end{cases}.$$

Equations (9) are the general steady-state equations for determining radiation exchange in a gray, diffuse enclosure of n surfaces by the net radiation method. The only assumptions are the five postulates stated previously. Equations (9) are a set of n linear (linear in T^4) algebraic equations containing n surface temperatures and n heat fluxes. Once any combination of n temperatures and fluxes has been specified, the remaining n unknown quantities may be obtained by simultaneous solution of the resulting equations.

For transient problems, the steady-state energy balance (Equation (6)) must be replaced by the unsteady-state energy balance:

$$\text{Rate of energy accumulation} = \text{Rate of heat generation} + \text{Rate of absorption of incident energy} - \text{Rate of energy emission.}$$

If the thermal conductivity of the material is great enough that the volume-averaged temperature and the surface temperature do not differ significantly, the energy balance for body i can be written:

$$\rho_i V_i c_i \frac{d T_i}{dt} = Q_i + \alpha_i H_i A_i - \epsilon_i \sigma T_i^4 A_i \quad (10)$$

where ρ = density,

V = volume,

c = specific heat capacity,

t = time,

and Q can be interpreted as the rate of heat generation or the rate at which energy is supplied to the body by other means. Rearranging Equation (10) to the form of Equation (6), one obtains

$$Q_i - \rho_i V_i c_i \frac{d T_i}{dt} = (\epsilon_i \sigma T_i^4 - \epsilon_i H_i) A_i. \quad (11)$$

The remainder of the development is analogous to that for the steady-state case. The resulting set of equations for the unsteady-state problem, using the net radiation method, is

$$\sum_{j=1}^n (F_{ij} - \delta_{ij}) \sigma T_j^4 = \sum_{j=1}^n \left(F_{ij} \cdot \frac{1 - \epsilon_j}{\epsilon_j} - \frac{\delta_{ij}}{\epsilon_j} \right) \left(\frac{Q_j}{A_j} - \frac{\rho_j V_j c_j}{A_j} \frac{d T_j}{dt} \right),$$

$$i = 1, \dots, n. \quad (12)$$

To integrate these equations, n of the $3n$ variables $\frac{d T_i}{dt}$, T_i , and Q_i must be known for all time. An additional n variables must be known at time zero to fix the initial conditions.

III. GEBHART'S METHOD

A second method of analyzing radiative exchange within a diffuse-gray enclosure is that originated by Gebhart (7-10). Gebhart introduced the concept of the absorption factor G_{ij} which is the fraction of the emission from surface i that reaches surface j and is absorbed. This includes all the paths by which radiation may reach A_j after emission from A_i , that is, the direct path, paths by means of one reflection, and paths by multiple reflections. The absorption factor G_{ij} is similar to the view factor F_{ij} except that it represents the fraction of the energy absorbed by A_j from the emission of A_i , rather than the fraction of the energy incident on A_j from A_i . For all black surfaces, the two quantities are the same.

The steady-state energy balance for a typical surface is

$$Q_i = A_i \epsilon_i \sigma T_i^4 - \sum_{j=1}^n A_j \epsilon_j \sigma T_j^4 G_{ji} \quad (13)$$

where Q_i is the net energy loss from surface i . The first term on the right-hand side of Equation (13) is the energy emitted by A_i , while the second term sums the energy absorbed by surface i from all sources.

There remains the problem of finding the absorption factors.

The total emitted energy from A_j is $A_j \epsilon_j \sigma T_j^4$. The portion absorbed as a consequence of direct radiation to A_i is $A_j \epsilon_j \sigma T_j^4 F_{ji} \alpha_i$ or $A_j \epsilon_j \sigma T_j^4 F_{ji} \epsilon_i$, since for gray surfaces $\epsilon_i = \alpha_i$. All other radiation from A_j absorbed by A_i will have first undergone at least one reflection. The emission from A_j that arrives at a typical surface A_k and is then reflected is $A_j \epsilon_j \sigma T_j^4 F_{jk} (1 - \epsilon_k)$, where the reflectivity γ_k has been

replaced by $(1-\epsilon_k)$. If the incident energy is uniformly distributed and diffusely reflected, the fraction of the radiation reflected from surface k that is absorbed at A_i is the same as the fraction of emitted energy from A_k that is absorbed at A_i . Of the energy originating by emission from A_j , the portion ultimately absorbed at A_i is

$$A_j \epsilon_j \sigma T_j^4 F_{ji} \epsilon_i + \sum_{k=1}^n A_j \epsilon_j \sigma T_j^4 F_{jk} (1-\epsilon_k) G_{ki}.$$

Dividing this energy by the emission from A_j yields the fraction:

$$G_{ji} = F_{ji} \epsilon_i + \sum_{k=1}^n F_{jk} (1-\epsilon_k) G_{ki}. \quad (14)$$

Upon rearranging the above equation and letting j take on all values from 1 to n , the following set of equations is obtained:

$$\sum_{k=1}^n \left[F_{jk} (1-\epsilon_k) - \delta_{jk} \right] G_{ki} = -F_{ji} \epsilon_i, \quad j = 1, \dots, n. \quad (15)$$

Simultaneous solution of Equations (15) for G_{ki} , $k = 1, \dots, n$, provides the values of the absorption factors required in Equation (13). Since surface i may be chosen as any one of the n surfaces of the enclosure, the set of n equations represented by Equations (15) must be solved successively for $i = 1, \dots, n$ to provide the required absorption factors. Thus, there are a total of n^2 values of G_{ij} , the same as the number of view factors F_{ij} .

If $Q_{i \rightarrow j}$ is defined as the rate at which energy is radiated from surface i to surface j ,

$$Q_{i \rightarrow j} = A_i \epsilon_i \sigma T_i^4 G_{ij}$$

and

$$Q_{j \rightarrow i} = A_j \epsilon_j \sigma T_j^4 G_{ji}.$$

Since there is no net heat transfer between i and j when $T_i = T_j$, it follows that $Q_{i \rightarrow j} = Q_{j \rightarrow i}$, which can only be satisfied if

$$A_i \epsilon_i G_{ij} = A_j \epsilon_j G_{ji}. \quad (16)$$

A second relationship among the G_{ij} is found by noting that all the energy emitted by surface i must ultimately be absorbed within the enclosure.

Thus

$$\sum_{j=1}^n G_{ij} = 1. \quad (17)$$

Substitution of the reciprocity relation, Equation (16), into the energy balance yields

$$Q_i = A_i \epsilon_i \sigma T_i^4 - \sum_{j=1}^n A_i \epsilon_i \sigma T_j^4 G_{ij}. \quad (18)$$

Equation (17) can be used to rewrite Equation (18) in a form which will be found useful later:

$$Q_i = \sum_{j=1}^n A_i \epsilon_i G_{ij} \sigma (T_i^4 - T_j^4). \quad (19)$$

Rearranging Equation (18) and allowing the index i to take on values from 1 to n yields the set of equations:

$$\sum_{j=1}^n (\epsilon_i G_{ij} - \delta_{ij} \epsilon_i) \sigma T_j^4 = -\frac{Q_i}{A_i}, \quad i = 1, \dots, n \quad (20)$$

for the steady-state problem.

The unsteady-state energy balance for body i is

$$\rho_i V_i c_i \frac{d T_i}{dt} = Q_i + \sum_{j=1}^n A_j \epsilon_j \sigma T_j^4 G_{ji} - A_i \epsilon_i \sigma T_i^4 \quad (21)$$

if it is assumed that the surface temperature does not differ materially from the average temperature of the body. Rearranging Equation (21) with the aid of Equation (16) and letting the value of i range from 1 to n gives

$$\frac{d T_i}{dt} = \frac{A_i}{\rho_i V_i c_i} \left[\frac{Q_i}{A_i} + \sum_{j=1}^n (\epsilon_i G_{ij} - \delta_{ij} \epsilon_i) \sigma T_j^4 \right], \quad i = 1, \dots, n. \quad (22)$$

IV. HOTTEL'S METHOD

The analysis of radiative exchange within a diffuse-gray enclosure may also be carried out using a method developed by Hottel (14, 15). The net rate of energy outflow from surface i to surface j , Q_{ij} , is defined in terms of an exchange quantity \mathfrak{F}_{ij} as

$$Q_{ij} = A_i \mathfrak{F}_{ij} \sigma (T_i^4 - T_j^4). \quad (23)$$

The quantity \mathfrak{F}_{ij} may be regarded as a composite view factor which includes the effects of multiple reflections. The net loss Q_i from surface i may be found by summing Q_{ij} over the surfaces of the enclosure. Thus

$$Q_i = \sum_{j=1}^n Q_{ij} = \sum_{j=1}^n A_i \mathfrak{F}_{ij} \sigma(T_i^4 - T_j^4). \quad (24)$$

Obviously, the values of the gray-body view factors \mathfrak{F}_{ij} must be known in order for Equation (24) to have utility.

It is simplest to determine the \mathfrak{F}_{ij} by relating them to the absorption factors already presented in Gebhart's method. Comparison of Equation (24) and Equation (19) indicates that

$$\varepsilon_i G_{ij} = \mathfrak{F}_{ij}. \quad (25)$$

Furthermore, from Equation (16) it is clear that the reciprocity relation for \mathfrak{F}_{ij} becomes

$$A_i \mathfrak{F}_{ij} = A_j \mathfrak{F}_{ji} \quad (26)$$

and from Equation (17) that

$$\sum_{j=1}^n \mathfrak{F}_{ij} = \varepsilon_i. \quad (27)$$

The matrix of \mathfrak{F}_{ij} values may now be computed by substituting the relation $G_{ki} = \mathfrak{F}_{ki}/\varepsilon_k$ into Equation (15) to yield the result:

$$\sum_{k=1}^n \left[F_{jk} \left(\frac{1-\varepsilon_k}{\varepsilon_k} \right) - \frac{\delta_{jk}}{\varepsilon_k} \right] \mathfrak{F}_{ki} = -F_{ji} \varepsilon_i, \quad j = 1, \dots, n; \quad i = 1, \dots, n. \quad (28)$$

Combining of Equation (27) and Equation (24) and letting i range from 1 to n yields the following set of steady-state equations:

$$\sum_{j=1}^n (\mathfrak{F}_{ij} - \delta_{ij} \epsilon_i) \sigma T_j^4 = -\frac{Q_i}{A_i}, \quad i = 1, \dots, n. \quad (29)$$

Equations (29) could also have been derived by direct substitution of Equation (25) into Equations (20). Following this procedure for the transient problem by inserting Equation (25) into Equations (22) gives

$$\frac{dT_i}{dt} = \frac{A_i}{\rho_i V_i c_i} \left[\frac{Q_i}{A_i} + \sum_{j=1}^n (\mathfrak{F}_{ij} - \delta_{ij} \epsilon_i) \sigma T_j^4 \right], \quad i = 1, \dots, n. \quad (30)$$

V. COMPARISON OF THE METHODS

As noted previously, the net radiation approach, Gebhart's method, and Hottel's formulation yield identical numerical results since they are based on identical assumptions. However, the differences in computational detail may cause one of these to have greater application to a particular problem. Frequently, steady-state problems are most conveniently analyzed using the net radiation method because it does not require calculation of the G or \mathfrak{F} matrix. On the other hand, either Gebhart's or Hottel's method is generally more useful for unsteady-state problems because the derivatives appear explicitly. Once the G_{ij} or \mathfrak{F}_{ij} matrix has been determined, Equations (22) or Equations (30) may be numerically integrated simply by stepping in time. On the other hand, integration of Equations (12) requires simultaneous solution for the derivatives at each time step because of the implicit occurrence of the derivatives.

CHAPTER 3

APPLICATION OF THEORY

In this chapter the general equations that were developed for radiation exchange within a diffuse-gray enclosure (see Chapter 2) will be specialized to the class of radiation problems of interest in which a surface n of known temperature surrounds $m = n - 1$ surfaces of known heat loss. Formulations will be developed in terms of dimensionless variables which will reduce the number of independent variables considered.

I. STEADY STATE

Temperature levels in a fuel rod array after withdrawal from a nuclear reactor core are often controlled by radiative heat transfer between rods. At steady state the net heat loss from each of the rods must equal the heat generated within the rod by radioactive decay of fission products. The temperature of the shroud T_n can be found by an energy balance equating the total heat generated within the array of fuel rods to that dissipated by the shroud to the surroundings.

Net Radiation Method

The quantity

$$\sum_{j=1}^n (F_{ij} - \delta_{ij}) \sigma T_n^4 = \sigma T_n^4 \left(\sum_{j=1}^n F_{ij} - \sum_{j=1}^n \delta_{ij} \right) = \sigma T_n^4 (1 - 1) = 0$$

may be subtracted from the left-hand sides of Equations (9) to give

$$\sum_{j=1}^n (F_{ij} - \delta_{ij}) \sigma (T_j^4 - T_n^4) = \sum_{j=1}^n \left(F_{ij} \frac{1 - \epsilon_j}{\epsilon_j} - \frac{\delta_{ij}}{\epsilon_j} \right) \frac{Q_j}{A_j}, \quad i = 1, \dots, n. \quad (31)$$

Equations (31) are made dimensionless by dividing through by the heat flux of one of the surfaces. Choosing the surface designated k ($Q_k \neq 0$) as the reference,

$$\sum_{j=1}^n (F_{ij} - \delta_{ij}) Y_j = \sum_{j=1}^n \left(F_{ij} \frac{1 - \epsilon_j}{\epsilon_j} - \frac{\delta_{ij}}{\epsilon_j} \right) X_j, \quad i = 1, \dots, n. \quad (32)$$

The dimensionless variables X_j and Y_j are defined as

$$X_j = \frac{Q_j/A_j}{Q_k/A_k}$$

and

$$Y_j = \frac{\sigma (T_j^4 - T_n^4)}{Q_k/A_k}.$$

Obviously, $Y_n = 0$ so the summation on the left-hand sides of Equations (32) may be reduced to $j = 1$ to m , where $m = n - 1$. From the conservation of energy,

$$\sum_{i=1}^n Q_i = 0;$$

hence,

$$Q_n = - \sum_{i=1}^m Q_i.$$

For a nuclear fuel assembly, this equation is a statement that the energy absorbed by the shroud from the rods within the array is equal to the sum

of the heat losses from these rods. A relation for X_n in terms of X_j , $j = 1, \dots, m$, can now be developed as follows:

$$X_n = \frac{Q_n/A_n}{Q_k/A_k} = \frac{\left(-\sum_{j=1}^m Q_j\right)/A_n}{Q_k/A_k} = -\sum_{j=1}^m \frac{A_j}{A_n} \frac{Q_j/A_j}{Q_k/A_k} = -\sum_{j=1}^m \frac{A_j}{A_n} \cdot X_j. \quad (33)$$

With X_n given by Equation (33), the number of unknowns in Equations (32) is reduced by one. The final set of equations (also reduced by one) is

$$\sum_{j=1}^m (F_{ij} - \delta_{ij}) Y_j = \sum_{j=1}^n \left(F_{ij} \cdot \frac{1 - \epsilon_j}{\epsilon_j} - \frac{\delta_{ij}}{\epsilon_j} \right) X_j, \quad i = 1, \dots, m. \quad (34)$$

The unknowns are m values of Y_j , that is, m values of temperature.

Gebhart's Method

In this case, the quantity

$$\sum_{j=1}^n (\epsilon_i G_{ij} - \delta_{ij} \epsilon_i) \sigma T_n^4 = \epsilon_i \sigma T_n^4 \left(\sum_{j=1}^n G_{ij} - \sum_{j=1}^n \delta_{ij} \right) = 0$$

is subtracted from the left-hand sides of Equations (20) and both sides are divided by Q_k/A_k . The resulting equations in terms of dimensionless variables are

$$\sum_{j=1}^m (\epsilon_i G_{ij} - \delta_{ij} \epsilon_i) Y_j = -X_i, \quad i = 1, \dots, m. \quad (35)$$

The value of X_n is determined independently from Equation (33).

Hottel's Method

In a similar manner the subtraction of $\sum_{j=1}^n (\epsilon_i G_{ij} - \delta_{ij} \epsilon_i) \sigma T_n^4$ from the left-hand sides of Equations (29) and formulation in terms of dimensionless

variables gives

$$\sum_{j=1}^m (\mathfrak{F}_{ij} - \delta_{ij} \epsilon_i) Y_j = -X_i, \quad i = 1, \dots, m. \quad (36)$$

Discussion

Clearly, of the sets of equations for the calculation of the Y_j , Equations (34) are most easily solved since they obviate the need for prior calculation of either the G_{ij} or \mathfrak{F}_{ij} matrix. This is a significant savings in computational effort since it avoids solving the n sets of n equations (a total of n^2 equations) represented by Equations (15) or (28).

The Y_j can be seen to be functions of the geometry, the emissivities of the surfaces, and the dimensionless heat fluxes. Note that, even if the value of the reference heat flux Q_k/A_k is changed, the X_i will remain the same if all the heat losses are changed proportionally. For example, in a nuclear fuel assembly the heat generation rates of each of the rods are essentially equal so that $X_i = 1$, $i = 1, \dots, k, \dots, m$, and $X_n = -m\bar{A}_1/A_n$, independent of the magnitude of the heat generation rates. Once the equations are solved for the Y_j , the value of any surface temperature T_j may be found for any values of the shroud temperature and heat generation rate without resolving the equations. This is in contrast to the solution of the dimensional equations (Equations (9), (20), or (29)) for the T_j . A new solution would be required for any change in T_n or in the Q_i .

Reformulation of the Net Radiation Method

It will now be shown that the net radiation equations can be reformulated to remove the dependence of the dependent variables upon the emissivities of the surfaces. Equations (32) can be rearranged to the form:

$$\sum_{j=1}^n (F_{ij} - \delta_{ij}) \left[Y_j - \left(\frac{1 - \epsilon_j}{\epsilon_j} \right) X_j \right] = - \sum_{j=1}^n \delta_{ij} X_j = -X_i, \quad i = 1, \dots, n.$$

The quantity $\left(\frac{1 - \epsilon_n}{\epsilon_n} \right) X_n \sum_{j=1}^n (F_{ij} - \delta_{ij}) = 0$ can be added to the left-hand side of this equation without affecting the equality:

$$\sum_{j=1}^n (F_{ij} - \delta_{ij}) \left[Y_j - \left(\frac{1 - \epsilon_j}{\epsilon_j} \right) X_j + \left(\frac{1 - \epsilon_n}{\epsilon_n} \right) X_n \right] = -X_i, \quad i = 1, \dots, n.$$

The summation can be reduced to $j = 1$ to m since the term in brackets is zero for $j = n$. Further, X_n can be eliminated as an unknown by Equation (33), thus reducing the number of unknowns and the number of independent equations from n to m . The final set of equations is

$$\sum_{j=1}^m (F_{ij} - \delta_{ij}) Z_j = -X_i, \quad i = 1, \dots, m \quad (37)$$

where

$$Z_j = Y_j - \left(\frac{1 - \epsilon_j}{\epsilon_j} \right) X_j - \left(\frac{1 - \epsilon_n}{\epsilon_n} \right) \sum_{p=1}^m \frac{A_p}{A_n} \cdot X_p. \quad (37a)$$

Because the coefficients of the Z_j on the left-hand sides of Equations (37) are functions only of geometry (since the F_{ij} are functions only of geometry) and the right-hand sides are functions only of the surface heat fluxes, the values of the Z_j determined by solution of Equations (37) are independent of the emissivities of the various surfaces. For a fixed

geometry and a fixed set of dimensionless heat fluxes, Equations (37) need be solved only once for the Z_j . The actual temperature values for a particular combination of surface emissivities are found from Equation (37a), which introduces the emissivity dependence. This is in contrast to the formulation represented by Equations (34), which must be resolved each time the emissivities are altered.

There is no apparent way to restate either Gebhart's or Hottel's equations in terms of the variables Z_j . Thus, the merits of the net radiation method for solving the class of steady-state problems under discussion are even greater than previously shown.

II. UNSTEADY STATE

Only Gebhart's and Hottel's methods will be employed in the analysis of the transient problem. The temperature-time derivatives appear implicitly in the net radiation method, which makes it unwieldy for transient problems. The analysis will be limited to the case in which a shroud (body n) of known constant temperature surrounds $m = n - 1$ bodies of known heat generation or heat input by external means.

In general, it is unlikely that practical problems involving the unsteady-state heating of a nuclear fuel assembly would meet the condition of a constant shroud temperature. Instead, the shroud temperature probably also would be varying with time. In such cases, the following analysis in terms of dimensionless variables strictly would not be applicable. A rigorous solution would require the integration of Equations (22) or (30), with the changing temperature of the shroud being taken into account. Because of the diversity of possible boundary conditions for the energy

exchange between shroud and environment, it is not possible to frame the equations in a general manner; each problem must be solved separately. However, even for some of these problems, estimated results obtained with a constant shroud temperature can be useful. Furthermore, since results for a constant shroud temperature can be couched in terms of dimensionless variables with a consequent decrease in the number of variables, the estimates can be presented as a small number of dimensionless plots rather than requiring solution of a new set of differential equations for each problem.

If T_n is at a known fixed temperature, there remain m unknown temperatures which vary with time, and Equations (30) reduce to the set:

$$\frac{\rho_i V_i c_i}{A_i} \frac{d T_i^4}{dt} = 4(T_i^4)^{3/4} \left[\frac{Q_i}{A_i} + \sum_{j=1}^n (\mathfrak{F}_{ij} - \delta_{ij} \epsilon_i) \sigma T_j^4 \right], \quad i = 1, \dots, m$$

where $\frac{d T_i}{dt}$ has been replaced by $\frac{1}{4 T_i^3} \frac{d T_i^4}{dt}$. The above equations may also be written as

$$\frac{\rho_i V_i c_i}{A_i} \frac{d(T_i^4 - T_n^4)}{dt} = 4 \left[(T_i^4 - T_n^4) + T_n^4 \right]^{3/4} \left[\frac{Q_i}{A_i} + \sum_{j=1}^n (\mathfrak{F}_{ij} - \delta_{ij} \epsilon_i) \sigma (T_j^4 - T_n^4) \right]$$

for $i = 1, \dots, m$ since

$$\sum_{j=1}^n (\mathfrak{F}_{ij} - \delta_{ij} \epsilon_i) \sigma T_n^4 = \sigma T_n^4 \left(\sum_{j=1}^n \mathfrak{F}_{ij} - \epsilon_i \sum_{j=1}^n \delta_{ij} \right) = \sigma T_n^4 (\epsilon_i - \epsilon_i) = 0.$$

After successive division by the reference heat flux Q_k/A_k and by the quantity $\left(\frac{Q_k/A_k}{\sigma}\right)^{3/4}$, one obtains the dimensionless equations ($i = 1, \dots, m$):

$$\frac{d \left[\frac{\sigma(T_i^4 - T_n^4)}{Q_k/A_k} \right]}{d \left[\frac{t\sigma A_i}{\rho_i V_i c_i} \left(\frac{Q_k/A_k}{\sigma} \right)^{3/4} \right]} = 4 \left[\frac{\sigma(T_i^4 - T_n^4)}{Q_k/A_k} + \frac{\sigma T_n^4}{Q_k/A_k} \right]^{3/4}.$$

$$\left[\frac{Q_i/A_i}{Q_k/A_k} + \sum_{j=1}^m (\mathfrak{F}_{ij} - \delta_{ij} \epsilon_i) \frac{\sigma(T_j^4 - T_n^4)}{Q_k/A_k} \right].$$

Finally, if $\frac{\rho_i V_i c_i}{A_i}$ is constant for $i = 1$ to m , these equations become

$$\frac{d Y_i}{d\theta} = 4(Y_i + W)^{3/4} \left[X_i + \sum_{j=1}^m (\mathfrak{F}_{ij} - \delta_{ij} \epsilon_i) Y_j \right], \quad i = 1, \dots, m \quad (38)$$

with initial conditions:

$$Y_{i0} = \frac{\sigma(T_{i0}^4 - T_n^4)}{Q_k/A_k}, \quad i = 1, \dots, m \text{ at } \theta = 0.$$

The variables X_i and Y_i are defined as for the steady-state problem,

while

$$\theta = \frac{t\sigma A_i}{\rho_i V_i c_i} \left(\frac{Q_k/A_k}{\sigma} \right)^{3/4}$$

and

$$W = \frac{\sigma T_n^4}{Q_k/A_k} .$$

The required initial conditions are given by specification of T_i , $i = 1, \dots, n$ at time zero. Equations (38) are a set of first-order differential equations which can be integrated numerically to yield the Y_i as functions of θ and, thereby, the temperatures T_i as functions of time. In contrast to the steady-state problem, the Y_i values for the transient case are functions of T_n through the parameter W . Thus, both time and shroud temperature are introduced as additional variables for the transient problem. The effect of this increase in dimensionality is to greatly multiply the number of dimensionless plots required to display the variables. Consequently, the results for the transient case cannot be presented in as compact a manner as can results for the steady-state case.

CHAPTER 4

VIEW FACTORS

The analysis of radiant interchange among diffusely emitting and diffusely reflecting surfaces requires a knowledge of the view factors between the various surfaces. In this chapter the basic defining equations for view factors will be presented. A shorthand method will then be developed for treating surfaces that are greatly elongated in one dimension. Using this technique, the view factors between infinitely long parallel cylinders in arrays will be derived for cylinders on square and equilateral triangular pitches.

I. DEFINING EQUATIONS

The development of the basic defining equations for view factors presented in this section is based on information given in references (28), (31), and (32). Consider an elemental surface area dA as shown in Figure 1. Direction is measured by the angles θ and ϕ , where the angle θ is measured from the normal to dA . The intensity i of radiation leaving a surface in the direction (θ, ϕ) is defined as the radiant energy leaving the surface per unit time per unit elemental projected surface area normal to the (θ, ϕ) direction per unit elemental solid angle centered around the direction (θ, ϕ) . The radiosity B is the radiant energy leaving a surface per unit time per unit surface area. Note that intensity is defined on the basis of projected area, while radiosity is based on actual surface area. The relation between projected area A_p and surface area A is

ORNL DWG 75-8461

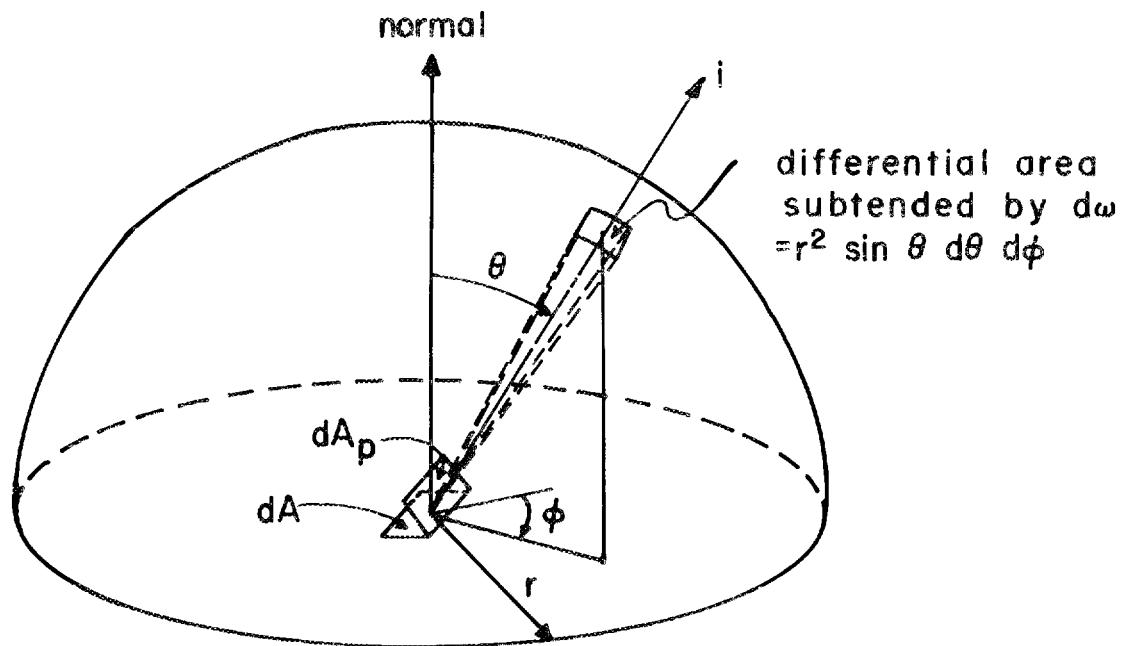


Figure 1. Integration of Intensity Over Solid Angle.

$$dA_p = \cos \theta dA.$$

The rate at which energy leaves the differential area dA in all directions is

$$B dA = \int i dA_p d\omega = \int i \cos \theta dA d\omega$$

or

$$B = \int i \cos \theta d\omega$$

where the integration with respect to the solid angle ω is over the entire hemisphere. As illustrated in Figure 1, the differential solid angle $d\omega$ may be expressed in terms of the angles θ and ϕ of a spherical coordinate system centered on dA . Since, by definition, a solid angle anywhere above dA is equal to the intercepted area on the hemisphere divided by the square of the hemisphere radius, it follows that $d\omega = \sin \theta d\theta d\phi$. Consequently, integration over the entire hemisphere yields

$$B = \int_0^{2\pi} \int_0^{\pi/2} i \cos \theta \sin \theta d\theta d\phi. \quad (39)$$

If the intensity is independent of direction as it is when a surface emits and reflects diffusely, i may be moved outside the integral signs and Equation (39), upon integration, reduces to

$$B = \pi i. \quad (40)$$

Attention is now directed toward the radiant interchange between a pair of infinitesimal surfaces, dA_i and dA_j , illustrated in Figure 2. The angles β_i and β_j are formed by the respective normals and the connecting

ORNL DWG 75-8462

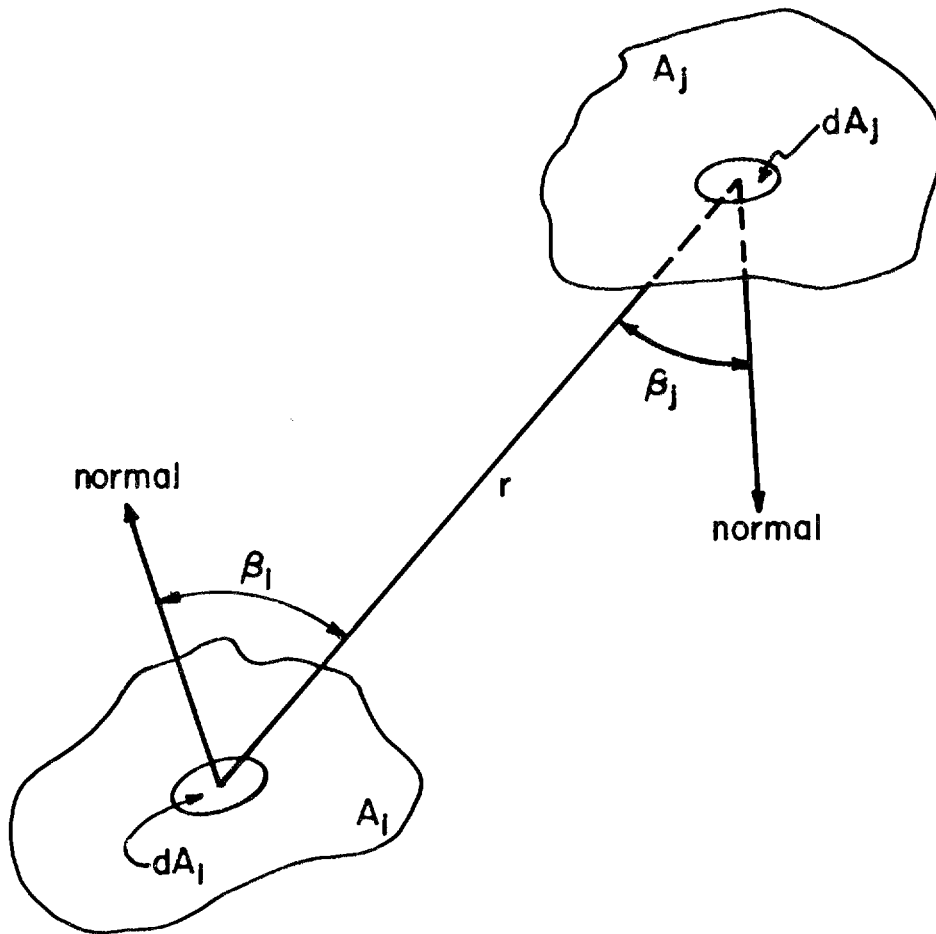


Figure 2. Geometry for Radiant Interchange Between Two Surfaces.

line of length r between the elements. The radiant energy which leaves dA_i and is intercepted by dA_j is

$$i_i (\cos \beta_i dA_i) d\omega, \quad (41)$$

in which $d\omega$ is the solid angle subtended by dA_j when viewed from dA_i . From the geometry, $d\omega = \cos \beta_j dA_j / r^2$. Introducing this result into expression (41) and eliminating i_i using Equation (40), one obtains

$$\frac{B_i \cos \beta_i \cos \beta_j dA_i dA_j}{\pi r^2} \quad (42)$$

as the energy incident on dA_j from dA_i .

The energy incident on the finite area A_j from dA_i may be found by integrating the foregoing expression over all the differential surface elements comprising A_j to give

$$\int_{A_j} \frac{B_i \cos \beta_i \cos \beta_j dA_i dA_j}{\pi r^2}. \quad (43)$$

The radiant energy intercepted by A_j from A_i is determined by integrating expression (43) over the area A_i to yield

$$\int_{A_i} \int_{A_j} \frac{B_i \cos \beta_i \cos \beta_j dA_i dA_j}{\pi r^2}. \quad (44)$$

The energy leaving dA_i in all directions is $B_i dA_i$, so that the energy leaving A_i in all directions is the integral:

$$\int_{A_i} B_i dA_i . \quad (45)$$

The ratio of expression (44) to expression (45) represents the fraction of the radiation outgoing from A_i that is incident on A_j . Since this is precisely the definition of the view factor F_{ij} , it follows that

$$F_{ij} = \frac{\int_{A_i} \int_{A_j} B_i \cos \beta_i \cos \beta_j dA_i dA_j / \pi r^2}{\int_{A_i} B_i dA_i} . \quad (46)$$

As it stands, the foregoing angle factor depends on the magnitude and the surface distribution of the radiosity B_i .

It is customary in the definition of the view factor to assume that the radiosity is constant over each surface. As shown in Equation (2), the radiosity consists of both emitted and reflected radiation. For an isothermal surface of constant emissivity (and hence uniform emission), the assumption of uniform radiosity over the surface is equivalent to the assumption that the reflected radiation is the same at each point on the surface. In turn, for the reflected radiation to be uniform over the surface, it is necessary that the incident radiation be constant along the surface. It is unlikely that this condition will be completely realized for finite surfaces for any but the simplest geometries, such as radiation exchange between infinitely large parallel plates.

With the assumption that B_i is constant, Equation (46) reduces to the standard form for diffuse interchange between two finite surfaces:

$$F_{ij} = \frac{1}{A_i} \int_{A_i} \int_{A_j} \frac{\cos \beta_i \cos \beta_j dA_i dA_j}{\pi r^2}. \quad (47)$$

The view factor as defined by Equation (47) depends only on geometrical parameters. A corresponding derivation for the fraction of the radiant energy leaving surface j that is intercepted by A_i leads to an equation identical to Equation (47) except that the subscripts i and j are interchanged. The result is as follows:

$$F_{ji} = \frac{1}{A_j} \int_{A_i} \int_{A_j} \frac{\cos \beta_i \cos \beta_j dA_i dA_j}{\pi r^2}. \quad (48)$$

From a comparison of Equations (47) and (48), it can be seen that

$$A_i F_{ij} = A_j F_{ji}, \quad (49)$$

which is known as the reciprocity rule.

II. HOTTEL'S CROSSED-STRING METHOD

In certain cases, mathematical techniques exist for the determination of configuration factors which avoid the need to perform the double-area integration required in the direct evaluation of Equation (47). One such technique is Hottel's crossed-string method (14, 15, 38), which is applicable to the calculation of view factors between surfaces that may be assumed to extend infinitely far along one coordinate. Surfaces of

$$A_1 F_{12} = \frac{A_1 + A_2 - A_3}{2} \quad (51)$$

Now examine the configuration shown in cross section in Figure 4, where some blockage of the radiant transfer between A_1 and A_2 occurs because of the presence of the surfaces A_3 and A_4 . The dashed lines abcd, efgh, ae, and dh can be considered to represent the locations of strings stretched tightly between the outer edges of A_1 and A_2 . Line segments ab and cd are tangent to A_3 at points b and c, respectively, while movement from b to c is along the surface of A_3 . Similarly, ef and gh are tangent to A_4 at f and g, while the line segment fg is along the surface of A_4 . Together with A_1 and A_2 , the surfaces abcd and efgh form an enclosure. Then, since $F_{11} = 0$,

$$F_{1-abcd} + F_{12} + F_{1-efgh} = 1$$

which, after multiplying through by A_1 , may be written as

$$A_1 F_{1-abcd} + A_1 F_{12} + A_1 F_{1-efgh} = A_1. \quad (52)$$

Applying Equation (51) to the three-sided enclosures abcdh and aefgh, the values of $A_1 F_{1-abcd}$ and $A_1 F_{1-efgh}$ are

$$A_1 F_{1-abcd} = \frac{A_1 + A_{abcd} - A_{dh}}{2}$$

and

$$A_1 F_{1-efgh} = \frac{A_1 + A_{efgh} - A_{ae}}{2}.$$

ORNL DWG. 76-146

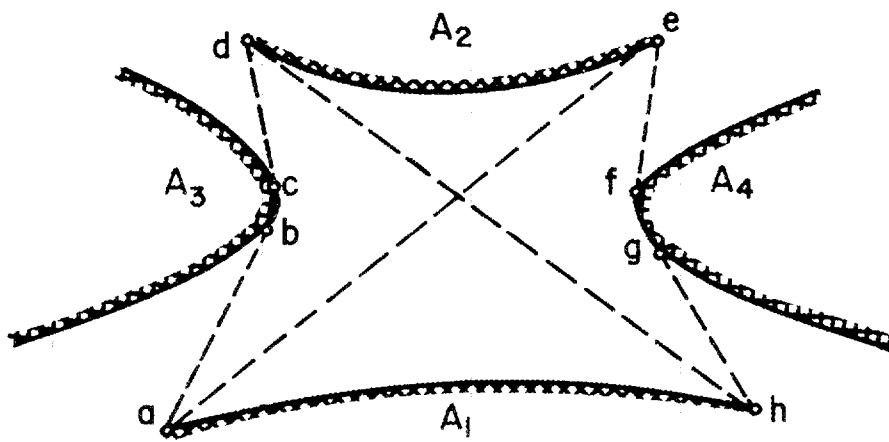


Figure 4. Hottel's Crossed-String Method.

Substituting these values into Equation (52) yields

$$F_{12} = \frac{(A_{ae} + A_{dh}) - (A_{abcd} + A_{efgh})}{2 A_1} . \quad (53)$$

Since Equation (53) is for infinitely long plane areas, the areas are proportional to the lengths shown in the two-dimensional representation, Figure 4. Exchanging areas for lengths in Equation (53) gives

$$F_{12} = \frac{(ae + dh) - (abcd + efgh)}{2 ah} . \quad (54)$$

Reverting to the interpretation of the dashed lines in Figure 4 as lengths of string stretched between the edges of A_1 and A_2 , Equation (54) may be expressed as follows:

$$F_{12} = \frac{(\text{sum of crossed strings}) - (\text{sum of uncrossed strings})}{2 \times \text{length of } A_1} . \quad (55)$$

III. VIEW FACTORS FOR CYLINDERS ON AN EQUILATERAL TRIANGULAR PITCH

Hottel's crossed-string method will be used to derive the view factors between infinitely long parallel cylinders in arrays on an equilateral triangular pitch. These configuration factors will subsequently be used in the calculation of radiant interchange between rods in hexagonal nuclear fuel rod assemblies.

The numbering system used in the following derivations is illustrated in Figure 5, which represents an array of cylinders on an equilateral triangular spacing. The notation F_{IJ} will be used to denote the view factor

ORNL DWG 69-12125 R1

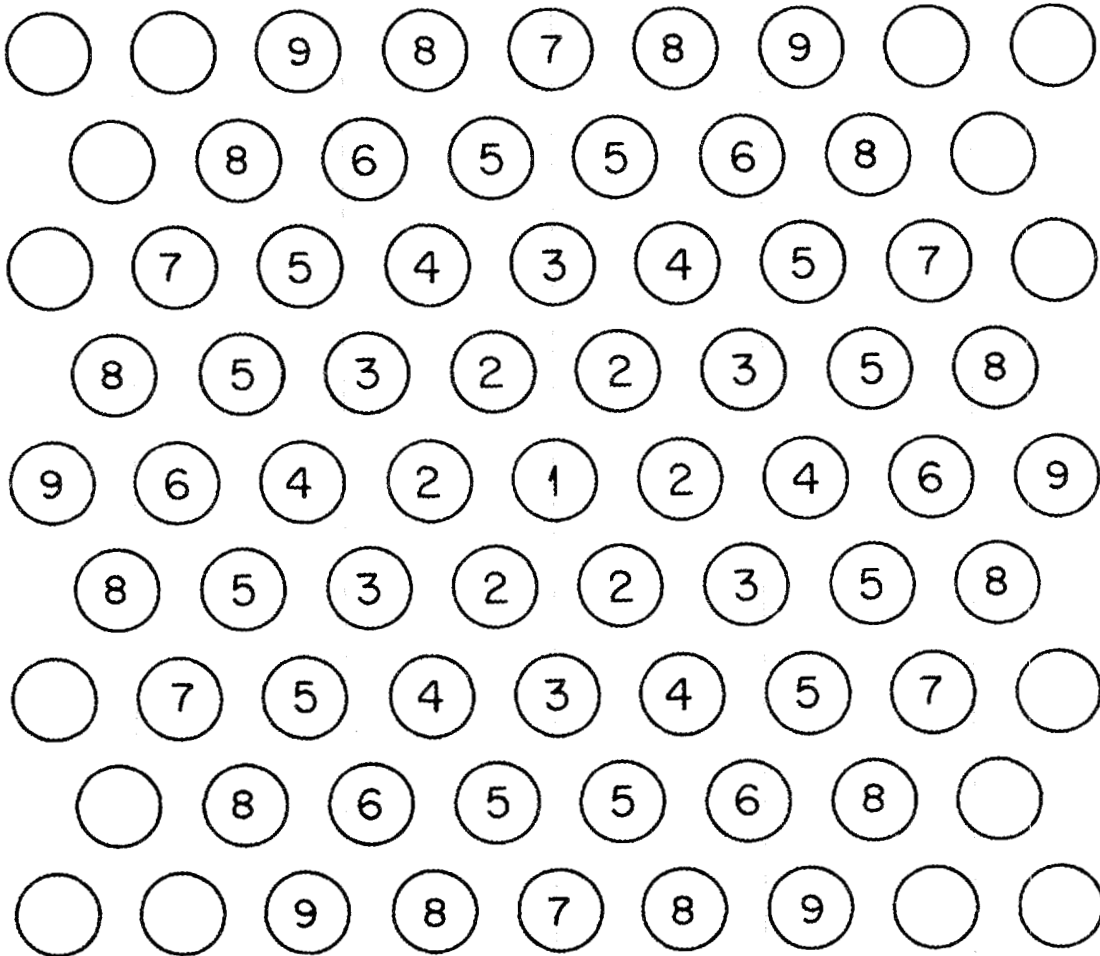


Figure 5. Parallel Cylinders on an Equilateral Triangular Pitch.

between a particular rod designated i and a particular rod designated j as opposed to the notation F_{ij} which denotes the view factor between the totality of the surfaces designated i and the totality of the surfaces designated j . For example, referring to Figure 5, F_{12} indicates the view factor between surface 1 and any one of the cylinders numbered 2, while F_{12} is the view factor between 1 and all six of the cylinders numbered 2. The relationship between F_{12} and F_{12} is obviously $F_{12} = 6 F_{12}$.

For the spacings (pitch-to-diameter ratios) that will be of interest here, view factor values are required for radiation exchange between rods up to four rows apart. This is equivalent to a knowledge of the view factors F_{12} , F_{13} , F_{15} , and F_{18} . The view factors F_{11} , F_{14} , F_{16} , F_{17} , and F_{19} are zero since surface 1 cannot see itself or any of the surfaces designated 4, 6, 7, and 9. The view factor relations that will be derived are strictly valid only for infinitely long cylinders. However, because of the large length-to-pitch ratios of rods in most nuclear fuel assemblies, these calculated view factors are very good approximations of the actual values.

Derivation of Equations for F_{12}

Partial shadowing. If the pitch-to-diameter ratio (PDR) is less than $2\sqrt{3}/3$, a portion of the radiation leaving cylinder 1 in the direction of cylinder 2 is blocked by other rods, as shown in Figure 6. The lengths of the various line segments in Figure 6 are

$$ad = ae = \text{PDR} \cdot R; \quad ac = rs = R$$

$$cd = es = (ad^2 - ac^2)^{1/2} = R(\text{PDR}^2 - 1)^{1/2}$$

$$\omega = \frac{\pi}{6} - \tan^{-1} \frac{cd}{ac} = \frac{\pi}{6} - \tan^{-1} (\text{PDR}^2 - 1)^{1/2}; \quad bc = R\omega$$

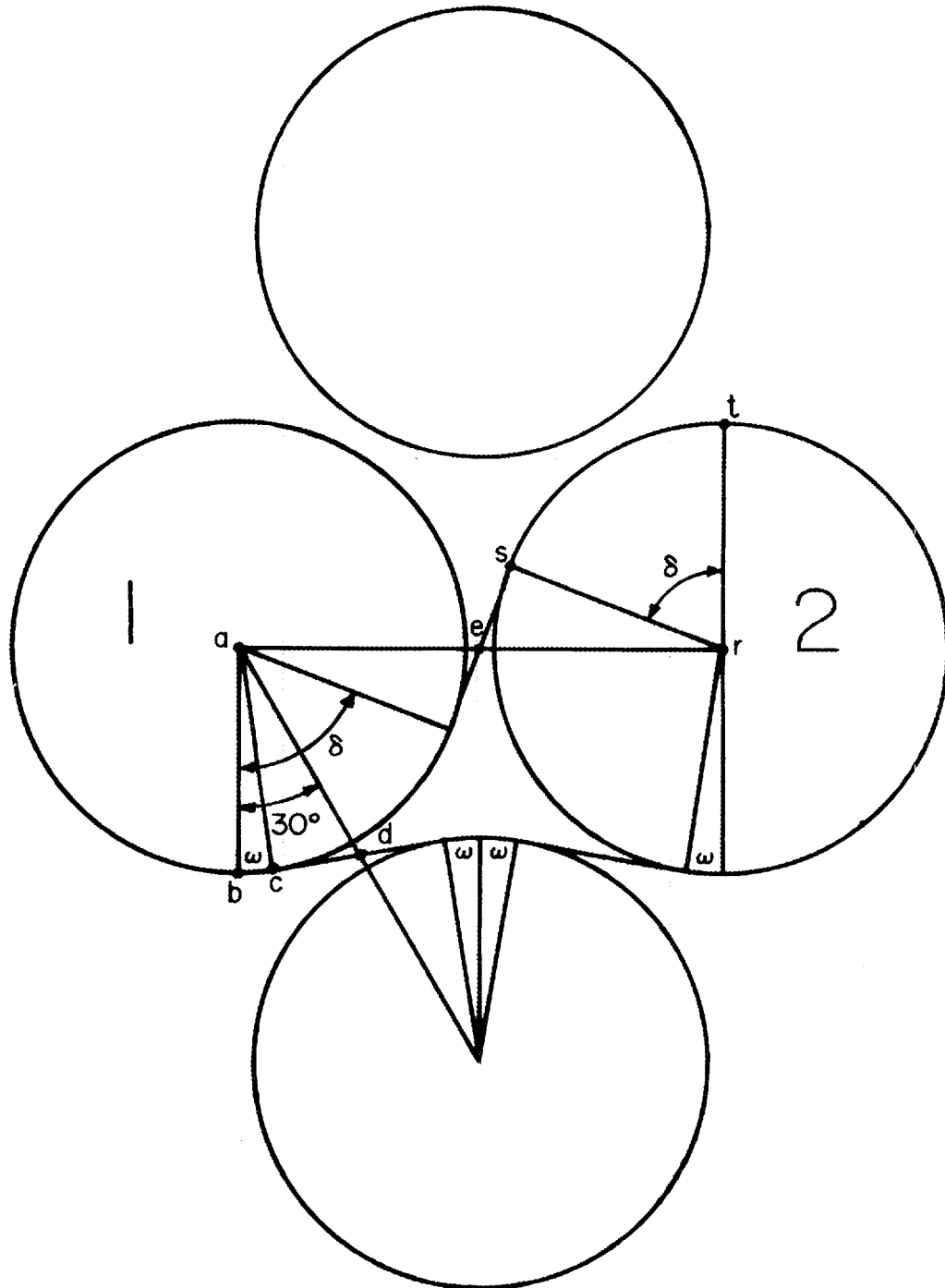


Figure 6. Determination of F_{12} with Partial Shadowing.

$$\delta = \frac{\pi}{2} - \tan^{-1} \frac{es}{er} = \frac{\pi}{2} - \tan^{-1} (\text{PDR}^2 - 1)^{1/2}; \quad st = R\delta$$

in which R is the radius of a cylinder. Application of Equation (55) gives

$$F_{12} = \frac{4(es + st) - 8(bc + cd)}{2 \cdot 2\pi R} = \frac{st - cd - 2bc}{\pi R},$$

$$F_{12} = \frac{1}{\pi} \left[\frac{\pi}{6} - (\text{PDR}^2 - 1)^{1/2} + \tan^{-1} (\text{PDR}^2 - 1)^{1/2} \right], \quad 1 \leq \text{PDR} \leq 2\sqrt{3}/3. \quad (56)$$

No shadowing. If the PDR is greater than $2\sqrt{3}/3$, no shadowing occurs and the lengths of the uncrossed strings are each $\text{PDR} \cdot 2R$ (see Figure 7). Then

$$F_{12} = \frac{4(es + st) - 2bg}{2 \cdot 2\pi R} = \frac{2(es + st) - bg}{2\pi R},$$

$$F_{12} = \frac{1}{\pi} \left[(\text{PDR}^2 - 1)^{1/2} - \tan^{-1} (\text{PDR}^2 - 1)^{1/2} - \text{PDR} + \frac{\pi}{2} \right], \quad \text{PDR} \geq 2\sqrt{3}/3. \quad (57)$$

Derivation of Equations for F13

Radiation to two rows only. For $\text{PDR} < 2\sqrt{3}/3$, cylinders more than two rows away from cylinder 1 receive no irradiation; thus

$$6 F_{12} + 6 F_{13} = 1$$

and

$$F_{13} = \frac{1}{6} - F_{12}.$$

Since F_{12} is known from Equation (56), it follows that

$$F_{13} = \frac{1}{\pi} \left[(\text{PDR}^2 - 1)^{1/2} - \tan^{-1} (\text{PDR}^2 - 1)^{1/2} \right], \quad 1 \leq \text{PDR} \leq 2\sqrt{3}/3. \quad (58)$$

ORNL DWG 75-8465

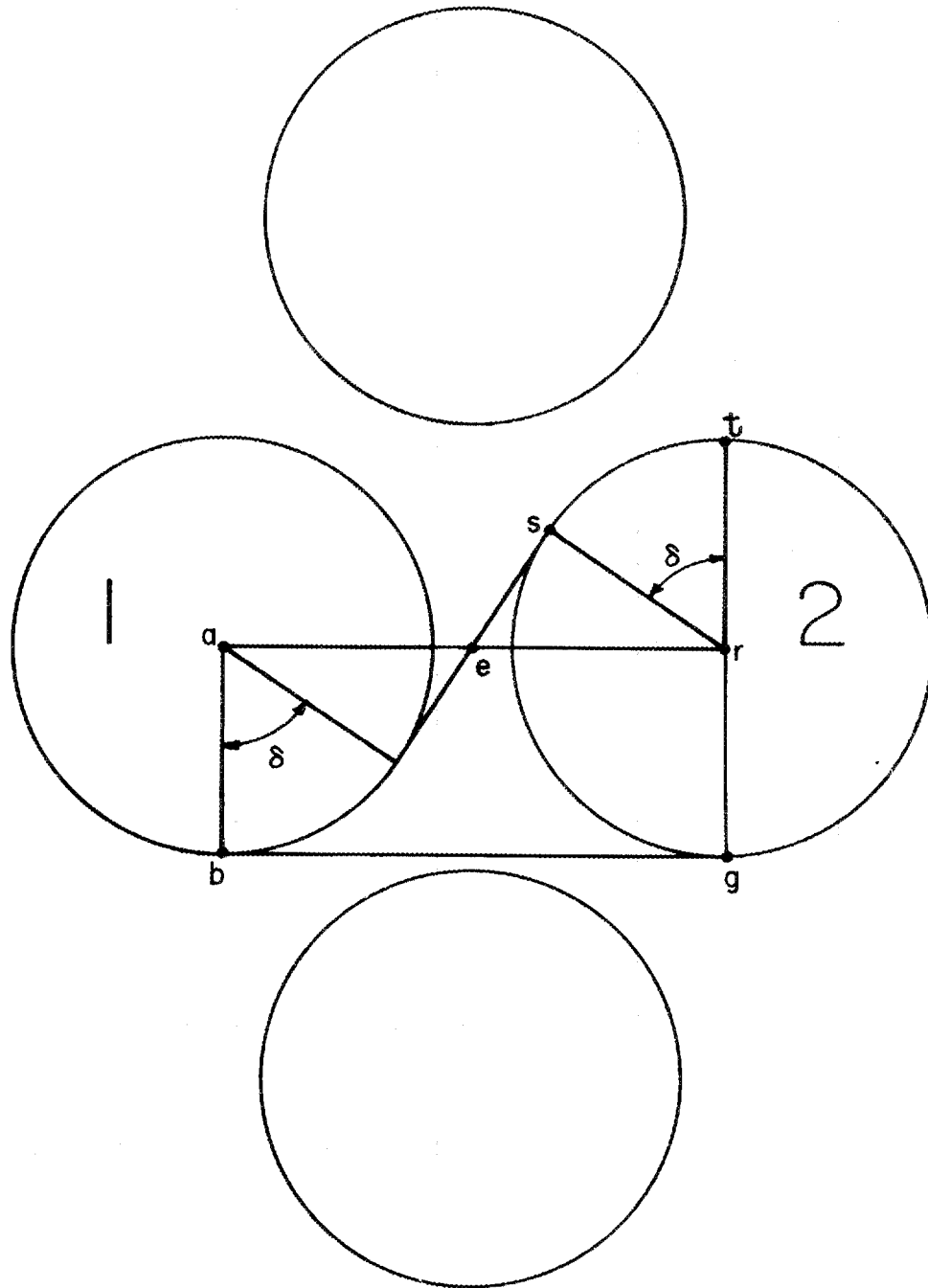


Figure 7. Determination of F12 with No Shadowing.

Partial shadowing. Rod 3 continues to be partially shadowed by rods between 1 and 3 under the conditions $2\sqrt{3}/3 < \text{PDR} < 2$. The upper limit of 2 for the range of PDR is found by referring to Figure 8 and noting that the obstructing cylinders must be separated by a center-to-center distance of $2D$ (D is the diameter of a cylinder) if they are not to block radiation interchange between 1 and 3. From Figure 8,

$$ah = \text{PDR} \cdot 2R; \quad ad = fh = \text{PDR} \cdot R; \quad fr = \text{PDR} \cdot 3R$$

$$cd = (ad^2 - ac^2)^{1/2} = R(\text{PDR}^2 - 1)^{1/2}; \quad af = (ah^2 - fh^2)^{1/2} = \sqrt{3} \text{PDR} \cdot R$$

$$\psi = \tan^{-1} \frac{fr}{af} - \tan^{-1} \frac{fh}{af} = \tan^{-1} \sqrt{3} - \tan^{-1} \frac{\sqrt{3}}{3} = \frac{\pi}{6}$$

$$\omega = \frac{\pi}{2} - \psi - \tan^{-1} \frac{cd}{ac} = \frac{\pi}{3} - \tan^{-1} (\text{PDR}^2 - 1)^{1/2}; \quad bc = R\omega$$

$$ar = (af^2 + fr^2)^{1/2} = 2\sqrt{3} \text{PDR} \cdot R; \quad er = \sqrt{3} \text{PDR} \cdot R$$

$$es = (er^2 - rs^2)^{1/2} = R(3 \text{PDR}^2 - 1)^{1/2}$$

$$\delta = \frac{\pi}{2} - \tan^{-1} \frac{es}{rs} = \frac{\pi}{2} - \tan^{-1} (3 \text{PDR}^2 - 1)^{1/2}; \quad st = R\delta$$

so that

$$F_{13} = \frac{4(es + st) - 8(bc + cd)}{2 \cdot 2\pi R} = \frac{es + st - 2(bc + cd)}{\pi R},$$

$$F_{13} = \frac{1}{\pi} \left[(3 \text{PDR}^2 - 1)^{1/2} - \tan^{-1} (3 \text{PDR}^2 - 1)^{1/2} - 2(\text{PDR}^2 - 1)^{1/2} + 2 \tan^{-1} (\text{PDR}^2 - 1)^{1/2} - \frac{\pi}{6} \right], \quad 2\sqrt{3}/3 \leq \text{PDR} \leq 2. \quad (59)$$

No shadowing. The equation for F_{13} when there is no shadowing can be found from Equation (57) if $\sqrt{3} \text{PDR}$ is substituted for PDR , where $\sqrt{3} \text{PDR}$

ORNL DWG 75-8466

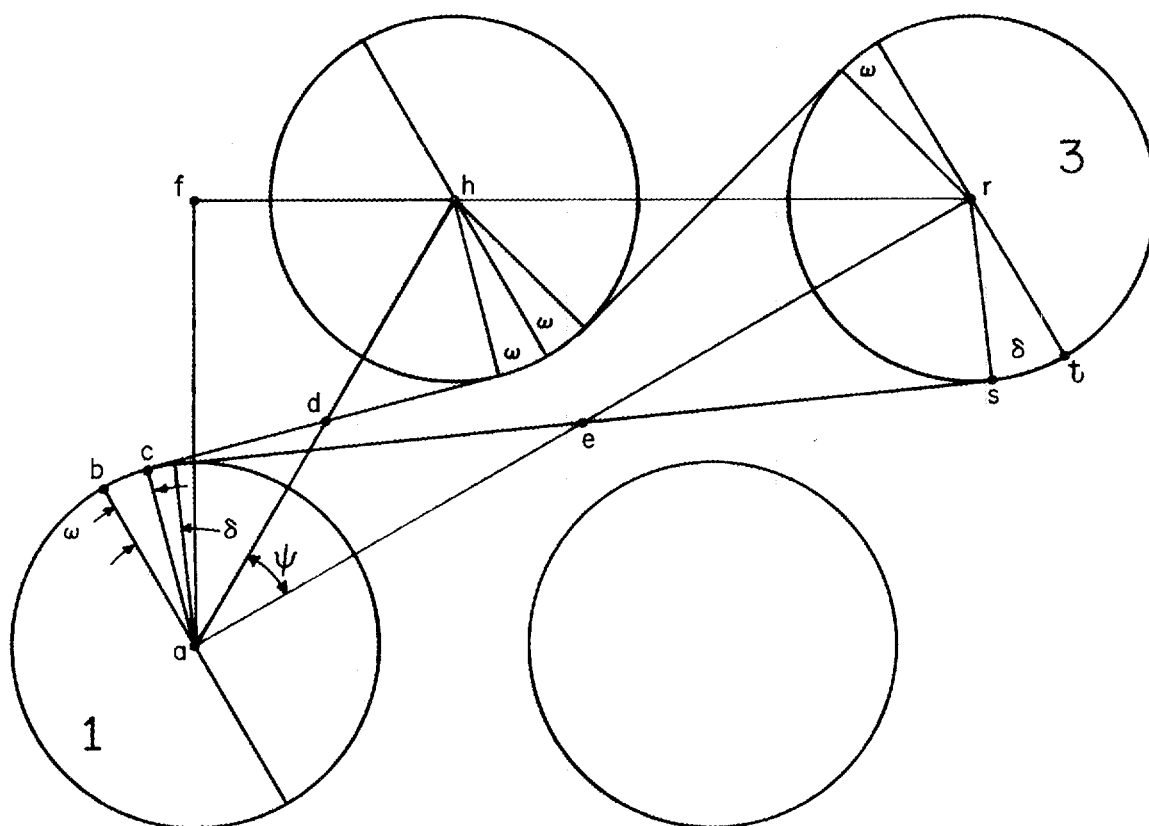


Figure 8. Determination of F13 with Partial Shadowing.

is the pitch-to-diameter ratio of cylinder 1 with respect to cylinder 3.

Then

$$F13 = \frac{1}{\pi} \left[(3 \text{ PDR}^2 - 1)^{1/2} - \tan^{-1} (3 \text{ PDR}^2 - 1)^{1/2} - \sqrt{3} \text{ PDR} + \frac{\pi}{2} \right],$$

$$\text{PDR} \geq 2. \quad (60)$$

Derivation of Equations for F15

No interchange. If the $\text{PDR} \leq 2\sqrt{3}/3$, rod 1 cannot see rod 5. Hence

$$F15 = 0, \quad 1 \leq \text{PDR} \leq 2\sqrt{3}/3. \quad (61)$$

Obstruction of one crossed string. For $2\sqrt{3}/3 \leq \text{PDR} \leq 2$ (the determination of the upper limit of 2 for the range of PDR will be demonstrated subsequently), one of the crossed strings is obstructed by other rods as shown in Figure 9. The lengths of the various line segments are

$$ah = 2\sqrt{3} \text{ PDR} \cdot R; \quad ad = \sqrt{3} \text{ PDR} \cdot R; \quad fh = \text{PDR} \cdot 3R; \quad fr = \text{PDR} \cdot 5R$$

$$cd = (ad^2 - ac^2)^{1/2} = R(3 \text{ PDR}^2 - 1)^{1/2}; \quad af = \sqrt{3} \text{ PDR} \cdot R$$

$$\psi = \tan^{-1} \frac{fr}{af} - \tan^{-1} \frac{fh}{af} = \tan^{-1} \frac{\sqrt{3}}{2} - \tan^{-1} \frac{\sqrt{3}}{3} = \tan^{-1} \frac{\sqrt{3}}{9}$$

$$\omega = \frac{\pi}{2} - \psi - \tan^{-1} \frac{cd}{ac} = \frac{\pi}{2} - \tan^{-1} \frac{\sqrt{3}}{9} - \tan^{-1} (3 \text{ PDR}^2 - 1)^{1/2}; \quad bc = R\omega$$

$$hn = eh = \text{PDR} \cdot R; \quad mn = el = (hn^2 - hm^2)^{1/2} = R(\text{PDR}^2 - 1)^{1/2}$$

$$ak = ah \cos \psi = 9\sqrt{7} \text{ PDR} \cdot R/7; \quad ar = (af^2 + fr^2)^{1/2} = 2\sqrt{7} \text{ PDR} \cdot R$$

$$kr = ar - ak = 5\sqrt{7} \text{ PDR} \cdot R/7; \quad hk = (hr^2 - kr^2)^{1/2} = \sqrt{21} \text{ PDR} \cdot R/7$$

$$\alpha = \tan^{-1} \frac{kr}{hk} - \tan^{-1} \frac{mn}{hm} = \tan^{-1} \frac{5\sqrt{3}}{3} - \tan^{-1} (\text{PDR}^2 - 1)^{1/2}; \quad jm = R\alpha$$

ORNL DWG 75-8467

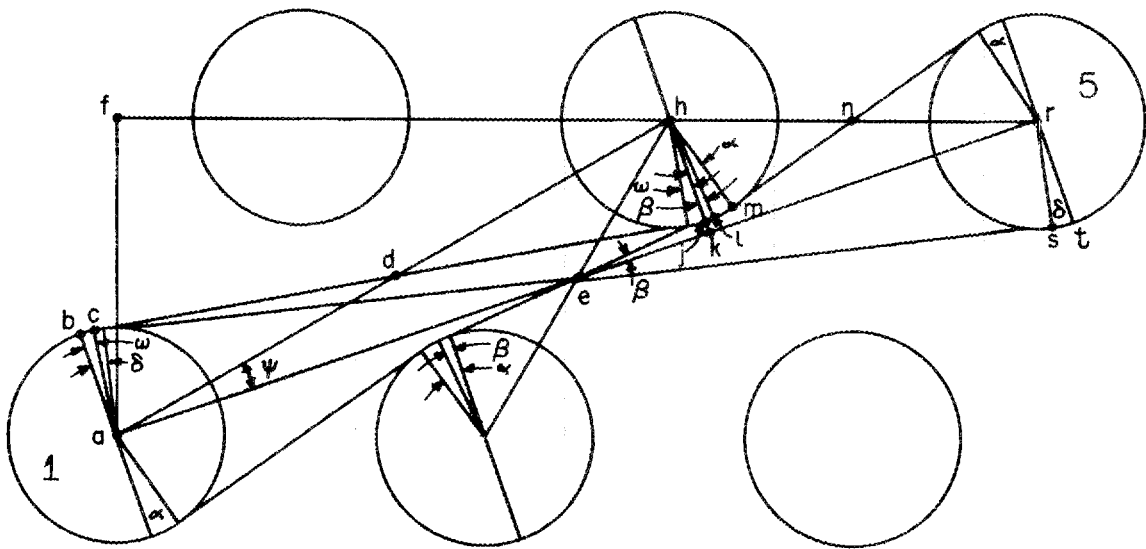


Figure 9. Determination of F15 with Partial Shadowing and Obstruction of One Crossed String.

$$ek = (eh^2 - hk^2)^{1/2} = 2\sqrt{7} \text{ PDR} \cdot R/7$$

$$\beta = \tan^{-1} \frac{hk}{ek} - \tan^{-1} \frac{hl}{el} = \tan^{-1} \frac{\sqrt{3}}{2} - \frac{\pi}{2} + \tan^{-1} (\text{PDR}^2 - 1)^{1/2}$$

$$\alpha - \beta = 2 \left[\frac{\pi}{3} - \tan^{-1} (\text{PDR}^2 - 1)^{1/2} \right]; \quad lm = R(\alpha - \beta) \quad (62)$$

$$er = \sqrt{7} \text{ PDR} \cdot R; \quad es = (er^2 - rs^2)^{1/2} = R(7 \text{ PDR}^2 - 1)^{1/2}$$

$$\delta = \tan^{-1} \frac{rs}{es} = \frac{\pi}{2} - \tan^{-1} (7 \text{ PDR}^2 - 1)^{1/2}; \quad st = R\delta.$$

Since α will become equal to β at the PDR for which obstruction of the crossed string ceases, this PDR may be found by setting $\alpha - \beta = 0$ in Equation (62) giving $\text{PDR} = 2$. The view factor F15 is found from the application of Equation (55) to yield

$$F15 = \frac{[2(st + es + jm + lm) + 6 mn] - 2[2(bc + cd + jm + mn)]}{2 \cdot 2\pi R},$$

$$F15 = \frac{st + es + lm + mn - jm - 2(bc + cd)}{2\pi R},$$

$$F15 = \frac{1}{2\pi} \left[(7 \text{ PDR}^2 - 1)^{1/2} - \tan^{-1} (7 \text{ PDR}^2 - 1)^{1/2} - 2(3 \text{ PDR}^2 - 1)^{1/2} \right. \\ \left. + 2 \tan^{-1} (3 \text{ PDR}^2 - 1)^{1/2} + (\text{PDR}^2 - 1)^{1/2} - \tan^{-1} (\text{PDR}^2 - 1)^{1/2} \right. \\ \left. - \tan^{-1} (\sqrt{3}/5) \right], \quad 2\sqrt{3}/3 \leq \text{PDR} \leq 2. \quad (63)$$

Partial shadowing with no obstruction of crossed strings. The upper limit of PDR for this case is the PDR which produces no shadowing of rod 5, that is, when $hk = 2R$ (see Figure 9). But, from the previous case, $hk = \sqrt{21} \text{ PDR} \cdot R/7$. Solving for PDR gives $2\sqrt{21}/3$ as the upper limit.

Referring to Figure 10 and using many of the results for the preceding case,

$$F_{15} = \frac{4(st + es) - 4(bc + cd + jm + mn)}{2 \cdot 2\pi R} = \frac{st + es - bc - cd - jm - mn}{\pi R},$$

$$F_{15} = \frac{1}{\pi} \left[(7 \text{ PDR}^2 - 1)^{1/2} - \tan^{-1} (7 \text{ PDR}^2 - 1)^{1/2} - (3 \text{ PDR}^2 - 1)^{1/2} + \right. \\ \left. \tan^{-1} (3 \text{ PDR}^2 - 1)^{1/2} - (\text{PDR}^2 - 1)^{1/2} + \tan^{-1} (\text{PDR}^2 - 1)^{1/2} - \frac{\pi}{3} \right],$$

$$2 \leq \text{PDR} \leq 2\sqrt{21}/3. \quad (64)$$

No shadowing. The equation for F_{15} with no shadowing is obtained by using the result for F_{12} with no shadowing and substituting $\sqrt{7}$ PDR for PDR, where $\sqrt{7}$ PDR is the pitch-to-diameter ratio of cylinder 1 with respect to cylinder 5. Then

$$F_{15} = \frac{1}{\pi} \left[(7 \text{ PDR}^2 - 1)^{1/2} - \tan^{-1} (7 \text{ PDR}^2 - 1)^{1/2} - \sqrt{7} \text{ PDR} + \frac{\pi}{2} \right],$$

$$\text{PDR} \geq 2\sqrt{21}/3. \quad (65)$$

Derivation of Equations for F_{18}

No interchange. If the $\text{PDR} \leq 2\sqrt{3}/3$, cylinder 1 cannot see cylinder 5; hence

$$F_{18} = 0, \quad 1 \leq \text{PDR} \leq 2\sqrt{3}/3. \quad (66)$$

Obstruction of one crossed string. For $2\sqrt{3}/3 < \text{PDR} < 2\sqrt{21}/3$, one of the crossed strings is obstructed by other rods as shown in Figure 11. The

lengths of the line segments are

$$ah = 2\sqrt{7} \text{ PDR} \cdot R; \quad ad = \sqrt{7} \text{ PDR} \cdot R; \quad fh = \text{PDR} \cdot 5R; \quad fr = \text{PDR} \cdot 7R$$

$$cd = (ad^2 - ac^2)^{1/2} = R(7 \text{ PDR}^2 - 1)^{1/2}; \quad af = \sqrt{3} \text{ PDR} \cdot R$$

$$\psi = \tan^{-1} \frac{fr}{af} - \tan^{-1} \frac{fh}{af} = \tan^{-1} \frac{7}{\sqrt{3}} - \tan^{-1} \frac{5}{\sqrt{3}} = \tan^{-1} \frac{\sqrt{3}}{19}$$

$$\omega = \frac{\pi}{2} - \psi - \tan^{-1} \frac{cd}{ac} = \frac{\pi}{2} - \tan^{-1} \frac{\sqrt{3}}{19} - \tan^{-1} (7 \text{ PDR}^2 - 1)^{1/2}; \quad bc = R\omega$$

$$hr = \text{PDR} \cdot 2R; \quad hn = \text{PDR} \cdot R; \quad mn = (hn^2 - hm^2)^{1/2} = R(\text{PDR}^2 - 1)^{1/2}$$

$$ak = ah \cos \psi = 19\sqrt{13} \text{ PDR} \cdot R/13; \quad ar = (af^2 + fr^2)^{1/2} = 2\sqrt{13} \text{ PDR} \cdot R$$

$$kr = ar - ak = 7\sqrt{13} \text{ PDR} \cdot R/13; \quad hk = (hr^2 - kr^2)^{1/2} = \sqrt{39} \text{ PDR} \cdot R/13$$

$$\alpha = \tan^{-1} \frac{kr}{hk} - \tan^{-1} \frac{mn}{hm} = \tan^{-1} \frac{7\sqrt{3}}{3} - \tan^{-1} (\text{PDR}^2 - 1)^{1/2}; \quad jm = R\alpha$$

$$eh = \sqrt{3} \text{ PDR} \cdot R; \quad el = (eh^2 - hl^2)^{1/2} = R(3 \text{ PDR}^2 - 1)^{1/2}$$

$$ek = (eh^2 - hk^2)^{1/2} = 6\sqrt{13} \text{ PDR} \cdot R/13$$

$$\beta = \tan^{-1} \frac{hk}{ek} - \tan^{-1} \frac{hl}{el} = \tan^{-1} \frac{\sqrt{3}}{6} - \frac{\pi}{2} + \tan^{-1} (3 \text{ PDR}^2 - 1)^{1/2}$$

$$\alpha - \beta = \frac{5\pi}{6} - \tan^{-1} (3 \text{ PDR}^2 - 1)^{1/2} - \tan^{-1} (\text{PDR}^2 - 1)^{1/2}; \quad lm = R(\alpha - \beta)$$

$$er = \sqrt{13} \text{ PDR} \cdot R; \quad es = (er^2 - rs^2)^{1/2} = R(13 \text{ PDR}^2 - 1)^{1/2}$$

$$\delta = \frac{\pi}{2} - \tan^{-1} \frac{es}{rs} = \frac{\pi}{2} - \tan^{-1} (13 \text{ PDR}^2 - 1)^{1/2}; \quad st = R\delta.$$

The upper limit of $2\sqrt{21}/3$ for the range of PDR is found by equating α and β since $\alpha = \beta$ at the minimum PDR for which there is no obstruction of either crossed string. The configuration factor Fl8 is given by

$$F_{18} = \frac{[2(st + es + jm + lm + el) + 4 mn] - 2[2(bc + cd + jm + mn)]}{2 \cdot 2\pi R},$$

$$F_{18} = \frac{st + es + lm + el - jm - 2(bc + cd)}{2\pi R},$$

$$F_{18} = \frac{1}{2\pi} \left[(13 \text{ PDR}^2 - 1)^{1/2} - \tan^{-1}(13 \text{ PDR}^2 - 1)^{1/2} - 2(7 \text{ PDR}^2 - 1)^{1/2} \right. \\ \left. + 2 \tan^{-1}(7 \text{ PDR}^2 - 1)^{1/2} + (3 \text{ PDR}^2 - 1)^{1/2} - \tan^{-1}(3 \text{ PDR}^2 - 1)^{1/2} \right. \\ \left. - \tan^{-1}\left(\frac{5\sqrt{3}}{87}\right) \right], \quad 2\sqrt{3}/3 \leq \text{PDR} \leq 2\sqrt{21}/3. \quad (67)$$

Partial shadowing with no obstruction of crossed strings. The upper limit of PDR for this case occurs when there is no shadowing of rod 8, that is, when $hk = 2R$ (Figure 11). But, $hk = \sqrt{39} \text{ PDR} \cdot R/13$ so that $\text{PDR} = 2\sqrt{39}/3$. This case differs from the previous one only in that both crossed strings are obstructed. The equation for F_{18} becomes

$$F_{18} = \frac{4(st + es) - 4(bc + cd + jm + mn)}{2 \cdot 2\pi R} = \frac{st + es - bc - cd - jm - mn}{\pi R},$$

$$F_{18} = \frac{1}{\pi} \left[(13 \text{ PDR}^2 - 1)^{1/2} - \tan^{-1}(13 \text{ PDR}^2 - 1)^{1/2} - (7 \text{ PDR}^2 - 1)^{1/2} + \right. \\ \left. \tan^{-1}(7 \text{ PDR}^2 - 1)^{1/2} - (\text{PDR}^2 - 1)^{1/2} + \tan^{-1}(\text{PDR}^2 - 1)^{1/2} - \right. \\ \left. \tan^{-1}\left(\frac{5\sqrt{3}}{3}\right) \right], \quad 2\sqrt{21}/3 \leq \text{PDR} \leq 2\sqrt{39}/3. \quad (68)$$

No shadowing. The equation for F_{18} with no shadowing is obtained by using the result for F_{12} with no shadowing and substituting $\sqrt{13} \text{ PDR}$ for PDR, where $\sqrt{13} \text{ PDR}$ is the pitch-to-diameter ratio of rod 1 with respect

to rod 8. Then

$$F_{18} = \frac{1}{\pi} \left[(13 \text{ PDR}^2 - 1)^{1/2} - \tan^{-1} (13 \text{ PDR}^2 - 1)^{1/2} - \sqrt{13} \text{ PDR} + \frac{\pi}{2} \right],$$

$$\text{PDR} \geq 2\sqrt{39}/3 . \quad (69)$$

An Approximation for Close Spacings

Calculated results for F_{12} , F_{13} , F_{15} , and F_{18} for selected values of PDR are shown in Table I. The quantity $\text{ERROR} = 1 - 6(F_{12} + F_{13}) - 12(F_{15} + F_{18})$ in the table represents the fraction of the radiation leaving a rod that is not intercepted by rods in the first four surrounding rows. Obviously, ERROR increases with PDR. For the spacings encountered in the designs of hexagonal nuclear fuel assemblies ($\text{PDR} < 1.4$; commonly, 1.2 to 1.3), it can be seen that to a very good approximation all the radiation outgoing from a cylinder may be assumed to be intercepted in the adjacent four rows of rods. In such cases, all the radiation falling on rods in rows beyond the fourth may be assumed, instead, to fall on rods in the fourth row for the purpose of radiant interchange calculations. This assumption has the advantage of introducing negligible error for close spacings while obviating the need to consider an excessively large number of surfaces in order to account for all the radiation leaving a given surface. In place of F_{18} , the pseudo view factor F_{18}^* is defined for such cases as

$$F_{18}^* = \frac{1 - 6(F_{12} + F_{13}) - 12 F_{15}}{12} . \quad (70)$$

Values of F_{18}^* are also given in Table I.

IV. VIEW FACTORS FOR CYLINDERS ON A SQUARE PITCH

The crossed-string method will now be used to derive the view factors between infinitely long parallel cylinders in arrays on a square pitch. The cylinders are designated as shown in Figure 12. For the spacings

TABLE I

View Factors for Parallel Cylinders on
an Equilateral Triangular Pitch

PDR	F12	F13	F15	F18	ERROR	F18*
1.00	0.16667	0.0	0.0	0.0	0.00000	0.00000
1.05	0.16338	0.00328	0.0	0.0	0.00000	0.00000
1.10	0.15758	0.00909	0.0	0.0	0.00000	0.00000
1.15	0.15030	0.01637	0.0	0.0	0.00000	0.00000
1.20	0.14274	0.02367	0.00010	0.00002	0.00014	0.00003
1.25	0.13601	0.02961	0.00041	0.00006	0.00059	0.00011
1.30	0.12997	0.03444	0.00088	0.00014	0.00132	0.00025
1.35	0.12449	0.03838	0.00146	0.00025	0.00228	0.00044
1.40	0.11949	0.04156	0.00215	0.00037	0.00347	0.00066
1.45	0.11491	0.04408	0.00291	0.00052	0.00484	0.00092
1.50	0.11070	0.04606	0.00375	0.00068	0.00638	0.00121
1.55	0.10679	0.04754	0.00464	0.00085	0.00808	0.00153
1.60	0.10317	0.04860	0.00558	0.00104	0.00992	0.00187
1.65	0.09980	0.04928	0.00656	0.00124	0.01188	0.00223
1.70	0.09665	0.04962	0.00758	0.00146	0.01395	0.00262
1.75	0.09371	0.04966	0.00863	0.00168	0.01613	0.00302
1.80	0.09094	0.04943	0.00971	0.00191	0.01840	0.00344
1.85	0.08834	0.04896	0.01081	0.00215	0.02076	0.00388
1.90	0.08588	0.04826	0.01194	0.00239	0.02320	0.00433
1.95	0.08357	0.04736	0.01308	0.00265	0.02572	0.00479
2.00	0.08138	0.04627	0.01425	0.00290	0.02830	0.00526

ORNL DWG 75-8469

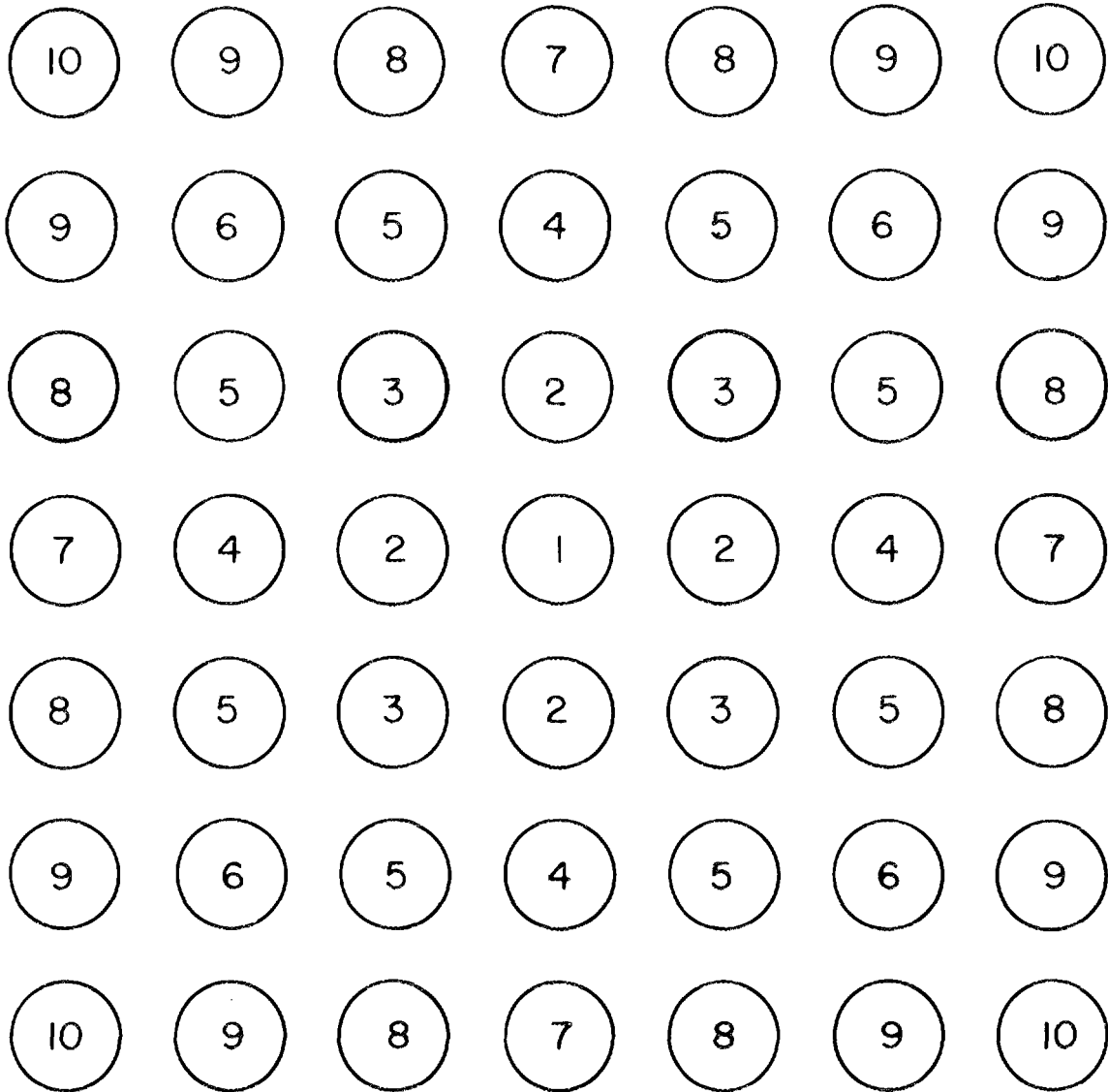


Figure 12. Parallel Cylinders on a Square Pitch.

that will be considered here, all but a very small fraction of the radiation leaving cylinder 1 is intercepted by cylinders 2, 3, 5, and 8.

Again, the notation F_{1J} denotes the fraction of the radiant energy outgoing from cylinder 1 that is intercepted by a single cylinder numbered J , not that intercepted by all cylinders J . Obviously, F_{11} , F_{14} , F_{16} , F_{17} , and F_{1-10} are zero since surface 1 cannot see itself or any of the surfaces numbered 4, 6, 7, and 10.

Derivation of Equation for F_{12}

The equation for F_{12} for cylinders on a square pitch is derived in the same manner as the equation for F_{12} for cylinders on an equilateral triangular pitch with no shadowing. Thus

$$F_{12} = \frac{1}{\pi} \left[(\text{PDR}^2 - 1)^{1/2} - \tan^{-1} (\text{PDR}^2 - 1)^{1/2} - \text{PDR} + \frac{\pi}{2} \right], \text{ all PDR. } (71)$$

The above formula, as noted, applies for all PDRs since there is no shadowing of rod 2 by other rods, even for $\text{PDR} = 1.0$, for cylinders on a square pitch.

Derivation of Equations for F_{13}

Partial shadowing. If the PDR is less than $\sqrt{2}$, rod 3 is shadowed by other rods as illustrated by Figure 13. Lengths of the line segments are

$$ad = \text{PDR} \cdot R; \quad cd = (ad^2 - ac^2)^{1/2} = R(\text{PDR}^2 - 1)^{1/2}$$

$$ah = hr = \text{PDR} \cdot 2R; \quad \psi = \tan^{-1} \frac{hr}{ah} = \tan^{-1} 1 = \frac{\pi}{4}$$

$$\omega = \frac{\pi}{2} - \psi - \tan^{-1} \frac{cd}{ac} = \frac{\pi}{4} - \tan^{-1} (\text{PDR}^2 - 1)^{1/2}; \quad bc = R\omega$$

ORNL DWG 75-8470

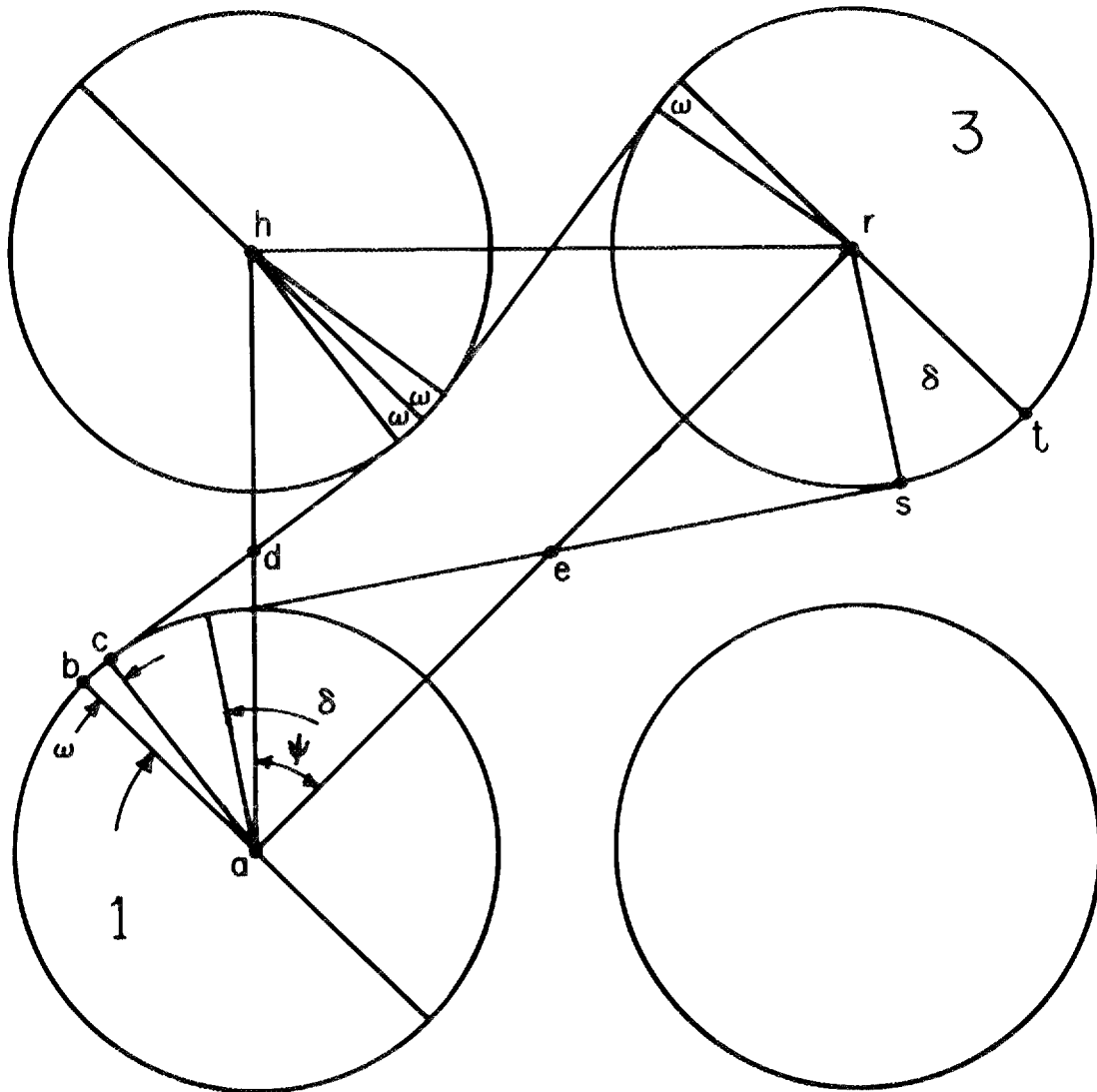


Figure 13. Derivation of F13 with Partial Shadowing.

$$ar = (ah^2 + hr^2)^{1/2} = 2\sqrt{2} \text{ PDR} \cdot R; \quad er = \sqrt{2} \text{ PDR} \cdot R$$

$$es = (er^2 - rs^2)^{1/2} = R(2 \text{ PDR}^2 - 1)^{1/2}$$

$$\delta = \frac{\pi}{2} - \tan^{-1} \frac{es}{rs} = \frac{\pi}{2} - \tan^{-1} (2 \text{ PDR}^2 - 1)^{1/2}; \quad st = R\delta.$$

The upper limit of $\sqrt{2}$ for the range of PDR is found by noting that there will be no shadowing when gh becomes equal to $2R$. Since $gh = \sqrt{2} \text{ PDR} \cdot R$, it follows that $\text{PDR} = \sqrt{2}$. Hottel's crossed-string method leads to the result:

$$F_{13} = \frac{4(st + es) - 8(bc + cd)}{2 \cdot 2\pi R} = \frac{st + es - 2(bc + cd)}{\pi R},$$

$$F_{13} = \frac{1}{\pi} \left[(2 \text{ PDR}^2 - 1)^{1/2} - \tan^{-1} (2 \text{ PDR}^2 - 1)^{1/2} - 2(\text{PDR}^2 - 1)^{1/2} + 2 \tan^{-1} (\text{PDR}^2 - 1)^{1/2} \right], \quad 1 \leq \text{PDR} \leq \sqrt{2}. \quad (72)$$

No shadowing. The equation for F_{13} with no shadowing can be derived by substituting $\sqrt{2} \text{ PDR}$ for PDR in Equation (71) since $\sqrt{2} \text{ PDR}$ is the pitch-to-diameter ratio of cylinder 3 relative to cylinder 1. Then

$$F_{13} = \frac{1}{\pi} \left[(2 \text{ PDR}^2 - 1)^{1/2} - \tan^{-1} (2 \text{ PDR}^2 - 1)^{1/2} - \sqrt{2} \text{ PDR} + \frac{\pi}{2} \right], \quad \text{PDR} \geq \sqrt{2}.$$

(73)

Derivation of Equations for F15

Obstruction of one crossed string. For $1 < \text{PDR} < \sqrt{2}$, one of the crossed strings is obstructed. Referring to Figure 14, the lengths of the line segments are

$$ah = (af^2 + fh^2)^{1/2} = 2\sqrt{2} \text{PDR} \cdot R; \quad ad = \sqrt{2} \text{PDR} \cdot R$$

$$ac = R; \quad cd = (ad^2 - ac^2)^{1/2} = R(2 \text{PDR}^2 - 1)^{1/2}$$

$$\psi = \tan^{-1} \frac{fr}{af} - \tan^{-1} \frac{fh}{af} = \tan^{-1} 2 - \tan^{-1} 1 = \frac{\pi}{2} - \tan^{-1} 3$$

$$\omega = \frac{\pi}{2} - \psi - \tan^{-1} \frac{cd}{ac} = \tan^{-1} 3 - \tan^{-1} (2 \text{PDR}^2 - 1)^{1/2}; \quad bc = R\omega$$

$$hn = eh = \text{PDR} \cdot R; \quad mn = el = (hn^2 - hm^2)^{1/2} = R(\text{PDR}^2 - 1)^{1/2}$$

$$\alpha = \frac{3\pi}{4} - \tan^{-1} \frac{mn}{hm} - \omega - \tan^{-1} \frac{cd}{ac} = \tan^{-1} 2 - \tan^{-1} (\text{PDR}^2 - 1)^{1/2}; \quad jm = R\alpha$$

$$\beta = \tan^{-1} \frac{fr}{af} - \tan^{-1} \frac{hl}{el} = \tan^{-1} 2 - \frac{\pi}{2} + \tan^{-1} (\text{PDR}^2 - 1)^{1/2}$$

$$\alpha - \beta = \frac{\pi}{2} - 2 \tan^{-1} (\text{PDR}^2 - 1)^{1/2}; \quad lm = R(\alpha - \beta)$$

$$ar = (af^2 + fr^2)^{1/2} = 2\sqrt{5} \text{PDR} \cdot R; \quad er = \sqrt{5} \text{PDR} \cdot R$$

$$es = (er^2 - rs^2)^{1/2} = R(5 \text{PDR}^2 - 1)^{1/2}$$

$$\delta = \frac{\pi}{2} - \tan^{-1} \frac{es}{rs} = \frac{\pi}{2} - \tan^{-1} (5 \text{PDR}^2 - 1)^{1/2}; \quad st = R\delta.$$

The PDR at which the crossed string is no longer obstructed may be found by setting $\alpha - \beta = 0$ to yield $\text{PDR} = \sqrt{2}$. The value of F15 is

$$F15 = \frac{[2(st + es) + 2(jm + lm) + 6 mn] - 2[2(bc + cd + jm + mn)]}{2 \cdot 2\pi R},$$

ORNL DWG 75-8471

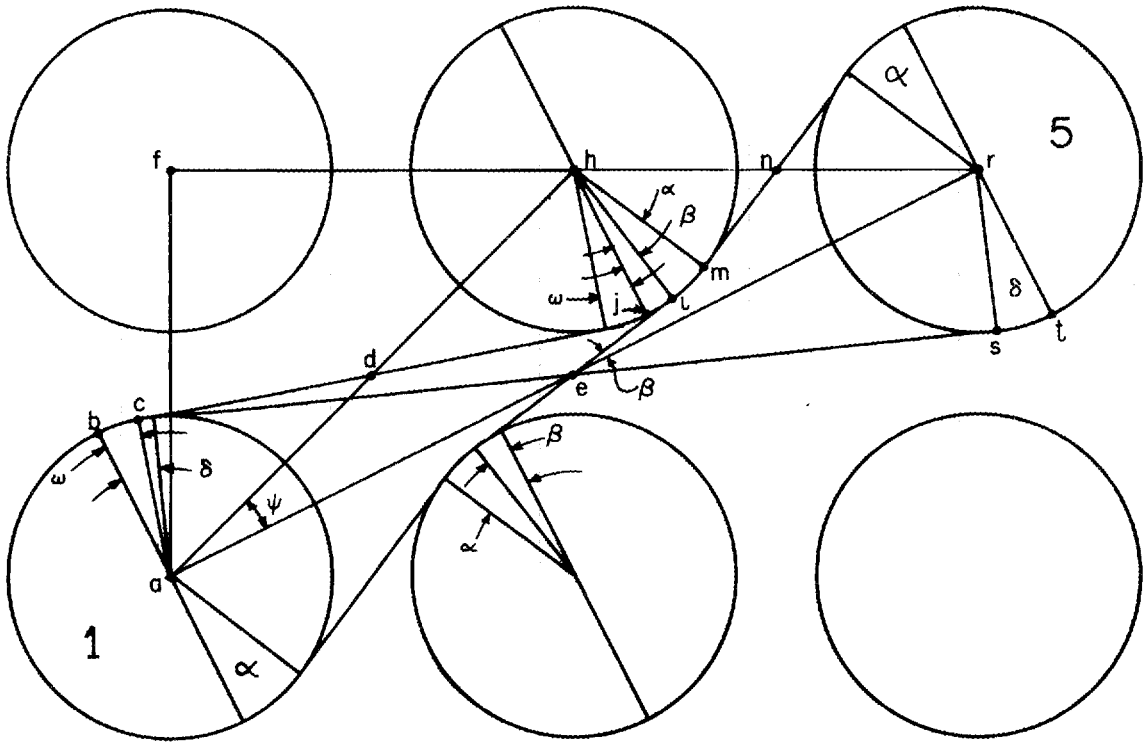


Figure 14. Derivation of F15 with Partial Shadowing and Obstruction of One Crossed String.

$$F_{15} = \frac{st + es + lm + mn - jm - 2(bc + cd)}{2\pi R}$$

$$F_{15} = \frac{1}{2\pi} \left[(5 \text{ PDR}^2 - 1)^{1/2} - \tan^{-1}(5 \text{ PDR}^2 - 1)^{1/2} - 2(2 \text{ PDR}^2 - 1)^{1/2} + \right. \\ \left. 2 \tan^{-1}(2 \text{ PDR}^2 - 1)^{1/2} + (\text{PDR}^2 - 1)^{1/2} - \tan^{-1}(\text{PDR}^2 - 1)^{1/2} - \tan^{-1}(1/2) \right],$$

$$1 \leq \text{PDR} \leq \sqrt{2}. \quad (74)$$

Partial shadowing with no obstruction of crossed strings. The upper limit for this case occurs when there is no longer any shadowing. The PDR at which this happens may be determined by setting either ω or α equal to zero, which gives a value of PDR of $\sqrt{5}$. Since this case differs from the previous one only in that both crossed strings are unobstructed, one obtains (see Figure 15)

$$F_{15} = \frac{st + es - bc - cd - jm - mn}{\pi R},$$

$$F_{15} = \frac{1}{\pi} \left[(5 \text{ PDR}^2 - 1)^{1/2} - \tan^{-1}(5 \text{ PDR}^2 - 1)^{1/2} - (2 \text{ PDR}^2 - 1)^{1/2} + \right. \\ \left. \tan^{-1}(2 \text{ PDR}^2 - 1)^{1/2} - (\text{PDR}^2 - 1)^{1/2} + \tan^{-1}(\text{PDR}^2 - 1)^{1/2} - \frac{\pi}{4} \right],$$

$$\sqrt{2} \leq \text{PDR} \leq \sqrt{5}. \quad (75)$$

No shadowing. The equation for F_{15} with no shadowing can be derived by using the equation for F_{12} and substituting $\sqrt{5}$ PDR for PDR, where $\sqrt{5}$ PDR represents the effective pitch-to-diameter ratio of rod 1 with respect to rod 5. Then

$$F15 = \frac{1}{\pi} \left[(5 \text{ PDR}^2 - 1)^{1/2} - \tan^{-1} (5 \text{ PDR}^2 - 1)^{1/2} - \sqrt{5} \text{ PDR} + \frac{\pi}{2} \right], \text{ PDR} \geq \sqrt{5}. \quad (76)$$

Derivation of Equations for F18

Obstruction of one crossed string. Figure 16 shows radiation inter-
change between rods 1 and 8 when one of the crossed strings is obstructed.
The lengths of the line segments are

$$ah = (af^2 + fh^2)^{1/2} = 2\sqrt{5} \text{ PDR} \cdot R; \quad ad = \sqrt{5} \text{ PDR} \cdot R$$

$$ac = R; \quad cd = (ad^2 - ac^2)^{1/2} = R(5 \text{ PDR}^2 - 1)^{1/2}$$

$$\psi = \tan^{-1} \frac{fr}{af} - \tan^{-1} \frac{fh}{af} = \tan^{-1} 3 - \tan^{-1} 2 = \frac{\pi}{2} - \tan^{-1} 7$$

$$\omega = \frac{\pi}{2} - \psi - \tan^{-1} \frac{cd}{ac} = \tan^{-1} 7 - \tan^{-1} (5 \text{ PDR}^2 - 1)^{1/2}; \quad bc = R\omega$$

$$hn = \text{PDR} \cdot R; \quad mn = (hn^2 - hm^2)^{1/2} = R(\text{PDR}^2 - 1)^{1/2}$$

$$eh = \sqrt{2} \text{ PDR} \cdot R; \quad el = (eh^2 - hl^2)^{1/2} = R(2 \text{ PDR}^2 - 1)^{1/2}$$

$$\alpha = \frac{\pi}{2} + \tan^{-1} 2 - \tan^{-1} \frac{mn}{hm} - \omega - \tan^{-1} \frac{cd}{ac} = \tan^{-1} 3 - \tan^{-1} (\text{PDR}^2 - 1)^{1/2};$$

$$jm = R\alpha$$

$$\beta = \tan^{-1} \frac{fr}{af} - \tan^{-1} \frac{hl}{el} - \frac{\pi}{4} = \tan^{-1} 3 - \frac{3\pi}{4} + \tan^{-1} (2 \text{ PDR}^2 - 1)^{1/2}$$

$$\alpha - \beta = \frac{3\pi}{4} - \tan^{-1} (\text{PDR}^2 - 1)^{1/2} - \tan^{-1} (2 \text{ PDR}^2 - 1)^{1/2}; \quad lm = R(\alpha - \beta)$$

$$ar = (af^2 + fr^2)^{1/2} = 2\sqrt{10} \text{ PDR} \cdot R; \quad er = \sqrt{10} \text{ PDR} \cdot R$$

$$es = (er^2 - rs^2)^{1/2} = R(10 \text{ PDR}^2 - 1)^{1/2}$$

$$\delta = \frac{\pi}{2} - \tan^{-1} \frac{es}{rs} = \frac{\pi}{2} - \tan^{-1} (10 \text{ PDR}^2 - 1)^{1/2}; \text{ st} = R\delta.$$

Setting $\alpha - \beta = 0$ and solving for PDR gives $\sqrt{5}$ as the pitch-to-diameter ratio at which the crossed string is no longer obstructed. The value of F18 is

$$F18 = \frac{[2(st + es) + 2(jm + lm + el) + 4 mn] - 2[2(bc + cd + jm + mn)]}{2 \cdot 2\pi R},$$

$$F18 = \frac{st + es + lm + el - jm - 2(bc + cd)}{2\pi R},$$

$$F18 = \frac{1}{2\pi} \left[(10 \text{ PDR}^2 - 1)^{1/2} - \tan^{-1} (10 \text{ PDR}^2 - 1)^{1/2} - 2(5 \text{ PDR}^2 - 1)^{1/2} + \right. \\ \left. 2 \tan^{-1} (5 \text{ PDR}^2 - 1)^{1/2} + (2 \text{ PDR}^2 - 1)^{1/2} - \tan^{-1} (2 \text{ PDR}^2 - 1)^{1/2} \right. \\ \left. - \tan^{-1} (2/11) \right], \quad 1 \leq \text{PDR} \leq \sqrt{5}. \quad (77)$$

Partial shadowing with no obstruction of crossed strings. Setting α equal to zero gives $\text{PDR} = \sqrt{10}$ as the upper limit for this case. Using results from the previous case but with both crossed strings unobstructed, one obtains

$$F15 = \frac{st + es - bc - cd - jm - mn}{\pi R},$$

$$F15 = \frac{1}{\pi} \left[(10 \text{ PDR}^2 - 1)^{1/2} - \tan^{-1} (10 \text{ PDR}^2 - 1)^{1/2} - (5 \text{ PDR}^2 - 1)^{1/2} + \right. \\ \left. \tan^{-1} (5 \text{ PDR}^2 - 1)^{1/2} - (\text{PDR}^2 - 1)^{1/2} + \tan^{-1} (\text{PDR}^2 - 1)^{1/2} - \tan^{-1} 2 \right],$$

$$\sqrt{5} \leq \text{PDR} \leq \sqrt{10}. \quad (78)$$

No shadowing. The PDR of rod 1 relative to rod 8 is $\sqrt{10}$, so that

$$F_{18} = \frac{1}{\pi} \left[(10 \text{ PDR}^2 - 1)^{1/2} - \tan^{-1} (10 \text{ PDR}^2 - 1)^{1/2} - \sqrt{10} \text{ PDR} + \frac{\pi}{2} \right],$$

$$\text{PDR} \geq 10. \quad (79)$$

Close Spacings

Values for F_{12} , F_{13} , F_{15} , and F_{18} are given in Table II for selected values of PDR. The quantity $\text{ERROR} = 1 - 4(F_{12} + F_{13}) - 8(F_{15} + F_{18})$ in the table is the fraction of the radiation leaving cylinder 1 that is not intercepted by rods 2, 3, 5, and 8 in the adjacent three rows. For close spacings, there is obviously little error in assuming that all the radiation falling on other rods is intercepted instead by rods in position 8. As noted previously, this assumption permits all the radiation leaving a surface to be accounted for, while producing only a slight redistribution of the radiant energy for rods of close spacings. This redistribution of energy introduces a much smaller error in the temperature calculations than is indicated by the value of ERROR because of the one-fourth power variation of temperature with changes in the view factors, as shown in Equations (34) for example. The pseudo view factor F_{18}^* (also given in Table II) is defined for rods on a square pitch as

$$F_{18}^* = \frac{1 - 4(F_{12} + F_{13}) - 8F_{15}}{8}. \quad (80)$$

TABLE II
View Factors for Parallel Cylinders
on a Square Pitch

PDR	F12	F13	F15	F18	ERROR	F18*
1.00	0.18169	0.06831	0.00000	0.00000	0.00000	0.00000
1.05	0.16906	0.07803	0.00136	0.00006	0.00025	0.00009
1.10	0.15895	0.08337	0.00350	0.00023	0.00095	0.00034
1.15	0.15031	0.08632	0.00596	0.00047	0.00203	0.00073
1.20	0.14274	0.08760	0.00861	0.00079	0.00344	0.00122
1.25	0.13601	0.08760	0.01140	0.00116	0.00514	0.00180
1.30	0.12997	0.08659	0.01427	0.00157	0.00708	0.00246
1.35	0.12449	0.08475	0.01720	0.00203	0.00924	0.00318
1.40	0.11949	0.08221	0.02018	0.00251	0.01159	0.00396
1.45	0.11491	0.07927	0.02308	0.00303	0.01438	0.00483
1.50	0.11070	0.07652	0.02554	0.00358	0.01823	0.00585
1.55	0.10679	0.07395	0.02761	0.00414	0.02304	0.00702
1.60	0.10317	0.07156	0.02932	0.00472	0.02870	0.00831
1.65	0.09980	0.06931	0.03073	0.00533	0.03510	0.00971
1.70	0.09665	0.06721	0.03185	0.00594	0.04216	0.01122
1.75	0.09371	0.06523	0.03273	0.00658	0.04982	0.01280
1.80	0.09094	0.06337	0.03337	0.00722	0.05801	0.01447
1.85	0.08834	0.06161	0.03382	0.00788	0.06669	0.01621
1.90	0.08588	0.05995	0.03407	0.00854	0.07580	0.01802
1.95	0.08357	0.05837	0.03415	0.00922	0.08531	0.01988
2.00	0.08138	0.05688	0.03407	0.00990	0.09518	0.02180

V. PREVIOUS WORK

The literature contains formulas, graphs, and tabulations of configuration factors for a large number of geometries which have received attention since the introduction of the view factor concept in about 1928 [see (28) for historical notes]. Among the more complete compilations of view factors are the works of Hamilton and Morgan (12), Leuenberger and Pearson (20), and Siegel and Howell (28). The last tabulate references to over 170 geometrical configurations for which angle factors have been determined.

The view factors between parallel cylinders in arrays, however, appear to have received little attention. Except for the derivation of the configuration factor between two infinitely long parallel cylinders with an unobstructed view of each other, no other analytical results are available. The usefulness of the crossed-string method in deriving analytical relations for the view factors between parallel cylinders in arrays does not seem to have been recognized. Investigators concerned with heat transfer in rod arrays have calculated the view factors that they needed using integration of the equation:

$$F_{ij} = \frac{1}{A_i} \int_{A_i} F_{dA_i-A_j} dA_i \quad (81)$$

where $F_{dA_i-A_j}$ is the configuration factor between the differential area dA_i and the finite area A_j . Equation (81) is merely a statement of the fact that the view factor for A_i with respect to A_j is the area-weighted average of the view factors from the differential areas comprising A_i . As shown by Jakob (17, p. 19) the view factor between a differential

surface dA_i and a finite surface A_j , whose generatrix is parallel to the differential surface, is

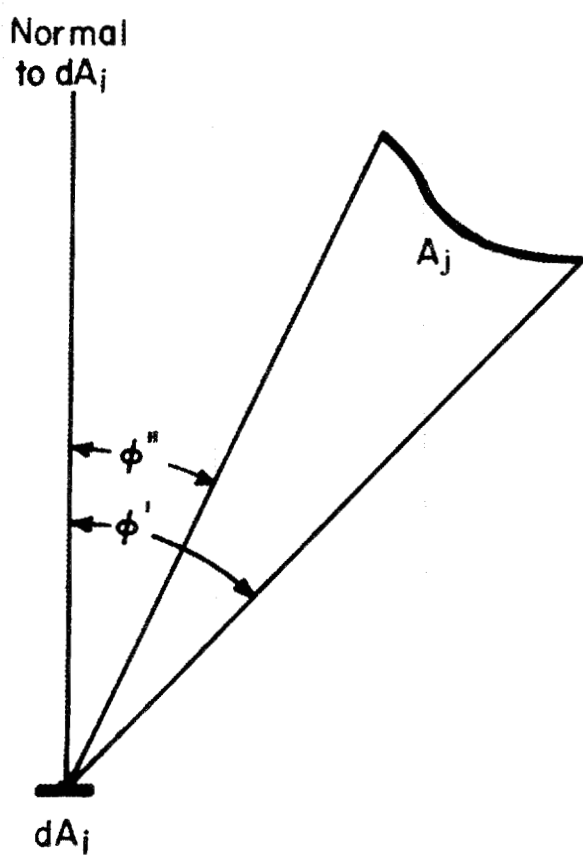
$$F_{dA_i-A_j} = \frac{\sin \phi' - \sin \phi''}{2}$$

if the surfaces are infinitely long (Figure 17). The symbols ϕ'' and ϕ' represent the angles measured clockwise from the normal to dA_i at which the surface A_j "appears" and subsequently "disappears" from the view of dA_i . If A_i is divided into n equal-sized incremental areas, the finite difference approximation for F_{ij} becomes

$$F_{ij} = \frac{1}{n} \sum_{k=1}^n \frac{\sin \phi'_k - \phi''_k}{2} . \quad (82)$$

Watson (37) determined F_{12} and F_{13} for rods on a square pitch using Equation (82). A comparison of his tabulated results covering a range of PDRs from 1.0 to 6.0 with the exact values calculated using the relations derived in this dissertation shows a maximum deviation of 0.4%. Klepper (19) has calculated values of F_{12} and F_{13} for cylinders on a triangular pitch and values of F_{12} , F_{13} , and F_{15} for rods on a square pitch at PDRs of 1.1, 1.2, 1.3, 1.4, and 1.5. Rods spaced on a triangular pitch were divided into twelve 30° segments, while rods on a square pitch were divided into eight 45° segments. As a result of inaccuracies caused by this coarse division and by graphical evaluation of the angles ϕ' and ϕ'' , Klepper's angle factors differ as much as 5% from the exact values. Singer (29) has developed a computer program to perform an evaluation of Equation (82) for the general case of radiation between two cylinders with

ORNL DWG 75-8474

Figure 17. Geometrical Relationship Between dA_i and A_j .

intervening upper and lower shadowing pins which is the configuration encountered for radiation between rods in arrays (see Figure 16, p. 63, for example). Except for two sample problems involving computation of F_{12} , F_{13} , and F_{15} for cylinders on square pitches of 1.0625 and 1.3341, Singer does not tabulate any view factors for parallel rod arrays. Results of his sample calculations using 100 increments differ no more than 0.04% from the exact values. A general computer program for the determination of view factors developed by Toups (35, 36) has been utilized by Evans (5) to calculate view factors between rods in square arrays.

It is obviously much simpler and more accurate to use the theoretical relations derived in Sections III and IV than to compute the view factors between parallel cylinders by evaluation of Equation (82), even if one uses the programs already developed by Singer or Toups. The crossed-string method could, of course, be used to derive equations for the view factors between cylinders farther apart in the array as would be needed in the case of cylinders on wide spacings.

CHAPTER 5

CONSTRUCTION OF VIEW FACTOR MATRICES

It is clear from an examination of the equations for radiant exchange within an enclosure (Chapters 2 and 3) that it is essential to know the view factors F_{ij} for each surface with respect to every other surface within the enclosure in order to effect a solution. The previous chapter was directed toward a determination of the individual view factors between rods in arrays for the two cases of cylinders on a square pitch and on an equilateral triangular pitch. In the present chapter, attention will be centered on the generation of the entire matrix of configuration factors. One of the major difficulties in evolving an algorithm to treat radiant exchange in a square or hexagonal rod array of any size is the development of a method for generating the F matrix for an array of arbitrary size. Obviously, however, this is necessary in order to produce a program of general utility and to avoid the necessity for solving the problem anew each time another size array is encountered.

I. HEXAGONAL ARRAYS

Two possibilities are considered. The first is the general case, which allows for an arbitrary variation of the surface heat flux from rod to rod. The second is the special case in which the distribution of heat fluxes is symmetrical. A particular example would be that of equal heat generation rate in each of the cylinders.

Arbitrary Heat Flux Distribution

The manner in which the rods are numbered for an arbitrary heat flux distribution is illustrated in Figure 18 for a 217-rod array. The numbering of the cylinders for larger or smaller arrays conforms to the pattern given in Figure 18. In general, each rod will be at a different temperature. The spacing between cylinders is assumed to be such that radiant exchange between rods more than four rows apart is negligible. Then, knowledge of the values of F_{12} , F_{13} , F_{15} , and F_{18} (defined in Chapter 4) will allow one to determine all the view factors between rods in the array. Thus, for example, $F_{1-7} = F_{12}$, $F_{14-31} = F_{13}$, $F_{29-53} = F_{15}$, and $F_{18-86} = F_{18}$. Elements of the F matrix for a 37-rod, or four-row, array are shown in Figure 19. Examination of the elements of F matrices for rod arrays of various numbers of cylinders (1, 7, 19, 37, 61, 91, 127, 169, 217, etc.) shows that a pattern exists for the location and magnitude of the nonzero elements. (A much larger array than that of Figure 19 is required to allow detection and definition of this pattern.) The observed pattern was programmed into the computer subroutine HEX, which can construct the F matrix for a hexagonal rod array of arbitrary size. The subroutine consists essentially of a large number of DO loops, each of which generates a portion of the matrix. For example, elements of the matrix in Figure 19 that have a left-hand superscript of 3 can be generated by the FORTRAN statements:

```

NROWS = 3
M(1) = 1
DO 1 I = 2, NROWS
1 M(I) = M(I - 1) + 6 * (I - 1)
DO 3 K = 2, NROWS

```

ORNL DWG 75-8475

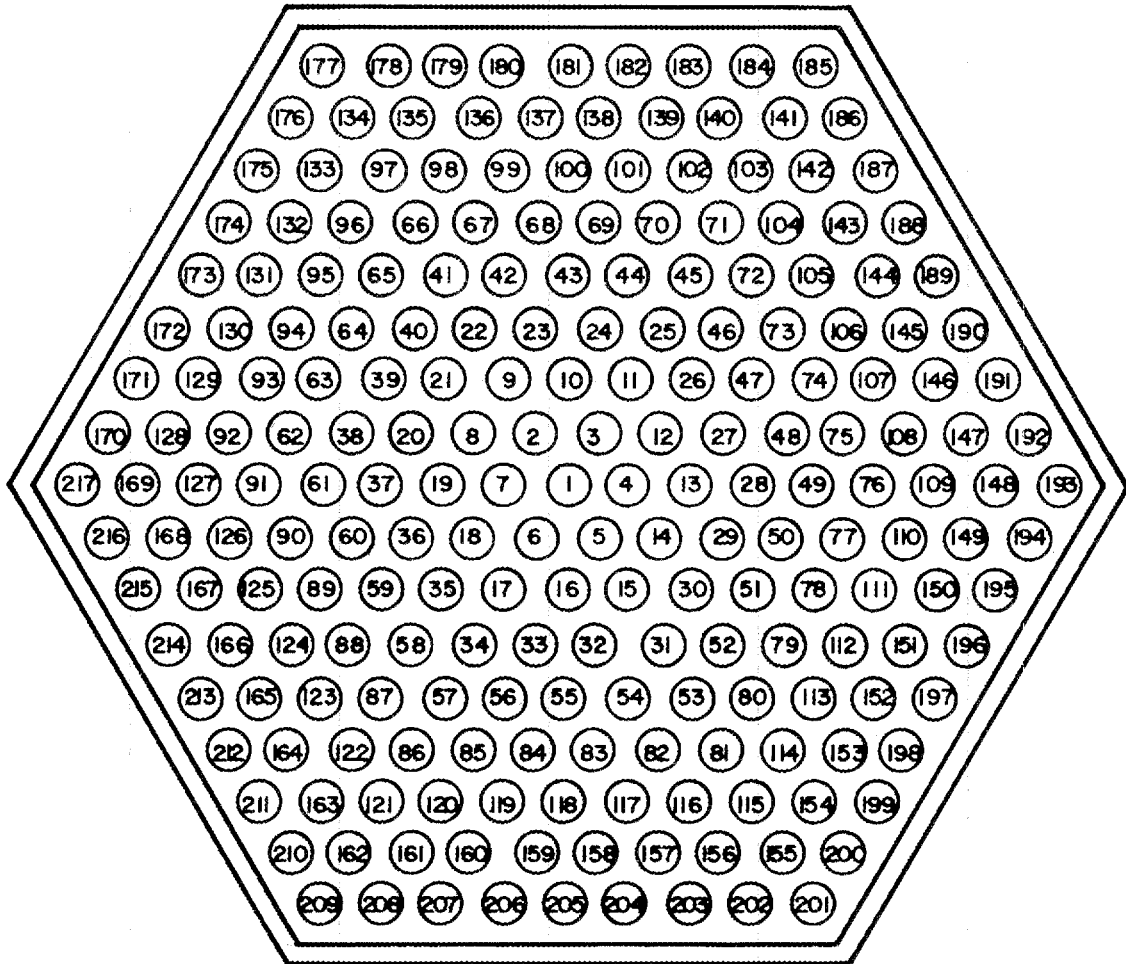


Figure 18. Numbering of Cylinders for a Hexagonal Array with Arbitrary Temperature Distribution.


```

I1 = M(K - 1) + 1
I2 = M(K) - 1
DO 3 I = I1, I2
  J = I + 1
  3 F(I,J) = F12

```

Other elements of the matrix are generated in a similar, although usually more complex, manner.

Once the $m \times m$ element matrix for the view factors between rods has been produced, the complete $n \times n$ matrix, which includes the interactions between the rods and shroud, is found by making use of the relations (n denotes shroud):

$$F_{in} = 1 - \sum_{j=1}^m F_{ij}, \quad i = 1, \dots, m$$

$$F_{ni} = \frac{A_i}{A_n} \cdot F_{in}, \quad i = 1, \dots, m$$

$$F_{nn} = 1 - \sum_{i=1}^m F_{ni}$$

Symmetrical Heat Flux Distribution

If the distribution of the heat fluxes is symmetrical such that rods at corresponding positions in the array have equal heat fluxes, the temperature distribution is also symmetrical. The surfaces may then be numbered as shown in Figure 20, where rods with the same number are considered as one surface of uniform temperature. The numbering of the cylinders for larger arrays follows the pattern set forth on Figure 20.

The motivation for regarding the condition of a symmetrical heat flux distribution as a special case is the large reduction in the number of

ORNL DWG 75-8476

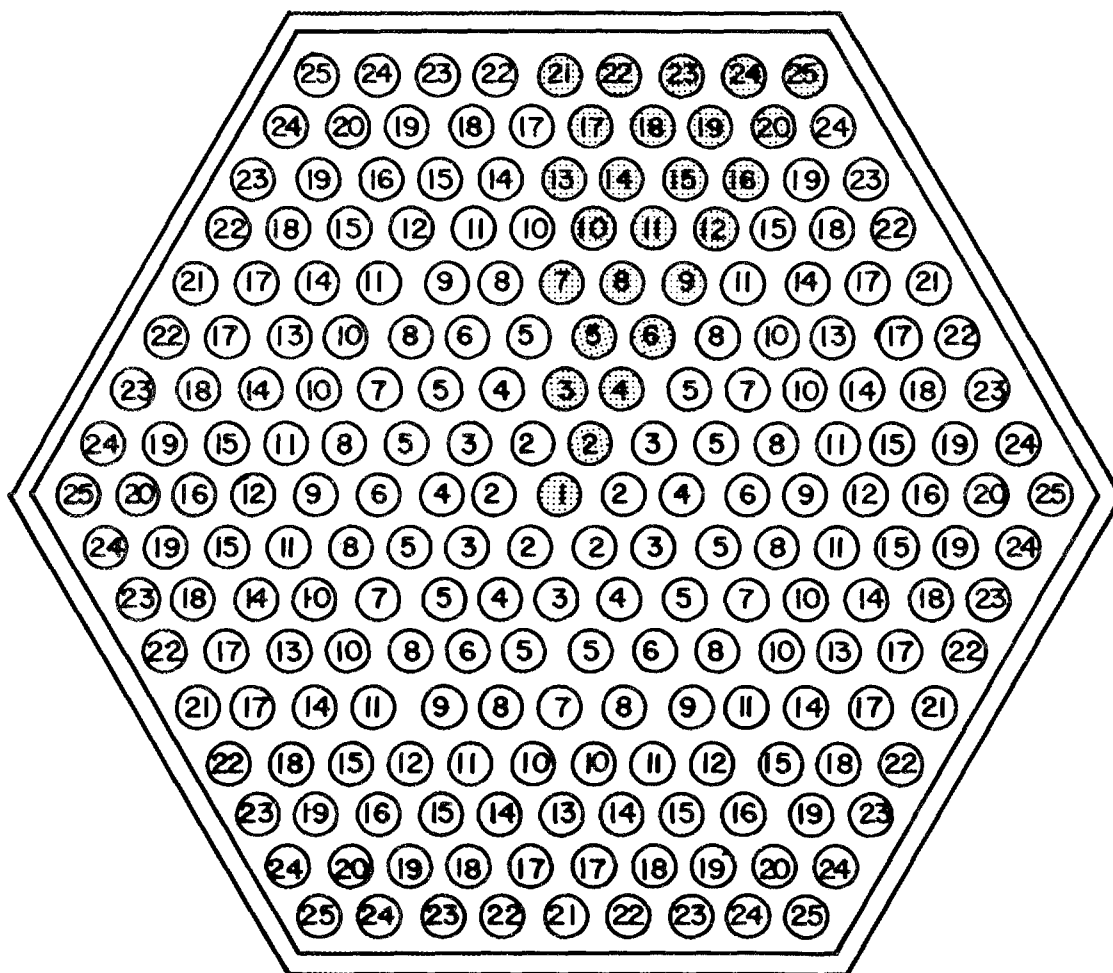


Figure 20. Designation of Cylinders for a Hexagonal Array with Symmetrical Temperature Distribution.

equations relative to the general case of an arbitrary distribution of heat fluxes. In the case of a 217-rod array there would be a reduction from 217 equations to only 25 equations, one equation for each surface in each instance. The savings in computing time is particularly significant in the solutions of unsteady-state problems where the integration of a large number of differential equations is involved. Since heat generation rates in nuclear fuel assemblies are usually nearly uniform across an assembly, symmetry does indeed exist.

If the radiation interchange between rods more than four rows apart is insignificant, knowledge of F_{12} , F_{13} , F_{15} , and F_{18} is sufficient to calculate all the view factors. For example, $F_{4-5} = 2 F_{12} + 2 F_{13}$ since each of the rods designated as 4, which together compose surface 4, has the same fraction ($2 F_{12} + 2 F_{13}$) of the radiation leaving it intercepted by rods in the grouping that comprises surface 5. The F matrix for a 91-rod array is shown in Figure 21. As before, a computer subroutine (HXSVM) was written to construct the F matrix for an arbitrary-size array from an inspection of the pattern of nonzero elements in the matrices for various-sized arrays.

II. SQUARE ARRAYS

Arbitrary Heat Flux Distribution

For square arrays with a nonsymmetrical temperature distribution, the use of a double-index notation as illustrated by Figure 22 greatly simplifies writing an algorithm to construct the matrix of view factors. Thus, one can write for rod (i,j) that $F_{(i,j)-(i-1,j)} = F_{12}$, $F_{(i,j)-(i-1,j+1)} = F_{13}$, and so forth. Radiation exchange between rods

	1	2	3	4	5	6	7	8	9	10	11	12
1		6F12	6F13		12F15			12F16				
2		2(F12+F13)	2(F12+F15)	F12+2(F13+F15)	2(F13+F15+F18)	2(F15+F18)	2(F15+F18)	2F15	2F18	2F18	2F18	
3			2F13	2(F12+F15+F18)	2(F12+F15+F18)	2F13	F13	2(F15+F18)	2F15	2(F15+F18)		2F18
4					2(F12+F13+F16)	F12+2F15		2(F13+F15+F18)		2F15	2(F15+F18)	
5					F12+F13+2F15	F12+F18	F12+F15+F18	F13+F13	F13+F15	F13+F18	2F15+F18	F15
6							2F13	2(F12+F15)	F12+2F18	2F15	2F13	
7								2(F12+F15)		2(F12+F18)	2F15	2F15
8								F13+2F18	F12	F12+F13+F15	F12+F15	F15+F18
9										2(F15+F15)	2(F12+F18)	F12
10										F12	F12+F15+F18	
11											F13	F12
12												

Only upper half of matrix is shown since

$$F_{ij} = \frac{A_j}{A_i} \cdot F_{ji}$$

Figure 21. Matrix of F_{ij} Values for a 91-Rod Hexagonal Array with a Symmetrical Temperature Distribution.

ORNL DWG. 75-8509

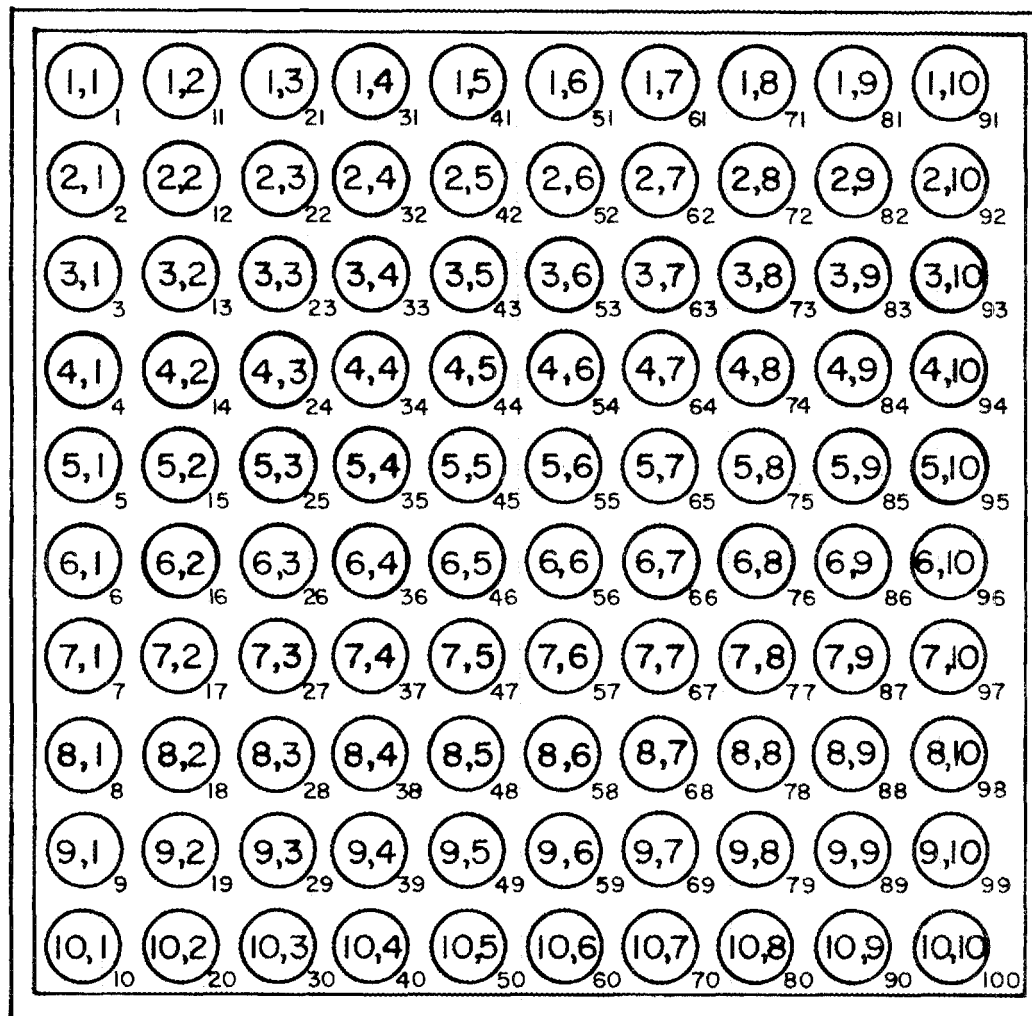


Figure 22. Numbering of Cylinders for a Square Array with Arbitrary Temperature Distribution.

more than three rows apart is assumed to be negligible (see Table II, p. 66, for the range of PDRs for which this assumption is valid). After the F matrix has been generated using a double-index notation for rod position (quadruple indexes for the view factors), a conversion is accomplished to achieve a single-index notation (shown outside the circles in Figure 22) for position and a double-index notation for the view factor. For instance, $F_{(7,4)-(7-5)}$ becomes F_{37-47} in the case of the array shown. This conversion is carried out to avoid the awkwardness that would arise in using double-index notation in the identification of the terms in the energy balance equations. For larger or smaller arrays, the single-index indication of rod position is similar to that shown in Figure 22 with cylinders numbered sequentially in column order. Construction of the F matrix for nonsymmetrical square arrays is performed by the computer algorithm SQUARE.

Symmetrical Heat Flux Distribution

Illustrations of the numbering sequences for rods in arrays with a symmetrical heat flux distribution are shown in Figures 23 and 24. Different numbering systems are required for arrays with an even number of rows and those with an odd number of rows because of the different symmetry for such arrays. Construction of the F array is accomplished by subroutine SQSYM, which incorporates the pattern observed from an examination of the matrices for a number of array sizes. Subroutine SQSYM is valid for both even- and odd-rowed arrays which have rod spacings such that radiation between rods more than three rows apart is negligible.

ORNL DWG 75-8477

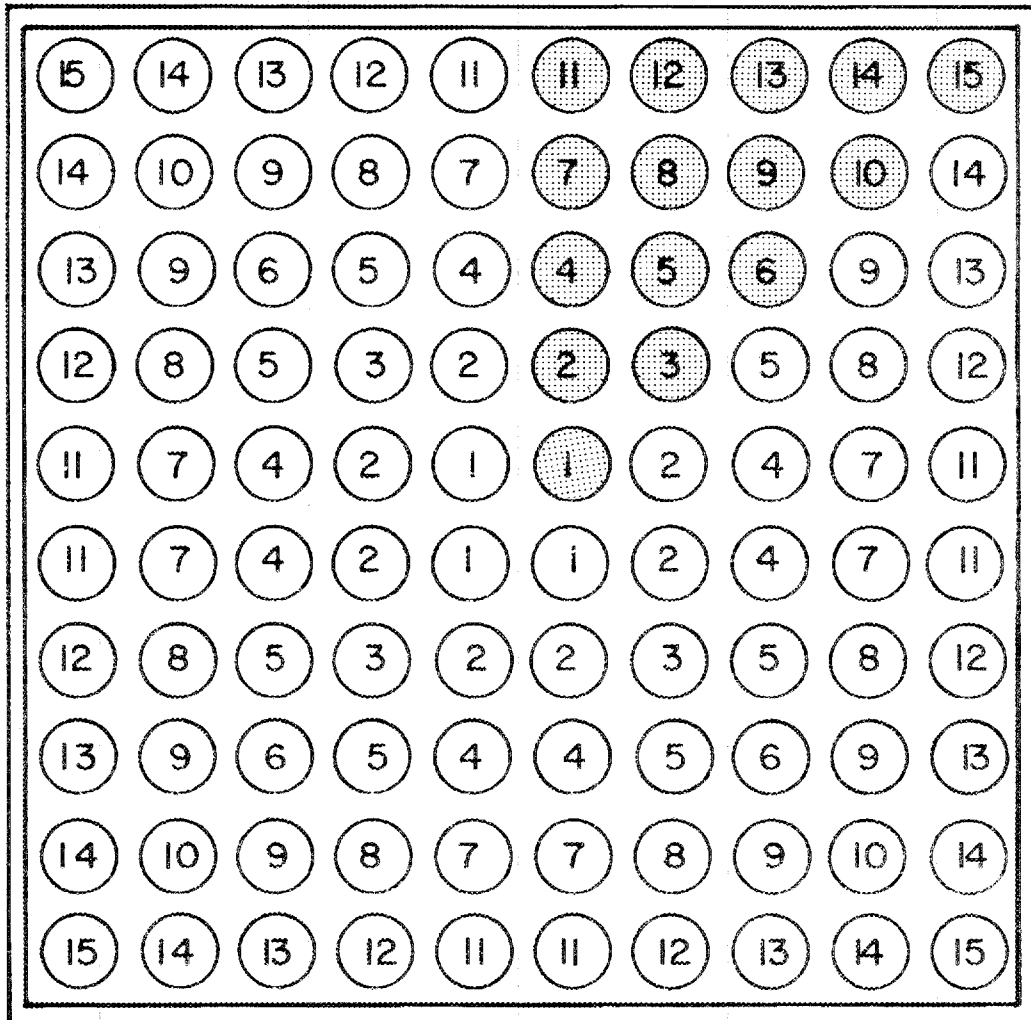


Figure 23. Designation of Cylinders for a Square Array with Symmetrical Temperature Distribution and an Even Number of Rows.

ORNL DWG 75-8478

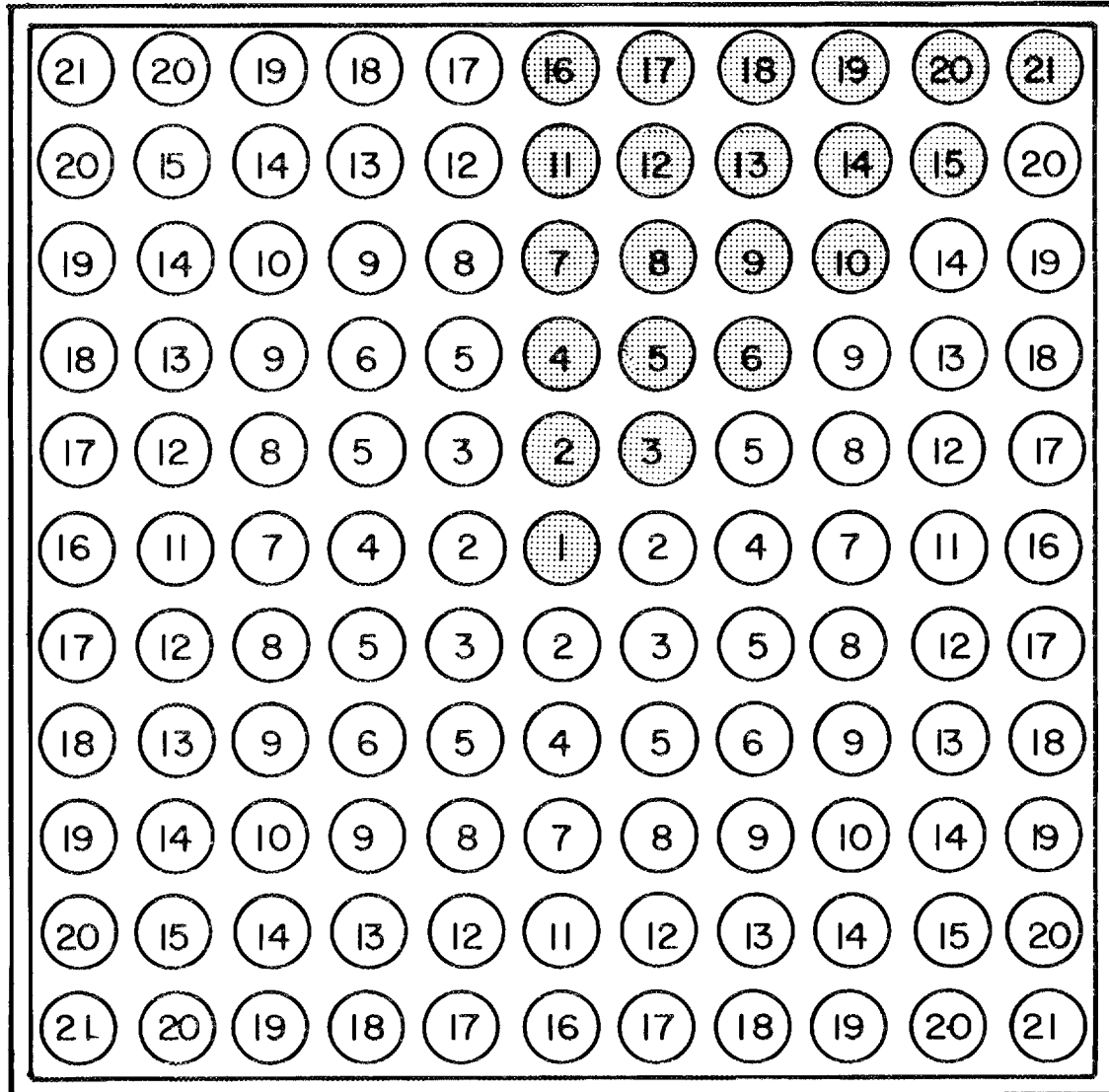


Figure 24. Designation of Cylinders for a Square Array with Symmetrical Temperature Distribution and an Odd Number of Rows.

CHAPTER 6

THEORETICAL RESULTS

I. STEADY STATE

Equations (37) of Chapter 3:

$$\sum_{j=1}^m (F_{ij} - \delta_{ij}) Z_j = -X_i, \quad i = 1, \dots, m \quad (37)$$

which are the dimensionless steady-state equations for a rod array with a constant shroud temperature can be written in the form:

$$\sum_{j=1}^m B_{ij} Z_j = C_i, \quad i = 1, \dots, m \quad (83)$$

where

$$B_{ij} = F_{ij} - \delta_{ij}$$

and

$$C_i = -X_i.$$

Now $B_{ii} = -1$ for $i = 1, \dots, m$ since $F_{ii} = 0$ as the rods are convex and cannot see themselves. Further,

$$\sum_{\substack{j=1 \\ j \neq i}}^m B_{ij} = \sum_{\substack{j=1 \\ j \neq i}}^m F_{ij} = 1 - F_{ii} - F_{in} \leq 1.$$

It follows that

$$|B_{ii}| \geq \sum_{\substack{j=1 \\ j \neq i}}^m |B_{ij}| \quad \text{for } i = 1, \dots, m$$

which is a sufficient condition for convergence to a solution of Equations (83) using Gauss-Seidel iteration. A complete description of the Gauss-Seidel method and its computer implementation may be found in references (21) and (22).

The computer algorithm STEADY was written to solve the steady-state problem. The program proceeds by first determining the view factors F_{12} , F_{13} , F_{15} , and the pseudo view factor F_{18}^* using subroutine EQVIEW for rods on an equilateral triangular pitch or subroutine SQVIEW for rods on a square pitch. The complete array of view factors F is then constructed using HEX, HXSYM, SQUARE, or SQSYM, depending on whether the array configuration is hexagonal or square and whether the distribution of rod heat fluxes is symmetrical or nonsymmetrical. The pseudo view factor F_{18}^* is used in constructing the F array rather than the true view factor F_{18} in order to take into account all the radiation leaving a rod as explained in Chapter 4. Finally, subroutine SIMEQ employs Gauss-Seidel iteration to solve Equations (37) to obtain the dimensionless variables Z_j from which the temperature values T_j are determined. An annotated listing of the computer program STEADY including a description of the necessary input data is given in Appendix D.

It is now of interest to consider the case in which the heat flux is the same for all the rods ($X_i = 1$ for $i = 1, \dots, n$) and all surfaces have the same emissivity. In such a case, Equations (37) become

$$\sum_{j=1}^m (F_{ij} - \delta_{ij}) Z_j = -1, \quad i = 1, \dots, m \quad (84)$$

where

$$Z_j = Y_j - \left(\frac{1 - \epsilon}{\epsilon}\right) \left(1 + \frac{m A_1}{A_n}\right).$$

An examination of Equations (84) shows that the values of the Z_j are functions only of the geometry. The use of the dimensionless variables Z_j then permits a highly compact presentation of the variation of temperature with array configuration, array size, PDR, heat generation rate, and emissivity. Figures 25 through 27 show the dependence of Z_1 (from which the center-rod temperature T_1 can be found) on PDR for various sizes of hexagonal arrays of cylinders on an equilateral triangular pitch. Similar results are presented in Figures 28 through 30 for square arrays of rods on a square pitch. The ranges of PDR values considered in Figures 25 through 30 correspond to those for which it is reasonable to assume that radiant exchange between rods more than three rows (square pitch), or four rows (triangular pitch), apart is negligible.

For spent nuclear fuel assemblies the heat flux Q_1/A_1 is dependent on the radioactive decay heat release rate which is determined from a knowledge of the fuel composition, conditions and period of irradiation in the reactor, and time elapsed since removal from the reactor. The temperature of the shroud T_n can be calculated from an independent energy balance which equates the heat generated within the rod array to that dissipated by the shroud to the surroundings. Emissivities of the surfaces must either be measured experimentally or estimated from literature values. The number of rods in the array, m , and the ratio of the surface area of a single rod to that of the sheath, A_1/A_n , are, of course, geometrical parameters. If the shroud is located at a distance $P - D$ ($P =$ pitch of the rods) from the last row of rods,

ORNL DWG 75-8479

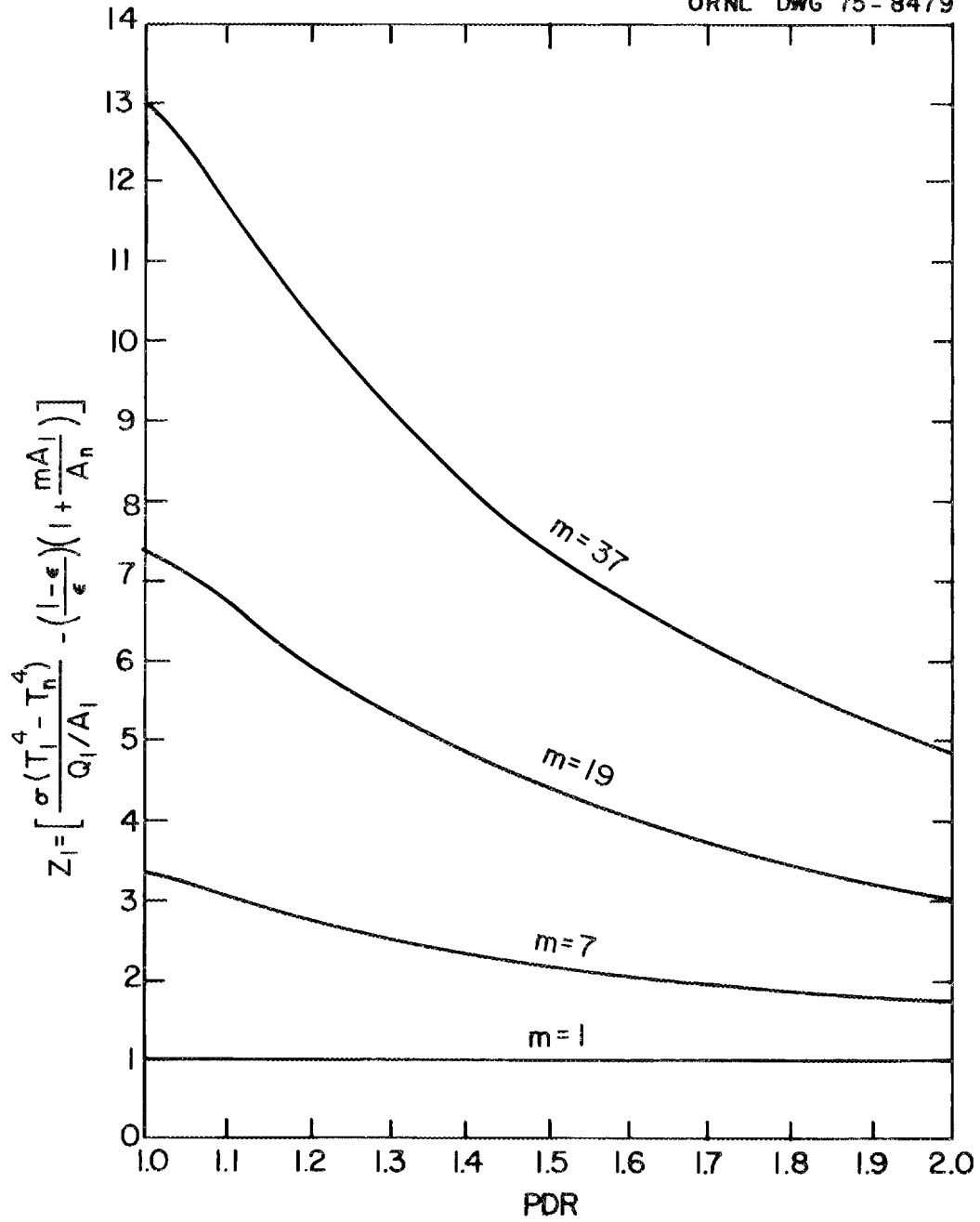


Figure 25. Center-Rod Temperatures for Hexagonal Arrays of 1, 7, 19, and 37 Cylinders.

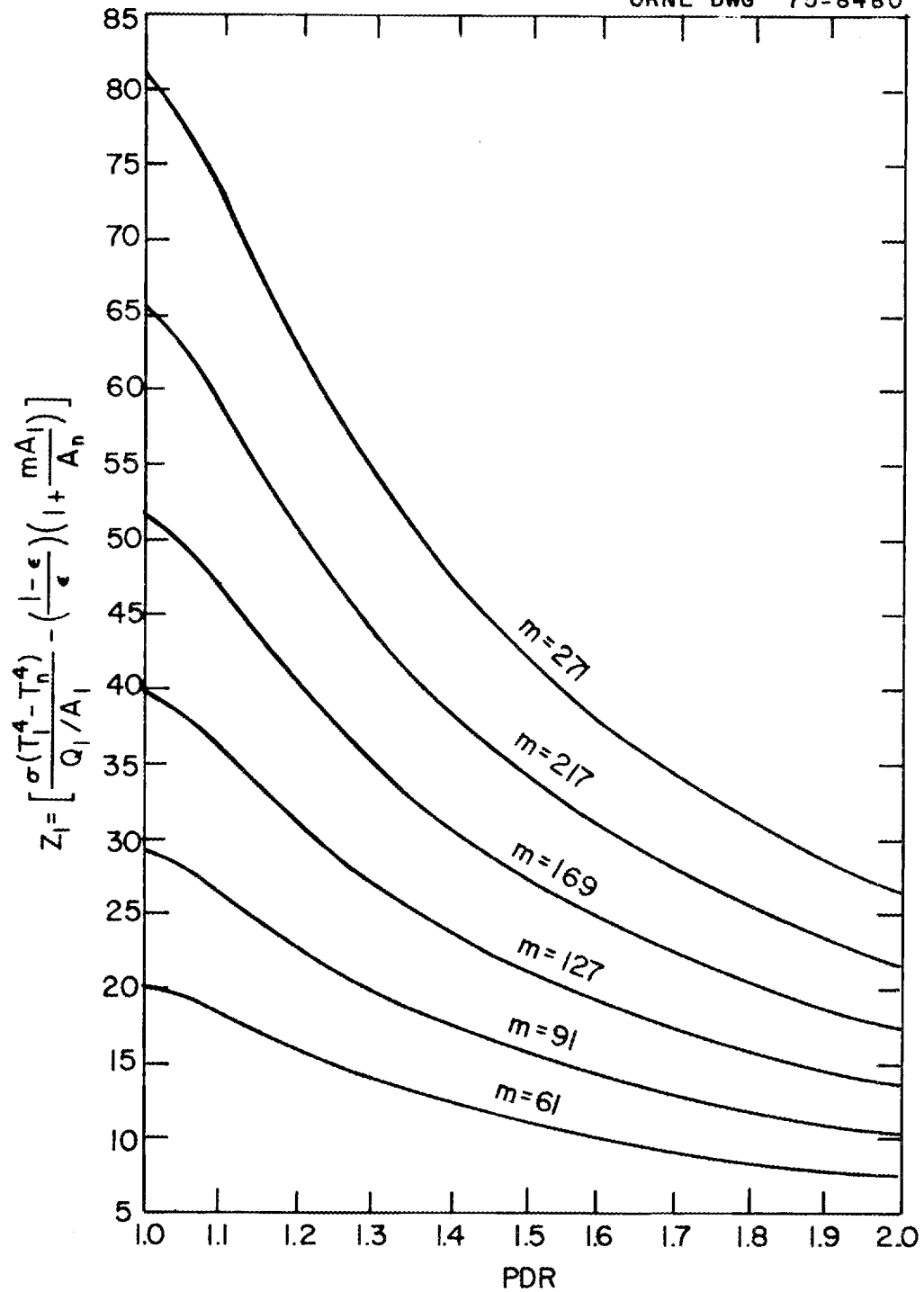


Figure 26. Center-Rod Temperatures for Hexagonal Arrays of 61, 91, 127, 169, 217, and 271 Cylinders.

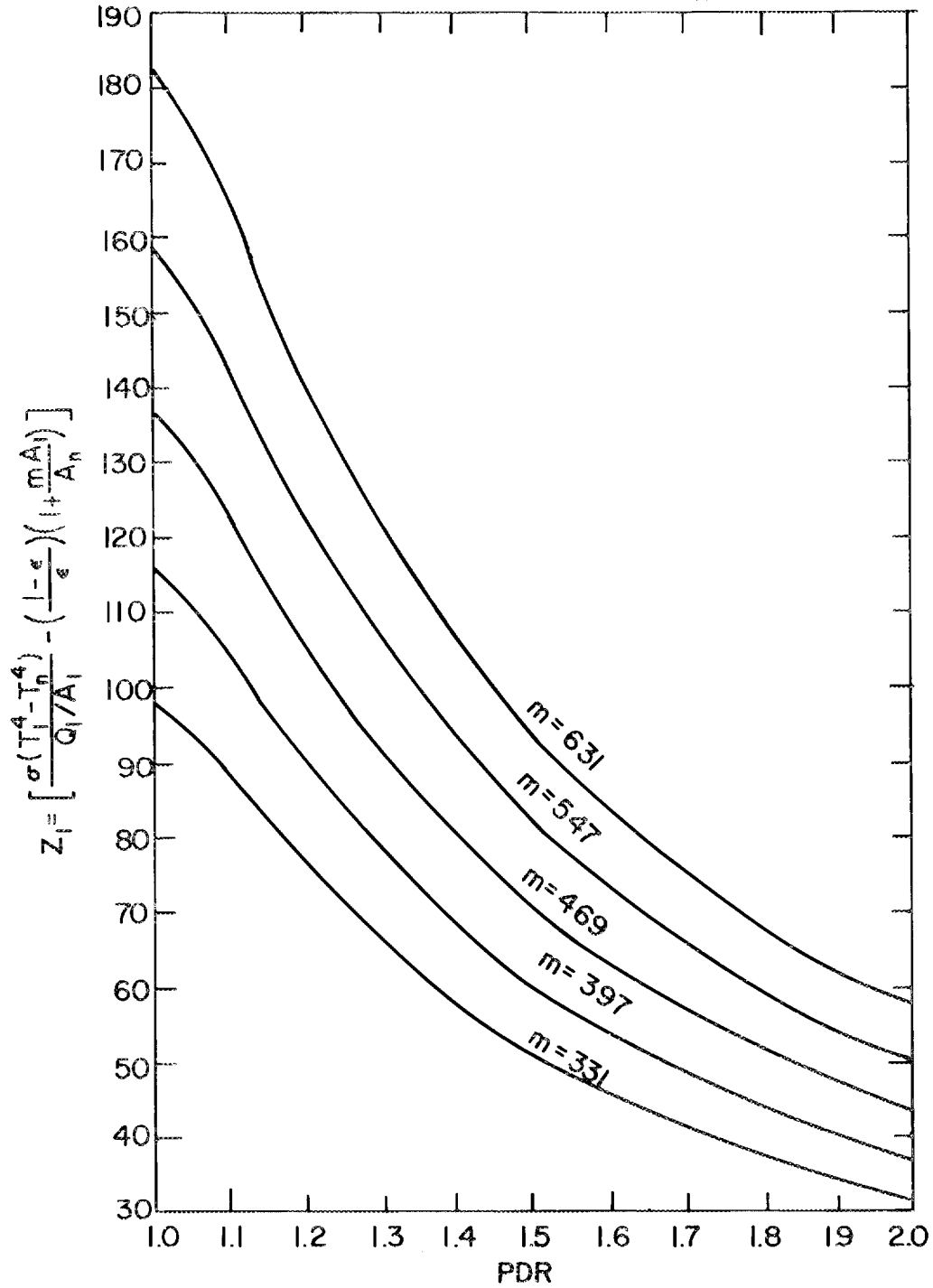


Figure 27. Center-Rod Temperatures for Hexagonal Arrays of 331, 397, 469, 547, and 631 Cylinders.

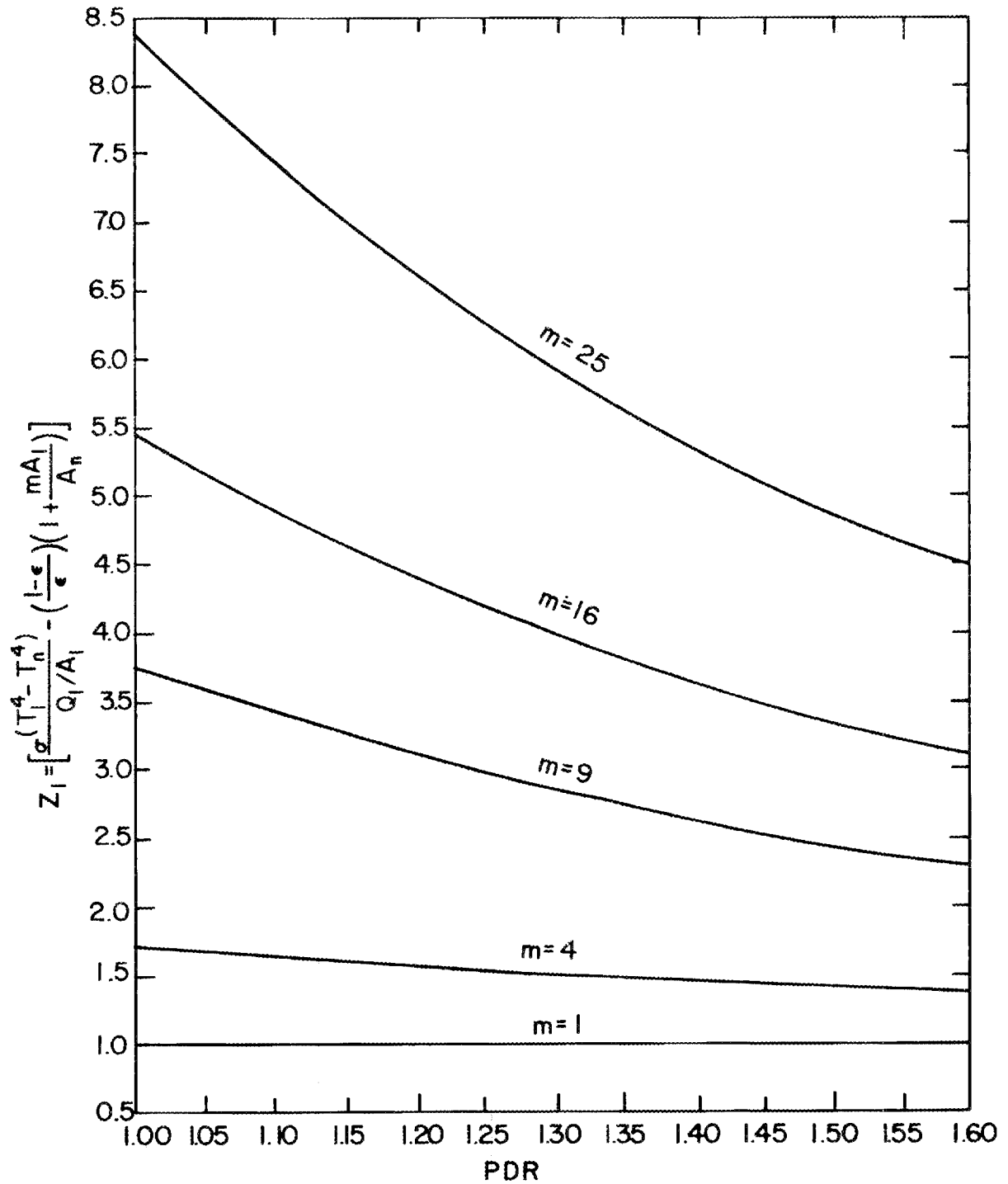


Figure 28. Center-Rod Temperatures for Square Arrays of 1, 4, 9, 16, and 25 Cylinders.

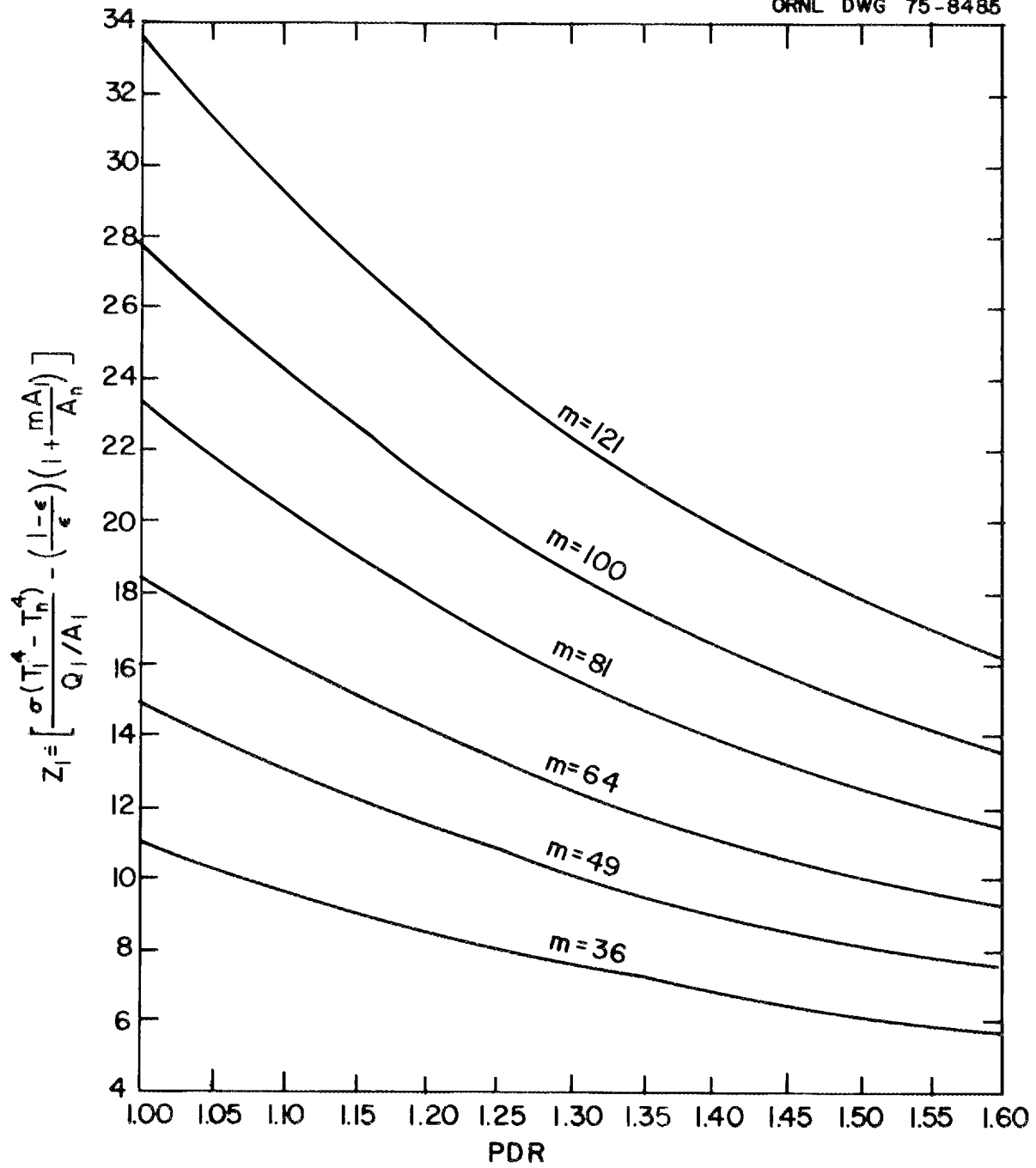


Figure 29. Center-Rod Temperatures for Square Arrays of 36, 49, 64, 81, 100, and 121 Cylinders.

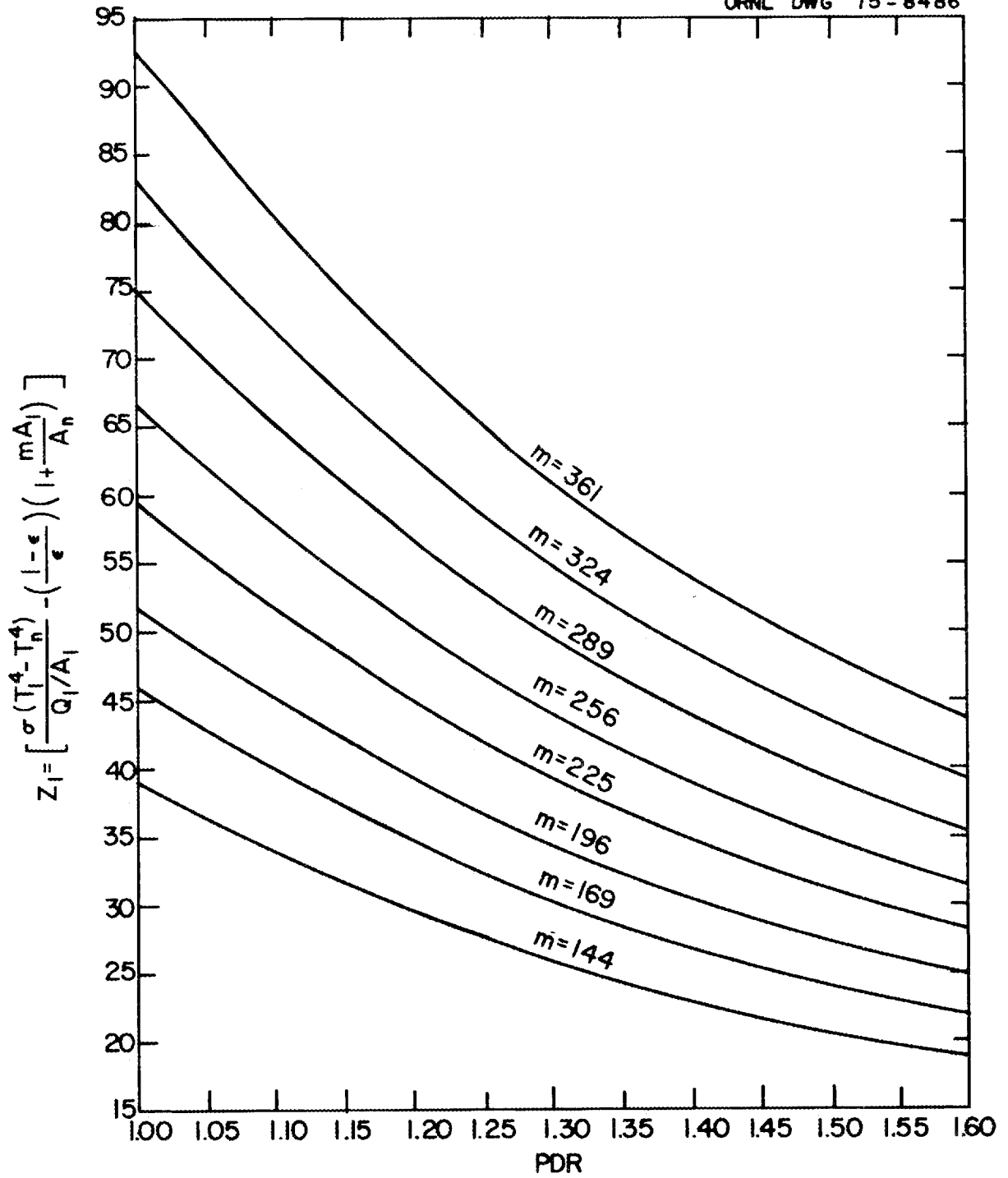


Figure 30. Center-Rod Temperatures for Square Arrays of 144, 169, 196, 225, 256, 289, 324, and 361 Cylinders.

$$\frac{A_1}{A_n} = \frac{\pi}{2\sqrt{3}} \cdot \frac{1}{[2 + \sqrt{3} (\text{NROWS}-1)]\text{PDR} - 1}$$

for hexagonal arrays and

$$\frac{A_1}{A_n} = \frac{\pi}{4[(\text{NROWS}+1)\text{PDR} - 1]}$$

for square arrays, where NROWS is the number of rows of rods. For unshrouded arrays the shroud may be considered to be located at infinity so that $A_1/A_n = 0$.

If it were desired to take into account the variation of the emissivities with temperature, it would be necessary to modify STEADY to solve Equations (37) in an iterative manner. The procedure would be to specify trial values for the emissivities of each of the surfaces, solve the set of equations for the temperature values, and calculate new emissivity values based on these temperatures. A new set of temperatures could then be obtained by resolving Equations (37) and these steps could be repeated until the temperatures converged.

II. UNSTEADY STATE

It was shown in Chapter 3 that the unsteady-state equations for a rod array with a constant-temperature shroud could be couched in terms of dimensionless variables as

$$\frac{dY_i}{d\theta} = 4(Y_i + w)^{3/4} \left[X_i + \sum_{j=1}^m (\mathfrak{F}_{ij} - \delta_{ij} \epsilon_i) Y_j \right], \quad i = 1, \dots, m \quad (38)$$

where the dimensionless time θ is defined as

$$\Theta = \frac{t\sigma A}{\rho V c} \left(\frac{Q_k/A_k}{\sigma} \right)^{3/4}$$

and the parameter W is defined as

$$W = \frac{\sigma T_n^4}{Q_k/A_k}.$$

Solution of Equations (38) for the Y_i as a function of Θ requires the numerical integration of a set of first-order differential equations, which was performed using Hamming's modified predictor-corrector method. This method is a stable fourth-order procedure that requires evaluation of the right-hand side of the differential equations twice during each step. A fourth-order procedure using Runge-Kutta-Gill integration, which requires four evaluations per step, was also tried but was found to be much slower for the same accuracy. The integration routine used was supplied by International Business Machines (IBM) in its System/360 Scientific Subroutine Package. An explanation of the predictor-corrector method and a description of this subroutine (DHPCG) are given in a recent IBM publication (16), while a more-detailed exposition of the mathematics may be found in references (13), (22), and (25).

Integration of Equations (38) first requires computation of the gray-body view factor matrix \mathfrak{F} using the equations derived in Chapter 2:

$$\sum_{k=1}^n \left[F_{ik} \left(\frac{1 - \epsilon_k}{\epsilon_k} \right) - \frac{\delta_{ik}}{\epsilon_k} \right] \mathfrak{F}_{kj} = -F_{ij} \epsilon_j, \quad i = 1, \dots, n; \quad j = 1, \dots, n \quad (28)$$

which may be written more compactly as

$$\sum_{k=1}^n B_{ik} \mathfrak{F}_{kj} = C_{ij}, \quad i = 1, \dots, n; \quad j = 1, \dots, n \quad (85)$$

where

$$B_{ik} = F_{ij} \left(\frac{1 - \epsilon_k}{\epsilon_k} \right) - \frac{\delta_{ik}}{\epsilon_k}$$

and

$$C_{ij} = -F_{ij} \epsilon_j .$$

Equations (85) represent n^2 relations in the form of n sets of n simultaneous linear algebraic equations which must be solved in order to define the n^2 values of \mathfrak{F}_{ij} . Gaussian elimination with pivoting as incorporated in the subroutine MATQ is employed to perform this task. MATQ is basically an algorithm developed at the Oak Ridge National Laboratory with further modifications suggested by Kee (18) to improve its speed. Discussions of the theory and programming of Gaussian elimination are available in references (21) and (22).

The computer program TRANS uses DHPCG, MATQ, and other subroutines, as required, to solve Equations (38) for the Y_i as a function of θ . Calculated results are presented in Figure 31 for a 217-rod array with equal heat generation in each of the rods and an initially flat temperature profile ($T_i = T_n$, $i = 1, \dots, m$ at $t = 0$ so that $Y_i = 0$, $i = 1, \dots, m$ at $\theta = 0$). The parameter W reflects the influence of the initial temperature level. For an array of the specified geometry and emissivity, Figure 31 can be used to find the variation of the center-rod temperature T_1 with time t for any heat generation rate, rod properties, and initial temperature level in the range of the parameters. The solution of unsteady-state

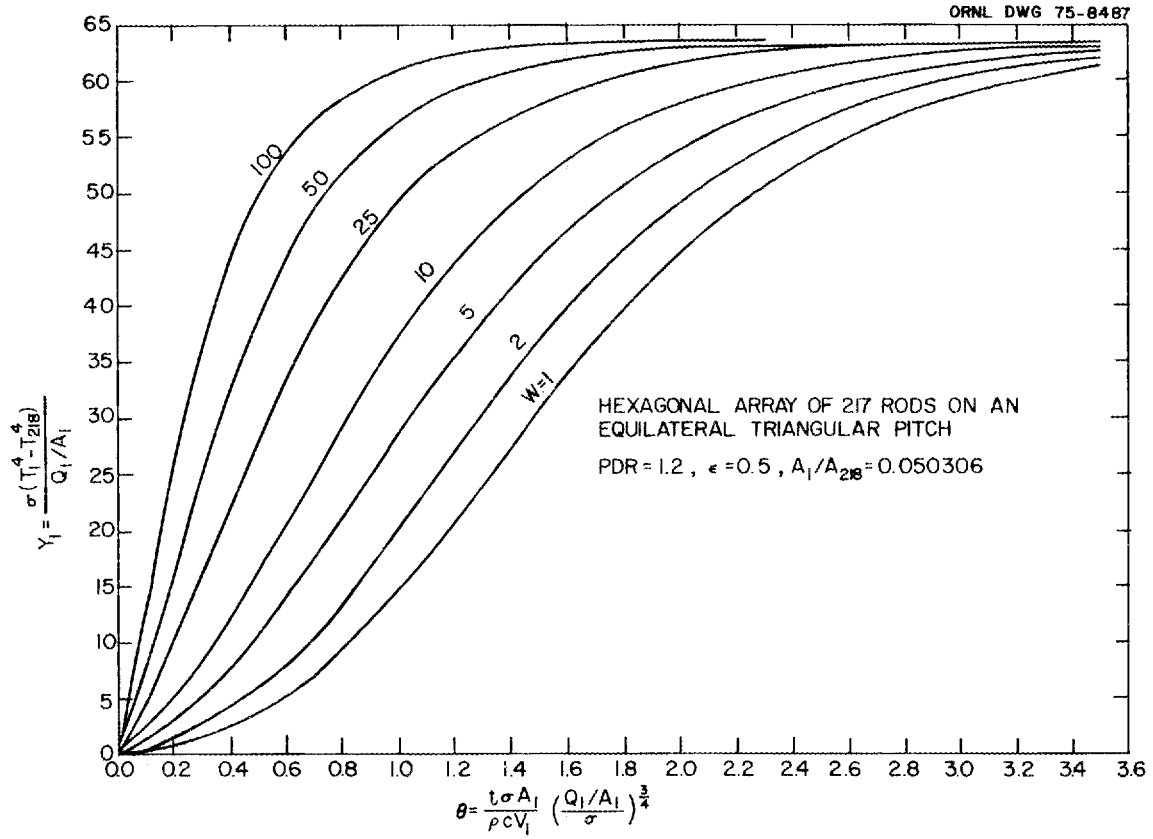


Figure 31. Unsteady-State Solution for Center-Rod Temperature.

problems for large rod arrays with nonsymmetrical heat generation rates quickly becomes impractical because of the excessive computer memory and computer execution time needed. Thus, the results of Figure 31 required the numerical integration of 25 simultaneous differential equations, while 217 equations would be necessary for the same array if the distribution of heat fluxes were nonsymmetrical. A listing of TRANS is given in Appendix D.

As pointed out previously, it is likely that the physical situation for unsteady-state problems of interest will be such that the shroud temperature is not constant. In such a case, it would be a simple matter to return to Equations (30) and to modify TRANS in order to deal with these problems. The absence of a constant shroud temperature precludes formulation of the equations in a useful dimensionless form, but it does not affect the ability to obtain solutions of these problems with only slight modification of the algorithms presented.

III. PREVIOUS WORK

Very few analyses of radiative heat transfer in rod clusters are presented in the literature. Pieczynski and Stewart (24) studied heat transfer in a hexagonal array of 7 rods using Hottel's method, while Fisher and Cowin (6) investigated a one-ring cluster of 6 rods, a two-ring cluster of 18 rods (rings of 6 and 12 rods), and a three-ring cluster of 36 rods (rings of 6, 12, and 18 rods) using the net radiation method. Evans (4) also chose the net radiation method to analyze square arrays of 49 and 64 rods. Each of these analyses, however, is restricted to writing out and solving the equations for the problem under consideration. None of the

authors presents a scheme that is useful for treating arbitrary-sized arrays in a general manner.

The most sophisticated analysis to date appears to be that presented by Watson (37) in his investigation of radiation exchange among rods on a square pitch in a square array. The calculational scheme evolved by Watson permits solution for any array which has equal heat generation in each of the rods. Hottel's method is used with Equation (24) written in the form:

$$T_i^4 = \frac{\frac{Q_i}{A_i \sigma} + \sum_{j=1}^n \mathfrak{F}_{ij} T_j^4}{\sum_{j=1}^n \mathfrak{F}_{ij}}, \quad i = 1, \dots, n$$

for each of the radiating surfaces, and these equations are solved by trial and error. The \mathfrak{F}_{ij} values required in the analysis are estimated from the empirical equation (all surfaces assumed to have the same emissivity):

$$\mathfrak{F}_{ij} = \frac{1}{\frac{1}{F_{ij}} + 2\left(\frac{1}{\epsilon} - 1\right)}.$$

This relation for the \mathfrak{F}_{ij} , although exact for $\epsilon = 1$, yields results which are increasingly in error [measured by comparison with the exact values of \mathfrak{F}_{ij} found using Equations (28)] as the emissivity of the surfaces decreases. The above equation overestimates the values of the \mathfrak{F}_{ij} with the consequence that the predicted values of temperature are too low.

The usefulness of framing the energy equations in terms of dimensionless variables has been overlooked by previous investigators.

Salmon (27), however, employed a dimensional variable which is equivalent to the dimensionless variable Y as defined here divided by the Stefan-Boltzmann constant σ . He used Watson's computer algorithm (37) to generate values of this variable for various PDRs and array sizes in a study of heat transfer in square fuel elements.

CHAPTER 7

EXPERIMENTAL

I. EXPERIMENTAL APPARATUS

Experimental temperature measurements were made for two 217-tube hexagonal arrays of differing PDRs. Table III lists the important geometrical characteristics of the two arrays, while Figure 32 is a photograph of one of the mock fuel elements prior to final assembly. Spacing between the tubes was accomplished by wrapping each tube with spiral-wound wire. One end of each tube was welded to a tube sheet as shown in Figure 33; the other end was plugged. The entire assembly was installed in a section of schedule 40 stainless steel pipe 10 in. in diameter and 17 ft long with the tube sheet forming one end of the closed pipe. The assembly was supported within the pipe by three-legged centering supports spaced to eliminate sagging. Figure 34 is a photograph of the test vessel.

Thermocouples and electrical heaters were inserted into the tubes at the tube sheet face. Electrical rod heaters were placed in 205 of the tubes to simulate heat generation by radioactive decay. The specifications of the heaters are shown in Figure 35. The heaters were arranged in 14 parallel circuits. Thirteen of the circuits consisted of three parallel groups of five heaters in series, while the remaining one contained two parallel groups of five heaters in series. The current to each circuit was monitored, and the current through each heater was calculated on the assumption of equal distribution of current between groups. The

TABLE III

Geometrical Characteristics of Experimental Arrays

Characteristic	Apparatus 1	Apparatus 2
Tubes (304 L stainless steel)		
Number	217	217
Outside diameter, in.	0.25	0.25
Wall thickness, in.	0.016	0.035
Pitch, in.	0.341	0.31
PDR	1.364	1.240
Total length, in.	138	138
Heated length, in.	47.5	47.5
Surface area per foot, in. ²	9.425	9.425
Metal cross-sectional area, in. ²	0.01176	0.02364
Wire wrap (304 L stainless steel)		
Diameter, in.	0.091	0.060
Spiral pitch, in.	8	8
Surface area per foot of tube, in. ²	3.890	2.537
Cross-sectional area, in. ²	0.006504	0.002827
Sheath (304 L stainless steel)		
Inside distance across flats, in.	5.160	4.670
Wall thickness, in.	0.125	0.125
Inside surface area per foot, in. ²	214.5	194.1
Metal cross-sectional area, in. ²	2.288	2.076

PHOTO 93753A

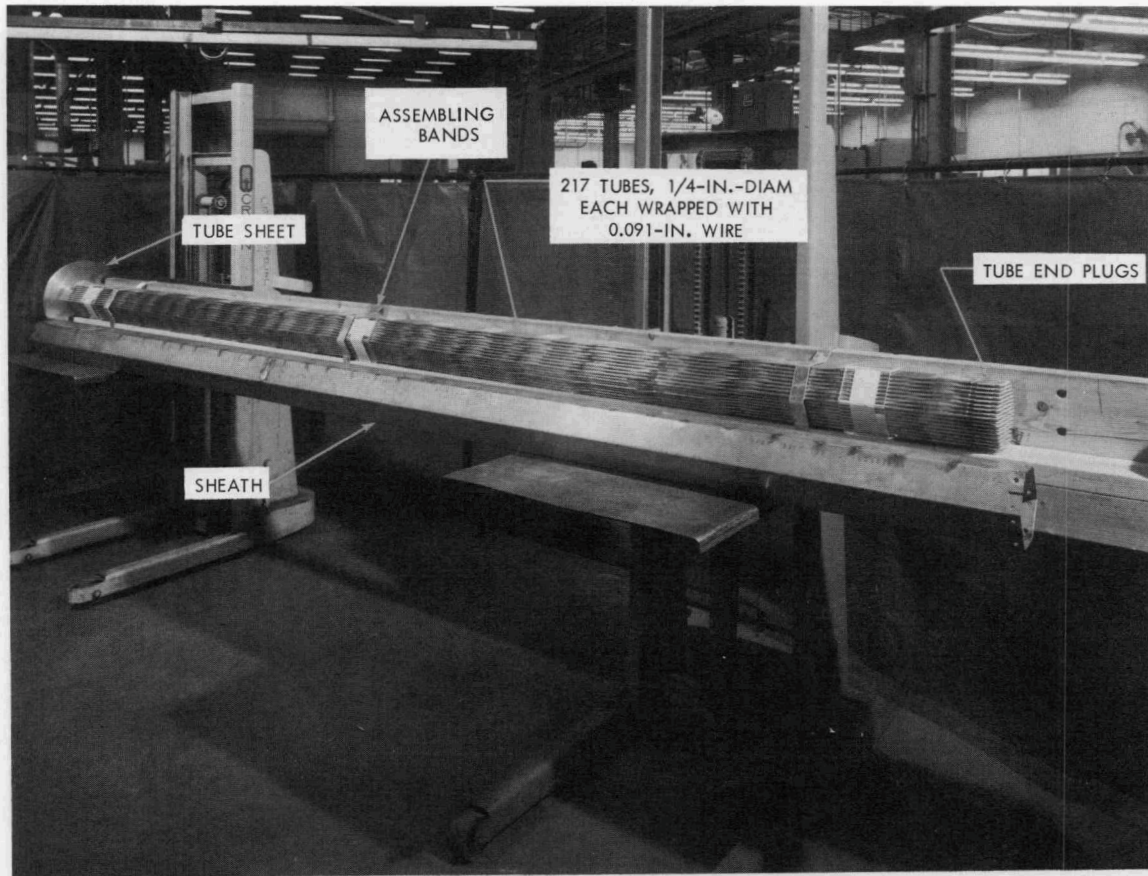


Figure 32. Tube Bundle and Sheath Prior to Assembly and Insertion into Test Vessel.

PHOTO 93752A1

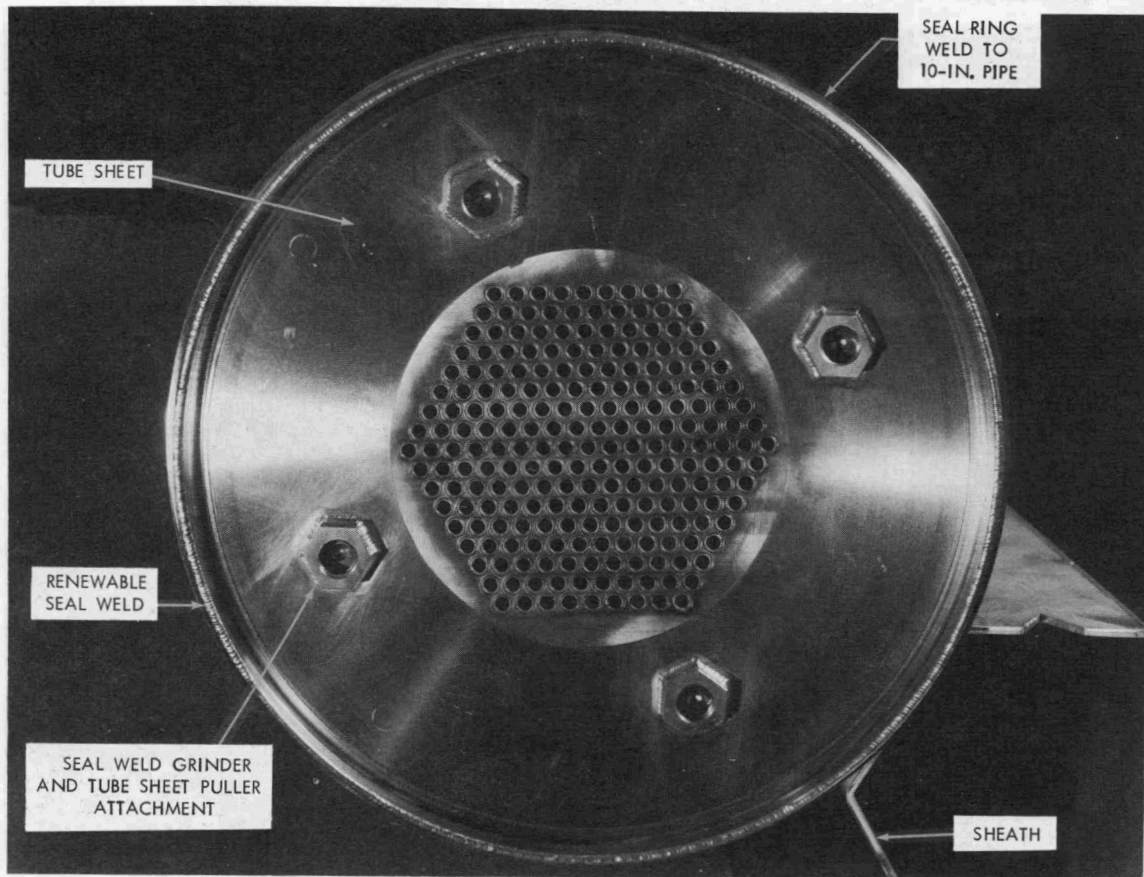


Figure 33. Tube Sheet.

PHOTO NO. 76911 A1

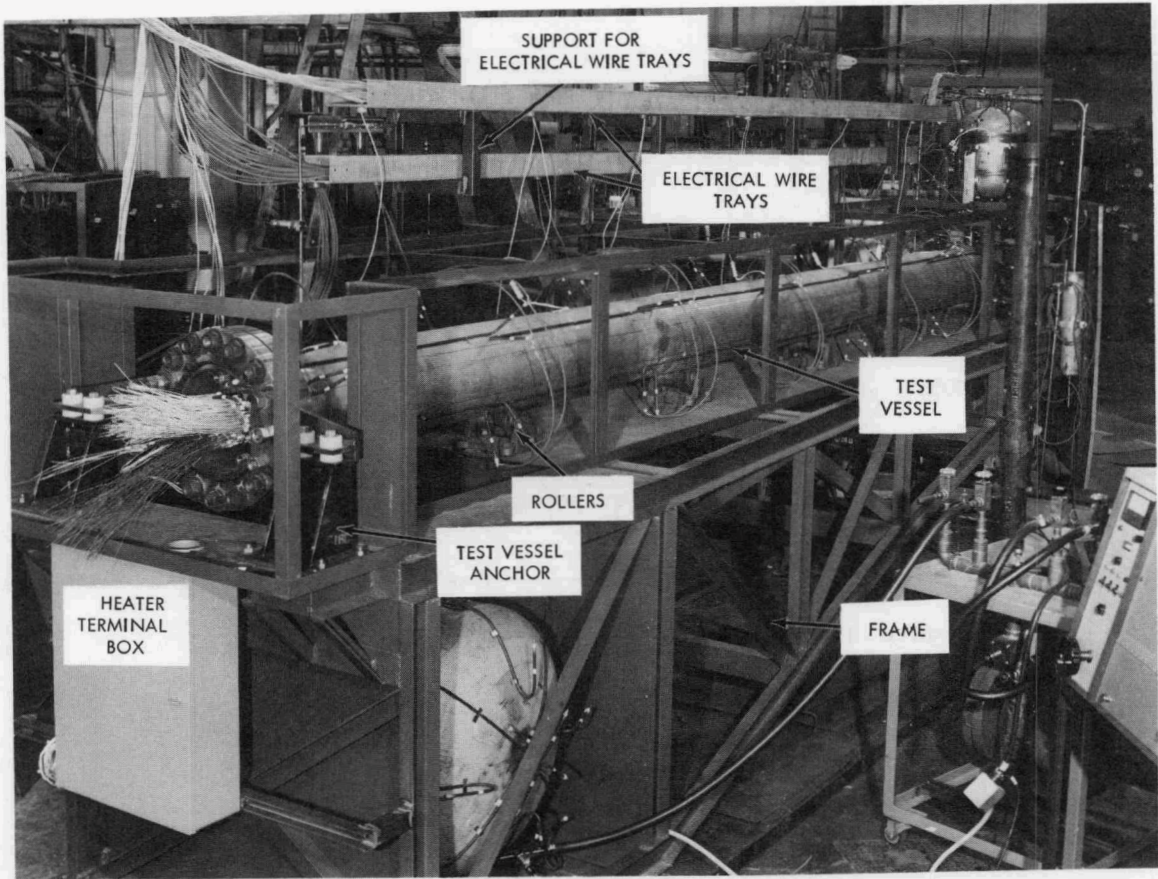


Figure 34. Test Vessel.

ORNL DWG 75 - 8488

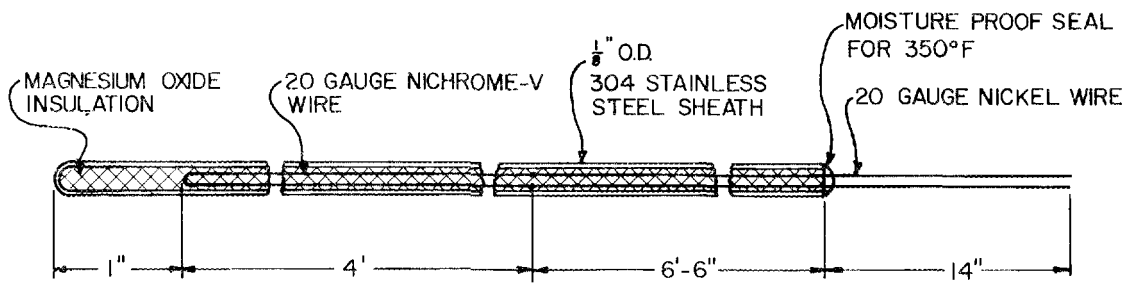


Figure 35. Specifications of Electrical Heaters.

power dissipated in the Nichrome portion of each heater was the product of the square of the current through the heater and the electrical resistance of the length of Nichrome. The resistivity of Nichrome V is essentially constant at 113.5×10^{-8} ohm-meter over a temperature range of 800 to 1400°F.

One-eighth-inch-diameter Chromel-Alumel thermocouples were inserted in the remaining 12 tubes. These thermocouples could be moved up and down the length of the tubes to measure the axial temperature profile. In addition, four fixed thermocouples were located on the outside of the hexagonal sheath at the axial position corresponding to the centerline of the heated zone. The specifications stipulated when thermocouples were purchased allowed a maximum error of $\pm 4^\circ\text{F}$ at temperatures up to 525°F. At higher temperatures, the maximum permissible error was 0.75% of the temperature. The usual variance of the thermocouples from true values was found to be far less than that allowed by the specifications. Positions of the tube thermocouples as well as those on the sheath are shown in Figure 36.

II. TEST CONDITIONS AND EXPERIMENTAL DATA

In order to reduce the contributions of energy transfer by gaseous natural convection and conduction to negligible values, the test vessel was evacuated and the experiments were performed under vacuum. The test procedure consisted of adjusting the power input to attain the desired center tube temperature, allowing the temperatures to reach their steady-state values, and recording the thermocouple, voltage, and current values. It was necessary to reposition the tube thermocouples several times during

ORNL DWG 75-8489

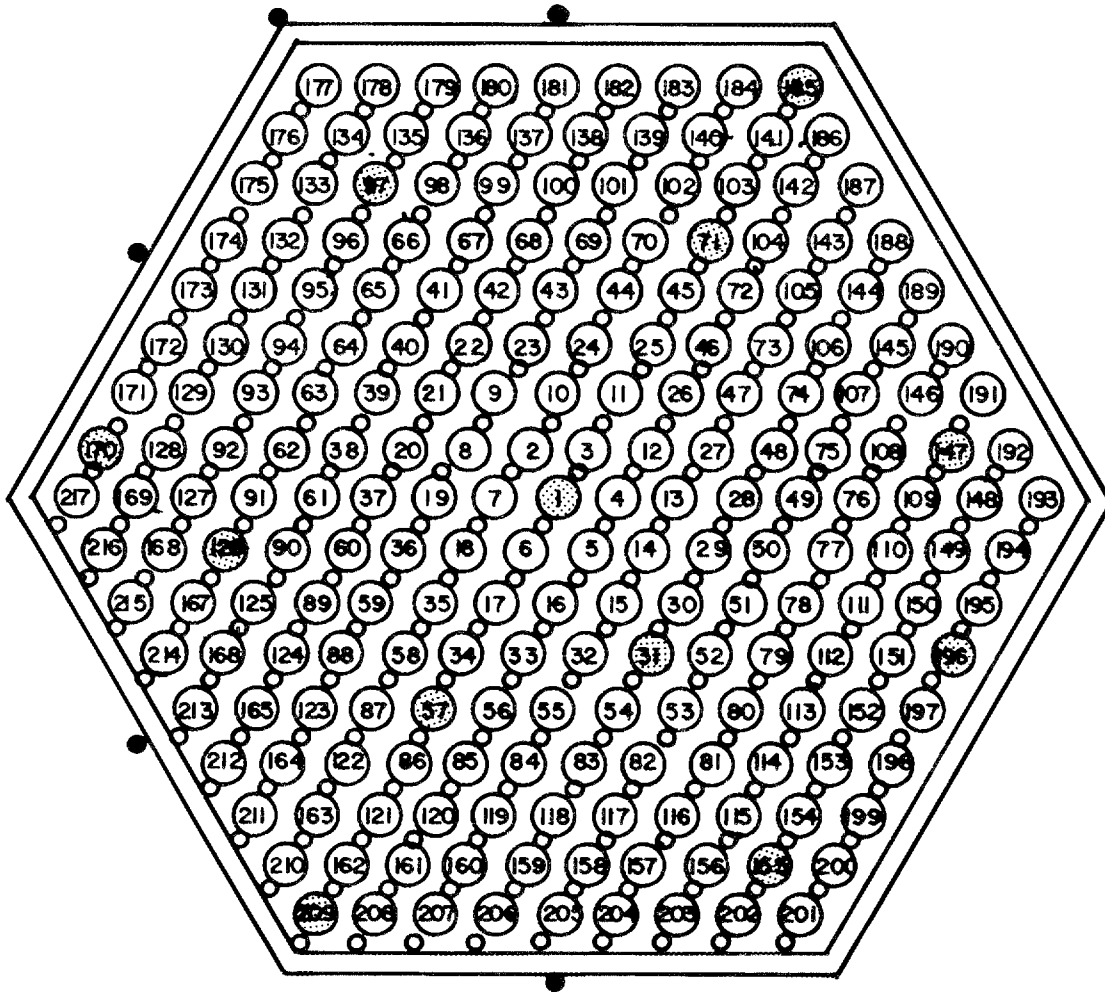


Figure 36. Cross Section of Experimental Array Showing Positions of Thermocouples.

each run in order to measure the axial temperature profile. Sufficient time was allowed after each relocation of the thermocouple cluster to permit the sensors to reach steady state.

Experimental data are reported for five runs, three at a PDR of 1.364 and two at a PDR of 1.240. A brief summary of the data for these runs is given in Table IV. The shroud temperature shown is the average value recorded for the sheath thermocouples. Variation from the top to the bottom of the sheath was approximately 25° to 30°. Detailed temperature data obtained with the tube thermocouples are presented in Figures 37 through 41. Thermocouple locations are given relative to the centerline of the heated zone, which was 92.5 in. from the tube sheet face. The more positive a position, the nearer it is to the tube sheet. Although measurements were made from -2.5 ft to +7.0 ft from the bundle midpoint at 6-in. intervals, the data presented show only the temperature values from -2.5 ft to +2.5 ft, representing data taken from 6 in. beyond one end of the 4-ft heated zone to 6 in. beyond the other end since the centerline of the heaters is the zero position. Skewing of the temperature profiles is attributable to heat dissipation in the nickel heater leads (positive side of the heated zone).

It can be seen from the figures that the temperature profiles are nearly flat at the center of the heated zone. The heated length is long enough that heat conduction in the axial direction has little effect on the temperature at the centerline of the heaters. An estimate of axial heat conduction from the central 1 ft of the heated zone was made using Fourier's law in the form:

TABLE IV

Summary of Thermal Data for Experimental Runs

Run No.	PDR	Pressure (microns Hg)	Core Power (Btu/hr)	Heat Flux [Btu/(hr-ft ²)]	Shroud Temperature (°F)	Center Tube Temperature (°F)
1	1.364	20	1565	29.5	441	799
2	1.364	33	2960	55.7	556	1002
3	1.364	50	1620	30.5	469	804
4	1.240	6	1650	31.1	503	805
5	1.240	10	2820	53.0	616	998

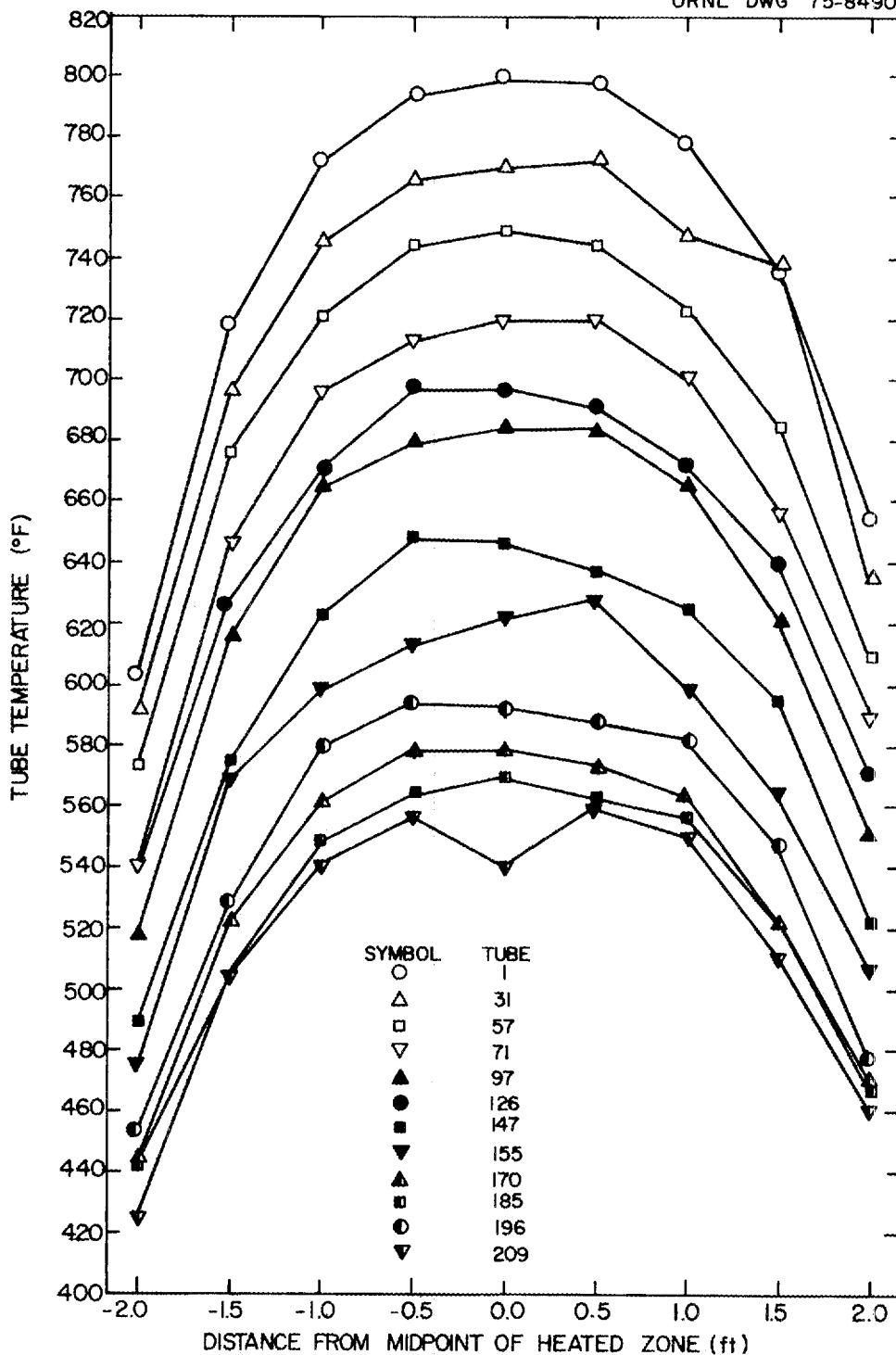


Figure 37. Experimental Data for Run 1.

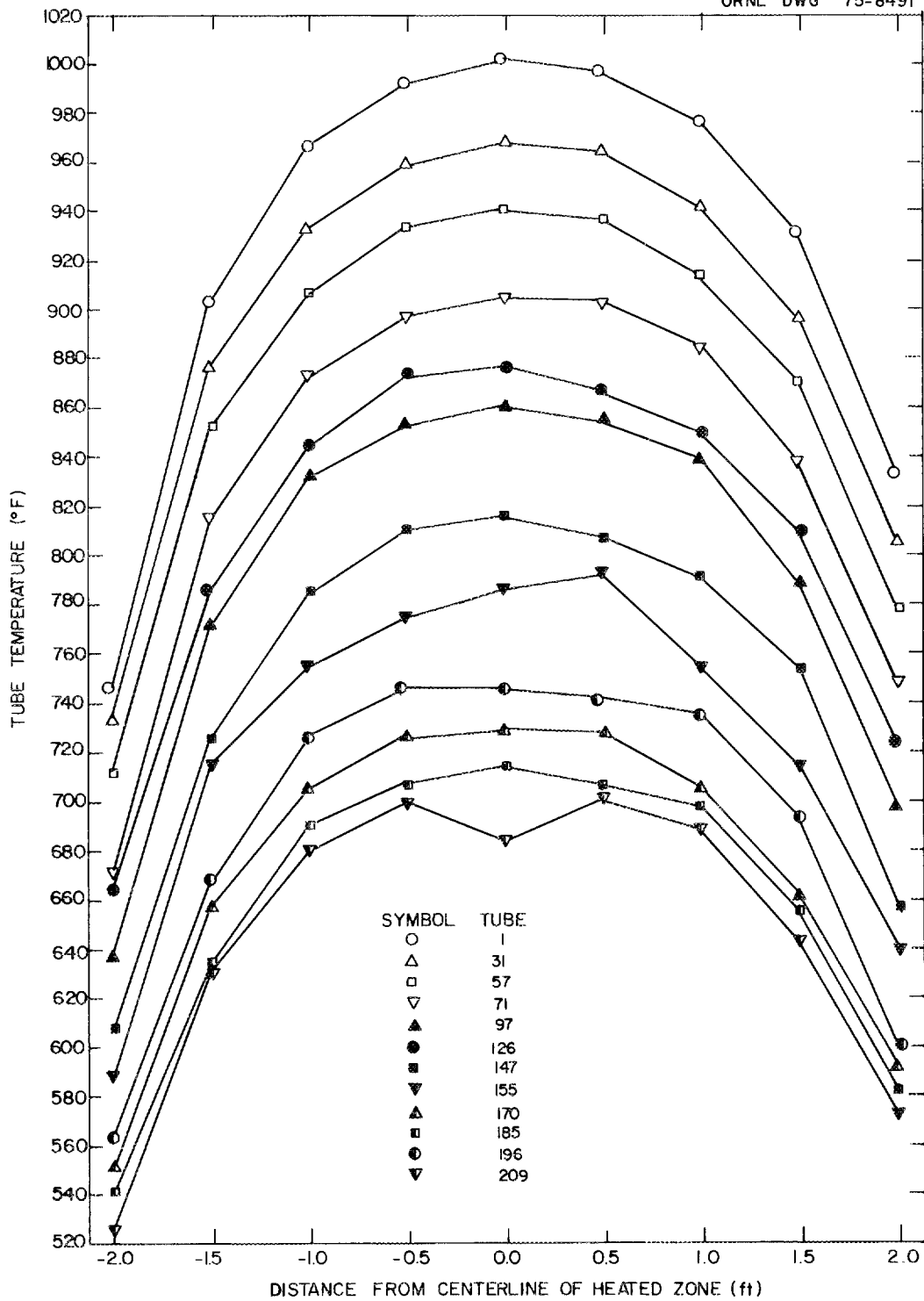


Figure 38. Experimental Data for Run 2.

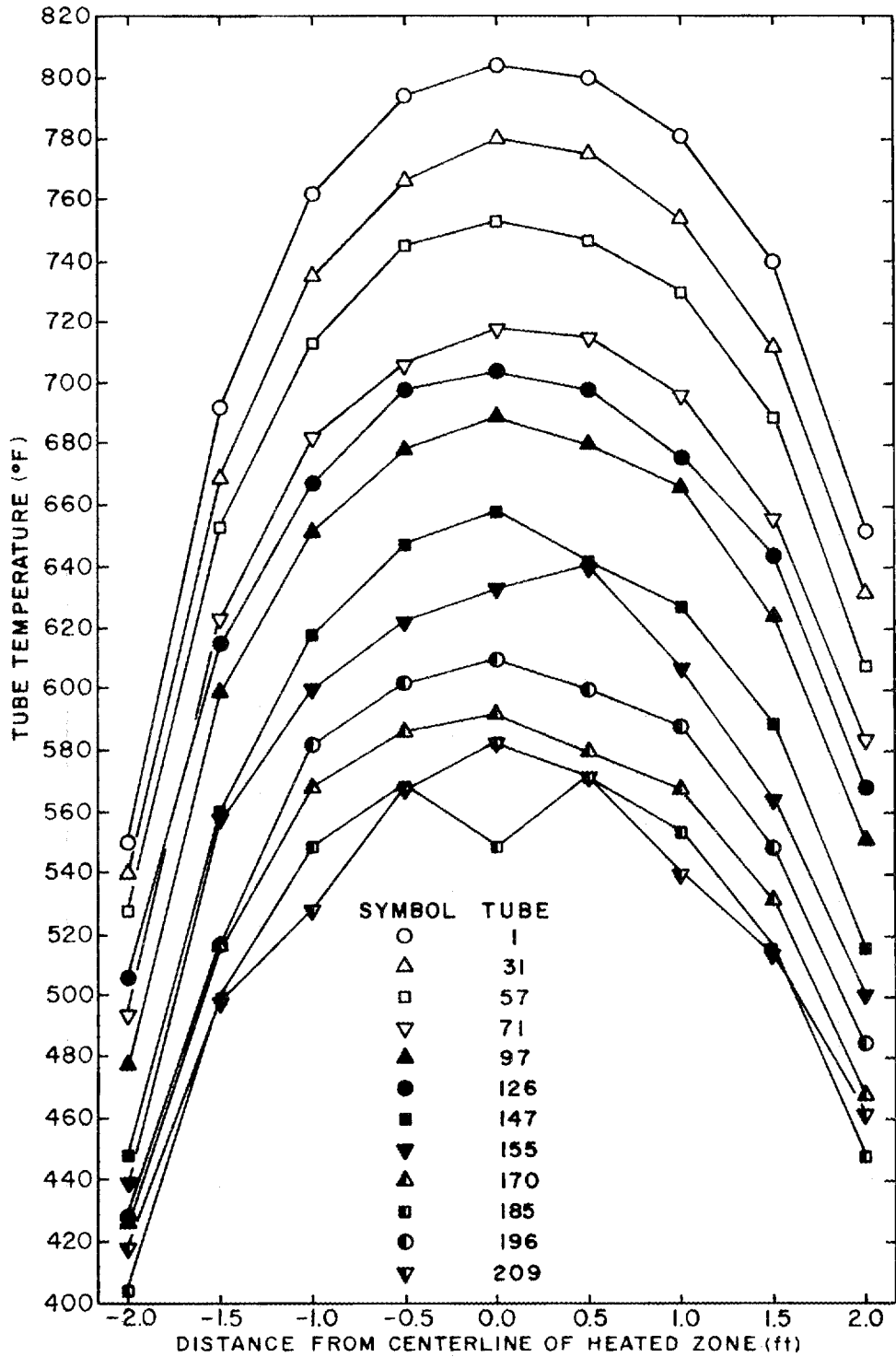


Figure 39. Experimental Data for Run 3.

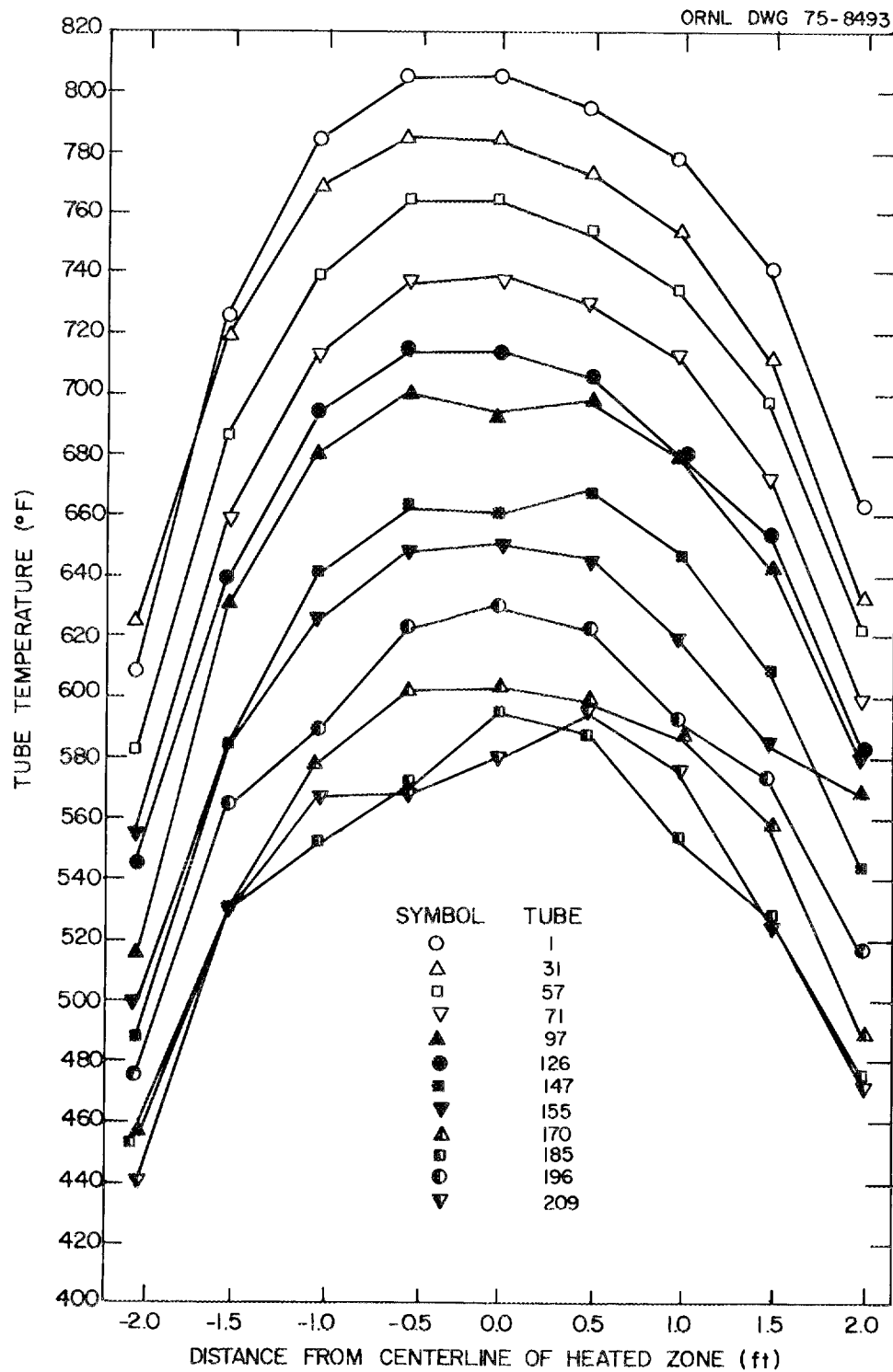


Figure 40. Experimental Data for Run 4.

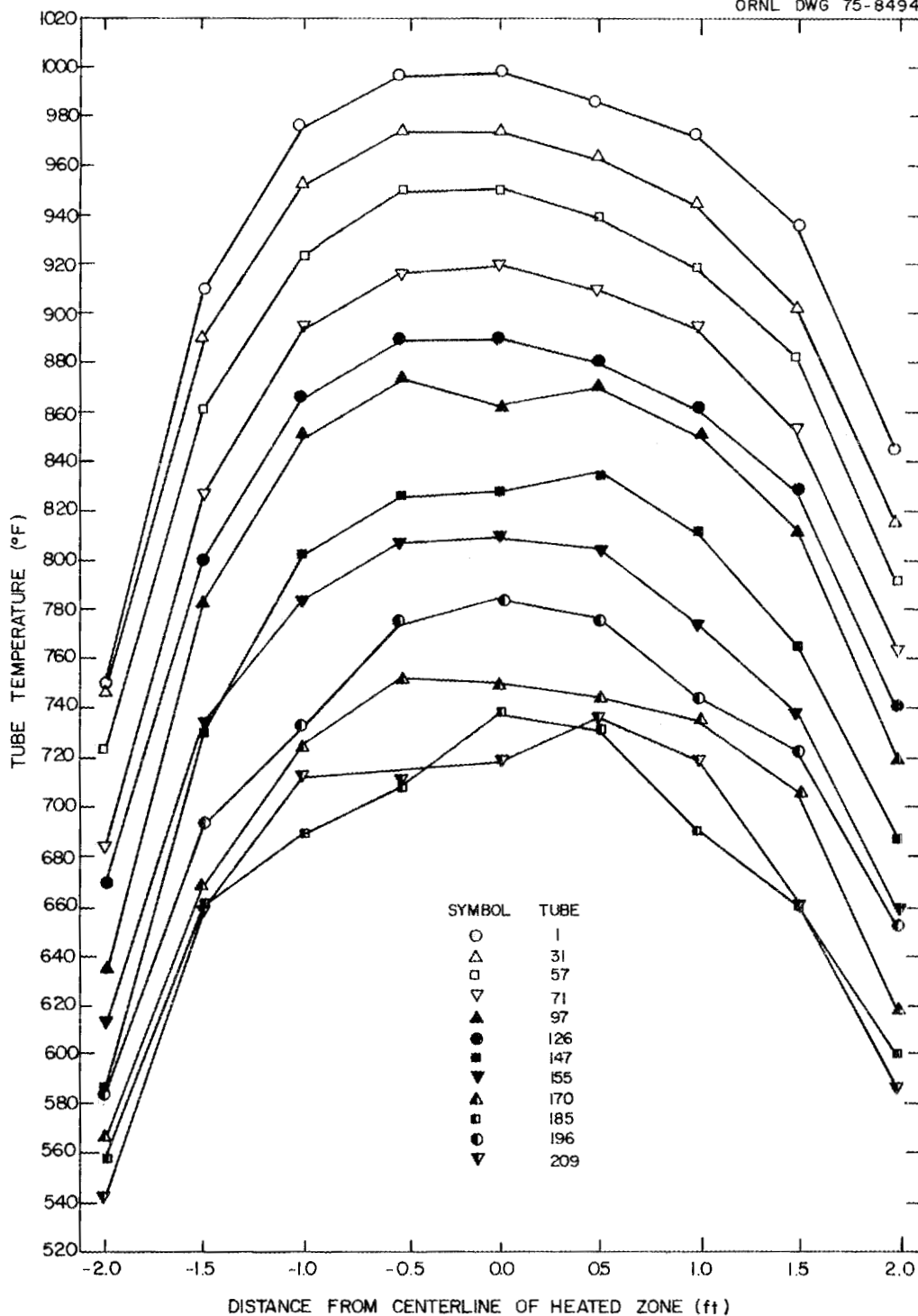


Figure 41. Experimental Data for Run 5.

$$Q = - kS \left(\left. \frac{dT}{dx} \right|_+ + \left. \frac{dT}{dx} \right|_- \right)$$

where S is the combined cross-sectional areas of metal for the tubes, spiral wire wrap, and the sheath; k is the thermal conductivity of 304 L stainless steel; $(dT/dx)|_+$ is the temperature derivative at +0.5 ft, and $(dT/dx)|_-$ is the temperature derivative at -0.5 ft. Axial conduction losses from the central 1 ft of the heaters were found to be approximately 6 to 7% of the heat generated in this section for the 800°F runs and 3 to 4% for the 1000°F runs. The assumption was then made that the temperatures measured at the centerline of the heaters approximated those that would be measured if the heated length was infinitely long. A comparison of the experimental values with theoretical calculations will be made in the next chapter.

CHAPTER 8

COMPARISON OF EXPERIMENTAL RESULTS AND THEORETICAL CALCULATIONS

A problem arises immediately in the comparison of the experimental results presented in Chapter 7 with theoretical predictions using the computer program discussed in Chapter 6. Because the experimental assembly was constructed to simulate a Liquid Metal Fast Breeder Reactor (LMFBR) fuel rod assembly, spiral wire wrap was used to separate the tubes. Clearly, the view factors between wire-wound tubes differ from those between parallel cylinders as derived in Chapter 4. Two approaches were taken to estimate the effects of the wire wrap.

The first approach was to ignore the presence of the wire wrap completely, reasoning that the blockage of radiation between tubes as a result of the wire wrap was offset by the increased area available for radiative transfer. The computer program STEADY was employed to simulate the experimental array with zero heat generation in the tubes containing thermocouples and equal heat generation in the remaining tubes containing heaters. The tube surface heat fluxes Q/A were determined by dividing the total power input to the 4-ft heated section by the surface area of the 205 heated tubes, ignoring the surface area of the wire wrap. Likewise, in the ratio A_1/A_n , A_1 was taken as the surface area of a tube alone. The quantity A_n (A_{218}), of course, was the surface area of the shroud. View factors were those derived in Chapter 4. Figures 42 through 46 show a comparison of the experimental results with theoretical predictions for several assumed values of emissivity. Before discussing these results, the alternate treatment of the wire wrap will be considered.

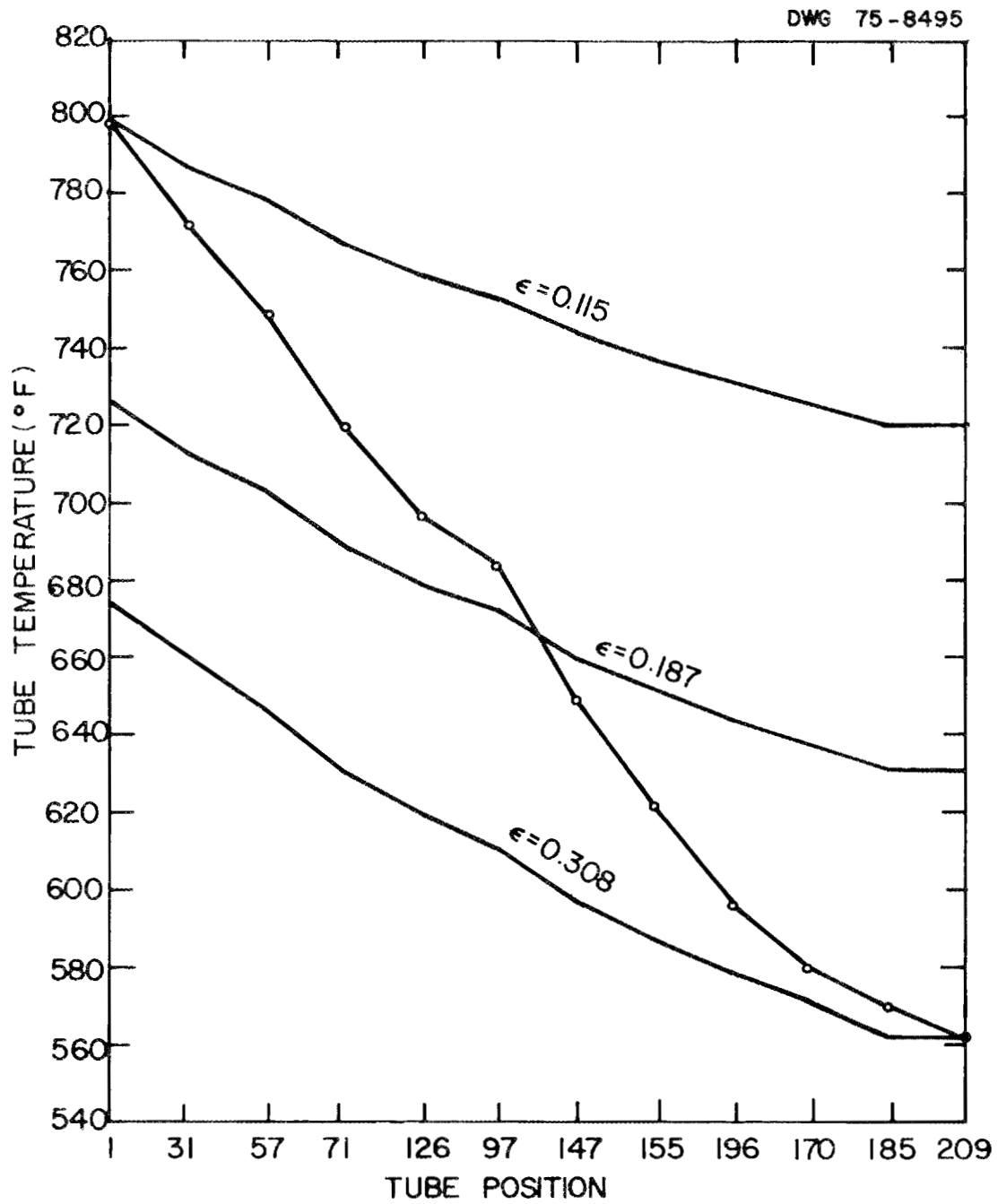


Figure 42. Comparison of Experimental Temperature Profile with Theoretical Calculations--Run 1.

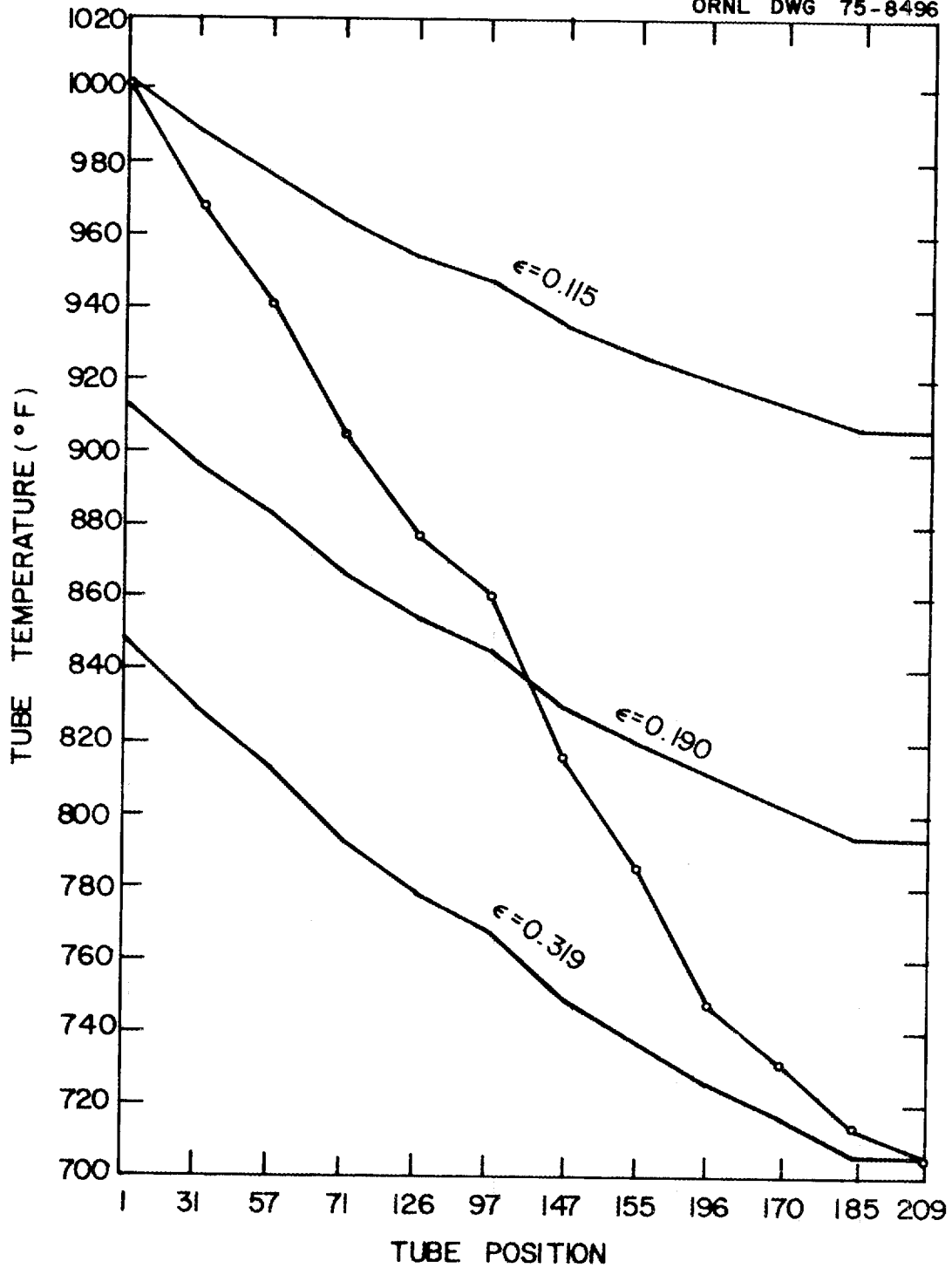


Figure 43. Comparison of Experimental Temperature Profile with Theoretical Calculations--Run 2.

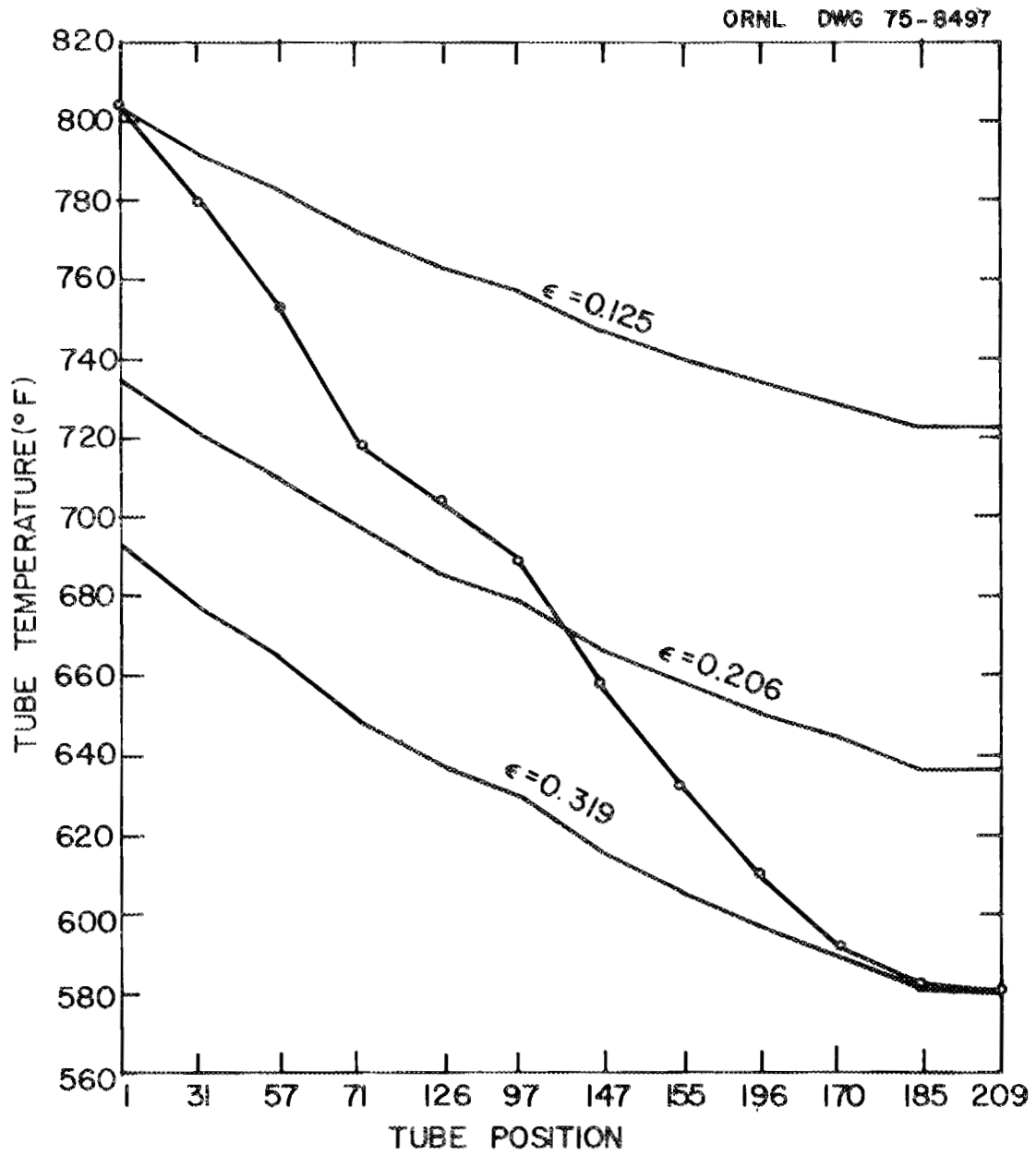


Figure 44. Comparison of Experimental Temperature Profile with Theoretical Calculations--Run 3.

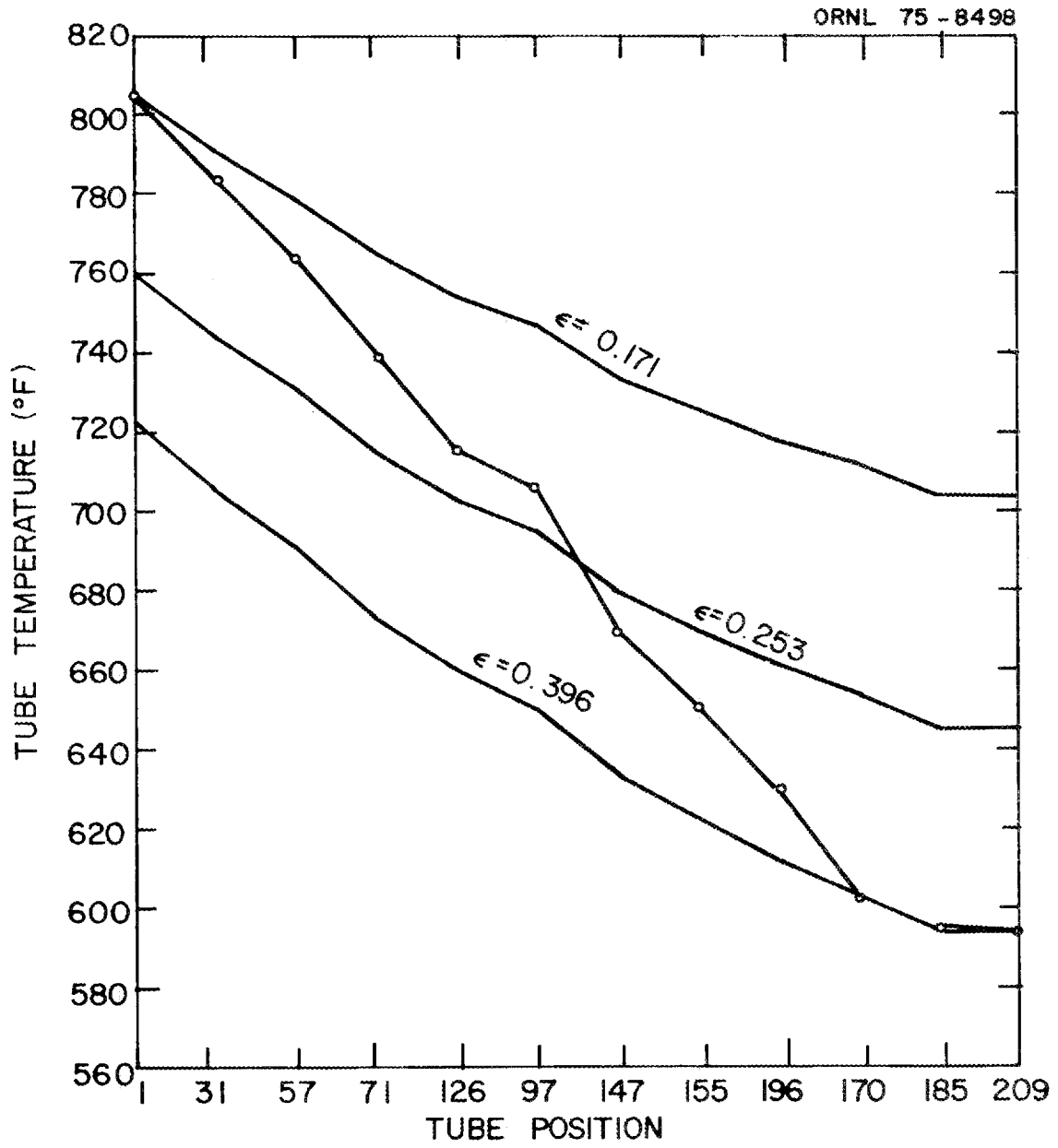


Figure 45. Comparison of Experimental Temperature Profile with Theoretical Calculations--Run 4.

ORNL 75-8499

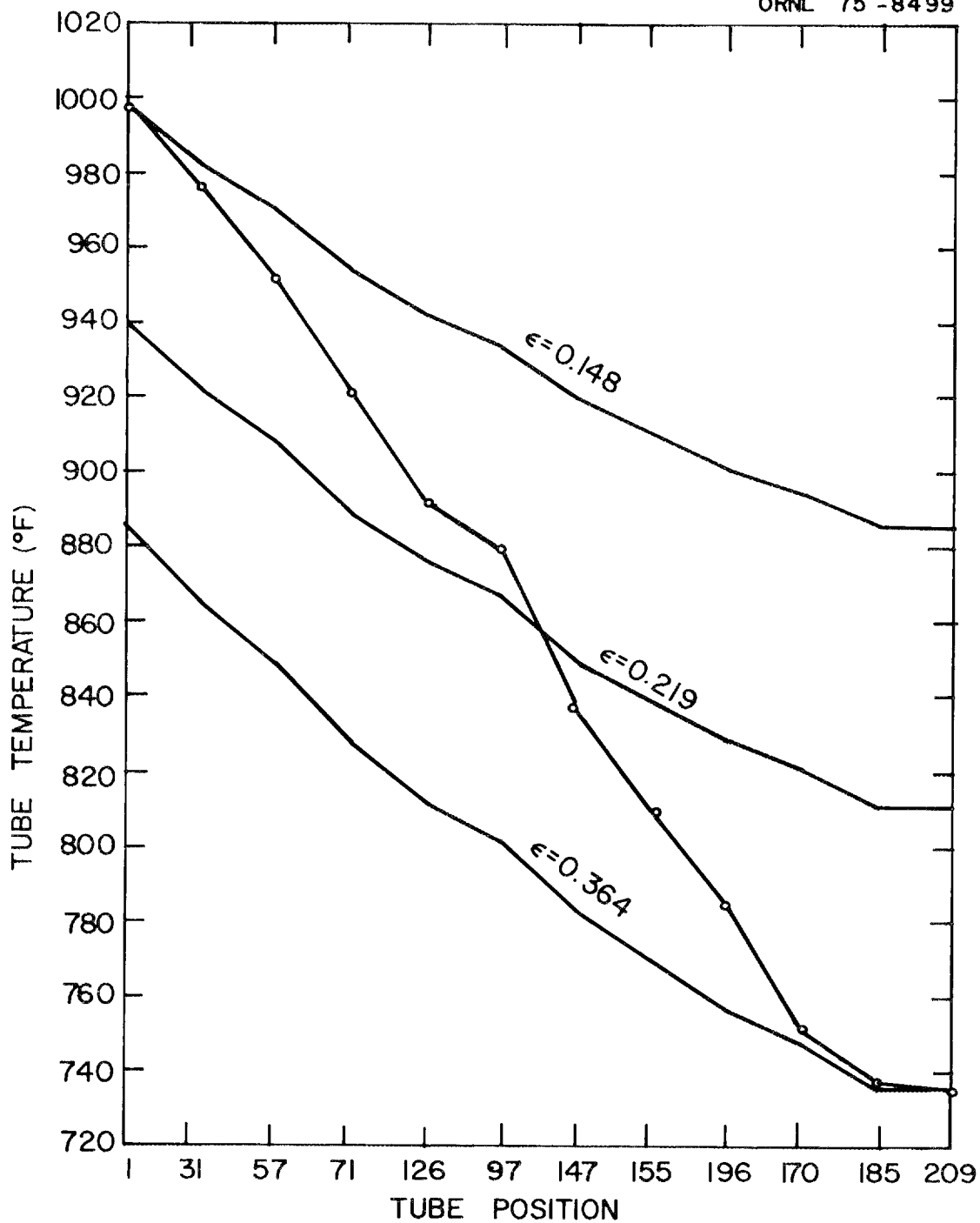


Figure 46. Comparison of Experimental Temperature Profile with Theoretical Calculations--Run 5.

The second approach to handling the wire wrap was to treat a tube and its associated wire wrap spacer as one surface of uniform temperature. The view factors between tube-wire wrap surfaces were estimated as shown in Appendix B, where $F1'1'$, $F1'2'$, $F1'3'$, $F1'5'$, and $F1'8'$ are the view factors between tube-wire wrap surfaces as opposed to the previously defined view factors between bare tubes, $F12$, $F13$, $F15$, and $F18$. Since a tube-wire wrap surface can see itself, $F1'1'$ is not zero as is $F11$. The subroutine HEX was used to construct the view factor array with a single additional statement inserted to generate the $F1'1'$ values. Surface heat fluxes and the ratio A_1/A_n were computed based on the combined surface areas of a tube and its wire wrap. The results of this more rigorous approach, however, were temperature values almost identical (maximum difference of 3°F) to those for the first approach.

Various emissivity values were used, as shown in Figures 42 through 46, in an attempt to fit the experimental results. The emissivities that gave the best fits to the data are lower than those usually reported in the literature for 304 stainless steel of comparable surface conditions, although the reported values show a large amount of scatter. Literature data (11, 15, 26, 34, 37, 39) indicate that the emissivities of stainless steel surfaces are a strong function of surface condition, particularly its degree of oxidation. Rolling and Funai (26) appear to have carried out the most extensive emissivity measurements to date for 304 stainless steel. Their data showing the influence of oxide film thickness are given in Figure 47. As can be seen from Equation (37a), the calculated temperature of a tube which has no heat generation ($X_j = 0$) is a function only of the emissivity of the shroud, not of the emissivity of the tube itself

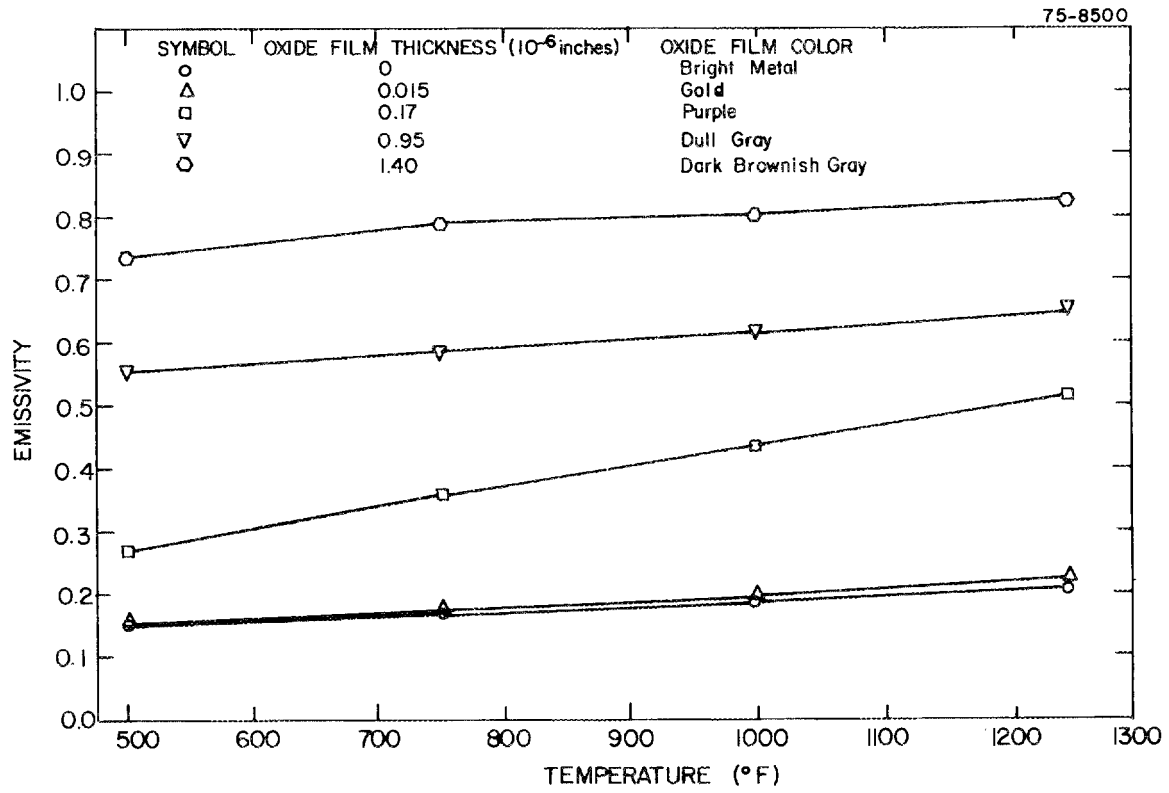


Figure 47. Emissivity of 304 Stainless Steel as a Function of Oxidation [Data of Rolling and Funai (26)].

or the emissivities of other tubes. Since a dull gray oxide film was observed on the shroud (during fabrication) and experimental shroud temperatures were 450 to 650°F, the sheath emissivity was estimated from Figure 47 to be approximately 0.55. A similar value has also been measured experimentally by Watson (37).

It is clear from Figures 42 through 46 that the experimentally measured temperature gradient across an array is much greater than predicted by theory. As a consequence, the predicted temperature profile is much flatter than the measured profile and the theoretical and experimental temperature profiles do not match for any sheath emissivity. Evans (2,4) encountered similar difficulties in his analysis of experimental data for a square array of 64 rods on a square pitch. Using the net radiation method, he also found the predicted temperature profile to be flatter than the experimental profile. Further, an emissivity of 0.05 to 0.10 was required in his calculations to achieve any measure of agreement with the experimental data, whereas the actual emissivity of the Zircaloy surfaces was estimated as 0.22.

This poor agreement between theoretical and experimental results indicates that one or more of the assumptions underlying the theoretical model is not correctly describing the experiments. To the extent that it is feasible, each of the five basic postulates upon which the theory is based will be examined to evaluate its validity for the experimental tube array.

The first postulate (see Chapter 2) is that each surface is isothermal. Temperature variations around the circumference of each tube and around the periphery of the shroud were assumed to be effectively damped

out by thermal conduction. If a significant temperature variation existed from one side of a tube to the other as a consequence of the net radial heat flux that exists in the array, a steeper temperature gradient than calculated would occur across the array. However, the empirical analysis given in Appendix A shows that, even under the most conservative assumptions, the temperature drops across the tubes are not large enough to account for the differences between theoretical and observed temperature profiles.

The second assumption is that the emissivities of the surfaces are independent of wavelength. For the experimental runs, the temperature range of the tubes was 560 to 1000°F (1020 to 1460°R). For this temperature range, 80% of the emitted energy has a wavelength of 2 to 14 microns. The data of Rolling and Funai (26, pp. 92-94) show that the emissivity of 304 stainless steel is relatively constant over this wavelength range.

The third postulate is diffuse reflection. For real surfaces, the concept of a diffusely reflecting surface appears to be more of an abstraction than a reality. Data given in the literature (1, 3, 23, 33) indicate that the directional distribution of reflected radiation is often highly dependent on the incident angle and wavelength of the incident radiation, the roughness of the surface, and the surface composition. The absence of any literature data for 304 stainless steel, however, makes it difficult to ascertain the extent to which this assumption is justifiable.

For most materials, the fourth assumption of diffuse emission appears to be more realistic than the assumption of diffuse reflection. Data reported by Eckert and Drake (3) indicate that metallic surfaces follow Lambert's cosine law fairly well for angles up to about 50° from the

surface normal; for larger angles, the emission is greater than predicted by the cosine law.

The final assumption is that the total radiant flux leaving a surface (i.e., the radiosity) is uniform over the surface. This assumption is valid only if the incident energy flux does not vary over the surface. If calculational methods based on uniform radiosity are used when, in fact, the incident flux is nonuniform, one has, in effect, made the physically inaccurate assumption that each incident ray is reflected uniformly from the entire surface rather than from the point of incidence. Thus, if the incident flux were much greater on one side of a tube than the other, the reflected flux would be represented as uniform over the surface in the calculation while, in reality, the reflected flux would be greater along the portions of the surface experiencing a higher incident flux. For the rod arrays under consideration, there is an increase in the energy flux moving radially from the center rod to the shroud. Consequently, the radiant flux impinging on a tube can be expected to vary to some degree around the periphery of a tube. If this variation is significant, a tube can no longer be considered a single surface but, instead, must be subdivided into smaller surfaces which more nearly approximate areas of uniform radiosity.

Fisher and Cowin (6) have reported theoretical calculations for radiant heat transfer in one-, two-, and three-ring clusters of 6, 18, and 36 rods enclosed by circular sleeves in which successive computations were performed with each rod considered as one surface, two surfaces, and four surfaces in order to investigate the effects of nonuniform radiosity around the circumference of a rod. Circumferential temperature variations, however, were assumed to be damped out by thermal conduction in the rod.

A comparison of theoretical calculations with experimental temperature values for both polished and oxidized nickel-copper tubes showed that, although even the single-surface representation gave reasonable results, agreement between theory and experiment improved with increasing subdivision of the rods. Increasing the subdivision resulted in larger calculated temperature decreases from row to row, more closely approximating the experimentally observed gradient. These larger temperature decreases may be explained as follows. When the incident flux is nonuniform and a single-surface representation is used which levels the reflected flux over each tube, the calculated temperature gradient underestimates the actual temperature gradient across the array. Subdivision of the tubes results in a more realistic representation of distribution of reflected energy and a calculated temperature gradient closer to the actual gradient since the smaller surfaces provide a better approximation of the actual point reflection of an incident ray.

Subdividing the surfaces of tubes, however, greatly increases the number of equations that must be solved. In addition, the view factors must be reevaluated, as they are now based on exchange between portions of tubes rather than between whole tubes. The resulting complexity makes it impractical to seek a general solution for large arrays of rods. Since the need for the assumption of uniform radiosity in the standard calculation methods arises from the use of view factors based on this assumption, another possible approach in the formulation of the energy balance equations is to use interchange factors which do not assume uniform radiosity. Obviously, however, these interchange factors would then become functions not only of geometry but also of the assumed distribution of reflected radiation.

Klepper (19) has calculated interchange factors between whole rods which do not assume uniform radiosity over the entire surface of a tube. An individual tube is considered to have a uniform surface temperature (and hence uniform emissive power), but the reflected flux is assumed to be constant only over each of several areas into which the tube is subdivided. Tubes in arrays on a square pitch are divided into eight equal-sized areas, while cylinders in arrays on an equilateral triangular pitch are divided into 12 segments. Evaluation of the interchange factors proceeds by considering the temperature of a central tube to be elevated, while the remaining tubes in a large array are at absolute zero. This assumption does not affect the value of the calculated interchange factors since they are not a function of temperature. Therefore, these interchange factors are applicable to any combination of rod temperatures. The size of the array selected is sufficiently large that the calculated interchange factors approximate those which would exist in an infinite array. The path of a unit emission of radiant energy from the central rod is followed as it is partially absorbed and partially reflected by segments of various cylinders in the array. The calculation is terminated when the initial unit of released energy is 96 to 98% absorbed. (Complete absorption would require following an infinite number of successively weaker reflections.) The fractions of the unit of energy absorbed by the segments of a given rod are summed to give the fraction absorbed by the whole rod.

The interchange factors determined by Klepper represent the fraction of energy emitted by one rod that is absorbed by another rod as a consequence of direct exchange and multiple reflections. This, however, is

simply the definition of Gebhart's absorption factor G_{ij} (or $\mathfrak{F}_{ij}/\epsilon_i$), and the interchange factors calculated by Klepper could alternately be computed using Equations (15). If one considers an array of n rods, each subdivided into N areas, the summation in Equations (15) would be over $n \times N + 1$ surfaces. (The additional surface is the shroud enclosing the rods.) The view factors required in the computation are those between segments of rods. The absorption factors between segments of rods resulting from a solution of Equations (15) could be used to find the absorption factors between entire rods in the following manner. Let i' and j' denote segments of rods i and j , respectively. Then the fraction of the radiation emitted by a segment i' that is absorbed by rod j is

$$G_{i'j} = \sum_{j'=1}^N G_{i'j'} ,$$

where $G_{i'j'}$ is the fraction of the radiation emitted by segment i' on rod i that is absorbed by area j' on the rod j . The fraction of the total radiation emitted by rod i that is absorbed by rod j is the weighted average of the $G_{i'j}$. That is,

$$G_{ij} = \frac{\sum_{i'=1}^N G_{i'j} \sigma \epsilon_{i'} T_{i'}^4 A_{i'}}{\sum_{i'=1}^N \sigma \epsilon_{i'} T_{i'}^4 A_{i'}} .$$

For rods of uniform temperature and emissivity which are divided into N equal-sized areas, the radiation emitted by each segment of rod i is the same, so that

$$G_{ij} = \frac{1}{N} \sum_{i'=1}^N G_{i'j} = \frac{1}{N} \sum_{i'=1}^N \sum_{j'=1}^N G_{i'j'} \quad (86)$$

Let N_{\min} designate the minimum number of areas into which each rod must be subdivided in order to approximate uniform radiosity over each rod segment. For every N greater than N_{\min} , the values calculated for the absorption factors between whole rods will be the same. For values of N less than N_{\min} , however, the G_{ij} will be a function of N , approaching the true values as N approaches N_{\min} . Thus far, the work reported in this paper has been based on $N = 1$, the assumption of uniform radiosity over the entire surface of each rod. Values of G_{ij} for $N = 1$ can be found by using Equations (15) and the configuration factors between whole rods derived in Chapter 4. If a comparison of these G_{ij} is made with the G_{ij} computed by Klepper, it is found that quite different values result from the two sets of calculations, and there is a corresponding difference in the manner in which the energy leaving a rod is found to be distributed. Table V shows this comparison for rods on an equilateral triangular pitch for $\epsilon = 0.3, 0.6,$ and 0.9 at PDRs of 1.2, 1.3, and 1.4. Results for the G_{ij} with $N = 12$ show a larger fraction of the radiation to be absorbed by the radiating rod itself and by immediately adjacent rods, while there is a wider dispersal of energy for $N = 1$. Thus, the absorption factors calculated with $N = 12$ indicate that the array is less permeable to thermal radiation than do the absorption factors calculated with $N = 1$. The result is a greater temperature gradient (because of the lower effective thermal conductivity of the array) when the G_{ij} for $N = 12$ are used in place of the G_{ij} for $N = 1$ in solving Equations (20).

TABLE V

Comparison of Absorption Factors for $N = 1$ and
 $N = 12$ for Rods on a Triangular Pitch

	$\epsilon = 0.3$		$\epsilon = 0.6$		$\epsilon = 0.9$	
	$N = 1$	$N = 12$	$N = 1$	$N = 12$	$N = 1$	$N = 12$
Pitch-to-Diameter Ratio = 1.2						
G11	0.04662	0.188	0.03807	0.137	0.01183	0.0407
G12	0.07296	0.111	0.10629	0.125	0.13388	0.140
G13	0.02894	0.0161	0.02914	0.0156	0.02539	0.0184
G14	0.01808	0.00359	0.01207	0.000108	0.00330	
G15	0.00841		0.00401		0.00085	
G16	0.00526		0.00181		0.00020	
G17	0.00310		0.00087		0.00009	
G18	0.00255		0.00059		0.00005	
G19	0.00157		0.00027		0.00001	
Pitch-to-Diameter Ratio = 1.3						
G11	0.04075	0.156	0.03316	0.117	0.01024	0.0350
G12	0.06650	0.102	0.09719	0.116	0.12210	0.127
G13	0.03025	0.0230	0.03414	0.0252	0.03461	0.0310
G14	0.01768	0.00650	0.01221	0.00244	0.00342	
G15	0.00911	0.00126	0.00512		0.00178	
G16	0.00582		0.00237		0.00037	
G17	0.00365		0.00129		0.00020	
G18	0.00303		0.00097		0.00029	
G19	0.00192		0.00044		0.00004	
Pitch-to-Diameter Ratio = 1.4						
G11	0.03618	0.138	0.02945	0.105	0.00907	0.0316
G12	0.06100	0.0967	0.08950	0.111	0.11236	0.120
G13	0.03079	0.0265	0.03729	0.0301	0.04067	0.0373
G14	0.01707	0.00822	0.01206	0.00334	0.00343	
G15	0.00968	0.00195	0.00626		0.00306	
G16	0.00625	0.00128	0.00288		0.00054	
G17	0.00413		0.00172		0.00033	
G18	0.00351		0.00147		0.00071	
G19	0.00227		0.00066		0.00008	

Since previous calculations using $N = 1$ yielded temperature gradients much smaller than those found experimentally, the computations were repeated using Klepper's interchange factors. For the PDRs encountered in the experimental arrays, Klepper's results show that the radiation leaving a rod is essentially absorbed in the first two surrounding rows of rods as indicated in Table V. Because G_{14} was very small, it was assumed to be zero in order to use the subroutine HEX without modification for setting up the matrix of interchange factors. The values of G_{15} were increased so that the sum of the absorption factors remained unity. The assumption was made that values of G_{ij} given by Klepper, although derived for rods in infinite arrays, can be used with reasonable accuracy even for rods near the sheath. After construction of the G matrix using HEX, Equations (35) were solved simulating the experimental conditions. Comparisons of calculated results with data for the experimental runs with the 217-rod hexagonal assembly are presented in Figures 48 through 52. Clearly, the calculated temperature profiles are in much closer agreement with the experimental data than the theoretical results presented previously in Figures 42 through 46 (pp. 116-20). Further, the values of emissivity that generate theoretical curves most closely approximating the experimental profiles are in the range which would be expected for the experimental surfaces, while the theoretical emissivity values required to fit the experimental data in Figures 42 through 46 (pp. 116-20) were much lower than the expected values.

Based on these results, it appears that the assumption of uniform radiosity around the entire periphery of a tube is not met in practice, at least for the arrays employed in the experiments reported here. Further experimentation with arrays of other sizes (particularly, small

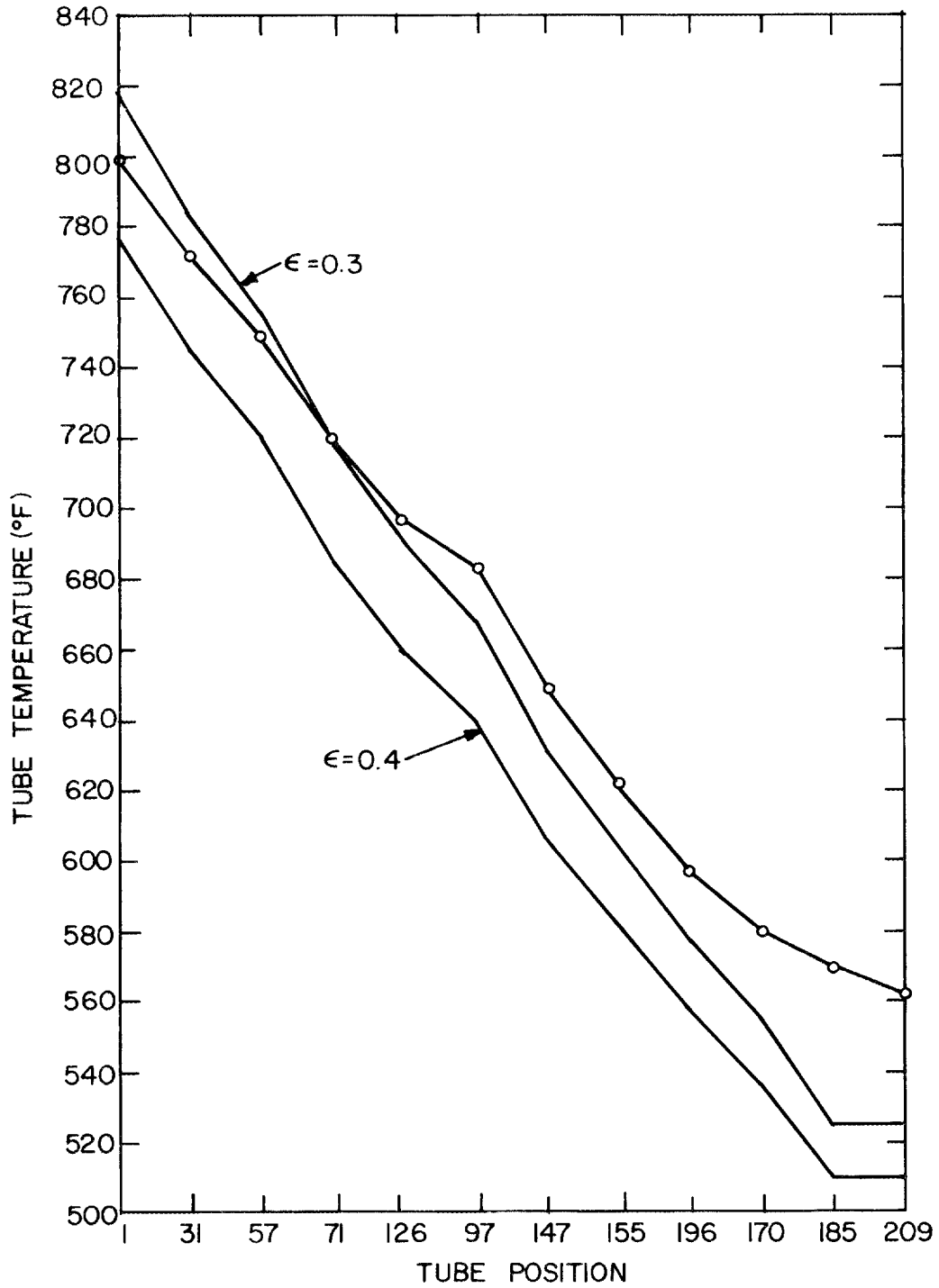


Figure 48. Comparison of Experimental Data and Theoretical Calculations (Nonuniform Radiosity)--Run 1.

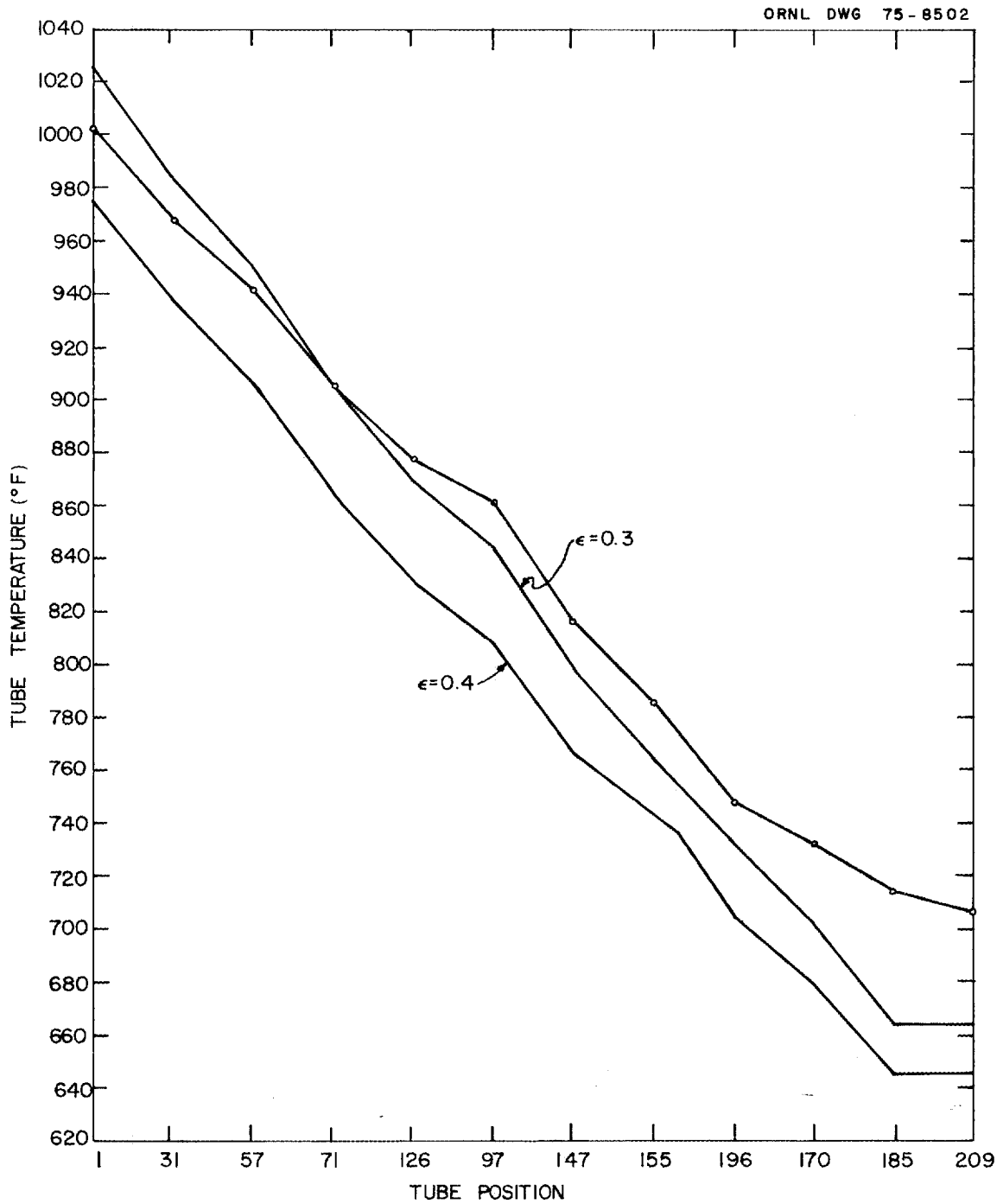


Figure 49. Comparison of Experimental Data and Theoretical Calculations (Nonuniform Radiosity)--Run 2.

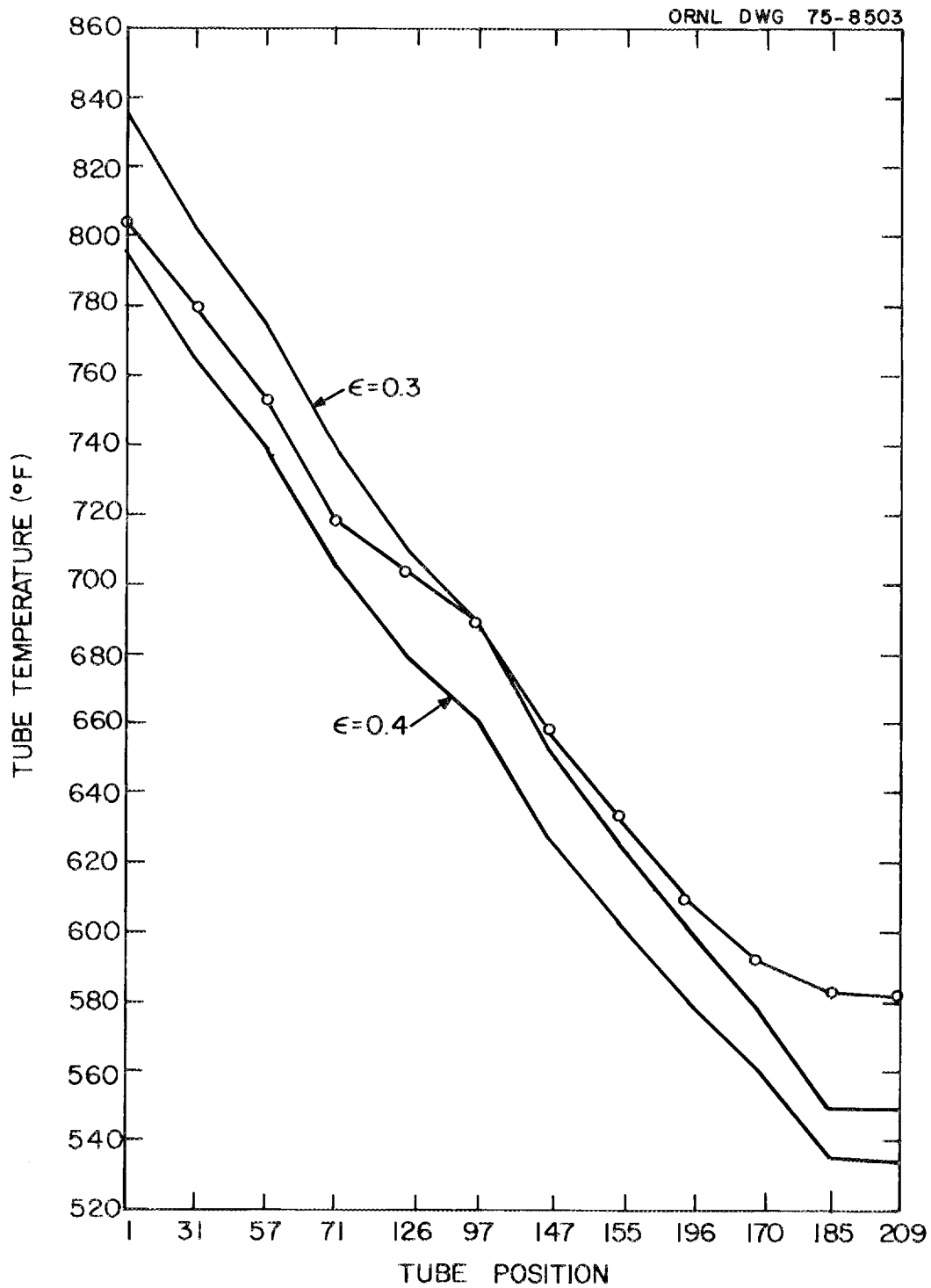


Figure 50. Comparison of Experimental Data and Theoretical Calculations (Nonuniform Radiosity)--Run 3.

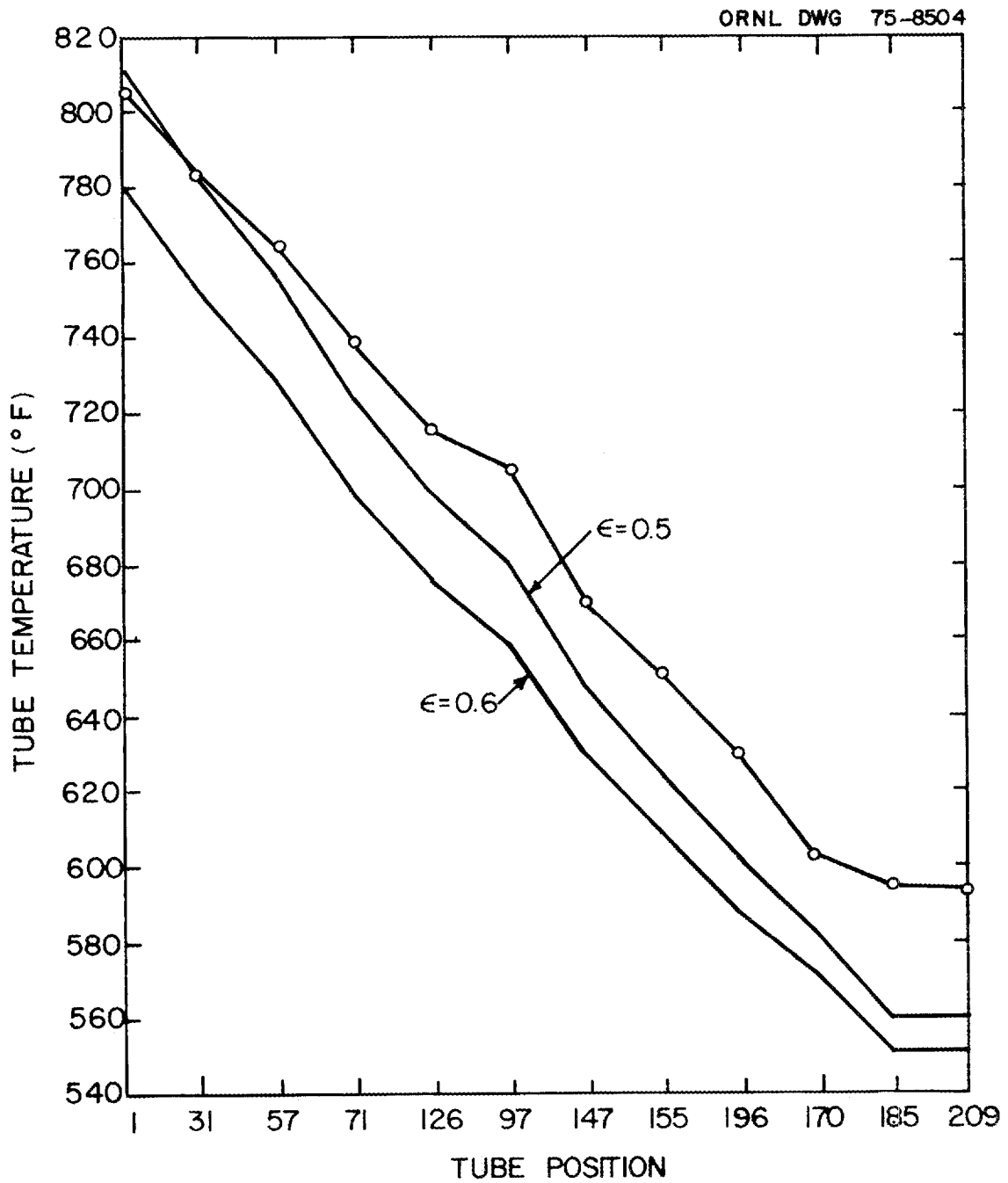


Figure 51. Comparison of Experimental Data and Theoretical Calculations (Nonuniform Radiosity)--Run 4.

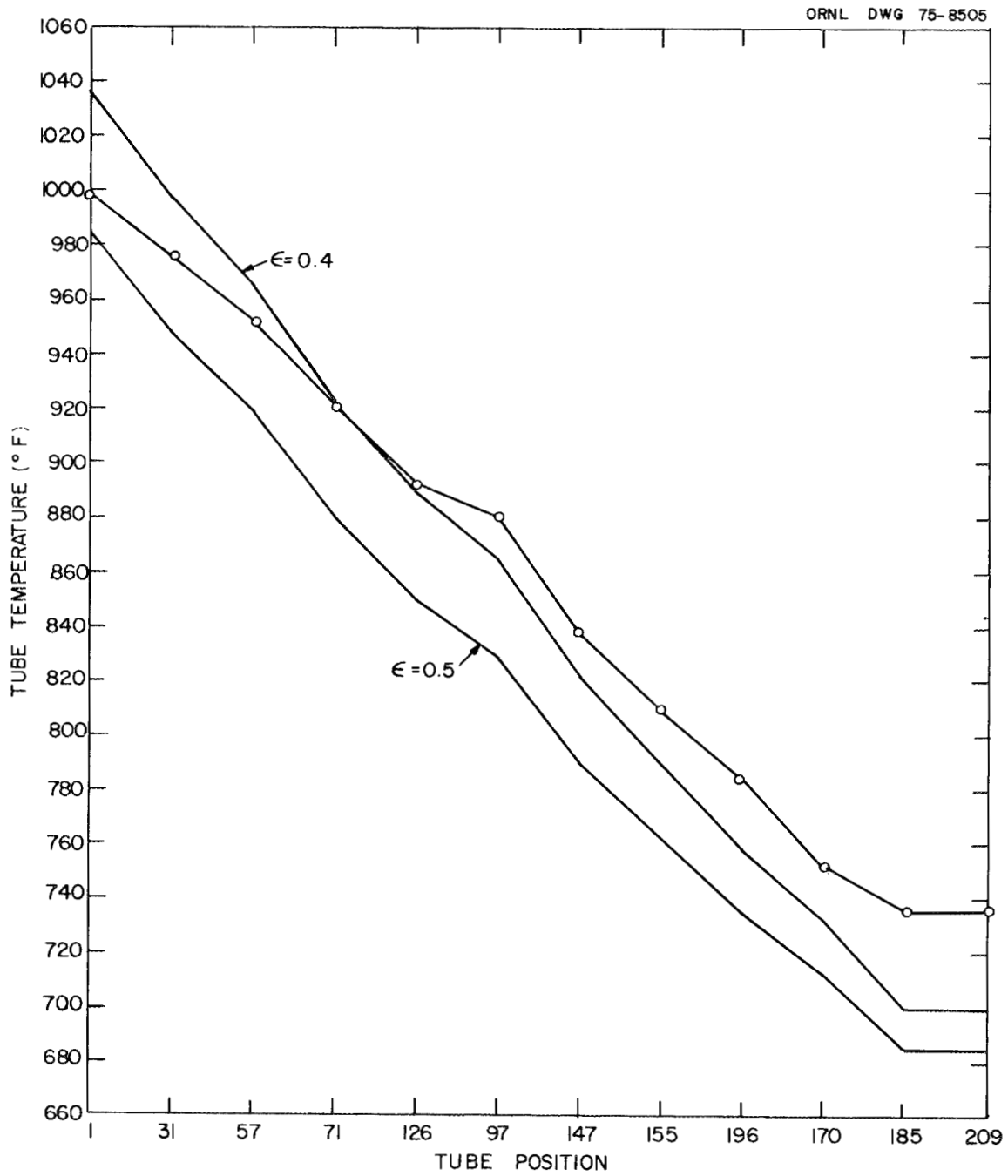


Figure 52. Comparison of Experimental Data and Theoretical Calculations (Nonuniform Radiosity)--Run 5.

arrays) is needed to more thoroughly check the theory and establish that this is indeed the case. However, on the basis of the results reported here, it is recommended that the energy balance equations be solved using Gebhart's or Hottel's method and that the G and \mathcal{F} matrices be constructed using the absorption factors given by Klepper. This procedure will replace the assumption of uniform radiosity over the entire surface of a cylinder with the much less stringent assumption that the reflected energy flux is uniform over 30° segments for rods on a triangular pitch and over 45° segments for rods on a square pitch. As an aid to computation, the absorption factors determined by Klepper are reproduced in Appendix C.

CHAPTER 9

CONCLUSIONS AND RECOMMENDATIONS

I. CONCLUSIONS

The following conclusions were deduced from this study of radiative heat transfer in arrays of parallel cylinders:

1. Explicit theoretical equations can be derived for the view factors between rods in arrays of parallel rods on square and equilateral pitches using Hottel's crossed-string method.
2. An analysis of the steady-state temperatures prevailing in hexagonal arrays of rods on a triangular pitch and in square arrays of rods on a square pitch can be made by using the theory of radiant exchange among diffuse-gray surfaces. A computer algorithm can be written to solve the sets of linear equations arising from the theoretical formulation in such a manner that a rod array of any size can be handled (within the limitations of computer memory). Development of the analysis in terms of dimensionless variables allows presentation of calculational results in a highly compact form with a minimum of variables.
3. Unsteady-state solutions can be calculated for these same rod arrays by numerical integration of the differential equations resulting from a transient analysis based on diffuse-gray surfaces. The number of variables in the transient problem can also be reduced using dimensionless

variables, particularly for the case in which the shroud temperature is constant.

4. For the array tested -- a 217-tube hexagonal array on a triangular pitch -- the assumption of uniform radiosity around the periphery of each tube yielded theoretical results which were in poor agreement with the experimental observations.
5. The use of absorption factors derived on the basis of more finely divided surface areas for each tube (thereby replacing the assumption of uniform radiosity over the entire tube with an assumption of uniform radiosity over each of the subdivisions) produced theoretical temperature profiles within 7% of the experimental profiles.

II. RECOMMENDATIONS

The theoretical analysis presented here should be further tested by comparison with experimental data from arrays of different sizes. In particular, the apparent shortcomings of the assumption of uniform radiosity around entire tubes should be studied further. Future experiments should be designed to employ grid spacers at intervals along the length of bare tubes, thus removing the complicating factor of the spiral wire wrap spacers employed in the experiments reported here. Nevertheless, these spiral spacers must be considered in simulating LMFBR fuel assemblies. Fabrication of the tubes of a highly conducting material (such as copper) would remove any concern about significant temperature gradients across individual tubes. Tubes with known and stable emissivities are needed so that this parameter is fixed a priori in making

theoretical calculations for comparison with the experimental data. For metallic surfaces, however, this is difficult to accomplish even under high vacuum because of the susceptibility of these surfaces to oxidation or reduction at high temperatures. At least in the range of high emissivities (0.9 to 1.0), stable surfaces can be attained through the use of high-temperature paints. Many of these paints have the added advantage that their emissivities are nearly constant over a broad temperature range.

LIST OF REFERENCES

LIST OF REFERENCES

1. Birkebak, R. C., and E. R. G. Eckert, "Effects of Roughness of Metal Surfaces on Angular Distribution of Monochromatic Reflected Radiation," J. Heat Transfer 87, 85-94 (1965).
2. Dietz, K. A. (ed.), Quarterly Technical Report LOFT Program Office July 1-September 30, 1968, IDO-17266 (February 1969).
3. Eckert, E. R. G., and R. M. Drake, Heat and Mass Transfer, 2d ed., McGraw-Hill, New York, 1959.
4. Evans, D. R., MOXY: A Digital Computer Code for Core Heat Transfer Analysis, IN-1392 (August 1970).
5. Evans, D. R., Idaho Nuclear Corporation, private communication.
6. Fisher, S. A., and M. Cowin, "An Investigation of Radiant Heat Transfer in Clusters of Parallel Rods," Proceedings of the Third International Heat Transfer Conference, Vol. V, pp. 174-183, Chicago, Ill., 1966.
7. Gebhart, B., Heat Transfer, 2d ed., McGraw-Hill, New York, 1971.
8. Gebhart, B., "Unified Treatment for Thermal Radiation Transfer Processes-Gray, Diffuse Radiators and Absorbers," Paper No. 57-A-34, ASME, December 1957.
9. Gebhart, B., "A New Method for Calculating Radiant Exchanges," Trans. ASHRAE 65, 321-32 (1959).
10. Gebhart, B., "Surface Temperature Calculations in Radiant Surroundings of Arbitrary Complexity-For Gray, Diffuse Radiation," Intern. J. Heat Mass Transfer 3, 341-46 (1961).
11. Gubareff, G. G., J. E. Jansen, and R. H. Torborg, Thermal Radiation Properties Survey, 2d ed., Honeywell Research Center, Minneapolis, 1960.
12. Hamilton, D. C., and W. R. Morgan, Radiant-Interchange Configuration Factors, NACA TN 2836 (December 1952).
13. Hamming, R. W., Numerical Methods for Scientists and Engineers, 2d ed., McGraw-Hill, New York, 1973.
14. Hottel, H. C., "Radiant Heat Transmission," Chap. 4 in Heat Transmission, ed. by W. H. McAdams, 3d ed., McGraw-Hill, New York, 1954.
15. Hottel, H. C., and A. F. Sarofin, Radiative Transfer, McGraw-Hill, New York, 1967.

16. IBM System/360 Scientific Subroutine Package (360A-CM-03X) Version III Programmer's Manual, IBM Technical Publications, White Plains, New York, 1968.
17. Jakob, M., Heat Transfer, Vol. II, Wiley, New York, 1957.
18. Kee, C. W., ORNL, private communication.
19. Klepper, O. H., Radiant Interchange Factors for Heat Transfer in Parallel Rod Arrays, ORNL-TM-583 (December 1963).
20. Leuenberger, H., and R. A. Pearson, "Compilation of Radiation Shape Factors for Cylindrical Assemblies," Paper No. 56-A-144, ASME, November 1956.
21. McCracken, D. D., FORTRAN with Engineering Applications, pp. 92-100, Wiley, New York, 1967.
22. McCracken, D. D., and W. S. Dorn, Numerical Methods and FORTRAN Programming, pp. 250-61, Wiley, New York, 1964.
23. Münch, B., Directional Distribution in the Reflection of Heat Radiation and Its Effect on Heat Transfer, NASA TT F-497 (April 1968).
24. Pieczynski, A. T., and W. A. Stewart, Decay Heat Transfer from Reactor Fuel Rods in Test Holders in a Hot Cell, WERL-TAADM-1 (September 1968).
25. Ralston, A., and H. S. Wilf, Mathematical Methods for Digital Computers, pp. 95-109, Wiley, New York, 1960.
26. Rolling, R. E., and A. I. Funai, Investigation of the Effect of Surface Conditions on the Radiant Properties of Metals, Part II, Measurements on Roughened Platinum and Oxidized Stainless Steel, AFML-TR-64-363, Part II (April 1967).
27. Salmon, R., A Computer Code (CDC 1604A or IBM 7090) for Calculating the Cost of Shipping Spent Reactor Fuels as a Function of Burnup, Specific Power, Cooling Time, Fuel Composition, and Other Variables, ORNL-3648 (August 1964).
28. Siegel, R., and J. R. Howell, Thermal Radiation Heat Transfer, McGraw-Hill, New York, 1972.
29. Singer, G. L., VIEWPIN-A FORTRAN Program to Calculate View Factors for Cylindrical Pins, ANCR-1054 (March 1972).
30. Sparrow, E. M., "On the Calculation of Radiant Interchange Between Surfaces," pp. 181-212 in Modern Developments in Heat Transfer, ed. by W. E. Ibele, Academic, New York, 1963.

31. Sparrow, E. M., "Radiation Heat Transfer Between Surfaces," pp. 399-452 in Advances in Heat Transfer, Vol. 2, ed. by T. F. Irvine and J. P. Hartnett, Academic, New York, 1965.
32. Sparrow, E. M., and R. D. Cess, Radiation Heat Transfer, rev. ed., Brooks/Cole Publishing Co., Belmont, Calif., 1970.
33. Torrance, K. E., and E. M. Sparrow, "Off-Specular Peaks in the Directional Distribution of Reflected Thermal Radiation," J. Heat Transfer 88, 223-30 (1965).
34. Touloukian, Y. S., and D. P. DeWitt (eds.), Thermal Radiative Properties Metallic Elements and Alloys, IFI/Plenum, New York, 1970.
35. Toups, K. A., A General Computer Program for the Determination of Radiant-Interchange Configuration and Form Factors-CONFAC I, NASA CR-65256 (October 1965).
36. Toups, K. A., A General Computer Program for the Determination of Radiant-Interchange Configuration and Form Factors-CONFAC II, NASA CR-65257 (October 1965).
37. Watson, J. S., Heat Transfer from Spent Reactor Fuels During Shipping: A Proposed Method for Predicting Temperature Distribution in Fuel Bundles and Comparison with Experimental Data, ORNL-3439 (May 1963).
38. Wiebelt, J. A., Engineering Radiation Heat Transfer, Holt, Rinehart, and Winston, New York, 1966.
39. Wood, W. D., H. W. Deem, and C. F. Lucks, Thermal Radiative Properties, Plenum Press, New York, 1964.

APPENDIXES

APPENDIX A

THERMAL CONDUCTION ACROSS TUBES

A rough estimate of the temperature drop across a tube as a consequence of the noninfinite thermal conductivity of the tube walls can be made using Fourier's law for thermal conduction in the finite difference form:

$$\Delta T = \frac{Q\ell}{kS} \quad (87)$$

The quantity Q represents the steady-state net heat flow across the tube. For a tube in row i , Q is some fraction of the energy generated in rows 1 to $i-1$ as well as some part of the heat generated within the tube itself. The heat crossing a tube in row i as a result of heat generation in more inwardly located tubes may be approximated as

$$pQ_1 \cdot \frac{D}{q \cdot PDR \cdot D} = \frac{pQ_1}{q \cdot PDR} ,$$

where p is the number of tubes with heat generation interior to row i , q is the number of tubes in row i , and Q_1 is the heat generation rate for a single tube. The term $D/(q \cdot PDR \cdot D)$ represents an estimate of the fraction of the energy that would be intercepted by a single tube since D is approximately the width of a single tube and $q \cdot PDR \cdot D$ is roughly the perimeter of row i . In addition, the heat flowing across a tube because of heat generation within the tube itself is taken to be $0.5 Q_1$; therefore, for a tube in row i ,

$$Q = Q_1 \left(\frac{p}{q \cdot PDR} + 0.5 \right) .$$

The area S normal to heat flow is $2L\Delta r$, where L is the length of a tube, Δr is its thickness, and the factor of 2 arises because heat may flow in either direction around the tube. The length ℓ of the path for heat flow is estimated as one-half of the distance along one side of a tube, or $\pi D/4$. This distance is assumed to be roughly the average distance that energy absorbed on one side of the tube is conducted along the tube wall before being radiated. Equation (87) then becomes

$$(-\Delta T) = \frac{\pi Q_1 D}{8 k L \Delta r} \left(\frac{p}{q \cdot PDR} + 0.5 \right).$$

Table VI gives estimated values of the temperature differentials across tubes in rows 2 to 9 for the experimental run with the highest heat generation rate for both the apparatus with 16-mil-wall tubes (run 2) and the apparatus with 35-mil tubes (run 5). A value of 11 Btu/(hr-ft-°F) was used for the thermal conductivity of stainless steel. It is readily apparent that the temperature drops are quite small and that even the cumulative effect of these drops could not account for the differences between theoretical and observed temperature profiles discussed in Chapter 8.

TABLE VI
Estimates of the Temperature Differentials
Across Individual Tubes

Row	p	q	$-\Delta T$ ($^{\circ}\text{F}$)	
			Run 2	Run 5
2	1	6	1.2	0.5
3	7	12	1.8	0.8
4	19	18	2.4	1.1
5	37	24	3.1	1.5
6	61	30	3.8	1.8
7	91	36	4.5	2.1
8	127	42	5.2	2.5
9	169	48	5.9	2.8

APPENDIX B

VIEW FACTORS BETWEEN WIRE-WRAPPED TUBES

As previously, the notation F_{IJ} denotes the configuration factor between two single rods, I and J. Further, the symbol I'' will be used to stipulate the wire wrap for a bare tube I, while the symbol I' will designate a tube plus its associated wire wrap (i.e., I plus I'').

In the case of tube-wire wrap surfaces, the surfaces can see themselves; thus $F_{I'I'}$ is not zero. Referring to Figure 53, the following relations can be written:

$$F_{I'I'} = F_{I'I} + F_{I'I''} = F_{I'I''} \text{ since } F_{I'I} = 0 ,$$

$$F_{I''I'} = F_{I''I} + F_{I''I''} = F_{I''I} \text{ since } F_{I''I''} = 0 .$$

Using the reciprocity relation and the above equations one obtains

$$F_{I'I} = \frac{A_I}{A_{I'}} \cdot F_{I'I'} = \frac{A_I}{A_{I'}} \cdot F_{I'I''} .$$

and

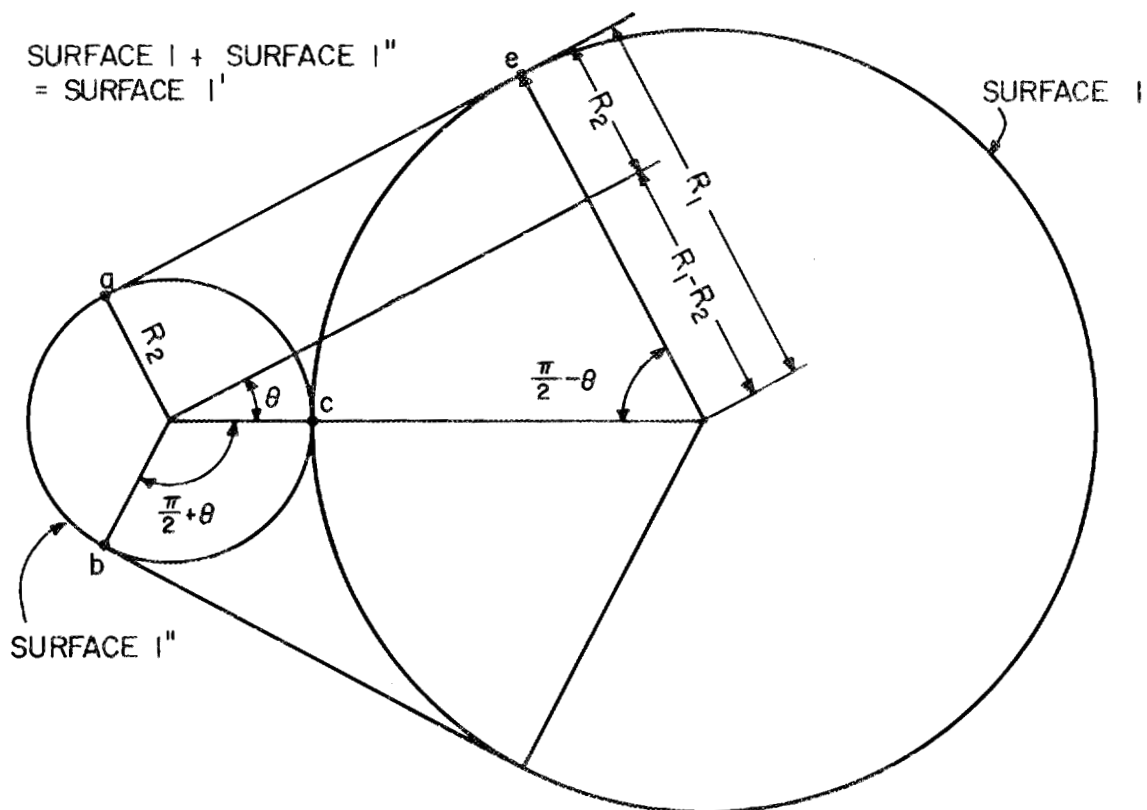
$$F_{I''I} = \frac{A_{I''}}{A_{I'}} \cdot F_{I''I'} = \frac{A_{I''}}{A_{I'}} \cdot F_{I''I} = \frac{A_I}{A_{I'}} \cdot F_{I'I''} .$$

Then

$$F_{I'I'} = F_{I'I} + F_{I'I''} = \frac{2A_I \cdot F_{I'I''}}{A_{I'}} .$$

From Equation (55) it can be seen that the quantity $(2A_I \cdot F_{I'I''})$ equals the sum of the crossed strings minus the sum of the uncrossed strings stretched between A_I and $A_{I''}$. Referring to Figure 53, the length of a crossed string bce is

ORNL DWG 75-8506

Figure 53. Determination of R_1 .

$$R_1 \left(\frac{\pi}{2} - \theta \right) + R_2 \left(\frac{\pi}{2} + \theta \right),$$

while that of an uncrossed string as is

$$\left[(R_1 + R_2)^2 - (R_1 - R_2)^2 \right]^{1/2} = 2(R_1 R_2)^{1/2}.$$

The value of θ is

$$\theta = \sin^{-1} \left(\frac{R_1 - R_2}{R_1 + R_2} \right).$$

Then $F1'1'$ is

$$F1'1' = \frac{2 \left[R_1 \left(\frac{\pi}{2} - \theta \right) + R_2 \left(\frac{\pi}{2} + \theta \right) - 2(R_1 R_2)^{1/2} \right]}{2\pi(R_1 + R_2)},$$

$$F1'1' = 0.5 - \frac{1}{\pi} \left[\frac{(R_1 - R_2) \sin^{-1} \left(\frac{R_1 - R_2}{R_1 + R_2} \right) + 2(R_1 R_2)^{1/2}}{R_1 + R_2} \right].$$

If D is the diameter of a tube and d is the diameter of its wire wrap, the above equation can be written for a tube-wire wrap surface as

$$F1'1' = 0.5 - \frac{1}{\pi} \left[\frac{(D - d) \sin^{-1} \left(\frac{D - d}{D + d} \right) + 2(Dd)^{1/2}}{D + d} \right]. \quad (88)$$

Figures 54 and 55 show cross sections of an array at two different axial locations. The position of the wire wrap relative to a tube as it spirals around the tube will always be between these two locations. The view factors $F1'2'$, $F1'3'$, $F1'5'$, and $F1'8'$ could be approximated by successively estimating their values for case one of Figure 54 and for case

ORNL DWG. 75-8507

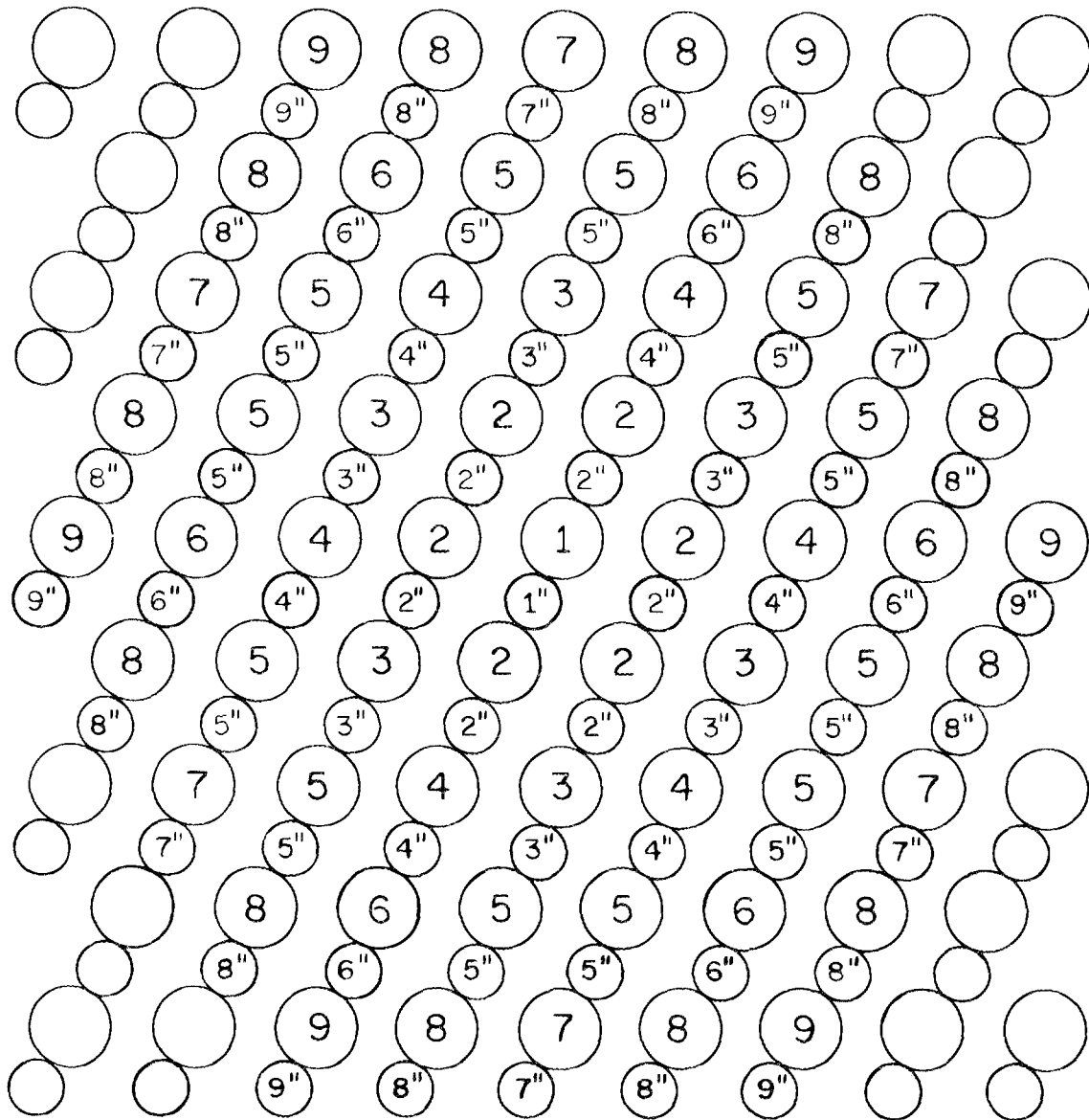


Figure 54. Cross Section of Array at Axial Position at Which Wire Wrap Contacts Adjacent Tube.

ORNL DWG 75-8508

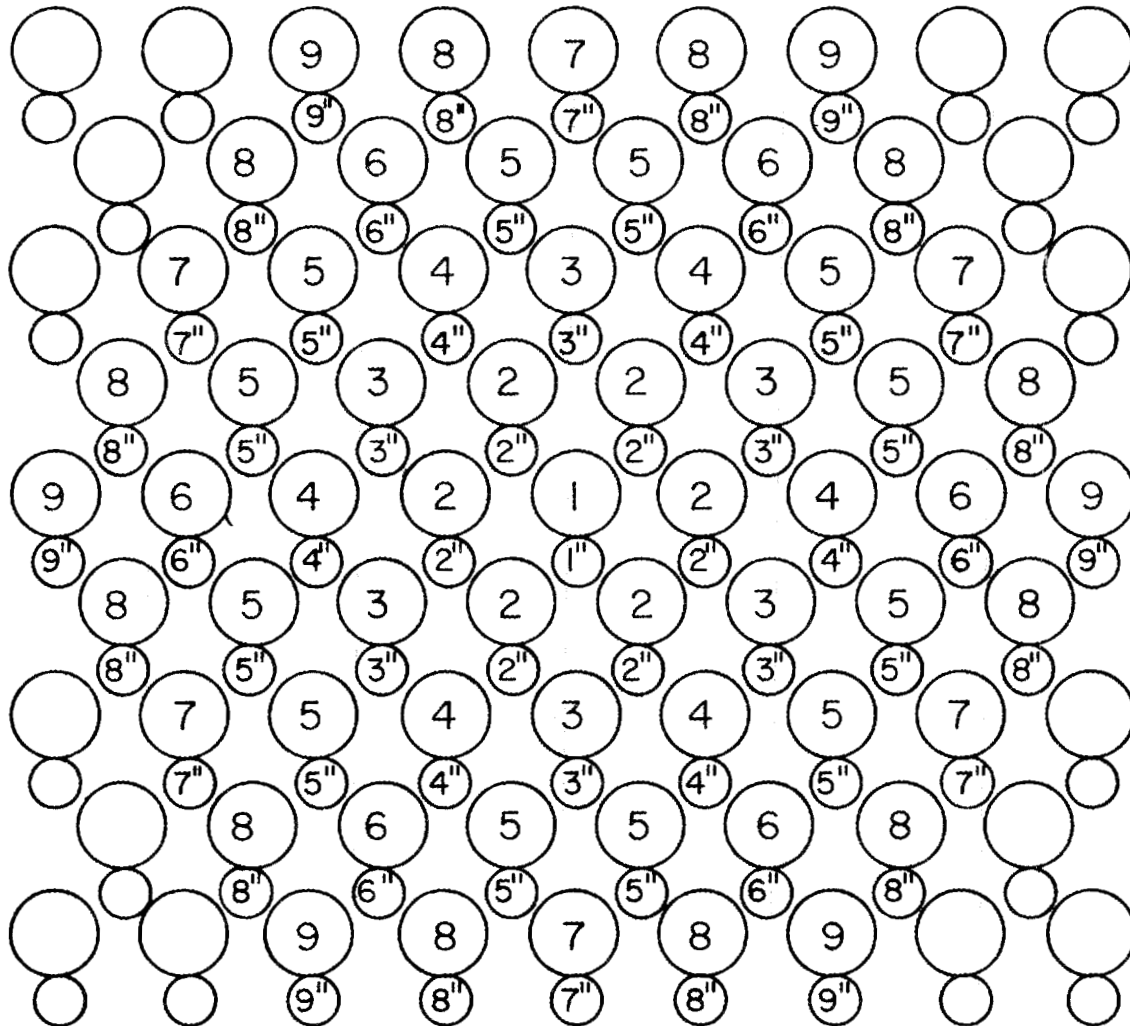


Figure 55. Cross Section of Array at Axial Position at Which Wire Wrap is Farthest from Adjacent Tube.

two of Figure 55 and then averaging the results. Within the accuracy of the estimates, the view factors for the two cases appear to be equal; consequently, only the development of the view factors for case one will be presented.

For a fixed axial location, the values of $F_{1'5'}$ and $F_{1'8'}$ for those surfaces 5' and 8' which 1' is able to see can be related to the values of F_{15} and F_{18} by the following equations:

$$F_{1'5'} = \frac{A_1}{A_{1'}} \cdot F_{15} = \frac{F_{15}}{PDR} ,$$

$$F_{1'8'} = \frac{A_1}{A_{1'}} \cdot F_{18} = \frac{F_{18}}{PDR} .$$

These equations follow from the fact that 1' sees the same areas of 5' and 8' as 1 does of 5 and 8; however, the surface area of a wire-wrapped tube is larger by a factor of PDR than the area of a bare tube so that the view factors $F_{1'5'}$ and $F_{1'8'}$ are similarly reduced. The values of $F_{1'5'}$ and $F_{1'8'}$ are, of course, zero for those surfaces 5' and 8' which 1' cannot see. However, during each spiral of the wire wrap around a tube, the particular tubes 5' and 8' seen by 1' change for each of the six positions corresponding to the configuration shown in Figure 54. At each of these positions, 4 of 12 of the tubes labeled 5' (or 8') are visible so that the length-averaged values are

$$F_{1'5'} = \frac{F_{15}}{3 PDR} , \tag{89}$$

$$F_{1'8'} = \frac{F_{18}}{3 PDR} . \tag{90}$$

In a similar but more approximate manner, the length-averaged value of

F1'3' is estimated to be

$$F1'3' = \frac{F13}{2 \text{ PDR}} . \quad (91)$$

The value of F1'2' is then found by difference from the equation:

$$F1'2' = \frac{1 - 6F1'3' - 12(F1'5' + F1'8')}{6} . \quad (92)$$

APPENDIX C

KLEPPER'S ABSORPTION FACTORS

Absorption factors calculated by O. H. Klepper and reported in reference (19) are reproduced here for the convenience of users of the programs in this report. Interchange factors for cylinders on an equilateral triangular pitch are tabulated in Table VII for emissivities of 0.3, 0.4, 0.5, 0.6, 0.7, 0.8, 0.9, and 0.95 and for PDRs from 1.1 to 1.5 in steps of 0.1. For cylinders on a square pitch, Klepper's values for the interchange factors are given in Table VIII at identical values of emissivity and PDR.

TABLE VII

Klepper's Absorption Factors for Cylinders on
an Equilateral Triangular Pitch

	Emissivity							
	0.3	0.4	0.5	0.6	0.7	0.8	0.9	0.95
Pitch-to-Diameter Ratio = 1.1								
G11	0.225	0.209	0.186	0.160	0.128	0.0901	0.0478	0.0252
G12	0.115	0.120	0.124	0.129	0.135	0.141	0.147	0.152
G13	0.00923	0.00856	0.00833	0.00849	0.00878	0.00929	0.00989	0.0104
G14	0.00111							
Pitch-to-Diameter Ratio = 1.2								
G11	0.188	0.177	0.159	0.137	0.110	0.0772	0.0407	0.0215
G12	0.111	0.116	0.120	0.125	0.130	0.135	0.140	0.143
G13	0.0161	0.0153	0.0152	0.0156	0.162	0.0172	0.0184	0.0193
G14	0.00359	0.00236	0.00158	0.00108				
Pitch-to-Diameter Ratio = 1.3								
G11	0.156	0.149	0.136	0.117	0.0944	0.0665	0.0350	0.0185
G12	0.102	0.108	0.112	0.116	0.120	0.123	0.127	0.129
G13	0.0230	0.0233	0.0239	0.0252	0.0267	0.0287	0.0310	0.0325
G14	0.00650	0.00479	0.00341	0.00244	0.00162			
G15	0.00126							
Pitch-to-Diameter Ratio = 1.4								
G11	0.138	0.134	0.122	0.105	0.0851	0.0600	0.0316	0.0166
G12	0.0967	0.103	0.107	0.111	0.114	0.117	0.120	0.122
G13	0.0265	0.0273	0.0284	0.0301	0.0321	0.0345	0.0373	0.0391
G14	0.00822	0.00625	0.00458	0.00334	0.00226	0.00135		
G15	0.00195	0.00137						
G16	0.00128							
Pitch-to-Diameter Ratio = 1.5								
G11	0.121	0.118	0.108	0.0942	0.0762	0.0538	0.0284	0.0150
G12	0.0899	0.0966	0.101	0.104	0.107	0.109	0.112	0.113
G13	0.0295	0.0314	0.0331	0.0354	0.0380	0.0410	0.0443	0.0464
G14	0.00939	0.00755	0.00566	0.00419	0.00287	0.00174		
G15	0.00260	0.00199	0.00149	0.00121	0.00102			
G16	0.00191	0.00151	0.00115					

TABLE VIII

Klepper's Absorption Factors for Cylinders on a Square Pitch

	Emissivity							
	0.3	0.4	0.5	0.6	0.7	0.8	0.9	0.95
Pitch-to-Diameter Ratio = 1.1								
G11	0.193	0.179	0.160	0.137	0.111	0.0777	0.0415	0.0219
G12	0.125	0.130	0.133	0.138	0.142	0.145	0.149	0.152
G13	0.0605	0.0622	0.0645	0.0679	0.0717	0.0766	0.0819	0.0858
G14	0.00417	0.00332	0.00269	0.00216	0.00167	0.00113		
G15	0.00247	0.00219	0.00207	0.00206	0.00210	0.00221	0.00234	0.00247
Pitch-to-Diameter Ratio = 1.2								
G11	0.156	0.148	0.134	0.115	0.0928	0.0653	0.0345	0.0182
G12	0.114	0.120	0.125	0.130	0.134	0.137	0.141	0.144
G13	0.0602	0.0627	0.0654	0.0687	0.0723	0.0767	0.0814	0.0848
G14	0.00992	0.00782	0.00618	0.00487	0.00367	0.00243	0.00124	
G15	0.00663	0.00580	0.00538	0.00528	0.00532	0.00555	0.00585	0.00614
G17	0.00237	0.00182	0.00143	0.00113				
G18	0.00139	0.00111						
Pitch-to-Diameter Ratio = 1.3								
G11	0.126	0.122	0.111	0.0968	0.0781	0.0551	0.0290	0.0153
G12	0.101	0.108	0.113	0.117	0.121	0.124	0.127	0.129
G13	0.0591	0.0622	0.0650	0.0681	0.0713	0.0748	0.0785	0.0811
G14	0.0132	0.0106	0.00836	0.00652	0.00480	0.00312	0.00151	
G15	0.0118	0.0111	0.0110	0.0113	0.0118	0.0125	0.0134	0.0141
G16	0.00182	0.00109						
G17	0.00381	0.00297	0.00234	0.00185	0.00139			
G18	0.00242	0.00193	0.00165	0.00152	0.00145	0.00145	0.00148	0.00154
Pitch-to-Diameter Ratio = 1.4								
G11	0.110	0.107	0.0987	0.0861	0.0696	0.0492	0.0258	0.0136
G12	0.0921	0.0993	0.104	0.109	0.112	0.115	0.118	0.120
G13	0.0573	0.0607	0.0633	0.0659	0.0684	0.0709	0.0734	0.0753
G14	0.0143	0.0118	0.00937	0.00731	0.00535	0.00345	0.00163	
G15	0.0153	0.0154	0.0157	0.0165	0.0175	0.0188	0.0203	0.0214
G16	0.00269	0.00179	0.00112					
G17	0.00427	0.00340	0.00266	0.00208	0.00154	0.00101		
G18	0.00284	0.00229	0.00192	0.00173	0.00161	0.00157	0.00157	0.00162

TABLE VIII (continued)

	Emissivity							
	0.3	0.4	0.5	0.6	0.7	0.8	0.9	0.95
Pitch-to-Diameter Ratio = 1.5								
G11	0.102	0.100	0.0921	0.0804	0.0650	0.0460	0.0241	0.0127
G12	0.0880	0.0952	0.100	0.104	0.108	0.111	0.113	0.115
G13	0.0565	0.0601	0.0628	0.0654	0.0678	0.0702	0.0725	0.0743
G14	0.0152	0.0127	0.0102	0.00803	0.00592	0.00385	0.00182	
G15	0.0166	0.0169	0.0174	0.0183	0.0195	0.0209	0.0225	0.0237
G16	0.00316	0.00214	0.00136					
G17	0.00486	0.00393	0.00311	0.00245	0.00183	0.00121		
G18	0.00337	0.00281	0.00242	0.00224	0.00214	0.00212	0.00216	0.00224

APPENDIX D

LISTINGS OF COMPUTER PROGRAMS

On the following pages are given the listings of the steady-state (STEADY) and unsteady-state (TRANS) computer programs. As much as possible, the variable names used in the programs duplicate those employed in the report text. Comment cards within the program listing describe the character and format of the input data required.

.....
 LISTING OF THE COMBINED STEADY STATE (STEADY) AND
 UNSTEADY STATE (TRANS) PROGRAMS FOR THE CALCULATION
 OF RADIATIVE HEAT TRANSFER IN HEXAGONAL ARRAYS OF
 CYLINDERS ON AN EQUILATERAL TRIANGULAR PITCH AND IN
 SQUARE ARRAYS OF CYLINDERS ON A SQUARE PITCH

IMPLICIT REAL*8(A-H,O-Z)
 DIMENSION STATEMENT AND VALUE OF NMAX AND MXROWS
 MUST BE CHANGED IF CALCULATIONS ARE TO BE DONE
 FOR ARRAYS OF MORE THAN 37 CYLINDERS IN THE CASE
 OF UNSYMMETRICAL HEAT GENERATION, OR FOR HEX
 ARRAYS OF MORE THAN 331 CYLINDERS AND SQUARE
 ARRAYS OF MORE THAN 256 RODS IN THE CASE OF
 SYMMETRY IN THE DISTRIBUTION OF HEAT FLUXES.
 DIMENSION STATEMENTS MUST ALSO BE CHANGED IN
 SUBROUTINES DERIV AND OUTP.
 INDICES OF G IN DIMENSION STATEMENT MUST
 CORRESPOND TO VALUE OF MXROWS, THOSE OF F TO NMAX,
 AND THAT OF H TO MXROWS*MXROWS*MXROWS*MXROWS.
 DIMENSION G(6,6,6,6),ALX(16,38),C(38,38),F(38,38),
 > A(38),D(38),E(38),X(38),Y(38),Z(38),PRMT(5),IC(38)
 COMMON/MD/C,X,W,M
 COMMON/MD/TPI,NC,KP
 EQUIVALENCE (C(1),G(1))
 EXTERNAL DERIV,OUTP
 NMAX=38
 MXROWS=6
 CDNV=0.5D-10
 SIGMA=0.1712D-8

INPUT DATA CONSISTS OF THE FOLLOWING:
 CARD 1: NVIEW,NGEOM,NSYM,NMETH,NSTATE,
 NEMISS,NFLUX - FORMAT OF 16 IS
 CARD 2: NROWS,NRODS - FORMAT OF 16 IS
 CARD 3: PDR,E(1),AR - FORMAT OF 8F10.0
 (DECIMAL MUST BE PUNCHED)
 IF NSTATE=2, (PRMT(I),I=1,4),W,TPI MUST BE INPUT
 ON FORMAT OF 8F10.0 (PUNCH DECIMAL)
 IF NEMISS=2, (E(I),I=1,N) MUST BE INPUT ON
 FORMAT OF 8F10.0 (PUNCH DECIMAL)
 IF NFLUX=2, (X(I),I=1,M) MUST BE INPUT ON
 FORMAT OF 8F10.0 (PUNCH DECIMAL)
 IF NVIEW=2, KLEPPER'S VALUES FOR ABSORPTION
 FACTORS G11,G12,G13,G14,G15,G16,G17,G18 MUST BE
 INPUT ON A FORMAT OF 8F10.0 (PUNCH DECIMAL)

WHERE:

NVIEW=1 DENOTES UNIFORM RADIOSITY
 NVIEW=2 DENOTES NONUNIFORM RADIOSITY
 NGEOM=1 DENOTES HEXAGONAL ARRAY OF CYLINDERS
 ON AN EQUILATERAL TRIANGULAR PITCH
 NGEOM=2 DENOTES SQUARE ARRAY OF CYLINDERS
 ON A SQUARE PITCH
 NSYM=1 DENOTES SYMMETRICAL HEAT GENERATION
 NSYM=2 DENOTES UNSYMMETRICAL HEAT GENERATION
 NMETH=1 DENOTES NET RADIATION METHOD
 NMETH=2 DENOTES HOTTTEL'S METHOD
 NSTATE=1 DENOTES STEADY STATE
 NSTATE=2 DENOTES UNSTEADY STATE
 NEMISS=1, ALL SURFACES HAVE SAME EMISSIVITY
 NEMISS=2, SURFACES VARY IN EMISSIVITY
 NFLUX=1, CYLINDERS HAVE SAME HEAT GENERATION RATE
 NFLUX=2, CYLINDERS VARY IN HEAT GENERATION
 NROWS=NUMBER OF ROWS IN ARRAY
 NRODS=NUMBER OF CYLINDERS IN ARRAY

```

C      PDR=PITCH-TO-DIAMETER RATIO OF CYLINDERS
C      AR=RATIO OF SURFACE AREA OF A SINGLE
C      CYLINDER TO SURFACE AREA OF SHROUD
C      E(1)=EMISSIVITY OF SURFACE 1
C      E(I)=EMISSIVITY OF SURFACE I
C      X(I)=RATIO OF HEAT FLUX FOR SURFACE I
C      TO HEAT FLUX FOR REFERENCE SURFACE
C      M=NUMBER OF INDEPENDENT SURFACES (EXCLUDING
C      SHROUD), M=NRODS IF NSYM=2, OTHERWISE
C      M<NRODS (SEE CHAPTER 5)
C      N=M+1 (N IS SURFACE NUMBER ASSIGNED TO SHROUD)
C      PRMT IS DESCRIBED IN SUBROUTINE DHPCG
C      TPI=INTERVAL OF INDEPENDENT VARIABLE THETA AT
C      WHICH OUTPUT IS DESIRED FOR TRANSIENT SOLUTION.
C      TPI MUST BE AN INTEGER MULTIPLE OF PRMT(3).
C      W=DIMENSIONLESS SHROUD TEMP. (SEE CHAPTER 3)
1 READ 100,NVIEW,NGEOM,NSYM,NMETH,NSTATE,NEMISS,NFLUX
IF (NVIEW .EQ. 0) GO TO 70
READ 100,NROWS,NRODS
READ 101,PDR,E(1),AR
IF (NSTATE .EQ. 2) READ 101,(PRMT(I),I=1,4),W,TPI
C      DETERMINATION OF NUMBER OF INDEPENDENT SURFACES
M=NRODS
IF (NSYM .EQ. 2) GO TO 7
GO TO (3,5),NGEOM
3 M=0
DO 4 I=1,NROWS
4 M=M+(I+1)/2
GO TO 7
5 M=0
I2=(NROWS+1)/2
DO 6 I=1,I2
6 M=M+I
7 N=M+1
C      SET OR READ IN EMISSIVITIES AND HEAT FLUXES
DO 8 I=1,M
E(I)=E(1)
8 X(I)=1.D0
E(N)=E(1)
IF (NEMISS .EQ. 2) READ 101,(E(I),I=1,N)
IF (NFLUX .EQ. 2) READ 101,(X(I),I=1,M)
GO TO (10,35),NVIEW
10 EMISS=1.D0
GO TO (11,14),NGEOM
C      CALCULATION OF BLACK BODY VIEW FACTORS
C      FOR CYLINDERS ON A TRIANGULAR PITCH
11 CALL EQVIEW(PDR,F11,F12,F13,F15,F18,F18A,ERROR)
GO TO (12,13),NSYM
C      CONSTRUCTION OF MATRIX OF BLACK BODY VIEW FACTORS
C      FOR HEXAGONAL ARRAY WITH SYM. HT. GENERATION
12 CALL HXSYM(F,A,NROWS,N,NMAX,AR,EMISS,
> F11,F12,F13,F15,F18A,IC)
GO TO 17
C      CONSTRUCTION OF MATRIX OF BLACK BODY VIEW FACTORS
C      FOR HEXAGONAL ARRAY WITH ARBITRARY HT. GENERATION
13 CALL HEX(F,A,NROWS,N,NMAX,AR,EMISS,
> F11,F12,F13,F15,F18A,IC)
GO TO 17
C      CALCULATION OF BLACK BODY VIEW FACTORS
C      FOR CYLINDERS ON A SQUARE PITCH
14 CALL SQVIEW(PDR,F11,F12,F13,F15,F18,F18A,ERROR)
GO TO (15,16),NSYM
C      CONSTRUCTION OF MATRIX OF BLACK BODY VIEW FACTORS
C      FOR SQUARE ARRAY WITH SYM. HT. GENERATION
15 CALL SQSYM(F,A,NROWS,N,NMAX,AR,EMISS,
> F11,F12,F13,F15,F18A,IC)
GO TO 17
C      CONSTRUCTION OF MATRIX OF BLACK BODY VIEW FACTORS
C      FOR SQUARE ARRAY WITH ARBITRARY HT. GENERATION
16 CALL SQUARE(F,A,NROWS,N,NMAX,AR,EMISS,F11,F12,

```

```

    > F13,F15,F18A,G,MXRQWS)
17 GO TO (18,30),NMETH
18 GO TO (19,29),NSTATE
C     SOLUTION OF STEADY STATE PROBLEM
C     BY NET RADIATION METHOD
19 X(N)=0.D0
    DO 20 I=1,M
      X(N)=X(N)-X(I)*A(I)
      C(I,1)=-X(I)
      F(I,I)=F(I,I)-1.D0
20 Z(I)=C(I,1)/F(I,I)
    IF (M .EQ. 1) GO TO 21
    CALL SIMEQ(F,C(1,1),Z,M,NMAX,CCNV)
21 Z(N)=0.D0
    ALPHA=-(1.D0-E(N))/E(N)*X(N)
    DO 22 I=1,N
      Y(I)=Z(I)*(1.D0-E(I))/E(I)*X(I)+ALPHA
22 GO TO 60
29 PRINT 215
    STOP
C     DETERMINE MATRIX OF SCRIPT F FACTORS
30 CONTINUE
    DO 33 I=1,N
      DO 32 J=1,N
        C(I,J)=-F(I,J)*E(J)
32 F(I,J)=F(I,J)*(1.D0-E(J))/E(J)
33 F(I,I)=F(I,I)-1.D0/E(I)
    CALL MATQ(F,C,N,N,DET,NMAX,NMAX,IC)
    GO TO 47
C     NONUNIFORM RADIOSITY
C     READ IN KLEPPER'S VALUES FOR ABSORPTION FACTORS
C     VALID ONLY IF ALL SURFACES HAVE SAME EMISSIVITY
35 READ 101,G11,G12,G13,G14,G15,G16,G17,G18
    G1=G11
    G2=G12
    G3=G13
    G4=G14
    G5=G15
    G6=G16
    G7=G17
    G8=G18
    GO TO (36,37),NGEOM
36 SUM=G11+6.D0*(G12+G13+G14+G16+G17)+12.D0*(G15+G18)
C     BECAUSE KLEPPER'S ABSORPTION FACTORS DO NOT SUM TO
C     ONE, THE ABSORPTION FACTOR G18 IS ADJUSTED SO THAT
C     ALL THE RADIATION LEAVING A CYLINDER IS CONSIDERED
    G18=G18+(1.D0-SUM)/12.D0
C     BECAUSE THE GRAY EDDY VIEW FACTOR MATRIX IS BEING
C     CONSTRUCTED USING A SUBROUTINE DESIGNED FOR ELACK
C     BODY VIEW FACTOR MATRIX CONSTRUCTION, THE VALUES
C     OF G13,G15,G18 ARE INCREASED TO COMPENSATE FOR
C     ZERO VALUES OF G14,G16,G17 IN THE MATRIX
    G13=G13+G14
    G15=G15+0.5D0*G16
    G18=G18+0.5D0*G17
    GO TO 38
37 SUM=G11+4.D0*(G12+G13+G14+G16+G17)+8.D0*(G15+G18)
    G18=G18+(1.D0-SUM)/8.D0
    G15=G15+0.5D0*(G14+G16)
    G18=G18+0.5D0*G17
38 EMISS=E(1)
C     CALCULATION OF HOTTEL'S GRAY EDDY VIEW FACTORS
    F11=EMISS*G11
    F12=EMISS*G12
    F13=EMISS*G13
    F15=EMISS*G15
    F18=EMISS*G18
    GO TO (41,44),NGEOM
41 GO TO (42,43),NSYM
C     CONSTRUCTION OF MATRIX OF GRAY BODY VIEW FACTORS

```

```

C      FOR HEXAGONAL ARRAY WITH SYM. HT. GENERATION
42 CALL HXSVM(C,A,NROWS,N,NMAX,AR,EMISS,
  > F11,F12,F13,F15,F18,IC)
  GO TO 47
C      CONSTRUCTION OF MATRIX OF GRAY BODY VIEW FACTORS
C      FOR HEXAGONAL ARRAY WITH ARBITRARY HT. GENERATION
43 CALL HEX(C,A,NROWS,N,NMAX,AR,EMISS,
  > F11,F12,F13,F15,F18,IC)
  GO TO 47
44 GO TO (45,46),NSYM
C      CONSTRUCTION OF MATRIX OF GRAY BODY VIEW FACTORS
C      FOR SQUARE ARRAY WITH SYM. HT. GENERATION
45 CALL SQSYM(C,A,NROWS,N,NMAX,AR,EMISS,
  > F11,F12,F13,F15,F18,IC)
  GO TO 47
C      CONSTRUCTION OF MATRIX OF GRAY BODY VIEW FACTORS
C      FOR SQUARE ARRAY WITH ARBITRARY HT. GENERATION
46 CALL SQUARE(F,A,NROWS,N,NMAX,AR,EMISS,F11,F12,
  > F13,F15,F18,G,MXROWS)
  DO 461 I=1,N
  DO 461 J=1,N
461 C(I,J)=F(I,J)
47 GO TO (48,51),NSTATE
C      SOLUTION OF STEADY STATE PROBLEM
C      BY HOTTEL'S METHOD
48 X(N)=0.DO
  DO 49 I=1,M
  X(N)=X(N)-X(I)*A(I)
  C(I,I)=C(I,I)-E(I)
  D(I)=-X(I)
49 Y(I)=D(I)/C(I,I)
  IF (M .EQ. 1) GO TO 50
  CALL SIMEQ(C,D,Y,M,NMAX,CONV)
50 Y(N)=0.DO
  GO TO 60
C      SOLUTION OF TRANSIENT PROBLEM
C      BY HOTTEL'S METHOD
51 EW=M
  EW=1.DO/EW
  X(N)=0.DO
  DO 52 I=1,M
  X(N)=X(N)-X(I)*A(I)
  C(I,I)=C(I,I)-E(I)
  D(I)=EW
52 Y(I)=0.DO
  GO TO 60
53 NC=-1
  KP=0
  CALL DHPCG(FRMT,Y,C,M,IHLF,DERIV,OUTP,ALX)
  IF (IHLF .GT. 10) PRINT 216
  IF (IHLF .EQ. 11) PRINT 217
  IF (IHLF .EQ. 12) PRINT 218
  IF (IHLF .EQ. 13) PRINT 219
  GO TO 1
60 IF (NGEQM .EQ. 1) PRINT 201,NROWS,NRODS
  IF (NGECM .EQ. 2) PRINT 202,NROWS,NRODS
  IF (NMETH .EQ. 1) PRINT 221
  IF (NMETH .EQ. 2) PRINT 222
  IF (NVIEW .EQ. 1) PRINT 223
  IF (NVIEW .EQ. 2) PRINT 224
  IF (NSYM .EQ. 1) PRINT 225
  IF (NSYM .EQ. 2) PRINT 226
  PRINT 203,AR
  PRINT 204,PDR
  IF (NSTATE .EQ. 2) PRINT 220,W
  IF (NVIEW .EQ. 1) PRINT 205,F12,F13,F15,F18,F18A
  IF (NVIEW .EQ. 2) PRINT 206,G1,G2,G3,G4,G5,G6,G7,G8
  GO TO (61,53),NSTATE
61 PRINT 207
  PRINT 208

```

```

      IF (NMETH .EQ. 1) PRINT 209, (I, E(I), X(I), Z(I),
1 Y(I), I=1, N)
      IF (NMETH .EQ. 2) PRINT 210, (I, E(I), X(I), Y(I),
1 I=1, N)
      PRINT 211
      GO TO 1
70 STOP
100 FORMAT(16I5)
101 FORMAT(8F10.0)
102 FORMAT(2F10.0)
201 FORMAT(' HEXAGONAL ARRAY OF', I3, ' ROWS OF', I4,
1 ' RODS ON AN EQUILATERAL TRIANGULAR PITCH')
202 FORMAT(' SQUARE ARRAY OF', I3, ' ROWS OF', I4,
1 ' RODS ON A SQUARE PITCH')
203 FORMAT(' RATIO OF SURFACE AREA OF A SINGLE ROD ',
1 ' TO THAT OF SHROUD IS ', 1PE11.3)
204 FORMAT(' PITCH-TO-DIAMETER-RATIO=', F6.3)
205 FORMAT(' BLACK BODY VIEW FACTORS ARE F12=', F13.10,
1 2X, 'F13=', F13.10, '/', 5X, 'F15=', F13.10, 2X, 'F18=',
2 F13.10, 2X, 'F18*=', F13.10, '/')
206 FORMAT(' KLEPPER'S ABSORPTION FACTORS ARE G11=',
1 F13.10, ' G12=', F13.10, '/', 5X, 'G13=', F13.10, ' G14=',
2 F13.10, ' G15=', F13.10, '/', 5X, 'G16=', F13.10, ' G17=',
3 F13.10, ' G18=', F13.10, '/')
207 FORMAT(' SURFACE EMISSIVITY DIMENSIONLESS ',
1 ' DIMENSIONLESS DIMENSIONLESS')
208 FORMAT(25X, 'HEAT FLUX, X TEMPERATURE, Z ',
1 ' TEMPERATURE, Y', '/')
209 FORMAT(16, 0PF13.3, 1P3D16.3)
210 FORMAT(16, 0PF13.3, 1PC16.3, 16X, D16.3)
211 FORMAT(1H1)
215 FORMAT(' NET RADIATION METHOD CANNOT BE USED ',
1 ' FOR TRANSIENT PROBLEM')
216 FORMAT(' TRANSIENT SOLUTION ABORTED DURING',
1 ' INTEGRATION IN SUBROUTINE DHFCG')
217 FORMAT(' NUMBER OF BISECTIONS OF INITIAL INCREMENT',
1 ' IS GREATER THAN 10')
218 FORMAT(' EITHER INPUT VALUE OF STEP SIZE OR OF THE',
1 ' INTEGRATION INTERVAL IS ZERO')
219 FORMAT(' SIGN OF INTEGRATION STEP SIZE DOES NOT',
1 ' EQUAL THE SIGN OF THE DIFFERENCE OF THE UPPER',
2 ' AND LOWER BOUNDS OF THE INTEGRATION RANGE')
220 FORMAT(' W=', F10.3)
221 FORMAT(' SOLUTION BY NET RADIATION METHOD')
222 FORMAT(' SOLUTION BY HOTTEL'S METHOD')
223 FORMAT(' UNIFORM RADIOSITY')
224 FORMAT(' NONUNIFORM RADIOSITY')
225 FORMAT(' SYMMETRICAL HT. GENERATION DISTRIBUTION')
226 FORMAT(' UNSYMMETRICAL HT. GENERATION DISTRIBUTION')
      END

```

.....

SUBROUTINE DHPCG

PURPOSE

TO SOLVE A SET OF FIRST ORDER ORDINARY GENERAL
DIFFERENTIAL EQUATIONS WITH GIVEN INITIAL VALUES

USAGE

CALL DHPCG (PRMT,Y,DERY,NDIM,IHLF,FCT,OUTP,AUX)
PARAMETERS FCT,OUTP REQUIRE EXTERNAL STATEMENT

DESCRIPTION OF PARAMETERS

PRMT, INPUT AND OUTPUT VECTOR MADE UP OF:

PRMT(1), LOWER BOUND OF INTEGRATION INTERVAL

PRMT(2), UPPER BOUND OF INTEGRATION INTERVAL

PRMT(3), INITIAL STEP SIZE OF INDEPENDENT VARIABLE

PRMT(4), ERROR BOUND. IF ABSOLUTE ERROR > PRMT(4),

STEP SIZE IS HALVED. IF ERROR < PRMT(4)/50 AND

STEP SIZE < PRMT(3), STEP SIZE IS DOUBLED. USER

MAY CHANGE PRMT(4) DURING INTEGRATION IN OUTP.

PRMT(5), NOT INPUT. DHPCG INITIALIZES PRMT(5)=0. IF

USER WISHES TO END INTEGRATION AT ANY OUTPUT POINT,

PRMT(5) IS MADE NON-ZERO IN OUTP.

Y, INPUT VECTOR OF INITIAL VALUES (DESTROYED).

LATER, Y IS VECTOR OF DEPENDENT VARIABLES COMPUTED

AT INTERMEDIATE POINTS X.

DERY, INPUT VECTOR OF ERROR WEIGHTS. SUM OF ITS

COMPONENTS MUST = 1. LATER, DERY IS VECTOR OF

DERIVATIVES OF Y AT POINT X.

NDIM, NUMBER OF EQUATIONS IN SYSTEM

IHLF, OUTPUT VALUE WHICH SPECIFIES NUMBER OF

BISECTIONS OF INITIAL STEP SIZE.

FCT, EXTERNAL SUBROUTINE SUPPLIED BY USER TO COMPUTE

RIGHT HAND SIDE OF DERY GIVEN VALUES OF X AND Y. ITS

PARAMETER LIST MUST BE X,Y,DERY AND IT MUST NOT

DESTROY X AND Y.

OUTP, EXTERNAL SUBROUTINE SUPPLIED BY USER FOR OUTPUT

PURPOSES. ITS PARAMETERS ARE X,Y,DERY,IHLF,NDIM,

AND PRMT. NONE OF THESE PARAMETERS (EXCEPT PRMT(4)

OR PRMT(5)) SHOULD BE CHANGED BY OUTP.

AUX, AUXILIARY STORAGE ARRAY WITH 16 ROWS AND

NDIM COLUMNS

METHOD

EVALUATION IS DONE BY HAMMING'S MODIFIED PREDICTOR-

CORRECTOR METHOD. IT IS A FOURTH ORDER METHOD USING

4 PRECEDING POINTS FOR COMPUTATION OF NEW Y. FOURTH

ORDER RUNGE-KUTTA METHOD SUGGESTED BY RALSTON IS

USED FOR INITIAL ADJUSTMENT OF INCREMENT AND FOR

COMPUTATION OF STARTING VALUES. DHPCG AUTOMATICALLY

ADJUSTS STEP SIZE DURING COMPUTATION BY HALVING OR

DOUBLING. FOR REFERENCE, SEE -

(1) RALSTON/IHLF, MATHEMATICAL METHODS FOR DIGITAL

COMPUTERS, PP. 95-100.

(2) RALSTON, RUNGE-KUTTA METHODS WITH MINIMUM ERROR

BOUNDS, MTAC, VOL 16, ISSUE 80(1962), PP. 431-7.

.....

SUBROUTINE DHPCG(PRMT,Y,DERY,NDIM,IHLF,FCT,OUTP,AUX)

IMPLICIT REAL*8(A-H,O-Z)

DIMENSION PRMT(1),Y(1),DERY(1),AUX(16,1)

N=1

IHLF=0

X=PRMT(1)

H=PRMT(3)

PRMT(5)=0.D0

DO 1 I=1,NDIM

AUX(16,I)=0.D0

AUX(15,I)=DERY(I)

1 AUX(1,I)=Y(I)


```

      CALL FCT(X,Y,DERY)
      X=PRMT(1)
      DO 22 I=1,NDIM
      AUX(11,I)=DERY(I)
22  Y(I)=AUX(1,I)+H*(.375D0*AUX(8,I)+.7916666666666667D0*
1  AUX(9,I)-.2083333333333333D0*AUX(10,I)+
2  .0416666666666667D0*DERY(I))
23  X=X+H
      N=N+1
      CALL FCT(X,Y,DERY)
      CALL OUTP(X,Y,DERY,H,NDIM,PRMT)
      IF(PRMT(5))6,24,6
24  IF(N-4)25,200,200
25  DO 26 I=1,NDIM
      AUX(N,I)=Y(I)
26  AUX(N+7,I)=DERY(I)
      IF(N-3)27,29,200
C
27  DO 28 I=1,NDIM
      DELT=AUX(9,I)+AUX(9,I)
      DELT=DELT+DELT
28  Y(I)=AUX(1,I)+.3333333333333333D0*H*(AUX(8,I)+
1  DELT+AUX(10,I))
      GOTO 23
C
29  DO 30 I=1,NDIM
      DELT=AUX(9,I)+AUX(10,I)
      DELT=DELT+DELT+DELT
30  Y(I)=AUX(1,I)+.375D0*H*(AUX(8,I)+DELT+AUX(11,I))
      GOTO 23
C
C *****
C THE FOLLOWING PART OF SUBROUTINE DHPCG COMPUTES BY
C MEANS OF RUNGE-KUTTA METHOD STARTING VALUES FOR THE
C NOT SELF-STARTING PREDICTOR-CORRECTOR METHOD.
100 DO 101 I=1,NDIM
      Z=H*AUX(N+7,I)
      AUX(5,I)=Z
101 Y(I)=AUX(N,I)+.4D0*Z
      Z IS AN AUXILIARY STORAGE LOCATION
C
      Z=X+.4D0*H
      CALL FCT(Z,Y,DERY)
      DO 102 I=1,NDIM
      Z=H*DERY(I)
      AUX(6,I)=Z
102 Y(I)=AUX(N,I)+.2969776092477536D0*AUX(5,I)+
1  .15875964497103583D0*Z
C
      Z=X+.45573725421878943D0*H
      CALL FCT(Z,Y,DERY)
      DO 103 I=1,NDIM
      Z=H*DERY(I)
      AUX(7,I)=Z
103 Y(I)=AUX(N,I)+.21810038822592047D0*AUX(5,I)-
1  3.0509651486929308D0*AUX(6,I)+3.8328647604670103D0*Z
C
      Z=X+H
      CALL FCT(Z,Y,DERY)
      DO 104 I=1,NDIM
104 Y(I)=AUX(N,I)+.17476028226269037D0*AUX(5,I)-
1  .55148066287873294D0*AUX(6,I)+1.2055355993965235D0*
2  AUX(7,I)+.17118478121951903D0*H*DERY(I)
      GOTO(9,13,15,21),ISW
      *****
C
C POSSIBLE BREAK-POINT FOR LINKAGE
C
C STARTING VALUES ARE COMPUTED.
C START HAMMING'S MODIFIED PREDICTOR-CORRECTOR METHOD.

```

```

200 ISTEP=3
201 IF(N-8)204,202,204
C
C N=8 CAUSES ROWS OF AUX TO CHANGE STORAGE LOCATIONS.
202 DO 203 N=2,7
DO 203 I=1,NDIM
AUX(N-1,I)=AUX(N,I)
203 AUX(N+6,I)=AUX(N+7,I)
N=7
C
C N LESS THAN 8 CAUSES N+1 TO GET N
204 N=N+1
C
C COMPUTATION OF NEXT VECTOR Y
DO 205 I=1,NDIM
AUX(N-1,I)=Y(I)
205 AUX(N+6,I)=DERY(I)
X=X+H
206 ISTEP=ISTEP+1
DO 207 I=1,NDIM
DELT=AUX(N-4,I)+1.3333333333333333D0*H*(AUX(N+6,I)+
1 AUX(N+6,I)-AUX(N+5,I)+AUX(N+4,I)+AUX(N+4,I))
Y(I)=DELT-.9256198347107438D0*AUX(16,I)
207 AUX(16,I)=DELT
C
C PREDICTOR GENERATED IN ROW 16 OF AUX, MODIFIED
C PREDICTOR GENERATED IN Y, DELT IS AUXILIARY STORAGE.
C
C CALL FCT(X,Y,DERY)
C DERIVATIVE OF MODIFIED PREDICTOR IS GENERATED IN DERY
C
DO 208 I=1,NDIM
DELT=.125D0*(5.00*AUX(N-1,I)-AUX(N-3,I)+3.00*H*
1 (DERY(I)+AUX(N+6,I)+AUX(N+6,I)-AUX(N+5,I)))
AUX(16,I)=AUX(16,I)-DELT
208 Y(I)=DELT+.07438016528925620D0*AUX(16,I)
C
C TEST WHETHER H MUST BE HALVED OR DOUBLED
DELT=0.00
DO 209 I=1,NDIM
209 DELT=DELT+AUX(15,I)*DABS(AUX(16,I))
IF(DELT-PRMT(4))210,222,222
C
C H MUST NOT BE HALVED. THAT MEANS Y(I) ARE GOOD.
210 CALL FCT(X,Y,DERY)
CALL OUTP(X,Y,DERY,H,NDIM,PRMT)
IF(PRMT(5))212,211,212
211 IF(IHLF-1)213,212,212
212 RETURN
213 IF(H*(X-PRMT(2)))214,212,212
214 IF(DABS(X-PRMT(2))-1D0*DABS(H))212,215,215
215 IF(DELT-.02D0*PRMT(4))216,216,201
C
C H COULD BE DOUBLED IF ALL NECESSARY PRECEEDING
C VALUES ARE AVAILABLE.
216 IF(IHLF)201,201,217
217 IF(N-7)201,218,218
218 IF(ISTEP-4)201,219,219
219 CHEK=(PRMT(2)-X)/(H+H)+.0000001D0
NCHEK=NCHEK
XCHEK=NCHEK
IF (DABS(CHEK-XCHEK) .GT. .00001D0) GO TO 201
H=H+H
IHLF=IHLF-1
ISTEP=0
DO 221 I=1,NDIM
AUX(N-1,I)=AUX(N-2,I)
AUX(N-2,I)=AUX(N-4,I)
AUX(N-3,I)=AUX(N-6,I)
AUX(N+6,I)=AUX(N+5,I)
AUX(N+5,I)=AUX(N+3,I)

```

```

      AUX(N+4,I)=AUX(N+1,I)
      DELT=AUX(N+6,I)+AUX(N+5,I)
      DELT=DELT+DELT+DELT
221 0AUX(16,I)=8.962962962962963D0*(Y(I)-AUX(N-3,I))
      1-3.361111111111111D0*H*(DERY(I)+DELT+ALX(N+4,I))
      GOTO 201
C
C      H MUST BE HALVED
222 IHLF=IHLF+1
      IF(IHLF-10)223,223,210
223 H=.5D0*H
      ISTEP=0
      DO 224 I=1,NDIM
      Y(I)=.390625D-2*(8.D0*AUX(N-1,I)+135.D0*AUX(N-2,I)+
1 4.D0*AUX(N-3,I)+AUX(N-4,I))- .1171875D0*(AUX(N+6,I)-
2 6.D0*AUX(N+5,I)-AUX(N+4,I))*H
      AUX(N-4,I)=.390625D-2*(12.D0*AUX(N-1,I)+135.D0*
1 AUX(N-2,I)+108.D0*AUX(N-3,I)+AUX(N-4,I))- .0234375D0*
2 (AUX(N+6,I)+18.D0*AUX(N+5,I)-9.D0*AUX(N+4,I))*H
224 AUX(N+4,I)=AUX(N+5,I)
      X=X-H
      DELT=X-(H+H)
      CALL FCT(DELT,Y,DERY)
      DO 225 I=1,NDIM
      AUX(N-2,I)=Y(I)
      AUX(N+5,I)=DERY(I)
225 Y(I)=AUX(N-4,I)
      DELT=DELT-(H+H)
      CALL FCT(DELT,Y,DERY)
      DO 226 I=1,NDIM
      DELT=AUX(N+5,I)+AUX(N+4,I)
      DELT=DELT+DELT+DELT
      0AUX(16,I)=8.962962962962963D0*(AUX(N-1,I)-Y(I))
      1-3.361111111111111D0*H*(AUX(N+6,I)+DELT+DERY(I))
226 AUX(N+3,I)=DERY(I)
      GOTO 206
      END

```

```

C .....
C
C SUBROUTINE OUTP
C
C OUTP IS THE OUTPUT SUBROUTINE FOR THE
C TRANSIENT SOLUTION ALGORITHM DFPCG
C .....
C
C SUBROUTINE OUTP(THETA,Y,DERY,DELTA,M,PRMT)
C IMPLICIT REAL*8(A-H,O-Z)
C COMMON/MD/TPI,NC,KP
C DIMENSION Y(1),DERY(1),PRMT(1),P(10),T(10),
C > YP(10,38),NSTEP(10)
C DATA CONV/0.5D0/
C NC=NC+1
C CHECK TO SEE IF AT AN OUTPUT POINT. IF SO STORE
C VALUES FOR LATER PRINTING.
C Q=THETA/TPI
C Q=Q+.0000001D0
C NQ=Q
C XNQ=NG
C IF (DABS(Q-XNQ) .GT. .00001D0) RETURN
C KP=KP+1
C NSTEP(KP)=NC
C H(KP)=DELTA
C T(KP)=THETA
C DO 1 I=1,M
C 1 YP(KP,I)=Y(I)
C IF (KP-10) 2,6,6
C CHECK TO SEE IF AT END OF INTEGRATION INTERVAL
C 2 IF (DELTA*(THETA-PRMT(2))) 3,5,5
C 3 IF (DABS(THETA-PRMT(2))- .1D0*DABS(DELTA)) 5,4,4
C USING CENTER ROD AS BASIS. CHECK TO SEE IF CLOSE
C TO STEADY STATE ( MAY NEED TO USE ANOTHER ROD AS
C BASIS IF ROD 1 HAS NO HT. GENERATION; MAY ALSO WISH TO
C CHANGE VALUE OF CONV ).
C 4 IF (DABS(DERY(1)) .GT. CONV) RETURN
C 5 PRMT(5)=1.D0
C 6 PRINT 200,(NSTEP(K),K=1,KP)
C PRINT 201,(H(K),K=1,KP)
C PRINT 202,(T(K),K=1,KP)
C PRINT 203
C DO 7 J=1,M
C 7 PRINT 204,J,(YP(K,J),K=1,KP)
C PRINT 205
C KP=0
C 200 FORMAT(1X,'STEP',7X,10I10)
C 201 FORMAT(/,' STEP SIZE ',10F10.4)
C 202 FORMAT(/,' THETA',8X,10F10.3)
C 203 FORMAT(/,6X,'ROD',5X,10(6X,' Y '),/)
C 204 FORMAT(6X,12,6X,10F10.3)
C 205 FORMAT(1H1)
C RETURN
C END

```


C
C
C
C
C
C
C

.....
SUBROUTINE SIMEQ

SIMEQ SOLVES A SET OF LINEAR ALGEBRAIC
EQUATIONS BY THE GAUSS-SEIDEL METHOD

.....
SUBROUTINE SIMEQ(B,C,Z,M,NMAX,CONV)
IMPLICIT REAL*8(A-H,O-Z)
DIMENSION B(NMAX,NMAX),C(NMAX),Z(NMAX)
ITER=0

```

1  ERROR=0.D0
   ITER=ITER+1
   IF (ITER .GT. 1000) PRINT 200
   IF (ITER .GT. 1000) STOP
   DO 7 I=1,M
     SUM=0.D0
     IF (I .EQ. 1) GO TO 4
     J1=I-1
     DO 3 J=1,J1
3    SUM=SUM+B(I,J)*Z(J)
     IF (I .EQ. M) GO TO 6
4    J2=I+1
     DO 5 J=J2,M
5    SUM=SUM+B(I,J)*Z(J)
6    ZZ=(C(I)-SUM)/B(I,I)
     ERR=DABS(Z(I)-ZZ)
     IF (ERR .GT. ERROR) ERRCOR=ERR
7    Z(I)=ZZ
     IF (ERROR .LT. CONV) RETURN
   GO TO 1
200 FORMAT(* NO CONVERGENCE IN SIMEQ IN 1000 ITERATIONS*)
   END

```



```
      IK=(K-1)*NA+I
16  X(IJ)=X(IJ)-A(IK)*X(KJ)
5   CONTINUE
      NRRN=(NR-1)*NA+NR
      IF(A(NRRN)) 17,9,17
17   PIVOT=1.00/A(NRRN)
      DO 18 J=1,NV
      NRJ=(J-1)*NX+NR
      X(NRJ)=X(NRJ)*PIVOT
      DO 18 K=1,NR1
      I=NR-K
      SUM=0.00
      DO 19 L=I,NR1
      IL=L*NA+I
      LJ=(J-1)*NX+(L+1)
      IF (A(IL) .EQ. 0.00) GO TO 19
      SUM=SUM+A(IL)*X(LJ)
19  CONTINUE
      IJ=(J-1)*NX+I
18  X(IJ)=X(IJ)-SUM
      RETURN
      END
```


C
C
C
C
C
C
C
C

.....
SUBROUTINE SQVIEW

SQVIEW CALCULATES THE BLACK BODY VIEW FACTORS FOR
INFINITELY LONG CYLINDERS ON A SQUARE PITCH

.....
SUBROUTINE SQVIEW(PDR,F11,F12,F13,F15,F18,F18A,ERROR)

IMPLICIT REAL*8(A-H,O-Z)

PI=3.141592653589793D0

D2=DSQRT(2.D0)

D5=DSQRT(5.D0)

D10=DSQRT(10.D0)

C1=PI+PI

C2=PI/2.D0

C3=PI/4.D0

C4=DATAN(.5D0)

C5=DATAN(2.D0/11.D0)

C6=CATAN(2.D0)

S1=DSQRT(PDR*PDR-1.D0)

S2=DSQRT(2.D0*PDR*PDR-1.D0)

S5=DSQRT(5.D0*PDR*PDR-1.D0)

S10=DSQRT(10.D0*PDR*PDR-1.D0)

T1=S1-DATAN(S1)

T2=S2-DATAN(S2)

T5=S5-DATAN(S5)

T10=S10-DATAN(S10)

F11=0.D0

F12=(T1-PDR+C2)/PI

IF (PDR .GT. D2) GO TO 1

F13=(T2-2.D0*T1)/PI

F15=(T5-2.D0*T2+T1-C4)/C1

F18=(T10-2.D0*T5+T2-C5)/C1

GO TO 5

1 F13=(T2-D2*PDR+C2)/PI

IF (PDR .GT. D5) GO TO 2

F15=(T5-T2-T1-C3)/PI

F18=(T10-2.D0*T5+T2-C5)/C1

GO TO 5

2 F15=(T5-D5*PDR+C2)/PI

IF (PDR .GT. D10) GO TO 3

F18=(T10-T5-T1-C6)/PI

GO TO 5

3 F18=(T10-D10*PDR+C2)/PI

5 ERROR=1.D0-4.D0*(F12+F13)-8.D0*(F15+F18)

F18A=(1.D0-4.D0*(F12+F13)-8.D0*F15)/8.D0

RETURN

END

C
C
C
C
C
C
C
C
C

.....
 SUBROUTINE SQUARE

SQUARE CONSTRUCTS THE MATRIX OF BLACK BODY VIEW
 FACTORS OR THE MATRIX OF GRAY BODY VIEW FACTORS
 FOR A SQUARE ARRAY OF CYLINDERS WITH AN ARBITRARY
 DISTRIBUTION OF HEAT GENERATION RATES

.....

```

SUBROUTINE SQUARE(F,A,NROWS,N,NMAX,AR,EMISS,
> F11,F12,F13,F15,F18,G,MXROWS)
  IMPLICIT REAL*8(A-H,C-Z)
  DIMENSION G(MXROWS,MXROWS,MXROWS,MXROWS),F(NMAX,NMAX),
> A(1)
  M=N-1
  DO 1 I=1,NROWS
  DO 1 J=1,NROWS
  DO 1 K=1,NROWS
  DO 1 L=1,NROWS
1  G(I,J,K,L)=0.00
  DO 25 I=1,NROWS
  DO 25 J=1,NROWS
  K=I-1
  L=J
  IF (K .LT. 1) GO TO 2
  G(I,J,K,L)=F12
2  K=I+1
  IF (K .GT. NROWS) GO TO 3
  G(I,J,K,L)=F12
3  K=I
  L=J-1
  IF (L .LT. 1) GO TO 4
  G(I,J,K,L)=F12
4  L=J+1
  IF (L .GT. NROWS) GO TO 5
  G(I,J,K,L)=F12
5  K=I-1
  IF (K .LT. 1) GO TO 7
  L=J-1
  IF (L .LT. 1) GO TO 6
  G(I,J,K,L)=F13
6  L=J+1
  IF (L .GT. NROWS) GO TO 7
  G(I,J,K,L)=F13
7  K=I+1
  IF (K .GT. NROWS) GO TO 9
  L=J-1
  IF (L .LT. 1) GO TO 8
  G(I,J,K,L)=F13
8  L=J+1
  IF (L .GT. NROWS) GO TO 9
  G(I,J,K,L)=F13
9  K=I-1
  IF (K .LT. 1) GO TO 13
  L=J-2
  IF (L .LT. 1) GO TO 10
  G(I,J,K,L)=F15
10 L=J+2
  IF (L .GT. NROWS) GO TO 11
  G(I,J,K,L)=F15
11 K=I-2
  IF (K .LT. 1) GO TO 13
  L=J-1
  IF (L .LT. 1) GO TO 12
  G(I,J,K,L)=F15
12 L=J+1
  IF (L .GT. NROWS) GO TO 13

```

```

      G(I,J,K,L)=F15
13  K=I+1
      IF (K .GT. NROWS) GO TO 17
      L=J-2
      IF (L .LT. 1) GO TO 14
      G(I,J,K,L)=F15
14  L=J+2
      IF (L .GT. NROWS) GO TO 15
      G(I,J,K,L)=F15
15  K=I+2
      IF (K .GT. NROWS) GO TO 17
      L=J-1
      IF (L .LT. 1) GO TO 16
      G(I,J,K,L)=F15
16  L=J+1
      IF (L .GT. NROWS) GO TO 17
      G(I,J,K,L)=F15
17  K=I-1
      IF (K .LT. 1) GO TO 21
      L=J-3
      IF (L .LT. 1) GO TO 18
      G(I,J,K,L)=F18
18  L=J+3
      IF (L .GT. NROWS) GO TO 19
      G(I,J,K,L)=F18
19  K=I-3
      IF (K .LT. 1) GO TO 21
      L=J-1
      IF (L .LT. 1) GO TO 20
      G(I,J,K,L)=F18
20  L=J+1
      IF (L .GT. NROWS) GO TO 21
      G(I,J,K,L)=F18
21  K=I+1
      IF (K .GT. NROWS) GO TO 25
      L=J-3
      IF (L .LT. 1) GO TO 22
      G(I,J,K,L)=F18
22  L=J+3
      IF (L .GT. NROWS) GO TO 23
      G(I,J,K,L)=F18
23  K=I+3
      IF (K .GT. NROWS) GO TO 25
      L=J-1
      IF (L .LT. 1) GO TO 24
      G(I,J,K,L)=F18
24  L=J+1
      IF (L .GT. NROWS) GO TO 25
      G(I,J,K,L)=F18
25  CONTINUE
C      VIEW FACTORS HAVE BEEN GENERATED USING
C      DOUBLE-INDEX NOTATION FOR ROD POSITION
C      AND QUADRUPLE INDEXES FOR VIEW FACTORS.
C      CONVERSION IS NOW ACCOMPLISHED TO ACHIEVE
C      SINGLE-INDEX NOTATION FOR POSITION AND
C      DOUBLE-INDEX NOTATION FOR VIEW FACTORS.
      DO 43 LL=1,NROWS
      DO 43 KK=1,NROWS
      DO 43 JJ=1,NROWS
      DO 43 II=1,NROWS
      I=II+NROWS*(JJ-1)
      J=KK+NROWS*(LL-1)
43  F(I,J)=G(II,JJ,KK,LL)
      TOTAL=0.00
      DO 51 I=1,M
      F(I,I)=F11
      A(I)=AR
      SUM=0.00
      DO 50 J=1,M
50  SUM=SUM+F(I,J)

```

```
F(I,N)=EMISS-SUM  
F(N,I)=AR*F(I,N)  
51 TOTAL=TOTAL+F(N,I)  
F(N,N)=EMISS-TOTAL  
RETURN  
END
```



```

F(2,3)=F12+F18
IF (NROWS .LT. 6) GO TO 80
F(1,4)=2.00*(F15+F18)
F(1,5)=2.00*(F15+F18)
F(2,4)=F12+F13+F15+F18
F(2,5)=F13+F15
F(2,6)=F15+F18
F(3,4)=2.00*(F13+F15)
F(3,5)=2.00*(F12+F18)
F(3,6)=F13
F(4,4)=F12
F(4,5)=F12+F15+F18
F(5,5)=F13
F(5,6)=F12
IF (NROWS .LT. 8) GO TO 80
F(1,7)=2.00*F18
F(1,8)=2.00*F18
F(2,7)=F15+F18
F(2,8)=F15
F(2,9)=F18
F(4,7)=F12+F13
F(4,8)=F13+F15+F18
F(4,9)=F15+F18
F(4,10)=F18
F(5,7)=F13+F15
F(5,8)=F12+F15+F18
F(5,9)=F13
F(6,7)=2.00*(F15+F18)
F(6,8)=2.00*F13
F(6,9)=2.00*F12
F(6,10)=F13
F(7,9)=F18
IF (NROWS .LT. 10) GO TO 50
F(8,11)=F13+F15
F(8,12)=F12+F18
F(8,13)=F13+F18
50 DO 8 K=2,K2
   I=M(K)
   J1=M(K+2)-3
   J2=J1+2
   F(I,J1)=2.00*F15
   8 F(I,J2)=2.00*F15
   DO 12 K=3,K1
     I1=M(K-1)+2
     I2=M(K)-1
     I4=K+2
     DO 12 I=I1,I2
       J=I+I4
   12 F(I,J)=F15
   DO 25 K=4,K0
     I1=M(K)-2
     J1=I1+1
     I2=I1+1
     J2=J1+1
     F(I1,J1)=F12+F15
     F(I2,J1)=F13
   25 F(I2,J2)=F12
   IF (NROWS .LT. 9)
   > GO TO 60
   DO 4 K=2,K3
     I=M(K)
     J1=M(K+3)-4
     J2=J1+2
     F(I,J1)=2.00*F18
   4 F(I,J2)=2.00*F18
     DO 7 K=3,K2
       I=M(K)-1
       J1=M(K+2)-3
       J2=J1+2
       F(I,J1)=F18

```

```

7 F(I,J2)=F18
DO 9 K=3,K2
I1=M(K-1)+2
I2=M(K)-1
I4=2*K
DO 9 I=I1,I2
J1=I+I4
J2=J1+2
F(I,J1)=F15
9 F(I,J2)=F15
DO 11 K=4,K1
I1=M(K-1)+2
I2=M(K)-2
I4=K+3
DO 11 I=I1,I2
J=I+I4
11 F(I,J)=F18
DO 16 K=4,K1
I=M(K)-1
J1=M(K+1)-2
J2=J1+1
F(I,J1)=F12+F15
16 F(I,J2)=F13
DO 17 K=4,K1
I=M(K)
J1=M(K+1)-4
J2=J1+1
J3=J2+1
J4=J3+1
J5=J4+1
F(I,J1)=2.00*F18
F(I,J2)=2.00*F15
F(I,J3)=2.00*F13
F(I,J4)=2.00*F12
17 F(I,J5)=F13
DO 23 K=5,K0
I1=M(K-1)+2
I2=M(K)-3
DO 23 I=I1,I2
J=I+1
23 F(I,J)=F12
DO 24 K=5,K0
I=M(K)-3
J=I+2
24 F(I,J)=F18
IF (NR0WS .LT. 11)
> GO TO 60
DO 5 K=3,K3
I1=M(K-1)+2
I2=M(K)-1
I4=3*K+2
DO 5 I=I1,I2
J1=I+I4
J2=J1+2
F(I,J1)=F18
5 F(I,J2)=F18
DO 15 K=5,K1
I=M(K)-2
J=M(K+1)-2
15 F(I,J)=F13+F18
DO 18 K=5,K1
I1=M(K-1)+3
I2=M(K)-2
DO 18 I=I1,I2
J=I+K
18 F(I,J)=F12
DO 20 K=5,K1
I1=M(K-1)+4
I2=M(K)-1
I4=K-3

```

```

DO 20 I=I1,I2
  J1=I+14
  J2=J1+1
  J3=J2+1
  F(I,J1)=F18
  F(I,J2)=F15
20 F(I,J3)=F13
  IF (NRDWS .LT. 13)
  > GO TO 60
  DO 14 K=6,K1
  I1=M(K-1)+3
  I2=M(K)-3
  I4=K+1
  DO 14 I=I1,I2
  J=I+14
14 F(I,J)=F13
60 IF (ITEST .EQ. C)
  > GO TO 70
  DO 6 K=2,K2
  I=M(K-1)+1
  J=M(K+1)+2
  6 F(I,J)=2.D0*F15
  DO 22 K=4,K0
  I=M(K-1)+1
  J=I+1
22 F(I,J)=2.D0*F12
  IF (NRDWS .LT. 9)
  > GO TO 80
  DO 3 K=2,K3
  I=M(K-1)+1
  J=M(K+2)+2
  3 F(I,J)=2.D0*F18
  DO 10 K=4,K1
  I=M(K-1)+1
  J1=M(K)+1
  J2=J1+1
  J3=J2+1
  J4=J3+1
  F(I,J1)=F12
  F(I,J2)=2.D0*F13
  F(I,J3)=2.D0*F15
10 F(I,J4)=2.D0*F18
  DO 19 K=4,K1
  I=M(K-1)+3
  J1=M(K)+1
  J2=J1+1
  F(I,J1)=F15
19 F(I,J2)=F13+F18
  IF (NRDWS .LT. 11)
  > GO TO 80
  DO 13 K=5,K1
  I=M(K-1)+2
  J1=M(K)+1
  J2=J1+1
  J3=J2+1
  F(I,J1)=F13
  F(I,J2)=F12+F15
13 F(I,J3)=F13+F18
  GO TO 80
70 DO 31 K=4,K0
  I=M(K-1)+1
  J1=I
  J2=J1+1
  F(I,J1)=F12
31 F(I,J2)=F12
  IF (NRDWS .LT. 10)
  > GO TO 80
  DO 26 K=2,K3
  I=M(K-1)+1
  J1=M(K+2)+1

```

```

      J2=J1+1
      F(I,J1)=F18
26  F(I,J2)=F18
      DO 27 K=3,K2
      I=M(K-1)+1
      J1=M(K+1)+1
      J2=J1+1
      F(I,J1)=F15
27  F(I,J2)=F15
      DO 28 K=4,K1
      I=M(K-1)+1
      J1=M(K)+1
      J2=J1+1
      J3=J2+1
      J4=J3+1
      F(I,J1)=F12+F13
      F(I,J2)=F13+F15
      F(I,J3)=F15+F18
28  F(I,J4)=F18
      DO 30 K=4,K1
      I=M(K-1)+3
      J1=M(K)+1
      J2=J1+1
      F(I,J1)=F15+F18
30  F(I,J2)=F13
      IF (NRDWS .LT. 12)
>   GO TO 80
      DO 29 K=5,K1
      I=M(K-1)+2
      J1=M(K)+1
      J2=J1+1
      J3=J2+1
      F(I,J1)=F13+F15
      F(I,J2)=F12+F18
29  F(I,J3)=F13
80  IF (ITEST .EQ. 0)
>   GO TO 90
      A(I)=1.D0
      DO 81 K=2,K0
      I=M(K)
81  A(I)=4.D0
      DO 82 K=1,K1
      I=M(K)+1
82  A(I)=4.D0
      DO 83 K=3,K0
      I1=M(K-1)+2
      I2=M(K)-1
      DO 83 I=I1,I2
83  A(I)=8.D0
      GO TO 100
90  DO 91 K=1,K0
      I=M(K)
91  A(I)=4.D0
      DO 92 K=2,K0
      I1=M(K-1)+1
      I2=M(K)-1
      DO 92 I=I1,I2
92  A(I)=8.D0
100 DO 101 I=1,MM
      DO 101 J=1,I
101 F(I,J)=A(J)/A(I)*F(J,I)
      DO 110 I=1,MM
      F(I,I)=F(I,I)+F11
110 A(I)=A(I)*AR
      TOTAL=0.D0
      DO 130 I=1,MM
      SUM=0.D0
      DO 129 J=1,MM
129 SUM=SUM+F(I,J)
      F(I,N)=EMISS-SUM

```

```
F(N,I)=F(I,N)*A(I)  
130 TOTAL=TOTAL+F(N,I)  
F(N,N)=EMISS-TOTAL  
RETURN  
END
```

```

C .....
C
C SUBROUTINE HEX
C
C HEX FORMS THE MATRIX OF BLACK BODY VIEW FACTORS OR
C THE MATRIX OF GRAY EDDY VIEW FACTORS FOR A HEX ARRAY
C OF CYLINDERS WITH AN ARBITRARY HT. GEN. DISTRIBUTION
C .....
C
C SUBROUTINE HEX(F,A,NROWS,N,NMAX,AR,EMISS,
> F11,F12,F13,F15,F18,M)
C IMPLICIT REAL*8(A-H,O-Z)
C DIMENSION F(NMAX,NMAX),A(1),M(1)
C NRODS=N-1
C K0=NROWS
C K1=NROWS-1
C K2=NROWS-2
C K3=NROWS-3
C K4=NROWS-4
C M(1)=1
C DO 1 I=2,NROWS
1 M(I)=M(I-1)+6*(I-1)
C DO 2 I=1,N
C DO 2 J=1,N
2 F(I,J)=0,DO
C IF (NROWS .LT. 2) GO TO 83
C F(1,2)=F12
C F(1,3)=F12
C F(1,4)=F12
C F(1,5)=F12
C F(1,6)=F12
C F(1,7)=F12
C F(2,4)=F13
C F(3,5)=F13
C F(3,7)=F13
C F(4,6)=F13
C F(5,7)=F13
C DO 3 K=2,K0
C I1=M(K-1)+1
C I2=M(K)-1
C DO 3 I=I1,I2
C J=I+1
3 F(I,J)=F12
C DO 4 K=2,K0
C I=M(K-1)+1
C J=M(K)
4 F(I,J)=F12
C DO 5 K=2,K0
C I=M(K-1)+1
C J=M(K)-1
5 F(I,J)=F13
C IF (NROWS .LT. 3) GO TO 83
C F(1, 8)=F13
C F(1,10)=F13
C F(1,12)=F13
C F(1,14)=F13
C F(1,16)=F13
C F(1,18)=F13
C F(2,13)=F15
C F(2,14)=F15
C F(2,16)=F15
C F(3,16)=F15
C F(3,18)=F15
C F(4, 8)=F15
C F(4, 9)=F15
C F(4,17)=F15
C F(4,18)=F15

```

```

F(5, 8)=F15
F(5,10)=F15
F(5,11)=F15
F(6, 9)=F15
F(6,10)=F15
F(6,12)=F15
F(6,13)=F15
F(7,11)=F15
F(7,12)=F15
F(7,14)=F15
F(7,15)=F15
F(8,11)=F15
F(9,12)=F15
F(10,13)=F15
F(10,19)=F15
F(11,14)=F15
F(12,15)=F15
F(13,16)=F15
F(14,17)=F15
F(15,18)=F15
F(16,19)=F15
F(8,13)=F18
F(8,15)=F18
F(9,14)=F18
F(9,16)=F18
F(10,15)=F18
F(10,17)=F18
F(11,16)=F18
F(11,18)=F18
F(12,17)=F18
F(12,19)=F18
F(13,18)=F18
F(14,19)=F18
DO 6 K=2,K1
I=M(K)
J=I+1
6 F(I,J)=F12
DO 7 K=2,K1
I1=M(K-1)+1
I2=I1+K-2
I4=6*K-6
DO 7 I=I1,I2
J=I+I4
7 F(I,J)=F12
DO 8 K=2,K1
I1=M(K-1)+1
I2=I1+2*K-3
I4=6*K-5
DO 8 I=I1,I2
J=I+I4
8 F(I,J)=F12
DO 9 K=2,K1
L1=M(K-1)+K-1
L2=M(K)-2*K+2
L3=K-1
L4=2*K-2
I4=6*K-5
DO 9 L=L1,L2,L3
I1=L
I2=I1+L4
I4=I4+1
DO 9 I=I1,I2
J=I+I4
9 F(I,J)=F12
DO 10 K=2,K1
I1=M(K)-K+1
I2=M(K)
I4=6*K
DO 10 I=I1,I2
J=I+I4

```

```

10 F(I,J)=F12
   DO 11 K=2,K1
     I=M(K)
     J=I+2
11 F(I,J)=F13
   DO 12 K=2,K1
     L1=M(K-1)+K
     L2=M(K)-K+2
     L3=K-1
     I4=6*K-7
     DO 12 L=L1,L2,L3
       I1=L
       I2=I1+K-2
       I4=I4+1
       DO 12 I=I1,I2
         J=I+I4
12 F(I,J)=F13
   DO 13 K=2,K1
     L1=M(K-1)+K-1
     L2=M(K)-K
     L3=K-1
     I4=6*K-4
     DO 13 L=L1,L2,L3
       I1=L
       I2=I1+K-2
       I4=I4+1
       DO 13 I=I1,I2
         J=I+I4
13 F(I,J)=F13
   DO 14 K=2,K1
     I1=M(K)-K+1
     I2=M(K)-1
     I4=6*K+1
     DO 14 I=I1,I2
       J=I+I4
14 F(I,J)=F13
   DO 15 K=2,K1
     I=M(K-1)+1
     J=M(K+1)
15 F(I,J)=F13
   DO 16 K=3,K0
     I1=M(K-1)+K-2
     I2=M(K)-K
     I3=K-1
     DO 16 I=I1,I2,I3
       J=I+2
16 F(I,J)=F13
   DO 17 K=2,K1
     I1=M(K)-K
     I2=I1+K-2
     I4=6*K+2
     DO 17 I=I1,I2
       J=I+I4
17 F(I,J)=F15
   DO 18 K=2,K1
     I1=M(K-1)+1
     I2=I1+1
     I4=12*K-10
     DO 18 I=I1,I2
       I4=I4+1
       J=I+I4
18 F(I,J)=F15
   DO 19 K=3,K0
     I1=M(K-1)+1
     I2=I1+1
     I4=6*K-9
     DO 19 I=I1,I2
       J=I+I4
19 F(I,J)=F15
   IF (NROWS .LT. 4)

```

```
> GO TO 83
F(2,21)=F13
F(3,24)=F13
F(4,27)=F13
F(5,30)=F13
F(6,33)=F13
F(7,36)=F13
F(1,20)=F15
F(1,21)=F15
F(1,23)=F15
F(1,24)=F15
F(1,26)=F15
F(1,27)=F15
F(1,29)=F15
F(1,30)=F15
F(1,32)=F15
F(1,33)=F15
F(1,35)=F15
F(1,36)=F15
F(2,25)=F15
F(2,26)=F15
F(3,28)=F15
F(3,29)=F15
F(4,31)=F15
F(4,32)=F15
F(5,34)=F15
F(5,35)=F15
F(6,37)=F15
F(7,23)=F15
F(2,28)=F18
F(2,30)=F18
F(2,32)=F18
F(2,34)=F18
F(3,31)=F18
F(3,33)=F18
F(3,35)=F18
F(3,37)=F18
F(4,20)=F18
F(4,22)=F18
F(4,34)=F18
F(4,36)=F18
F(5,21)=F18
F(5,23)=F18
F(5,26)=F18
F(5,37)=F18
F(6,24)=F18
F(6,26)=F18
F(6,28)=F18
F(7,25)=F18
F(7,27)=F18
F(7,29)=F18
F(7,31)=F18
F(8,26)=F18
F(8,33)=F18
F(9,27)=F18
F(9,35)=F18
F(10,29)=F18
F(10,36)=F18
F(11,20)=F18
F(11,30)=F18
F(12,21)=F18
F(12,32)=F18
F(13,23)=F18
F(13,33)=F18
F(14,24)=F18
F(14,35)=F18
F(15,26)=F18
F(15,36)=F18
F(16,20)=F18
F(16,27)=F18
```

```

F(17,21)=F18
F(17,29)=F18
F(18,23)=F18
F(18,30)=F18
F(19,24)=F18
F(19,32)=F18
F(21,25)=F18
F(22,26)=F18
F(23,37)=F18
F(24,28)=F18
F(25,29)=F18
F(27,31)=F18
F(28,32)=F18
F(30,34)=F18
F(31,35)=F18
F(33,37)=F18
DO 20 K=2,K2
I=M(K)
J=M(K+1)+1
20 F(I,J)=F13
DO 21 K=2,K2
I1=M(K-1)+K-1
I2=M(K)-K+1
I3=K-1
I4=12*K-5
DO 21 I=I1,I2,I3
I4=I4+2
J=I+I4
21 F(I,J)=F13
DO 22 K=3,K1
I1=M(K-1)+2
I2=I1+K-3
I4=6*K-7
DO 22 I=I1,I2
J=I+I4
22 F(I,J)=F13
DO 23 K=3,K1
I1=M(K-1)+1
I2=I1+K-3
I4=6*K-4
DO 23 I=I1,I2
J=I+I4
23 F(I,J)=F13
DO 24 K=2,K2
I=M(K)
J=M(K+1)+3
24 F(I,J)=F15
DO 25 K=2,K2
I1=M(K-1)+K
I2=M(K)-K+2
I3=K-1
I4=12*K-8
DO 25 I=I1,I2,I3
I4=I4+2
J=I+I4
25 F(I,J)=F15
DO 26 K=2,K2
I1=M(K-1)+K
I2=M(K)-K+2
I3=K-1
I4=12*K-7
DO 26 I=I1,I2,I3
I4=I4+2
J=I+I4
26 F(I,J)=F15
DO 27 K=2,K2
I=M(K-1)+1
J=M(K+2)-1
27 F(I,J)=F15
DO 28 K=2,K2

```

```

      I=M(K-1)+1
      J=M(K+2)
28  F(I,J)=F15
      DO 29 K=2,K2
      I=M(K)-1
      J=M(K+1)+1
29  F(I,J)=F15
      DO 30 K=3,K1
      I1=M(K)-1
      I2=M(K)
      DO 30 I=I1,I2
      J=I+3
30  F(I,J)=F15
      DO 31 K=3,K1
      L1=M(K-1)+K+1
      L2=M(K)-2*K+4
      L3=K-1
      I4=6*K-8
      DO 31 L=L1,L2,L3
      I1=L
      I2=I1+K-2
      I4=I4+1
      DO 31 I=I1,I2
      J=I+I4
31  F(I,J)=F15
      DO 32 K=3,K1
      I1=M(K)-K+3
      I2=M(K)
      I4=6*K-3
      DO 32 I=I1,I2
      J=I+I4
32  F(I,J)=F15
      DO 33 K=3,K1
      I1=M(K-1)+3
      I2=I1+K-3
      I4=6*K-8
      DO 33 I=I1,I2
      J=I+I4
33  F(I,J)=F15
      DO 34 K=3,K1
      L1=M(K-1)+K-2
      L2=L1+3*K-3
      L3=K-1
      I4=6*K-3
      DO 34 L=L1,L2,L3
      I1=L
      I2=I1+K-2
      I4=I4+1
      DO 34 I=I1,I2
      J=I+I4
34  F(I,J)=F15
      DO 35 K=4,K0
      L1=M(K-1)+K-3
      L2=M(K)-K-1
      L3=K-1
      DO 35 L=L1,L2,L3
      I1=L
      I2=I1+1
      DO 35 I=I1,I2
      J=I+3
35  F(I,J)=F15
      DO 36 K=2,K2
      I=M(K)-1
      J=M(K+1)+3
36  F(I,J)=F18
      DO 37 K=4,K0
      I1=M(K-1)+1
      I2=I1+2
      I4=6*K-10
      DO 37 I=I1,I2,2

```

```
J=I+I4
37 F(I,J)=F18
   IF (NROWS .LT. 5)
     > GO TO 83
   F(2,42)=F15
   F(2,43)=F15
   F(3,43)=F15
   F(3,44)=F15
   F(3,46)=F15
   F(3,47)=F15
   F(4,47)=F15
   F(4,48)=F15
   F(4,50)=F15
   F(4,51)=F15
   F(5,51)=F15
   F(5,52)=F15
   F(5,54)=F15
   F(5,55)=F15
   F(6,55)=F15
   F(6,56)=F15
   F(6,58)=F15
   F(6,59)=F15
   F(7,59)=F15
   F(7,60)=F15
   F(1,38)=F18
   F(1,40)=F18
   F(1,42)=F18
   F(1,44)=F18
   F(1,46)=F18
   F(1,48)=F18
   F(1,50)=F18
   F(1,52)=F18
   F(1,54)=F18
   F(1,56)=F18
   F(1,58)=F18
   F(1,60)=F18
   F(2,45)=F18
   F(2,47)=F18
   F(3,41)=F18
   F(3,49)=F18
   F(3,51)=F18
   F(4,45)=F18
   F(4,53)=F18
   F(4,55)=F18
   F(5,49)=F18
   F(5,57)=F18
   F(5,59)=F18
   F(6,53)=F19
   F(6,61)=F18
   F(7,43)=F18
   F(7,57)=F18
   F(8,44)=F19
   F(9,46)=F18
   F(10,48)=F18
   F(11,50)=F18
   F(12,52)=F18
   F(13,54)=F18
   F(14,56)=F18
   F(15,58)=F18
   F(16,60)=F18
   F(19,42)=F18
   DD 38 K=3,K2
   L1=M(K-1)+1
   L2=M(K)-K+2
   L3=K-1
   I4=12*K-7
   DD 38 L=L1,L2,L3
   I1=L
   I2=I1+K-2
   I4=I4+2
```

```

DO 38 I=I1,I2
J=I+I4
38 F(I,J)=F13
DO 39 K=2,K3
I=M(K)
J=M(K+2)+1
39 F(I,J)=F15
DO 40 K=2,K3
I=M(K)
J=M(K+2)+2
40 F(I,J)=F15
DO 41 K=2,K3
I1=M(K-1)+1
I2=I1+K-2
I4=18*K+1
DO 41 I=I1,I2
J=I+I4
41 F(I,J)=F15
DO 42 K=2,K3
I1=M(K-1)+1
I2=I1+K-2
I4=18*K+2
DO 42 I=I1,I2
J=I+I4
42 F(I,J)=F15
DO 43 K=3,K2
L1=M(K-1)+2
L2=M(K)-K+3
L3=K-1
I4=12*K-9
DO 43 L=L1,L2,L3
I1=L
I2=I1+K-3
I4=I4+2
DO 43 I=I1,I2
J=I+I4
43 F(I,J)=F15
DO 44 K=3,K2
L1=M(K-1)+K-1
L2=M(K)-K+1
L3=K-1
I4=12*K-3
DO 44 L=L1,L2,L3
I1=L
I2=I1+K-2
I4=I4+2
DO 44 I=I1,I2
J=I+I4
44 F(I,J)=F15
DO 45 K=3,K2
I1=M(K-1)+1
I2=I1+K-3
I4=12*K-3
DO 45 I=I1,I2
J=I+I4
45 F(I,J)=F15
DO 46 K=3,K2
I1=M(K-1)+K-2
I2=M(K)-K
I3=K-1
I4=12*K-4
DO 46 I=I1,I2,I3
I4=I4+2
J=I+I4
46 F(I,J)=F15
DO 47 K=4,K1
I1=M(K-1)+1
I2=I1+K-4
I4=6*K-3
DO 47 I=I1,I2

```

```

      J=I+I4
47  F(I,J)=F15
      DO 48 K=2,K3
         I1=M(K)-1
         I2=M(K)
         I4=12*K+8
         DO 48 I=I1,I2
            I4=I4+1
            J=I+I4
48  F(I,J)=F18
      DO 49 K=2,K3
         I1=M(K-1)+K
         I2=M(K)-K+2
         I3=K-1
         I4=18*K-3
         DO 49 I=I1,I2,I3
            I4=I4+3
            J=I+I4
49  F(I,J)=F18
      DO 50 K=2,K3
         I=M(K-1)+1
         J=M(K+3)-2
50  F(I,J)=F18
      DO 51 K=2,K3
         I=M(K-1)+1
         J=M(K+3)
51  F(I,J)=F18
      DO 52 K=3,K2
         L1=M(K-1)+K
         L2=L1+4*K-4
         L3=K-1
         L4=12*K-11
         DO 52 L=L1,L2,L3
            I1=L
            I2=I1+1
            L4=L4+2
            I4=0
            DO 52 I=I1,I2
               I4=I4+1
               J=I+L4+I4
52  F(I,J)=F18
      DO 53 K=3,K2
         I1=M(K-1)+1
         I2=I1+1
         I4=18*K-5
         DO 53 I=I1,I2
            I4=I4+1
            J=I+I4
53  F(I,J)=F18
      DO 54 K=3,K2
         I=M(K)-2
         J=M(K+1)+1
54  F(I,J)=F18
      DO 55 K=4,K1
         I1=M(K)-2
         I2=M(K)
         DO 55 I=I1,I2,2
            J=I+4
55  F(I,J)=F18
      DO 56 K=4,K1
         L1=M(K-1)+K+2
         L2=M(K)-K+4
         L3=K-1
         I4=6*K-9
         DO 56 L=L1,L2,L3
            I1=L
            I2=I1+K-4
            I4=I4+1
            DO 56 I=I1,I2
               J=I+I4

```

```

56 F(I,J)=F18
   DO 57 K=4,K1
     I1=M(K-1)+K+1
     I2=M(K)-K+3
     I3=K-1
     I4=6*K-10
     DO 57 I=I1,I2,I3
       I4=I4+1
       J=I+I4
57 F(I,J)=F18
   DO 58 K=4,K1
     L1=M(K-1)+K-1
     L2=M(K)-2*K+2
     L3=K-1
     I4=6*K-2
     DO 58 L=L1,L2,L3
       I1=L
       I2=I1+K-4
       I4=I4+1
       DO 58 I=I1,I2
         J=I+I4
58 F(I,J)=F18
   DO 59 K=4,K1
     I1=M(K)-K+1
     I2=I1+K-4
     I4=6*K+3
     DO 59 I=I1,I2
       J=I+I4
59 F(I,J)=F18
   DO 60 K=4,K1
     I1=M(K-1)+K-3
     I2=I1+4*K-4
     I3=K-1
     I4=6*K-2
     DO 60 I=I1,I2,I3
       I4=I4+1
       J=I+I4
60 F(I,J)=F18
   DO 61 K=4,K1
     I1=M(K-1)+2
     I2=I1+1
     I4=12*K-11
     DO 61 I=I1,I2
       I4=I4+1
       J=I+I4
61 F(I,J)=F18
   DO 62 K=5,K0
     L1=M(K-1)+K-4
     L2=M(K)-K-2
     L3=K-1
     DO 62 L=L1,L2,L3
       I1=L
       I2=I1+2
       DO 62 I=I1,I2,2
         J=I+4
62 F(I,J)=F18
   IF (NROWS .LT. 6)
     > GO TO E3
     F(8,68)=F18
     F(10,73)=F18
     F(12,78)=F18
     F(14,83)=F18
     F(16,88)=F18
     DO 63 K=3,K3
       L1=M(K-1)+K-1
       L2=M(K)-K+1
       L3=K-1
       I4=18*K+1
       DO 63 L=L1,L2,L3
         I1=L

```

```

I2=I1+K-2
I4=I4+3
DO 63 I=I1,I2
J=I+I4
63 F(I,J)=F15
DO 64 K=3,K3
L1=M(K-1)+K-1
L2=M(K)-K+1
L3=K-1
I4=18*K+2
DO 64 L=L1,L2,L3
I1=L
I2=I1+K-2
I4=I4+3
DO 64 I=I1,I2
J=I+I4
64 F(I,J)=F15
DO 65 K=3,K3
I1=M(K-1)+2*K-2
I2=M(K)
I3=K-1
I4=18*K+1
DO 65 I=I1,I2,I3
I4=I4+3
J=I+I4
65 F(I,J)=F15
DO 66 K=3,K3
I1=M(K-1)+2*K-2
I2=M(K)
I3=K-1
I4=18*K+2
DO 66 I=I1,I2,I3
I4=I4+3
J=I+I4
66 F(I,J)=F15
DO 67 K=2,K4
I=M(K)
J=M(K+3)+3
67 F(I,J)=F18
DO 68 K=2,K4
I=M(K)
J=M(K+3)+1
68 F(I,J)=F18
DO 69 K=2,K4
I1=M(K-1)+1
I2=I1+K-2
I4=24*K+13
DO 69 I=I1,I2
J=I+I4
69 F(I,J)=F18
DO 70 K=2,K4
I1=M(K-1)+1
I2=I1+K-2
I4=24*K+15
DO 70 I=I1,I2
J=I+I4
70 F(I,J)=F18
DO 71 K=2,K4
I1=M(K-1)+2*K-2
I2=M(K)
I3=K-1
I4=24*K+13
DO 71 I=I1,I2,I3
I4=I4+4
J=I+I4
71 F(I,J)=F18
DO 72 K=2,K4
I1=M(K-1)+2*K-2
I2=M(K)
I3=K-1

```

```

I4=24*K+15
DO 72 I=I1,I2,I3
I4=I4+4
J=I+I4
72 F(I,J)=F18
DO 73 K=2,K4
L1=M(K-1)+K-1
L2=M(K)-K+1
L3=K-1
I4=24*K+13
DO 73 L=L1,L2,L3
I1=L
I2=I1+K-2
I4=I4+4
DO 73 I=I1,I2
J=I+I4
73 F(I,J)=F18
DO 74 K=2,K4
L1=M(K-1)+K-1
L2=M(K)-K+1
L3=K-1
I4=24*K+15
DO 74 L=L1,L2,L3
I1=L
I2=I1+K-2
I4=I4+4
DO 74 I=I1,I2
J=I+I4
74 F(I,J)=F18
DO 75 K=3,K3
L1=M(K-1)+K
L2=M(K)-K+2
L3=K-1
I4=18*K-1
DO 75 L=L1,L2,L3
I1=L
I2=I1+K-2
I4=I4+3
DO 75 I=I1,I2
J=I+I4
75 F(I,J)=F18
DO 76 K=3,K3
I1=M(K-1)+2
I2=I1+K-3
I4=18*K-1
DO 76 I=I1,I2
J=I+I4
76 F(I,J)=F18
DO 77 K=3,K3
I1=M(K-1)+1
I2=I1+K-3
I4=18*K+4
DO 77 I=I1,I2
J=I+I4
77 F(I,J)=F18
DO 78 K=3,K3
L1=M(K-1)+K-1
L2=M(K)-K+1
L3=K-1
I4=18*K+4
DO 78 L=L1,L2,L3
I1=L
I2=I1+K-2
I4=I4+3
DO 78 I=I1,I2
J=I+I4
78 F(I,J)=F18
DO 79 K=4,K2
L1=M(K-1)+K-3
L2=M(K)-K-1

```

```

L3=K-1
L4=12*K-4
DO 79 L=L1,L2,L3
I1=L
I2=I1+1
L4=L4+2
I4=C
DO 79 I=I1,I2
I4=I4+1
J=I+I4+L4
79 F(I,J)=F18
DO 80 K=5,K1
I1=M(K-1)+4
I2=I1+K-5
I4=6*K-9
DO 80 I=I1,I2
J=I+I4
80 F(I,J)=F18
DO 81 K=5,K1
I1=M(K-1)+1
I2=I1+K-5
I4=6*K-2
DO 81 I=I1,I2
J=I+I4
81 F(I,J)=F18
IF (NROWS .LT. 7)
> GO TO 83
DO 82 K=4,K3
I1=M(K-1)+K-2
I2=M(K)-K
I3=K-1
I4=18*K+3
DO 82 I=I1,I2,I3
I4=I4+3
J=I+I4
82 F(I,J)=F18
83 DO 84 I=1,NRODS
F(I,I)=F11
A(I)=AR
DO 84 J=1,I
84 F(I,J)=F(J,I)
TOTAL=0.DO
DO 86 I=1,NRODS
SUM=0.DO
DO 85 J=1,NRODS
85 SUM=SUM+F(I,J)
F(I,N)=EMISS-SUM
F(N,I)=AR*F(I,N)
86 TOTAL=TOTAL+F(N,I)
F(N,N)=EMISS-TOTAL
RETURN
END

```



```

F(6,7)=2.D0*F13
F(6,8)=2.D0*(F12+F15)
F(6,9)=F12+2.D0*F18
F(7,2)=F(2,7)
F(7,5)=2.D0*F(5,7)
F(7,6)=F(6,7)
F(7,8)=2.D0*(F12+F15)
F(8,2)=F15
F(8,3)=F15+F18
F(8,4)=F13+F15+F18
F(8,5)=F(5,8)
F(8,6)=F12+F15
F(8,7)=F12+F15
F(8,8)=F13+2.D0*F18
F(9,2)=F(2,9)
F(9,3)=F(3,9)
F(9,5)=2.D0*F(5,9)
F(9,6)=F(6,9)
DO 10 K=5,K0
I1=M(K-1)+2
I2=M(K)-1
I4=2*K-3
DO 10 I=I1,I2
J=I-I4
10 F(I,J)=F18
DO 50 K=3,K2,2
I=M(K-1)+1
J=M(K+1)+1
F(I,J)=F13
50 F(J,I)=F13
DO 115 K=5,K0
I=M(K)-1
J=I+1
F(I,J)=F12
115 F(J,I)=2.D0*F12
IF (NROWS .LT. 6)
> GO TO 125
F(2,10)=2.D0*F18
F(3,10)=2.D0*(F15+F18)
F(4,10)=2.D0*F15
F(4,11)=2.D0*(F15+F18)
F(5,10)=F13+F18
F(5,11)=2.D0*F15+F18
F(5,12)=F15
F(6,10)=2.D0*F15
F(7,10)=2.D0*(F12+F18)
F(8,10)=F12+F13+F15
F(8,11)=F12+F15
F(8,12)=F13+F18
F(9,10)=2.D0*(F13+F15)
F(9,11)=2.D0*(F12+F18)
F(9,12)=F12
F(10,2)=F18
F(10,3)=F15+F18
F(10,5)=F(5,10)
F(10,6)=F15
F(10,7)=F12+F18
F(10,8)=F(8,10)
F(10,9)=F13+F15
F(10,11)=F12+F15+F18
F(11,4)=F15+F18
F(11,5)=F(5,11)
F(11,6)=F13
F(11,8)=F(8,11)
F(11,9)=F12+F18
F(11,10)=F(10,11)
F(12,5)=2.D0*F15
F(12,7)=2.D0*F15
F(12,8)=2.D0*F(8,12)
F(12,9)=F12

```

```

DO 4 K=2,K4
I=M(K)
J=M(K+4)-1
4 F(I,J)=2.D0*F18
DO 14 K=3,K3,2
I=M(K-1)+1
J=M(K+2)+3
14 F(I,J)=2.D0*F18
DO 35 K=6,K0
I=M(K)
J=M(K-3)-1
35 F(I,J)=2.D0*F18
DO 36 K=6,K0,2
I1=M(K-1)+1
I2=M(K)-2
I4=((K-2)/2)*3
DO 36 I=I1,I2
J=I-I4
36 F(I,J)=F15
DO 49 K=4,K2
I=M(K)
J=M(K+2)-1
49 F(I,J)=2.D0*F13
DO 68 K=5,K1,2
I=M(K-1)+1
J=M(K)+3
68 F(I,J)=2.D0*F15
DO 71 K=5,K1,2
I=M(K-1)+1
J=M(K)+2
F(I,J)=2.D0*F13
71 F(J,I)=F13
DO 119 K=6,K0,2
I=M(K-1)+1
J=I
119 F(I,J)=F12
DO 120 K=6,K0
I=M(K)-1
J=I
120 F(I,J)=F13
IF (NROWS .LT. 7)
> GO TO 125
F(5,14)=F15+F18
F(6,14)=2.D0*(F15+F18)
F(7,15)=2.D0*(F15+F18)
F(8,13)=F18
F(10,14)=F12+F13+F18
F(10,16)=F15+F18
F(11,14)=F12+2.D0*F15
F(11,15)=F12+F18
F(12,13)=2.D0*F15
F(12,14)=2.D0*(F13+F18)
F(12,16)=F12
F(13,8)=2.D0*F18
F(13,15)=2.D0*F18
F(14,5)=F(5,14)
F(14,6)=F15+F18
F(14,10)=F(10,14)
F(14,11)=F(11,14)
F(14,12)=F13+F18
F(15,7)=F15+F18
F(15,11)=F(11,15)
F(15,13)=F18
F(16,10)=2.D0*(F15+F18)
F(16,12)=F12
DO 3 K=3,K4,2
I=M(K-1)+1
J=M(K+3)+2
3 F(I,J)=2.D0*F18
DO 9 K=3,K4

```

```

I=M(K)
J=M(K+4)-3
9 F(I,J)=2.D0*F18
DO 11 K=7,K0
I=M(K-1)+1
J=M(K-5)+2
11 F(I,J)=2.D0*F18
DO 16 K=4,K3,2
I1=M(K-1)+1
I2=M(K)-1
I4=(K/2)*3+5
DO 16 I=I1,I2
J=I+I4
16 F(I,J)=F18
DO 17 K=4,K3,2
I=M(K-1)+1
J=M(K+2)+3
F(I,J)=F18
17 F(J,I)=F18
DO 20 K=4,K3
I=M(K)
J=M(K+3)-1
F(I,J)=2.D0*F15
20 F(J,I)=F15
DO 24 K=4,K3,2
I=M(K-1)+1
J=M(K+2)+1
F(I,J)=F15
24 F(J,I)=2.D0*F15
DO 43 K=5,K2
I=M(K)-1
J=M(K+2)
F(I,J)=F15
43 F(J,I)=2.D0*F15
DO 46 K=5,K2
I=M(K)-1
J=M(K+2)-1
F(I,J)=F15
46 F(J,I)=F15
DO 51 K=5,K2,2
I=M(K-1)+2
J=M(K+1)+2
F(I,J)=F13+F15
51 F(J,I)=F13+F15
DO 55 K=5,K2
I=M(K)
J=M(K+2)-3
55 F(I,J)=2.D0*F15
DO 59 K=7,K0,2
I1=M(K-1)+3
I2=M(K)-1
I4=K-1
DO 59 I=I1,I2
J=I-I4
59 F(I,J)=F13
DO 61 K=7,K0,2
I=M(K-1)+1
J=M(K-3)+3
61 F(I,J)=2.D0*F15
DO 69 K=6,K1,2
I=M(K-1)+1
J=M(K)+3
F(I,J)=F13+F15
69 F(J,I)=F13+F15
DO 70 K=6,K1,2
I1=M(K-1)+2
I2=M(K)-1
I4=K/2+2
DO 70 I=I1,I2
J=I+I4

```

```

70 F(I,J)=F13
   DO 81 K=6,K1,2
     I=M(K-1)+1
     J=M(K)+1
     F(I,J)=F12
81 F(J,I)=2.D0*F12
   DO 84 K=6,K1
     I=M(K)
     J=M(K+1)-1
     F(I,J)=2.D0*F12
84 F(J,I)=F12
   DO 87 K=6,K1,2
     I=M(K-1)+2
     J=M(K)+1
     F(I,J)=F13
87 F(J,I)=2.D0*F13
   DO 105 K=7,K0
     I=M(K)
     J=M(K-1)-1
105 F(I,J)=2.D0*F13
   DO 110 K=7,K0,2
     I=M(K-1)+1
     J=M(K-2)+3
110 F(I,J)=2.D0*F15
   DO 116 K=7,K0
     I=M(K)-2
     J=I+1
     F(I,J)=F12+F15
116 F(J,I)=F12+F15
   DO 117 K=7,K0
     I1=M(K-1)+1
     I2=M(K)-3
     DO 117 I=I1,I2
       J=I+1
       F(I,J)=F12
117 F(J,I)=F12
   DO 118 K=7,K0,2
     I=M(K-1)+1
     J=I+1
118 F(I,J)=2.D0*F12
     IF (NROWS .LT. 8)
       > GO TO 125
     F(3,18)=F15+2.D0*F18
     F(9,17)=2.D0*F18
     F(11,17)=F15+F18
     F(14,18)=F12+F15+F18
     F(15,18)=F12+F15+F18
     F(16,17)=2.D0*(F15+F18)
     F(17,9)=F18
     F(17,11)=F(11,17)
     F(17,16)=F15+F18
     F(18,8)=F(8,18)
     F(18,14)=F(14,18)
     F(18,15)=F(15,18)
     DO 5 K=4,K4,2
       I1=M(K-1)+1
       I2=M(K)-1
       I4=2*K+5
       DO 5 I=I1,I2
         J=I+I4
5 F(I,J)=F18
   DO 7 K=4,K4,2
     I=M(K-1)+1
     J=M(K+3)+1
     F(I,J)=F18
7 F(J,I)=F18
   DO 13 K=8,K0,2
     I1=M(K-1)+1
     I2=M(K)-3
     I4=2*K-5

```

```

DO 13 I=I1,I2
J=I-I4
13 F(I,J)=F18
DO 15 K=5,K3,2
I1=M(K-1)+2
I2=M(K)-1
I4=((K+1)/2)*3+3
DO 15 I=I1,I2
J=I+I4
15 F(I,J)=F18
DO 21 K=5,K3,2
I=M(K-1)+1
J=M(K+2)+1
F(I,J)=2.D0*F15
21 F(J,I)=F15
DO 27 K=5,K3
I=M(K)
J=M(K+3)-2
27 F(I,J)=2.D0*F15
DO 28 K=5,K3,2
I1=M(K-1)+2
I2=M(K)-1
I4=((K+1)/2)*3
DO 28 I=I1,I2
J=I+I4
28 F(I,J)=F15
DO 33 K=8,K0,2
I1=M(K-1)+3
I2=M(K)-1
I4=(K/2)*3
DO 33 I=I1,I2
J=I-I4
33 F(I,J)=F18
DO 42 K=6,K2
I=M(K)-2
J=M(K+2)-1
F(I,J)=F15+F18
42 F(J,I)=F15+F18
DO 47 K=6,K2,2
I=M(K-1)+1
J=M(K+1)+2
F(I,J)=F15
47 F(J,I)=F15
DO 48 K=6,K2,2
I1=M(K-1)+1
I2=M(K)-1
I4=K+1
DO 48 I=I1,I2
J=I+I4
48 F(I,J)=F13
DO 58 K=8,K0,2
I1=M(K-1)+1
I2=M(K)-1
I4=K-1
DO 58 I=I1,I2
J=I-I4
58 F(I,J)=F13
DO 60 K=8,K0,2
I1=M(K-1)+1
I2=M(K)-3
I4=K-3
DO 60 I=I1,I2
J=I-I4
60 F(I,J)=F15
DO 64 K=7,K1,2
I=M(K-1)+1
J=M(K)+4
64 F(I,J)=2.D0*F18
DO 67 K=7,K1
I1=M(K-1)+2

```

```

I2=M(K)-2
I4=K/2+3
DO 67 I=I1,I2
J=I+I4
67 F(I,J)=F15
DO 72 K=7,K1,2
I=M(K-1)+2
J=M(K)+3
F(I,J)=F13+F18
72 F(J,I)=F13+F18
DO 73 K=7,K1,2
I1=M(K-1)+3
I2=M(K)-1
I4=(K-1)/2+2
DO 73 I=I1,I2
J=I+I4
73 F(I,J)=F13
DO 78 K=7,K1
I1=M(K)-1
I2=M(K)
I4=K/2+1
DO 78 I=I1,I2
J=I+I4
F(I,J)=F12
78 F(J,I)=F12
DO 79 K=7,K1,2
I=M(K-1)+1
J=M(K)+1
F(I,J)=2.D0*F12
79 F(J,I)=F12
DO 85 K=7,K1,2
I=M(K-1)+2
J=M(K)+1
F(I,J)=F12+F13
85 F(J,I)=F12+F13
DO 90 K=7,K1
I=M(K)
J=M(K+1)-2
90 F(I,J)=2.D0*F13
DO 91 K=7,K1,2
I=M(K-1)+3
J=M(K)+1
F(I,J)=F13+F15
91 F(J,I)=F13+F15
DO 99 K=8,K0
I=M(K)
J=M(K-1)-3
99 F(I,J)=2.D0*F18
DO 102 K=8,K0
I=M(K)
J=M(K-1)-2
102 F(I,J)=2.D0*F15
DO 103 K=8,K0,2
I1=M(K-1)+3
I2=M(K)-1
I4=K/2+2
DO 103 I=I1,I2
J=I-I4
103 F(I,J)=F15
DO 107 K=8,K0,2
I1=M(K-1)+2
I2=M(K)-2
I4=(K-4)/2
DO 107 I=I1,I2
J=I-I4
107 F(I,J)=F13
DO 114 K=8,K0
I=M(K)-3
J=I+2
F(I,J)=F18

```

```

114 F(J,I)=F18
    IF (NROWS .LT. 9)
      > GO TO 125
    F(18,23)=F12+2.D0*F18
    F(23,18)=F(18,23)
    DO 6 K=5,K4,2
      I1=M(K-1)+2
      I2=M(K)-1
      I4=2*K+5
      DO 6 I=I1,I2
        J=I+14
  6 F(I,J)=F18
      DO 8 K=5,K4
        I1=M(K-1)+2
        I2=M(K)-1
        I4=2*K+3
        DO 8 I=I1,I2
          J=I+14
  8 F(I,J)=F18
      DO 12 K=9,K0,2
        I1=M(K-1)+2
        I2=M(K)-3
        I4=2*K-5
        DO 12 I=I1,I2
          J=I-14
 12 F(I,J)=F18
      DO 18 K=6,K3,2
        I1=M(K-1)+1
        I2=M(K)-2
        I4=(K/2)*3+3
        DO 18 I=I1,I2
          J=I+14
          F(I,J)=F15
 18 F(J,I)=F15
      DO 19 K=6,K3
        I=M(K)-1
        J=M(K+3)-2
        F(I,J)=F15+F18
 19 F(J,I)=F15+F18
      DO 25 K=6,K3,2
        I=M(K-1)+2
        J=M(K+2)+2
        F(I,J)=F15+F18
 25 F(J,I)=F15+F18
      DO 32 K=6,K3
        I=M(K)
        J=M(K+3)-4
 32 F(I,J)=2.D0*F18
      DO 34 K=9,K0,2
        I1=M(K-1)+4
        I2=M(K)-1
        I4=((K-1)/2)*3+2
        DO 34 I=I1,I2
          J=I-14
 34 F(I,J)=F18
      DO 37 K=9,K0,2
        I1=M(K-1)+3
        I2=M(K)-2
        I4=((K-1)/2)*3-1
        DO 37 I=I1,I2
          J=I-14
 37 F(I,J)=F15
      DO 39 K=9,K0,2
        I=M(K-1)+1
        J=M(K-4)+3
 39 F(I,J)=2.D0*F18
      DO 44 K=7,K2,2
        I=M(K-1)+1
        J=M(K+1)+3
 44 F(I,J)=2.D0*F15

```

```

DO 52 K=7,K2,2
  I1=M(K-1)+3
  I2=M(K)-1
  I4=K+1
DO 52 I=I1,I2
  J=I+I4
52 F(I,J)=F13
DO 53 K=7,K2
  I=M(K)-1
  J=M(K+2)-3
  F(I,J)=F18
53 F(J,I)=F18
DO 56 K=7,K2
  I1=M(K-1)+3
  I2=M(K)-1
  I4=K-1
DO 56 I=I1,I2
  J=I+I4
56 F(I,J)=F15
DO 57 K=9,K0,2
  I1=M(K-1)+3
  I2=M(K)-2
  I4=K+1
DO 57 I=I1,I2
  J=I-I4
57 F(I,J)=F15
DO 62 K=9,K0,2
  I1=M(K-1)+2
  I2=M(K)-3
  I4=K-3
DO 62 I=I1,I2
  J=I-I4
62 F(I,J)=F15
DO 63 K=8,K1,2
  I1=M(K-1)+1
  I2=M(K)-3
  I4=K/2+4
DO 63 I=I1,I2
  J=I+I4
63 F(I,J)=F18
DO 66 K=8,K1,2
  I=M(K-1)+1
  J=M(K)+4
  F(I,J)=F15+F18
66 F(J,I)=F15+F18
DO 74 K=8,K1,2
  I=M(K-1)+1
  J=M(K)+2
  F(I,J)=F12+F13
74 F(J,I)=F12+F13
DO 80 K=8,K1
  I=M(K-1)+2
  J=M(K)+2
  F(I,J)=F12+F15
80 F(J,I)=F12+F15
DO 83 K=8,K1
  I=M(K)-1
  J=M(K+1)-2
  F(I,J)=F12+F15
83 F(J,I)=F12+F15
DO 88 K=8,K1,2
  I=M(K-1)+3
  J=M(K)+2
  F(I,J)=F13+F18
88 F(J,I)=F13+F18
DO 92 K=8,K1,2
  I1=M(K-1)+3
  I2=M(K)-1
  I4=(K-4)/2
DO 92 I=I1,I2

```

```

      J=I+I4
92 F(I,J)=F15
   DO 93 K=8,K1
      I=M(K)
      J=M(K+1)-3
93 F(I,J)=2,DO*F15
   DO 96 K=8,K1
      I=M(K)
      J=M(K+1)-4
96 F(I,J)=2,DO*F18
   DO 106 K=9,K0
      I1=M(K-1)+4
      I2=M(K)-1
      I4=(K-1)/2+2
   DO 106 I=I1,I2
      J=I-14
106 F(I,J)=F13
   DO 108 K=9,K0,2
      I1=M(K-1)+3
      I2=M(K)-2
      I4=(K-3)/2
   DO 108 I=I1,I2
      J=I-14
108 F(I,J)=F13
   DO 109 K=9,K0
      I1=M(K-1)+2
      I2=M(K)-3
      I4=(K-5)/2
   DO 109 I=I1,I2
      J=I-14
109 F(I,J)=F15
   DO 112 K=9,K0,2
      I=M(K-1)+1
      J=M(K-2)+4
112 F(I,J)=2,DO*F18
   IF (NRDWS .LT. 10)
     > GO TO 125
   DO 22 K=7,K3,2
      I=M(K-1)+2
      J=M(K+2)+2
      F(I,J)=F15+F18
22 F(J,I)=F15+F18
   DO 29 K=7,K3,2
      I=M(K-1)+3
      J=M(K+2)+1
      F(I,J)=F18
29 F(J,I)=F18
   DO 38 K=10,K0,2
      I1=M(K-1)+1
      I2=M(K)-4
      I4=((K-4)/2)*3+1
   DO 38 I=I1,I2
      J=I-14
38 F(I,J)=F18
   DO 41 K=8,K2,2
      I1=M(K-1)+1
      I2=M(K)-3
      I4=K+3
   DO 41 I=I1,I2
      J=I+I4
      F(I,J)=F15
41 F(J,I)=F15
   DO 54 K=8,K2,2
      I=M(K-1)+2
      J=M(K+1)+1
      F(I,J)=F15
54 F(J,I)=F15
   DO 65 K=9,K1,2
      I1=M(K-1)+2
      I2=M(K)-3

```

```

      I4=(K-1)/2+4
      DO 65 I=I1,I2
      J=I+I4
65  F(I,J)=F18
      DO 77 K=9,K1
      I=M(K)-2
      J=M(K+1)-2
      F(I,J)=F12+F18
77  F(J,I)=F12+F18
      DO 86 K=9,K1,2
      I=M(K-1)+3
      J=M(K)+2
      F(I,J)=F12+F18
86  F(J,I)=F12+F18
      DO 89 K=9,K1
      I1=M(K-1)+4
      I2=M(K)-1
      I4=(K-2)/2
      DO 89 I=I1,I2
      J=I+I4
89  F(I,J)=F13
      DO 94 K=9,K1,2
      I=M(K-1)+4
      J=M(K)+1
      F(I,J)=F15+F18
94  F(J,I)=F15+F18
      DO 100 K=10,K0,2
      I1=M(K-1)+4
      I2=M(K)-1
      I4=K/2+3
      DO 100 I=I1,I2
      J=I-I4
100 F(I,J)=F18
      DO 111 K=10,K0,2
      I1=M(K-1)+1
      I2=M(K)-4
      I4=(K-8)/2
      DO 111 I=I1,I2
      J=I-I4
111 F(I,J)=F18
      IF (NR0WS .LT. 11)
      > GO TO 125
      DO 26 K=8,K3,2
      I1=M(K-1)+3
      I2=M(K)-1
      I4=(K/2)*3+2
      DO 26 I=I1,I2
      J=I+I4
26  F(I,J)=F15
      DO 30 K=8,K3,2
      I1=M(K-1)+3
      I2=M(K)-1
      I4=(K/2)*3
      DO 30 I=I1,I2
      J=I+I4
30  F(I,J)=F18
      DO 40 K=11,K0,2
      I1=M(K-1)+2
      I2=M(K)-4
      I4=((K-3)/2)*3
      DO 40 I=I1,I2
      J=I-I4
40  F(I,J)=F18
      DO 45 K=9,K2,2
      I1=M(K-1)+2
      I2=M(K)-3
      I4=K+3
      DO 45 I=I1,I2
      J=I+I4
45  F(I,J)=F15

```

```

DO 75 K=10,K1,2
I=M(K-1)+2
J=M(K)+3
F(I,J)=F12+F18
75 F(J,I)=F12+F18
DO 82 K=10,K1,2
I1=M(K-1)+3
I2=M(K)-2
I4=K/2
DO 82 I=I1,I2
J=I+I4
F(I,J)=F12
82 F(J,I)=F12
DO 97 K=10,K1,2
I1=M(K-1)+4
I2=M(K)-1
I4=(K-6)/2
DO 97 I=I1,I2
J=I+I4
97 F(I,J)=F18
DO 101 K=11,K0,2
I1=M(K-1)+5
I2=M(K)-1
I4=(K-1)/2+4
DO 101 I=I1,I2
J=I-I4
101 F(I,J)=F18
DO 104 K=11,K0,2
I1=M(K-1)+5
I2=M(K)-1
I4=(K-1)/2+3
DO 104 I=I1,I2
J=I-I4
104 F(I,J)=F15
DO 113 K=11,K0,2
I1=M(K-1)+2
I2=M(K)-4
I4=(K-7)/2
DO 113 I=I1,I2
J=I-I4
113 F(I,J)=F18
IF (NR0WS .LT. 12)
> GO TO 125
DO 23 K=9,K3,2
I1=M(K-1)+3
I2=M(K)-2
I4=((K+1)/2)*3+1
DO 23 I=I1,I2
J=I+I4
F(I,J)=F15
23 F(J,I)=F15
DO 31 K=9,K3,2
I1=M(K-1)+4
I2=M(K)-1
I4=((K-1)/2)*3+1
DO 31 I=I1,I2
J=I+I4
31 F(I,J)=F18
DO 76 K=11,K1
I1=M(K-1)+3
I2=M(K)-3
I4=K/2+1
DO 76 I=I1,I2
J=I+I4
F(I,J)=F12
76 F(J,I)=F12
DO 95 K=11,K1,2
I1=M(K-1)+5
I2=M(K)-1
I4=(K-5)/2

```

```

DO 95 I=I1,I2
J=I+I4
95 F(I,J)=F15
DO 98 K=11,K1,2
I1=M(K-1)+5
I2=M(K)-1
I4=(K-7)/2
DO 98 I=I1,I2
J=I+I4
98 F(I,J)=F18
DO 121 K=11,K1,2
I1=M(K-1)+4
I2=M(K)-2
I4=(K-1)/2
DO 121 I=I1,I2
J=I+I4
F(I,J)=F12
121 F(J,I)=F12
125 A(I)=AR
DO 126 K=2,NROWS
I=M(K)
126 A(I)=6.00*AR
DO 127 K=4,NROWS
I1=M(K-1)+1
I2=M(K)-1
DO 127 I=I1,I2
127 A(I)=12.00*AR
DO 128 K=3,NROWS,2
I=M(K-1)+1
128 A(I)=6.00*AR
TOTAL=0.00
DO 130 I=1,MM
F(I,I)=F(I,I)+F11
SUM=0.00
DO 129 J=1,MM
129 SUM=SUM+F(I,J)
F(I,N)=EMISS-SUM
F(N,I)=F(I,N)*A(I)
130 TOTAL=TOTAL+F(N,I)
F(N,N)=EMISS-TOTAL
RETURN
END

```

ORNL-5239
Dist. Category UC-79c

INTERNAL DISTRIBUTION

1. M. Bender
2. M. R. Bennett
3. R. E. Blanco
4. J. O. Blomeke
5. W. D. Bond
6. B. F. Bottenfield
7. N. C. Bradley
8. K. B. Brown
9. W. D. Burch
10. J. M. Chandler
11. W. E. Clark
12. M. E. Clifton
13. L. T. Corbin
14. R. M. Counce
- 15-24. R. L. Cox
25. D. J. Crouse
26. F. L. Culler
27. B. C. Duggins
28. D. E. Dunning
29. J. H. Evans
30. M. J. Feldman
31. D. E. Ferguson
32. J. H. Goode
33. N. R. Grant
34. W. S. Groenier
35. D. C. Hampson
36. B. A. Hannaford
37. W. O. Harms
38. J. N. Herndon
39. W. D. Holland
40. D. E. Horner
41. A. R. Irvine
42. P. R. Kasten
43. A. D. Kelmers
44. J. Q. Kirkman
45. J. A. Klein
46. C. E. Lamb
47. B. E. Lewis
48. A. L. Lotts
49. J. C. Mailen
50. A. P. Malinauskas
51. L. Maya
52. L. E. McNeese
53. J. G. Morgan
54. J. M. Morrison
55. R. F. Hibbs
56. J. P. Nichols
57. E. L. Nicholson
58. E. D. North
59. J. H. Pashley
60. F. L. Peishel
61. H. Postma
62. R. H. Rainey
63. W. F. Schaffer, Jr.
64. C. D. Scott
65. J. D. Sease
66. B. B. Spencer
67. R. G. Stacy
68. M. J. Stephenson
69. W. G. Stockdale
70. O. K. Tallent
71. D. B. Trauger
72. W. E. Unger
73. V. C. A. Vaughen
74. B. L. Vondra
75. C. D. Watson
76. J. S. Watson
77. B. S. Weil
78. M. E. Whatley
79. J. R. White
80. R. G. Wymer
81. O. O. Yarbrow
82. S. Beard (Consultant)
83. L. Burris, Jr. (Consultant)
84. A. B. Carson (Consultant)
85. W. K. Davis (Consultant)
86. E. L. Gaden, Jr. (Consultant)
87. C. H. Ice (Consultant)
88. W. H. Lewis (Consultant)
89. R. B. Richards (Consultant)
90. A. Schneider (Consultant)
91. M. J. Szulinski (Consultant)
92. J. S. Theilacker (Consultant)
93. A. K. Williams (Consultant)
- 94-95. Central Research Library
96. ORNL--Y-12 Technical Library
Document Reference Section
- 97-105. Laboratory Records
106. Laboratory Records, ORNL RC
107. ORNL Patent Office
108. Nuclear Safety Information
Center

EXTERNAL DISTRIBUTION

- 109. Director, Reactor Division, ERDA, ORO
- 110-111. Director, Division of Nuclear Fuel Cycle and Production, ERDA, Washington, D. C. 20014
- 112-113. Director, Division of Reactor Research and Development, ERDA, Washington, D. C. 20014
- 114. Research and Technical Support Division, ERDA, ORO
- 115-366. Given distribution as shown in TID-4500 under UC-79c -- Fuel Recycle category (Applied)